Mechanisms of clonal selection in myeloproliferative neoplasms (JAK2V617F) subclonal selection and transformation after TP53 inactivation

Panhong Gou

Université de Paris

École doctorale 561

Laboratoire UMRS 1131:Hématopoiese normale et pathologique: émergence, environnement et recherche translationnelle

Mechanisms of Clonal selection in myeloproliferative neoplasms (JAK2V617F) subclonal selection and transformation after TP53 inactivation

Présentée Par Panhong GOU

Thèse de doctorat de Hématologie

Dirigée par les Stéphane GIRAUDIER et Bruno CASSINAT

Présentée et soutenue publiquement à Paris le 05/07/2021

Devant un jury composé de :

Professeur Valerie UGO (Université d'Angers)	Présidente
Professeur Eric LIPPERT (Université de Brest)	Rapporteur
Professeur Loic GARCON (Université d'Amiens)	Rapporteur
Docteur Bruno CASSINAT (Université de Paris)	Co-Directeur de thèse
Professeur Stephane GIRAUDIER (Université de Paris)	Directeur de thèse

Titre: Mécanismes de transformation, sélection clonale et sous-clonale dans les néoplasies myéoprolifératives (*JAK2* V617F) après inactivation de TP53.

Résumé: Les néoplasies myéloprolifératives (NMP) forment un groupe hétérogène de pathologies caractérisées par la prolifération anormale de clones matures d'une ou plusieurs lignées myéloïdes.

Les NMPs sont des pathologies oligoclonales et acquises dans la cellule souche hématopoïétique (CSH). En effet, la présence de mutations somatiques sur un seul clone suffit à donner un avantage prolifératif et favorise une différenciation myéloïde aboutissant à un phénotype myéloprolifératif. Des anomalies dans certaines voies de signalisation intracellulaire jouent un rôle central dans la physiopathologie des NMPs. La mutation *JAK2* V617F est la plus fréquement retrouvée dans ces pathologies.

TP53 est aujourd'hui considéré comme un gardien de l'intégrité du génome en maintenant sa stabilité dans les états de stress cellulaire et est impliqué dans de nombreux processus. Les mutations de TP53 sont fréquentes dans de nombreuses pathologies malignes au vu des nombreux rôles de la protéine. En effet, plus de 50% des cancers présentent des mutations de TP53. En outre, les modèles murins mutés ou KO pour TP53 sont sujets au développement de tumeurs et particulièrement des lymphomes. De plus, dans les leucémies aiguës myéloïdes (LAM) secondaires à un NMP, TP53 fait parti des gènes les souvent mutés et impliqué dans leur acutisation.

Par conséquent, nous avons cherché dans ce projet à combiner une approche de modélisation mathématique avec des expériences in vivo sur des modèles murins pour déterminer quand et avec quelle

probabilité les mutations de TP53 survenaient dans les NMP. Dans un deuxième temps, nous avons essayé d'établir un modèle murin représentatif des mutations de TP53 retrouvées chez l'homme pour savoir si ces dernières étaient en cause dans les transformations en LAM chez les souris *JAK2* V617F.

En utilisant des souris Wild Type (WT), nous avons provoqué un stress aigü par du PHZ, , et stimulé l'hématopoïèse in vivo en combinant cette approche avec un modèle mathématique. Cette modélisation peut être utilisée pour étudier l'hématopoïèse sous d'autre conditions de stress. Dans un deuxième temps, nous avons eu pour objectif de soumettre le même stress chez des souris *JAK2* V617F pour établir la chronologie et la probabilité des mutations survenant dans les CSH. Cependant, les données in vivo ont montré que la réponse des souris JAK2 était différente des souris WT ce qui implique la création d'un nouveau modèle mathématique pour stimuler l'hématopoïèse efficacement. Dans les souris mutées pour JAK2 et TP53 nous avons trouvé que les mutations de TP53 ne favoriseraient pas la transformation des NMP en LAM. Toutefois, il semblerait que l'INF soit moins efficace sur les souris mutées JAK2 /TP53 que les souris JAK2 seules. Cette résistance pourrait expliquer la plus grande probabilité d'acutisation avec un délai retardé quand les sous-clones ont une faible charge allélique. Cela suggère que dans les MPN, comme dans les autres cancers, les mécanismes de régulation cellulaire sont importants et qu'il faut plus de deux gènes mutés pour induire un cancer.

mots clés: Néoplasies myéloprolifératives(NPM); JAK2V617F; TP53; Cellule souche hématopoïétique(CSH); modèle de souris Knock-in; Hématopoïèse.

Title: Mechanisms of Clonal selection in myeloproliferative neoplasms (JAK2V617F) subclonal selection and transformation after TP53 inactivation

Abstract: Myeloproliferative neoplasms (MPNs) are a heterogeneous group of disorders characterized by implication of one or more of the myeloid lineages and by a clonal proliferation of mature myeloid elements. MPNs arise in the HSC compartment as a result of a single HSC acquiring somatic mutations that theoretically give the mutant HSC a selective advantage, thereby promoting myeloid cell differentiation and producing a myeloproliferative phenotype. Abnormal cytokine signaling/signal transduction plays a key role in the pathogenesis of MPN. JAK2V617F is the most common driver mutation in MPN.TP53 is considered as the guardian of the genome, maintains genomic stability under cellular stress and is engaged in a variety of processeser. TP53 mutations are common in many malignancies due to the multiple activities of P53. In fact, more than 50% of cancers harbor P53 gene mutations. Therefore, P53 mutated or null mice are prone to the onset of tumor development, especially lymphomas. In the post-MPN AML TP53 is also one of the major genes which contribute transformation.

Therefore we aimed to combine mathematical modeling with in vivo experiments in a mouse model to determine when and with what probability mutant HSC occurs in the MPN. Secondly, we intended to create a mouse model that more closely resembles the human mutation level to determine if TP53 causes transform to AML in JAK2V617F mice.

We established acute stress by PHZ in normal mice and simulated in

vivo hematopoiesis by in vivo mouse experiments combined with a mathematical model. This model can be used to verify the hematopoietic process under other stress conditions. Secondly, we intended to use the same approach to establish the same stress state in JAK2V617F mice to determine the timing and probability of mutant HSC. However, the in vivo data showed that the response of JAK2V617F to stress was different from that of WT mice, so we need to recreate a new mathematical model to simulate the hematopoietic process under the mutation in the following. In the established JAK2V617F/TP53 mice, we found that TP53 did not promote the transfer of MPN mice to AML. However, JAK2V617F/TP53 mice were not as effective as JAK2V617F mice in treating IFN. This resistance to therapy could be an explanation to the higher probability for leukemia emergence with large delay when TP53 subclones are small. This suggesting that in MPN, like in other cancers, the cellular defense mechanisms are important and that more than two gene alterations are necessary to induce cancer.

Key words: Myeloproliferative neoplasms (MPN); JAK2V617F; TP53; Hematopoietic stem cell (HSC); Knock-in mouse model; Hematopoiesis

ACKNOWLEDGEMENT

I would like to express my gratitude to my thesis committee for agreeing to judge my work.

I am grateful to Pr. Valerie UGO for being the president of my thesis jury. I am thankful to Pr. Loic GARCON and Pr. Eric LIPPERT accepted to be the reviewers of my thesis jury.

I would like to give my gratitude to Pr. Christine Dosquet for accepting me into this lab. More than that, I appreciate your friendly, ever-welcoming and motivating attitude.

My deepest gratitude to my PhD supervisor Pr. Stephane GIRAUDIER! At first, his patient guidance was that I quickly gained a deep understanding of hematology. At the same time, his encouragement and guidance enabled me to have a deeper understanding of the project and a different understanding of scientific research. His active thinking is also an important treasure of my scientific research stage. I hope I can use your wisdom in my future work.

I owe my profound gratitude to Dr. Bruno CASSIANT, he is very nice to show me lots of things from I started to apply this lab to prepared my thesis defence. And he gives me lots of support in the thesis writing.

Thanks for Rose-Ann, she gives me much of helps in the animal work.At the same time she also shared lots of experience for the study. I earned many valuable experience and knowledge from you. Thanks for your help!

Please let me show my gratitude to Dr. Evelyne Lauret. She is one of my best teachers in my life. She gives me much of things on the flow cytometer and the study attitude.

I also want to show my gratitude to my lovely lab members. It’s all of you who give me plenty of help from study to live. Celia, it’s you who give me support and helping in every complicated thing especially I cannot speak French well. Celine, it’s your warming that gives me a different sense of study and life. Nabih who always gives me some useful suggestion in the study and many helps during my thesis manuscript prepared; Sarah who always gives me the bits of help once I came here four years ago; Gil, Saravanan, Loic although all of you are not in the lab now I still want to express my thanks for all of you.With the help of these kindly people my Paris life and study becomes interesting and meaningful.

I would like to thank Dr. Véronique PARIETTI-MONTCUQUET, her team give me a great support for the animal work. And I also like to show my gratitude to Dr. Niclas Setterblad,he is really nice to explain to me how to use the different tools of IRSL plate form.

I would like to show my gratitude to the CSC (China Scholarship Council), it’s your support I have the resources to come to Paris and experience this different period time.Finally, I want to deeply thanks to my families. They are always give me the great supports and advises when I get stuck. Deeply thank my husband, Wenchao ZHANG , he gives me tons of supports from life to study and accompany all the time.

Panhong GOU

03/05/2021

TABLE OF CONTENTS

LIST OF FIGURES

LIST OF TABLES

LIST OF ABBREVIATION

EMH: extramedullary hematopoiesis

MPNs: myeloproliferative neoplasms

MDS: myelodysplastic syndromes

HSC: hematopoietic Stem Cell

PV: polycythemia vera

ET: essential thrombocythemia

PMF: primary myelofibrosis

AML: acute myeloid leukemia

HCT: hematocrit

IFNα: Interferon alpha

CALR: calreticulin

MPL: thrombopoietin receptor gene

OS: median survival

ELN: Europe Leukemia Net

JAK2: janus kinase 2

IGF-1: insulin-like growth factor-1

EPO: erythropoietin

EPOR: erythropoietin receptor

IGF-1: insulin-like growth factor-1

TYK2: tyrosine kinase 2

TPO: thrombopoietin

TPOR: thrombopoietin receptor

GM-CSF: granulocyte-macrophage colony-stimulating factor

BM: bone marrow

SH2: src homology-2

JH1: janus homology domains 1

JH2: janus homology domains 2

TP53: tumor protein 53

TET2: tet methylcytosine dioxygenase 2

DNMT3A: DNA (cytosine-5)-methyltransferase 3A

EZH2: enhancer of zeste homolog 2

ASXL1: additional sex combs like 1

SRSF2: splicing factor arginine/serine enriched 2

BAC: bacterial artificial chromosome

FDA: Food and Drug Administration

BAC: bacterial artificial chromosome

pIpC: polyinosinic-polycytidine

RBC: red blood cell

WBC: white blood cell

PLT: platelet

HCT: hematocrit

LSK: $Lin^{-}Sca\text{-}1^{+}c\text{-}Kit^{+}$

MPP: myeloid progenitor populations

CMP: common myeloid progenitor

GMP: granulocyte-macrophage progenitors

MEP: megakaryocyte-erythroid progenitors

LT-HSC: long-term hematopoietic stem cells

ST-HSC: short-term hematopoietic stem cells

HPCs: hematopoietic progenitor cells

SLAM: signaling lymphocyte activation molecules

SCF: stem cell factor

FLT3: fms-like tyrosine kinase 3

IL-3: Interleukin 3

IL-6: Interleukin 6

TNF: tumor necrosis factor

G-CSF: granulocyte colony-stimulating factor

M-CSF: macrophage colony-stimulating factor

PAMPs: pathogen-associated molecular patterns

DAMPs: danger-associated molecular patterns

TLRs: toll-like receptors

IFNγ: Interferon gamma

IFNα: Interferon alpha

HIF2α: Hypoxia Inducible factor alpha 2

PHZ: Phenylhydrazine

LD50: lethal dose 50%

ROS: Reactive oxygen species

BMP4: bone morphogenetic protein 4

GDF15: growth/differentiation factor 15

HH: hedgehog

SEP: stress erythroid progenitors

MDM2: Murine double minute 2 homolog

PI3K: phosphatidylinositol 3-kinase

NGS: next-generation sequencing

VAF: variant allele frequency

IP: intraperitoneal injection

PBS: phosphate-buffered saline

PE: phycoerythrin

FITC: fluorescein isothiocyanate

PE/Cy7: phycoerythrin -Cyanine7

FBS: fetal bovine serum

APC-Cy7: allophycocyanin- Cyanine7

BMT: bone marrow transplantation

CFU: colony-forming unit

SD: standard deviation

Anova : Analysis of varianc

INTRODUCTION

CONTEXTE ET PRINCIPAUX RÉSULTATS

Les NMP sont un groupe hétérogène de maladies des cellules souches hématopoïétiques, caractérisées cliniquement par une augmentation des cellules hématopoïétiques matures du sang périphérique. Les NMP sont des pathologies clonale, ceci ayant été démontré initialement par des études basées l'étude de l'inactivation du chromosome X, des anomalies rares du caryotype et une analogie avec la leucémie myéloïde chronique et sa translocation clonale caractéristique BCR-ABL.

La mutation JAK2V617F a confirmé la nature clonale des NMP et a fourni des indices pour la compréhension du développement de la maladie. Ensuite, des mutations de l'exon 12 de JAK2, de CALR et de MPL ont également été identifiées dans les NMP. Toutes ces mutations ont une même caractéristique commune : Une activation de la voie de transduction JAK2.

La voie JAK2 joue un rôle majeur dans l'hématopoïèse. Différents modèles murins de NMP ont été largement utilisés dans diverses recherches au fil des ans. Les modèles de souris NMP ont également démontré que l'activation non régulée de la voie JAK2 est responsable du développement de la symptomatologie.

Chez la souris de type sauvage, les cellules souches hématopoïétiques à long terme (LT-HSC) sont quiescentes pour maintenir un état stable. Les MPP (progéniteurs primaires myéloïdes) et les ST-HSC (cellules souches hématopoïétiques à court terme) sont les principaux compartiments qui

maintiennent l'hématopoïèse de la souris. Les études ont montré que chez une souris de type sauvage, une cellule LT-HSC entre en mitose tous les 100 jours. Cela signifie qu'une LT-HSC ne peut faire des mitoses que 6 fois dans la durée de vie d'une souris (2 ans≈600 jours). Les LT-HSC mutées par JAK2 ont un avantage prolifératif par rapport aux cellules normales. Mais dans le modèle de souris MPN, les LT-HSC ont un léger avantage prolifératif par rapport aux cellules des souris normales.

Notre premier objectif est de combiner un modèle mathématique avec une étude in vivo pour déterminer à quel moment doit survenir la mutation JAK2V617F au cours de la vie pour qu'une pathologie puisse emerger. Nous esperons donc que la modélisation mathématique permettre de mieux comprendre les temps d'apparition de la premiere cellule souche pathologique.

Nous avons donc tout d'abord, étudié le comportement normal des cellules souches chez la souris. Il existe peu de modèles mathématiques axés sur les compartiments immatures, et la plupart des modèles mathématiques sont axés sur l'hématopoïèse à l'état stable. De plus, nous avons émis l'hypothèse que le stress est la principale raison pour laquelle les cellules mutées par JAK2V617F se développent et concurrencent les cellules de type sauvage puisque en état stationnaire, l'avantage prolifératif des cellules souches JAK2V617F n'est que d'un facteur 2 par rapport aux cellules normales. Nous avons donc modélisé l'hématopoïèse immature normale en combinant hématopoïèse à l'état d'équilibre et l'hématopoïèse de stress.

La phenylhydrazine (PHZ) a été utilisé comme stress capable d'induire une hémolyse importante et dose dépendante des globules rouges. Nous montrons que ceci s'accompagne d'un processus inflammatoire important. En combinant les données quantitatives et d'entrée en cycle des cellules des différents compartiments de cellules souches et de progéniteurs avec, nous avons modélisé la réponse des cellules matures au stress. En outre, notre modèle a été validé en utilisant différents stress "in silico" comme le traitement au 5-FU, la phlébotomie ou la suppression des LT-HSC. Après ces stress extrêmes, le modèle régulé récapitule ce qui se passe in-vivo et un retour à des valeurs hématopoïétiques normales selon les données biologiques obtenues dans la littérature.

Ce modèle étant validé, notre objectif est maintenant de déterminer l'issue d'une LT-HSC mutante (et ses propres propriétés prolifératives) afin de déterminer quand et avec quelle probabilité un phénotype NMP pourrait se développer après l'apparition d'une seule cellule souche mutante. À cette fin, nous avons reproduit chez des souris transgéniques JAK2V617F le stress précédemment analysé chez des souris normales. En appliquant les données des souris mutantes au modèle mathématique, nous espérons qu'il sera possible de déterminer 1- quels facteurs doivent être modifiés dans le modèle, illustrant mathématiquement les conséquences de la mutation de JAK2V617F sur l'hématopoïèse. 2- En utilisant les paramètres des souris mutantes, nous pourrons déterminer le nombre minimal de LT-HSC mutantes qui permettra

d'induire un phénotype MPN avec une probabilité égale à celle de l'émergence du MPN dans la population générale. Ce nombre de LT-HSC correspondra à la date d'émergence de la première LT-HSC mutante qui sera nécessaire pour induire un NMP. Nous espérons pouvoir démontrer clairement que le NMP est en fait une pathologie qui émerge pendant la vie fœtale. 3- Nous aimerions également démontrer que le stress est obligatoire pour induire l'émergence du phénotype NMP en utilisant des comparaisons entre les stress et l'état stable de l'hématopoïèse normale et pathologique. Les données in vivo ont été recueillies et la modélisation mathématique sera développée au cours des prochaines années.

Outre le temps d'émergence du NMP, nous avons étudié l'évolution des NMP.

Depuis des décennies, de plus en plus de mutations additionnelles ont été retrouvées chez un sous-ensemble de patients, en association avec les mutations initiatrices telles que JAK2V617F. Ces mutations supplémentaires interviennent dans diverses voies telles que l'épigénétique, l'épissage de l'ARNm, la signalisation intracellulaire et l'expression génétique. Des études cliniques ont montré que les mutations supplémentaires contribuent au mauvais pronostic des patients atteints de NMP. TP53 est l'un des gènes touché par des mutations supplémentaires dans la transformation du NMP. TP53 joue un rôle clé comme gardien du génome, et dans la majorité des cancers ont été identifiées des mutations de TP53. Cependant, dans les leucémies aiguës spontanées, la mutation TP53 a rarement été identifiée, elle est cependant plus

fréquente dans les leucémies acquises. Certaines études ont suggéré que la mutation TP53 était responsable de la transformation en leucémie aiguë des NMP. Certains modèles de souris confirment cette hypothèse. Cependant, une étude clinique a montré que certains patients atteints de NMP et porteurs de mutations TP53 ne développent pas de leucémie pendant une longue période, en particulier lorsque la charge allélique de la mutation TP53 est faible. Cela suggère que l'avantage de la mutation TP53 n'est pas plus élevé que celui de la mutation JAK2V617F chez les patients NMP.

Nous avons donc développé un modèle de souris triple transgénique pour identifier la fonction de la perte de fonction de TP53 dans le contexte de JAK2V617F. Dans notre modèle de souris, l'expression de JAK2V617F est assurée à un niveau physiologique avec la recombinaison vav-cre, (contrairement aux modèles précédants utilisant une surexpression importante de l'oncogène JAK2V617F induit par un promoteur viral) et TP53 est inactivé (knock-out).

Avec ce modèle de souris, nous avons constaté que les souris JAK2V617F/TP53-/- ont les mêmes caractéristiques de NMP que les souris JAK2V617F. Nous avons analysé le nombre de cellules sanguines, les poids de la rate, l'histologie de la moelle osseuse et de la rate, le cycle cellulaire de toutes les populations de progéniteurs et la survie, mais aucune différence significative n'a pu être identyifiée. Cela suggère que le TP53 ne joue pas un rôle clé dans le développement du phénotype NMP.

Par contre, les expressions géniques analysés par RNA-Seq dans les différentes populations de cellules souches et de progéniteurs nous a permis de mettre en évidence ce qui dans les modifications génnétiques induites par JAK2V617F était p53 dépendant ou non.

Les gènes régulés de façon indépendante de TP53 sont impliqués dans le phénotype NMP puisque le phénotype a été observé chez les souris transgéniques triples.

De plus, l'analyse comparative des voies a montré qu'une des principales voies régulées est la voie de signalisation de l'IFN-α. En effet, la souche JAK2V617F présente une surexpression significative des gènes impliqués dans la voie IFN alors que cette voie est quasi-normale dans les souches JAK2V617F/TP53-/-. Ceci suggère que les cellules JAK2V617F pourraient être hypersensibles à l'IFN alors que les souches JAK2V617F/TP53-/- seraient moins sensibles à l'IFN-α. Pour vérifier cette hypothèse, nous avons utilisé des greffes compétitives et traité les souris avec de l'IFN-α. De cette manière, nous avons constaté que les cellules mutées JAK2V617F/TP53-/- ont une sensibilité plus faible à l'IFN-α que les cellules JAK2V617F seules. Cette résistance au traitement pourrait être la raison de la probabilité plus élevée d'émergence de transformation leucémique même si l'inhbition de p53 n'est pas « en soi » un évènement oncologique.

En conclusion, nous avons combiné des données biologiques avec une approche mathématique pour modéliser l'hématopoïèse normale et sous stress et, comparé cete modélisation avec les résultats obtenus chez les souris

présentant un NMP. De plus, nous avons également montré que chez la souris et dans notre modèle transgénique, TP53 n'est pas un gène critique de la transformation des NMP en LAM, mais qu'il est responsable de la résistance à la thérapie IFN dans le contexte de JAK2V617F.

Background

Hematopoiesis is the production of all of the cellular components of blood. It occurs within the hematopoietic system, including organs and tissues such as the bone marrow, liver, and spleen. It begins early in the development of an embryo, well before birth, and continues all the life of an individual. During adult life, hematopoiesis occurs in the marrow of the long bones like femur and tibia, but mainly in the pelvis, cranium, vertebrae, and sternum[1]. Hematopoiesis represents approximately 5% of total body mass in human healthy adult[2], 3% of total body mass in rat[3] and 2% in dogs[4] . In pathological conditions, the lymph nodes, liver, and spleen may regain their hematopoietic function that is called extramedullary hematopoiesis (EMH). Pathological hematopoiesis may show alterations in the numbers and morphology of different cell lineages in peripheral blood and mono- or multilineage cell changes in the bone marrow. Both normal and pathological hematopoiesis can be divided into two different systems, myeloid and lymphoid, according to the different lineages. Myeloid neoplasms include acute myeloid leukemia (AML) and related aggressive myeloid neoplasms, myeloproliferative neoplasms

(MPN), mastocytosis, myelodysplastic syndromes (MDS), and MDS/MPN syndromes. JAK2V617F is one of the most common mutations expressed in myeloid neoplasms and more particularly in MPN where this mutation has been demonstrated as causative of the disorders. However, other genes can be abnormal in myeloid neoplasms. *TP53* which encodes the tumor suppressor P53 is the most frequently mutated gene in cancers. Surprisingly, it is not one of the most mutated genes in myeloid neoplasms, however it has been suggested that *TP53* could be associated to the evolution of MPN and MDS to acute leukemias.

The aim of this work was first to better understand the clonal advantage of JAK2V617F mutated cells based on the hypothesis that instead of steady state JAK2V617F hematopoiesis the clonal advantage may be due to stressed JAK2V617F stem cells, and second to better delineate what is *TP53* dependent or independent in MPN and verify if the *TP53* inactivation can transform the MPN into AML.

1.1 Myeloproliferative neoplasms

The myeloproliferative neoplasms (MPNs) are a heterogeneous group of disorders characterized not only by implication of one or more of the myeloid lineages and by a clonal proliferation of mature myeloid elements. These disorders are characterized the deregulation of signaling pathways (mostly tyrosine kinase) due to the acquisition of a molecular abnormality in a

hematopoietic stem cell (HSC). Indeed, MPNs arise in the HSC compartment as a result of a single HSC acquiring somatic mutations that theoretically give the mutant HSC a selective advantage over normal HSC, thereby promoting myeloid cell differentiation and producing a myeloproliferative phenotype. This population of somatic mutant HSC, which initiate and maintain myeloproliferative phenotypes, is called MPN stem cells compartment.

1.2 Subtypes of MPN

There are three subtypes of MPN, polycythemia vera (PV), which mainly characterized by an elevated number of red blood cells; essential thrombocythemia (ET), which refers to an increased number of platelets; and primary myelofibrosis (PMF), which exhibits bone marrow fibrosis[5].

1.2.1 Polycythemia Vera

Classical PV presentation comprised red blood cell mass increase, hematocrit (HCT) increase, and leukocyte count increase, frequently associated with splenomegaly and incidentally myelofibrosis, but may also manifest as isolated erythrocytosis, isolated thrombocytosis or isolated leukocytosis and/or splenomegaly, or any combination of these conditions. The HCT of peripheral blood is not always representative of the true volume of red cells in PV patients. In fact, the plasma volume can also vary, and genuine erythrocytosis is indistinguishable from pseudo-erythrocytosis related to plasma volume

contraction. Diagnosis is usually reached when there is splenomegaly, leukocytosis and thrombocytosis. But then, patient who expressed isolated thrombocytosis without increased HCT, can have an increased plasma volume and increased red cells mass.

The JAK2V617F mutation is present in at least 95 % of PV patients[6–8]. If PV is suspected but no JAK2V617F mutation is found, then mutations in the exon 12 of *JAK2* should be searched for.

Clinically, PV is characterized by a high frequency of thrombotic events concomitant to MPN, usually happening at the early course of disease but also during evolution of the disorder. PV is an unstable disease and may evolve toward myelofibrosis or leukemia. Treatment consists in venesections, anti-proliferative therapy or JAK2-targeting drugs. However, cytoreductive treatments like pipobroman or hydroxyurea not only does not eradicate the disease but have also been suggested as able to increase the progression rate to AML[9]. Interferon alpha (IFN-α) seems to be the safest treatment available to control leukocytosis, thrombocytosis, and extramedullary hematopoiesis, as well as to control symptoms caused by inflammatory cytokines. It is also able to reduce the development of the clonal population[10]. At last, ruxolitinib, a JAK2 inhibitor, has been recognized as able to induce hematological responses but the reduction of the clonal development[11] due to this drug is not clearly established.

Then, the best treatment to induce hematological and molecular responses in

PV is currently IFN-α, despite this drug cannot be given to all patients due to frequent secondary side effects.

1.2.2 Essential Thrombocythemia

ET is mostly identified in people older than 60 years. However, it can also be diagnosed in young people, especially among the female, around 20% of ET being younger than 40 years[12–14]. ET patients present with thrombocytosis, develop persistent and progressive thrombocytosis, and just like PV, arterial and/or venous thrombosis[15]. Splenomegaly are less frequently observed than in PV[16]. Bone marrow biopsy shows proliferative hematopoiesis mainly of the megakaryocyte lineage. In more than 75% of patients, acquired mutations targeting the JAK2 transduction pathway are associated ((JAK2V617F), calreticulin (*CALR*) or myeloproliferative leukemia virus (*MPL*)); all these mutations induce constitutive JAK2-dependant signaling. ET patients do not suffer from a significant reduction of overall survival (OS)[17], when effective treatments and management of the complications are prescribed, then this pathology can lead to an OS of 20 years and above. However, in 10% of cases, ET patients will develop MF during evolution. Bone marrow proliferation, reticular fibers deposits, anemia and age are the risk factors for poorer ET evolution. In addition, AML transformation can also occur and outcome of these secondary AML is very poor.

According to Europe Leukemia Net (ELN) recommendations, the goal of

treatment for patients with PV and ET is to prevent first/recurrent thrombosis and bleeding while effectively controlling and occurring (e.g., hematocrit, splenomegaly, histologic changes, etc.) to minimize the risk of developing MF or AML. Hydroxyurea treatment can decrease the rate of thrombosis from 24% to 3.6% in high-risk patients[18]. Anagrelide is as effective as hydroxyurea in controlling platelet counts, but hydroxyurea is superior to anagrelide in arterial thrombosis, hemorrhage, and progression to myelofibrosis. In contrast, anagrelide was superior to hydroxyurea in preventing venous thrombosis[19]. Low doses of aspirin are effective in reducing microvascular symptoms in patients with ET, but high doses can cause complications such as severe headaches or lupus erythematosus. However, recent studies have reported that twice-daily low-dose aspirin can improve once-daily under dosing while also eliminating adverse complications. Significant effect on improving vascular outcomes in ET patients[20].

1.2.3 Primary Myelofibrosis

Primary myelofibrosis (PMF) is characterized by erythro-megakaryocytic hyperplasia in the bone marrow, neo-angiogenesis, and osteosclerosis. The median age of PMF at diagnosis is over 60 years, 17% of patients only are younger than 50 and 5% younger than 40. There is a male bias just like in PV (and a female bias in ET)[21,22]. In PMF patients, common findings consist in anemia, fever, cachexia, bone pain, pruritus, splenomegaly, neutrophilia, and

thrombocytosis, or in a minority of patients, thrombocytopenia and leukopenia. Immature granulocytes, nucleated red cells, teardrop-shaped red cells in the blood are biological characteristics of this disorder. The bone marrow histology demonstrates magakaryocytosis with reticulin and/or collagen fibrosis grade 2 or 3[23]. After a variable delay, 20% of PMF transform to AML. Patients who didn't transform may also succumb from other complications, including cardiovascular disease and the effects of cytopenias such as bleeding or infection[24].

PMF pathogenic mutations are in JAK2V617F 50-60% of patients, CALR in 20% and about 10% have MPLW515/L mutations[25]. PMF therapy aims to improve survival and treat symptoms by preventing bone marrow failure and transformation to AML, treating common systemic symptoms, and preventing thrombohemorrhagic complications[26]. PMF treatment is given differently according to the risk classifications. Patients at low or intermediate risk but asymptomatic are generally given observation, but interferon, hydroxyurea or anagrelide are usually given in the presence of thrombocytosis; patients at intermediate or high risk have a significantly reduced survival time with varying symptoms, and allogeneic bone marrow transplantation is usually considered for patients under 65 years of age. Patients who are unable to undergo allogeneic bone marrow transplantation are generally treated symptomatically[27].

1.3 Janus kinase 2 (JAK2)

Abnormal cytokine signaling/signal transduction plays a key role in the pathogenesis of MPN. In 1951, a study reported that MPN was caused by some unknown stimulus leading to excessive proliferation of BM cells[28]. Further studies revealed that hematopoietic progenitor cells from MPN patients exhibit hypersensitivity to cytokines such as erythropoietin(EPO), insulin-like growth factor-1 (IGF-1), IL-3 and granulocyte-macrophage colony-stimulating factor (GM-CSF), and were able to form erythroid and megakaryocyte colonies despite reduced or even absent cytokine levels[29]. In 2005, the role of highly active cytokine signaling in MPN pathology was further enhanced with the discovery of JAK2 kinase activating mutations in the majority of MPN patients[6–8,30].

JAK2-STAT pathway is involved in cell division, cell death, tumor formation and immunity, and is a vital process to communicate chemical/cytokine signals from the outside of cells to nucleus[31,32]. Janus kinases (JAKs), signal transducer and activator of transcription proteins (STATs), and receptors are the key factors for these pathways. The STAT family in human are STAT1, STAT2, STAT3, STAT4, STAT5A, STAT5B, and STAT6[33]. The JAK family consist of JAK1, JAK2, JAK3, and tyrosine kinase 2 (TYK2), which can selectively couple with downstream transcription factors STATs to transduce the signals from more than 60 cytokines and growth factors (Figure 1)[34,35].

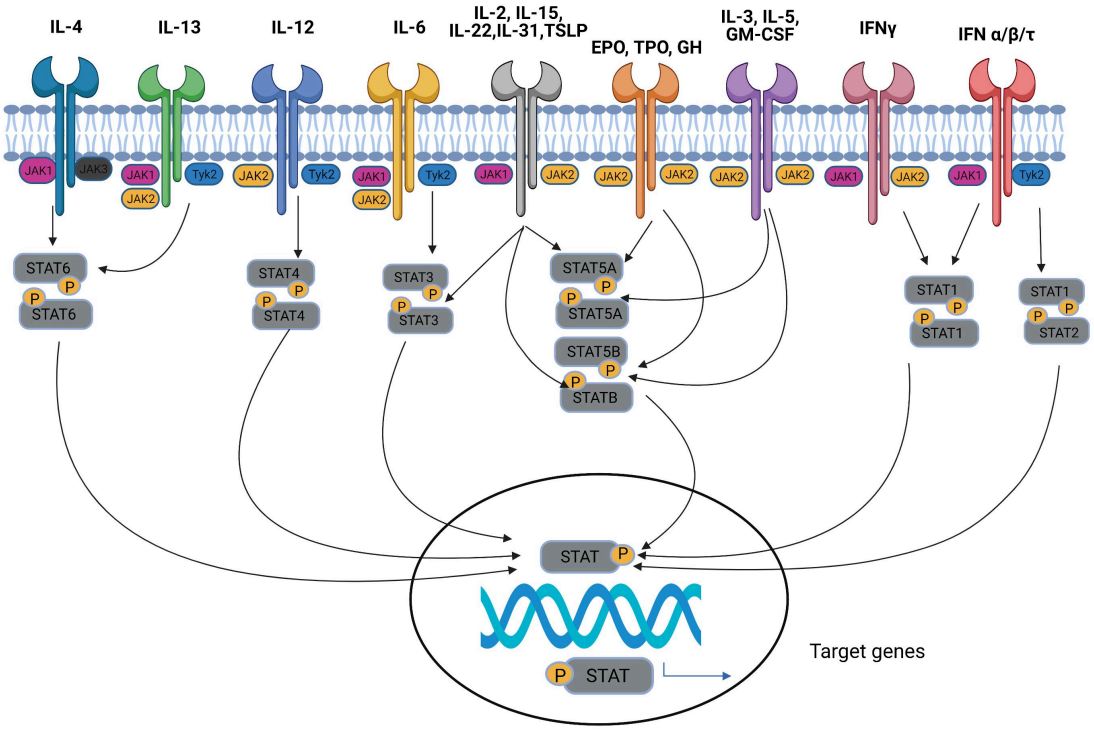

Figure 1: JAK-STAT signaling pathway and cytokines[34].

JAK2 is the mediator of erythropoietin (EPO) and thrombopoietin (TPO) receptor signaling pathways (Figure 1 and Table 1)[36]. Cytokine receptor experience a conformational change upon ligand binding, resulting in the activation of receptor-associated JAK molecules and the phosphorylation of specific tyrosine residues within the intracellular domain of the cognate receptor. These phosphotyrosine residues on the intracellular domain of the receptor with a src homology-2 (SH2) or a phosphotyrosine binding domain can serve as docking sites for downstream signaling proteins. Once these messengers bind to the receptor, they are phosphorylated by JAK kinase leading to its activation. In this way, extracellular signals can be delivered to the activation of several downstream effector processes, including STAT

transcription factors, the Ras/MAPK pathway, and the PI3K/AKT pathway (Figure 2)[36,37].

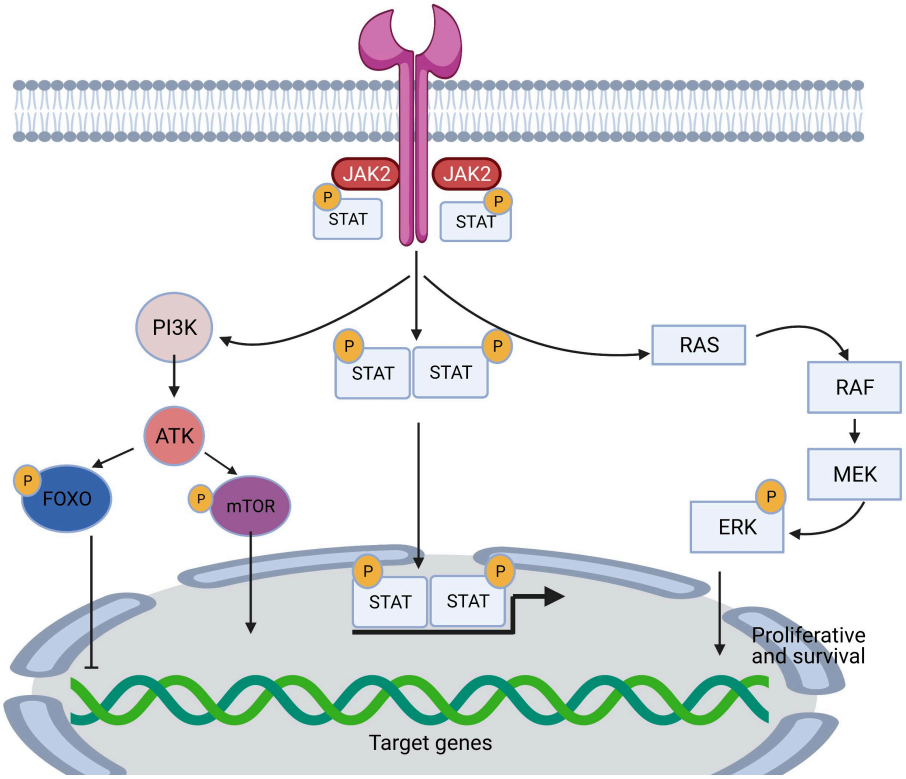

Figure 2: The activation pathway of JAK2[37] .

Table 1: Correlation of cytokines and growth factors with JAK-STAT signaling

Cytokine/hormone[b]	Genes of human receptor subunits	Downstream JAKs	Downstream STATs	Selected functions
Type I, common γ-chain (gene *IL2RG*) cytokines				
IL-2	*IL2RA/B-IL2RG*	JAK1/3	STAT3/5	Regulates T cell, B cell, and NK cell activities
IL-4	*IL4RA-IL2RG*	JAK1/3	STAT6	Induces differentiation of helper T cells; anti-inflammatory action on T cells and monocytes
IL-7	*IL7RA-IL2RG*	JAK1/3	STAT3/5	T cell development and homeostasis
IL-9	*IL9R-IL2RG*	JAK1/3	STAT1/3/5	T cell growth and differentiation
IL-15	*IL15RA-IL2RG*	JAK1/3	STAT3/5	Promotes T cell activation and proliferation
IL-21	*IL21R-IL2RG*	JAK1/3	STAT1/3/5	Down regulates NK cell activation
Type I/common β-chain (gene *CSF2RB*) cytokines				
GM-CSF	*CSF2RA-CSF2RB*	JAK2	STAT3/5	Growth of macrophages and granulocytes; stimulation and differentiation of stem cells; used to reverse neutropenia after chemotherapy
IL-3	*IL3RA/B-CSF2RB*	JAK2	STAT3/5/6	Differentiation of stem cells; proliferation of all cells in the myeloid lineage
IL-5	*IL5R-CSF2RB*	JAK2	STAT3/5/6	Stimulates B cell growth and immunoglobulin secretion
Type I, gp130 (gene *IL6RB* = *IL6ST*) cytokines				
IL-6	*IL6RA/B-IL6RB*	JAK1/2, TYK2	STAT1/3	Prototypic pro-inflammatory cytokine increases acute-phase protein production
IL-11	*IL11RA-IL6RB*	JAK1/2, TYK2	STAT3	Induces megakaryocyte colony formation and maturation
IL-27	*IL27RA-IL6RB*	JAK1/2, TYK2	STAT1/2/3/4/5	Regulation of B and T cell activity
Type I, heterodimeric cytokines				
IL-12 (35 kD/40 kD)	*IL12RB1-IL12RB2*	JAK1, TYK2	STAT4	Induces T_H1 T helper cell formation
IL-23	*IL23R-IL12RB1*	JAK1, TYK2	STAT3/4	Pro-inflammatory cytokine
Type I, hormone-like cytokines				
Erythropoietin	*EPOR-EPOR*	JAK2	STAT5	Control of red blood cell production; used to treat anemia
Thrombopoietin	*TPOR-TPOR*	JAK2	STAT1/3/5	Differentiation of megakaryocytes and platelets
G-CSF	*CSF3R-CSF3R*	JAK2	STAT5	Production of stem cells and granulocytes; used to treat neutropenia
Growth hormone	*GHR-GHR*	JAK2	STAT3/5a	Regulates post-natal body growth
Leptin	*LEPR-LEPR*	JAK2	STAT3/5a	Coordination of energy metabolism; increases satiety
Type II, IFN family cytokines				
IFN-α/β	*IFNAR1-IFNAR2*	JAK1, TYK2	STAT1/2/4	Promotes antiviral activity; stimulates T cell, macrophage, and NK cell activity; used to treat multiple sclerosis
IFN-γ	*IFNGR1-IFNGR2*	JAK1, TYK2	STAT1	Regulates macrophage and NK cell activation; used to treat chronic granulomatous disease and osteopetrosis
IL-28	*IFNLR1-IL10RB*	JAK1, TYK2	STAT1/2/3/4/5	Enhances immunity against infection
IL-29	*IFNLR1-IL10RB*	JAK1, TYK2	STAT1/2/3/4/5	Enhances immunity against infection
Type II, IL-10 family cytokines				
IL-10	*IL10RA-IL10RB*	JAK2, TYK2	STAT3	Anti-inflammatory actions
IL-19	*IL20RA-IL20RB*	JAK1/2, TYK2	STAT3	B-cell activation
IL-20	*IL20RA-IL20RB*	JAK1/2, TYK2	STAT3	Regulates differentiation and proliferation of keratinocytes during inflammation
IL-22	*IL22RA1-IL10RB*	JAK1/2, TYK2	STAT1/3/5	Targets non-hematopoietic cells such as hepatocytes, keratinocytes, lung, and intestinal epithelial cells
IL-24	*IL20RA-IL20RB*	JAK1/2, TYK2	STAT1/3	Targets skin, lung, and reproductive cells
IL-26	*IL10RB-IL20RA*	JAK1/2, TYK2	STAT1/3	Enhances IL-10 secretion from monocytes and IL-8 secretion from macrophages
Growth factors				
EGF	*EGFR-EGFR*	JAK1	STAT1//3/5a	Cell proliferation
PDGF	*PDGFRA/B-PDGFRA/B*	JAK1/2	STAT1/2/3/5/6	Stem cell proliferation

In more than 90% of cases of MPN, the driving mutations for the development of a MPN are caused by somatic mutations targeting *JAK2*, *CALR*, or *MPL* and these mutations occur (mostly) in a mutually exclusive manner[38,39]. The frequencies of each type of mutation differ from one MPN phenotype to another, but the most frequent in the three MPN phenotypes is the JAK2V617F

mutation (Figure 3.)[40].

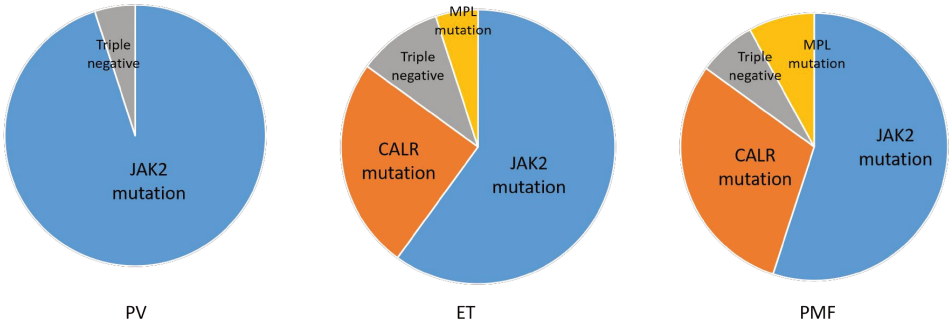

Figure 3: JAK2, CALR, and MPL mutation in MPN subtypes[40]

1.3.1 JAK2V617F

The MPN-associated JAK2 mutations are predominantly the V617F mutation, which occurs in 95% of patients with PV and 50% to 60% of patients with ET and MF respectively[6–8,41–43]. V617 amino acid residue located within the JH2 pseudokinase domain of JAK2 that is a domain able to inhibit the adjacent JH1 kinase domain, maintaining JAK2 in an inactive conformation (Figure 4). The dominant model in the field is that the V617F mutation disrupts the JH1/JH2 interaction through steric interference, thereby nullifying the inhibitory effect of JH2. The crystal structure of the JAK2 JH2 pseudokinase domain has been reported, with or without the V617F substitution, which is consistent with this model[44]. The V617F mutation, although only marginally affecting JH2 structure, is thought to alter at least two properties of the pseudokinase domain, which is important for JH1-JH2 interactions. The first alteration is that V617F stiffens the α-C(C) structure within the JH2 domain, which is consistent with an impaired ability of the pseudokinase domain to keep the kinase domain in an inactive

state[44–46]. V617F also abrogates the low-level bispecific kinase activity of the pseudokinase domain, a function that autophosphorylates residues S523 and Y570[47]. Together, these effects lead to a decrease in JH1 kinase activity inhibition by the JH2 pseudokinase domain inhibition, resulting in the formation of a constitutively active JAK2 molecule. The structure of the JAK2 protein or the fragments containing JH1 and JH2 domains remains elusive, and thus the details of JH1 inhibition by the JH2 domain remain unclear.

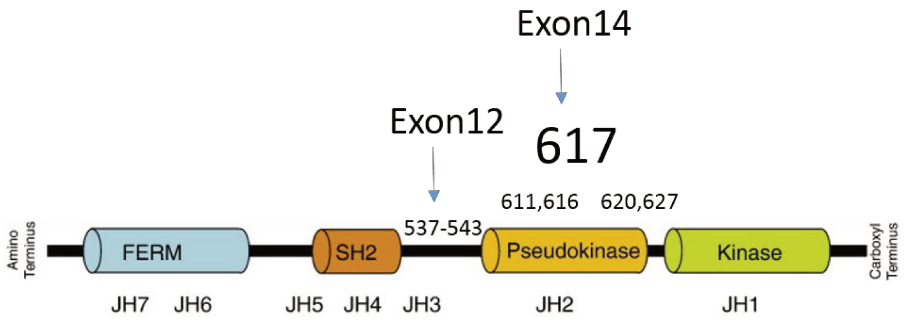

Figure 4: The structure of JAK2 mutation

From amino terminus to carboxyl terminus the structures are FERM domain (JH7 and JH6), SH2 domain (JH5 and JH4), pseudokinase domain (JH2), and kinase domain (JH1). FERM is 4.1 protein- ezrin-raixin-moesin for the identification of new cytokines receptors. SH2 is Src Homology 2 for enhance the interaction of tyrosine kinase with others. Pseudokinase for down-regulation of adjacent kinase structural domains (JH1). JAK2V617F is in JH2 domain.

A recent study showed that JAK2 exists in a dimeric form and remains in an inactive state through intermolecular interactions between the kinase domain of one molecule and the pseudokinase domain of another (Figure 5 left)[48]. The physical separation of the intracellular domain of the cytokine receptor that occurs when the ligand binds to the receptor results in a sliding motion of two JAK2 molecules, allowing the kinase domain to become apposed and to activate each other (Figure 5 center). Mutant JAK2 proteins retain a

dependence on cytokine receptor allosteric signaling and induction of cytokine-independent growth consistent with a JAK2 activation pattern[49–52]. Importantly, the transforming ability of JAK2V617F is eliminated when mutations in key residues on EPOR or disruption of the cytokine-binding region (FERM domain) of JAK2 affect the binding of JAK2 to EPOR. But how the V617F mutations affect JAK2 activation remains to be investigated (Figure 5, right).

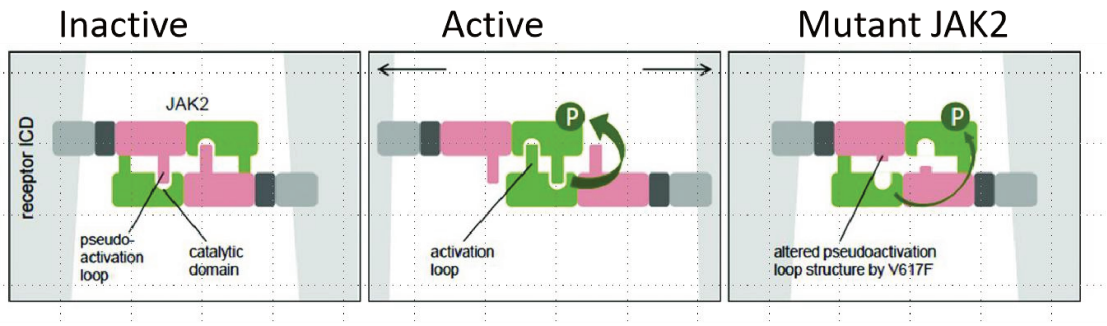

Figure 5: A model of JAK2 activation[53].

Left, JAK2 in an inactive state. Middle, the movement of the JAK2 dimer resulted in 2 JAK2 molecules with the kinase domain at the same site. Right, reduced inhibition of the catalytic activity of the JH1 domain on the JAK2 mutant model.

1.3.2 JAK2V617F in MPN

The fact that the clonal structure, microenvironment and mutational profile of a given patient change over time and lead to different phenotypes supports the view that MPN is not a specific self-limiting disease but can undergo ET to PV transformation or ET to PMF or even all three evolve further into AML[54].

Each somatic mutation in cancer cells, regardless of its structural nature, can be classified as the “driver” mutation and the “passenger” mutation according to its consequences for cancer development[55,56]. There is a causal relationship

between driver mutations and the oncogenesis, which not only induces a growth advantage in the expansion of cancer cells, but also has an active selective role in the microenvironment of oncogenesis[57,58]. The expression of JAK2V617F in the retroviral transduction models, transgenic mice and knock in mice models induces myeloproliferative phenotype but these models harbor some differences. These differences probably correlated with the JAK2V617 expression level suggesting that expression level of the driver mutation is able to modify the phenotype.

JAK2 mutation occurs in all hematopoietic stem cells, including not only the myeloid but also the lymphoid lineage[59]. In the PV patients JAK2V617F was identified in HSC[60] and LT-HSC[61] compartments. Except that, flow cytometric results showed an elevated percentage of progenitor compartments in the PV patients[60]. Anand S. et al. demonstrated that patients harboring JAK2V617F do not have increased the HSC compartment size (in PV and ET) but in PMF patients the HSC and GMP compartments were increased[60]. Except that, the JAK2V617F expressed in myeloid and lymphoid mature lineages of PV and PMF patients showing that the progenitors with JAK2V617F can create physiological hematopoiesis[62–64]. But the JAK2V617F was much expressed in B/NK/myeloid progenitors of PMF compared with PV suggesting the HSC compartment allele burden differs in PV and PMF[62]. However, several studies illustrate that JAK2V617F does not provide a proliferative advantage to the HSC population[64–67]. BM cells from patients with JAK2 mutations have been

xenografted into immunodeficient mice showing that the JAK2 mutated cells did not harbor a self-renewal advantage. Instead, JAK2V617F-positive cells do not have enhanced self-renewal, but rather expand the progenitor cell compartments. These results (and others) suggest that in humans, JAK2V617F mutation *per se* is not sufficient to initiate MPN disease without the involvement of other factors[68,69].

In addition to driver mutations, *de novo* mutations in genes encoding variable regulators of gene expression like epigenetic regulators, mRNA splicing or transcription factors may also serve as disease modifiers of MPN[70]. The most frequently mutated genes associated to the driver mutations are the epigenetic regulators TET methylcytosine dioxygenase 2 (*TET2*) and DNA (cytosine-5)-methyltransferase 3A (*DNMT3A*). Mutations in enhancer of zeste homolog 2 (*EZH2*), additional sex combs (*ASXL1*) and the splicing factor arginine/serine enriched 2 (*SRSF2*) are also associated with poorer prognosis and risk of AML transformation[71].

JAK2V617F mutations not only drive the pathogenesis of the three subtypes of MPN, but the expression level correlates with the phenotype of the disease. It has been shown that low expression levels of mutant JAK2 are mainly found in ET while high levels are frequent in PV[71]. This theory was also confirmed in a knock-in mouse model where the ratio of mutant to wild-type JAK2 correlated with the phenotype of MPN[68,72]. In addition, the order in which the mutations

occur is critical. TET2 mutations altered the transcriptional program of JAK2V617F activation in a cell-intrinsic manner and are more frequently seen as first event in the ET phenotype. Patients who acquire JAK2V617F first are more likely to develop PV[73].

In ET, PV and PMF, leukemic transformation may occurred in 1%, 4% and 20% of patients over 10 years, respectively[74]. Once leukemic transformation occurs in MPN patients, the outcome is dismal and the median survival is less than 6 months[75]. Advanced age (>60 y) and chemotherapy also increase the risk of leukemic transformation; however, the true mechanisms and pathways leading to the transformation of MPN to AML have not been well elucidated.

1.4 MPN MOUSE MODELS

Currently, JAK2 gene mutation testing becomes a key factor in the diagnostic criteria for MPN. Apart from the explorations in clinics on patient sample data and *in vitro* with cell lines that mimic the effects of known alterations on hematopoietic signaling pathways, a variety of experimental animal models have been established revealing the mechanisms and dynamics of JAK2V617F-induced MPN.

1.4.1 Retroviral Transduction Mouse Model

Several aberrant JAK2 signaling mouse models have been proposed to study MPN maintenance and progression including the retroviral transduction

JAK2V617F mouse model, transgenic mice and knock-in mice carrying JAK2V617F[76].

Retroviral transduction mouse model in which plasmid constructs containing JAK2V617F cDNAs were transduced into mouse BM cells in vitro before transplantation into irradiated recipients, have been the first to be described. In these models, retroviral expression of JAK2V617F in bone marrow cells induce a MPN-like phenotype in mice, demonstrating the oncogenic role of JAK2V617F. However, this approach has several limitations such as random insertion of constructs, which ultimately affects the expression level of the cDNA. The expression level of mutant proteins in this manner is usually much higher (~10- to 40-fold) than that of physiological wild-type proteins. Furthermore, mitotic progenitor cells are preferred targets, because LT-HSCs are normally mostly in a quiescent state and therefore less likely to be transduced, which may bias the results. Four studies have used this method to express JAK2V617F in mouse models and their results were similar[77–80]. The transduced JAK2V617F mice mostly exhibited PV-like disease with marked erythrocytosis, leukocytosis and splenomegaly. However, platelet counts were generally normal despite an increased megakaryocytosis.

Bone marrow analysis showed trilineage hyperplasia with increased cell proliferation in the bone marrow and more particularly an erythrocyte expansion. In the second stage of the disease (within 3 to 4 months after

reconstitution), a worsening pancytopenia developed with expanded EMH, and progressive development of reticulofibrosis. Furthermore, the mutant cells transplanted into irradiated secondary recipients also recapitulated the PV phenotype, consistent with the cellular autonomy of the mutant clone. The phenotype of C57Bl/6 mice in response to transduced JAK2V617F differs from that of BALB/c in that C57Bl/6 mice exhibit only a slight leukocytosis without subsequent stages of disease progression[79]. This suggests that strain-specific genetic modifications have an effect on JAK2V617F effects/gene expression levels and thus on the disease phenotype.

1.4.2 Transgenic mice model

The transgenic models were developed by injecting bacterial artificial chromosome (BAC) containing different JAK2V617F cDNA from different origins into the murine oocytes during embryogenesis. The models exhibited stable and genetically JAK2V617F expression with the different promoter control. In 2008, three different transgenic JAK2V617F mouse model were described with three different phenotypes of MPN. Shide et al. created two lines of mice with different expression levels of JAK2V617F under the control of H-2Kb promoter[81]. One mouse line with JAK2V617F mutation integrated on chromosome 18q showed mild polycythemia at 3 months-old in 19% mouse, thrombocytosis expressed in 34% mouse without splenomegaly at 3 months-old. The second mouse line which mutation integrated on

chromosome 7q D1 showed severe leukocytosis at one month-old increasing with time and reaching peak at 5 months[81]. Thrombocytosis and anemia were also identified in the mouse line at one month. Phenotypes of these two strains seem to correlate with JAK2V617F expression since JAK2V617F mRNA was lower in line one than line two (line 1 and 2 is 1.45- and 2.35-fold respectively compared with wild-type). Other mouse-lines were described by Xing et al. The authors used human JAK2V617F cDNA under the control of *Vav* promoter in C57Bl/6XDBA/2 mice[82]. They identified mild PV-like or high PV-like phenotype in different mouse lines. A third work was performed using again the human JAK2V617F cDNA construct containing an inactive reverse orientation JAK2V617F kinase, which was flanked by *lox* sites at both sides, JAK2V617F being expressed by *Cre* recombination under the control of *Vav* and *Mx* promoters. *Vav* promoter can promote *Cre* expression in all of the hematopoietic cells during the lifespan. The mice expressing JAK2V617F under *Vav* promoter displayed ET-like phenotype with normal hemoglobin, mildly increased neutrophils and severe thrombocytosis at 10 weeks. At 5 months the mice still showed ET phenotype with significantly increased platelet counts and mild decrease in hemoglobin consistent with the presence of myelofibrosis. The mice expressing JAK2V617F under *Mx1-Cre* promoter, which can be activated with interferon alpha, interferon beta or synthetic double-stranded RNA like the polyinosinic-polycytidine (pIpC) developed. 10 weeks after pIpC injection, a PV-like phenotype with increased

thrombocytosis, hemoglobin, and neutrophilia. At 5month these mice displayed high hemoglobin and pronounced neutrophilia in 75% mice[72]. Altogether, these studies illustrated that the JAK2V617F expression level correlated with the MPN phenotype. Moreover, despite transgenic mouse models provide a more stable state of JAK2V617F expression in hematopoietic compartments than retroviral transduction model, the insertion of transgene products is still random and could influence the JAK2V617F expression.

1.4.3 Knock-in Mouse Model

With the continuous advancement of biotechnology, the conditional knock-in mouse model has become available. JAK2V617F knock-in mouse under the management of the native promoter most faithfully recapitulates the expression of JAK2V617F in endogenous environment. JAK2V617F, in turn, is specifically induced in the BM compartment using *Cre*-mediated recombination under the control of the specific promoter. In 2010, different knock-in JAK2V617F mouse models have been described. One study showed that the knock-in mice under the control of *Mx-Cre* promoter displayed penetrant, severe PV-like phenotype with increased HCT, RBC, WBC and platelet, a huge splenomegaly and EMH. The disease was transplantable. The authors identified that EPO level was reduced as observed in PV patients. Total BM cells numbers were lowered in these mice maybe due to the fibrosis

development. The histopathology of bone marrow showed hypercellularity with trilineage hyperplasia and mild fibrosis. The spleen histology demonstrated a disappeared of the normal spleen architecture with attenuated white pulp and expanded red pulp, increased megakaryocytes numbers and clusters of immature erythroid precursors and fibrosis. The erythroid cells ($CD71^+$/$Ter\text{-}119^+$) and myeloid cells were also markedly increased in the spleen. These data suggest that the knock-in mouse generated a phenotype very similar to high-risk PV patients. The authors also analyzed the stem cell compartments in these knock-in mice. The LSK ($Lin^-Sca1^+c\text{-}kit^+$) population and myeloid progenitor populations (MPP) were increased in both BM and spleen, further MEP was also greatly elevated meanwhile CMP and GMP were increased at a lower extent in the BM and spleens. Myeloid colony numbers from BM and spleens were also increased when compared to the control mice. Homozygous JAK2V617F mice were also analyzed. The homozygous mice have more severe symptom (higher RBC, WBC, HCT, PLT, spleen size and fibrosis) than heterozygous mice. Confirming in a unique mouse strand that JAK2V617F allele burden influence the phenotype of MPN[83].

Mullally and colleagues also generated a heterozygous JAK2V617F conditional knock-in mice driven by E2A promoter. This mouse model demonstrated a PV-like phenotype with higher HCT, extramedullary erythropoiesis and splenomegaly. The erythroid cells numbers were also increased in the BM and

spleens. The histopathological findings were similar to those of the previous knock-in mouse models with an abnormal spleen structure, significant erythrocytosis and mild megakaryocyte hyperplasia in the red pulp. The erythroid elements in BM were also increased, but megakaryopoiesis was less developed in BM (correlated with normal platelet level in these mice). These mice do not exhibit the $Mac1^{+}Gr1^{+}$ increased previously noticed despite the WBC was increased. Meanwhile the fibrosis was also absent in both BM and spleen whatever the mice age. BM analysis exposed that the MEP population was markedly increased while the CMP and GMP populations were unchanged in JAK2V617F mice. This model showed no difference in the sensitivity to EPO of the erythroid progenitors or Stat5 over-activation, suggesting that the JAK2V617F promotes cell differentiation within the LSK compartment. Moreover, competitive graft of JAK2V617F bone marrow and normal cells showed that the JAK2V617F cells do not have selective proliferative advantage. Cell sorting and transplantation of the different stem cell populations to secondary graft, demonstrate that the long-term hematopoietic stem cells (LT-HSC) only were transplantable and able to regenerate MPN[67].

Li et al. generated a model in 2010 as well, this model characterized by a human JAK2V617F cDNA construct under the regulation of *Mx*-mediated recombination in the C57Bl/6 background. With the injection of pIpC, this model developed ET phenotype with mild increased of RBC, HCT and PLT, no elevated WBC or splenomegaly at 6 weeks. Plasma EPO level and spleen

histological analysis were normal no matter the age of the mice. Twenty-six weeks after induction, 10% of mice progressed to PV (erythroid and megakaryocytic hyperplasia increased in BM and spleen) with splenomegaly and platelet decrease. However, in this model reticular fibrosis was lacking in the BM and spleen of PV-like mice except one mouse, which developed fibrosis, splenomegaly and anemia. The sizes of LSK compartments, and myeloid progenitors (GMP and MEP) were decreased at 26 weeks compared with 6 weeks-old mice. Competitive graft in secondary recipients showed the JAK2V617F contribution to peripheral blood hematopoiesis gradually decreased with time, suggesting that JAK2V617F might impaired the number and/or function of HSC. They also identified that in this model the JAK2V617F did not increased LSK proliferative (cell cycle) but rather induced quiescence or senescence. This mouse model shared many features with human JAK2V617F ET, especially modest thrombocytosis and slightly elevated HCT at the early stage, with a disease progression in about 10% mice to PV-like phenotype. Homozygosity of JAK2V617F using this mouse model was generated. The homozygous mice developed a striking phenotypic switch from ET to PV. The EPO level significantly decreased in homozygous mice, indicating that the erythrocytosis is a cell-intrinsic event. The homozygous mice showed a more penetrant PV phenotype in transplanted mice and reduced survival. In addition to this, homozygous mice have reduced HSC frequency and impaired HSC

function resulting in the inability to maintain the PV phenotype over time in transplanted mice[84].

Table 2: Mutant JAK2V617F MPN models[76]

Author	Mouse	V617F species	JAK2 promoter	Cre-promoter	phenotype	LSK Frequency
Transgenic models						
Shide.et al(2008)	C57Bl/6/ DBA/2	Mouse	H-2Kb-	n/a	Low exp:ET(to PV) High exp: PV(to MF)	n/a
Xing et al.(2008)	C57Bl/6/ DBA/2	Human	Vav-	n/a	Low exp: mild PV-like High exp: PV-like (to MF)	n/a
Tiedt et al.(2008)	C57Bl/6	Human	Minimal human Jak2-	Mx- and Vav-	Vav-: ET-like (to MF) Mx-: PV-like (toMF)	n/a
Retroviral transduction models						
Wernig et al. (2006)	BALB/c and C57Bl/6	Mouse	n/a	n/a	PV-like (to MF)	n/a
Lacout et al. (2006)	C57Bl/6	Mouse	n/a	n/a	PV-like (to MF)	n/a
Zaleskas et al. (2006)	BALB/c and C57Bl/6	Mouse	n/a	n/a	PV-like (to MF)	n/a
Bumm et al. (2006)	BALB/c	Mouse	n/a	n/a	PV-like (to MF)	n/a
Knock-in models						
Akada et al. (2010)	129Sv/C 57Bl/6	Mouse	Jak2-	Mx-	PV-like (to MF)	Increased
Marty et al. (2010)	129Sv/C 57Bl/6	Mouse	Jak2-	n/a	PV-like (to MF)	Increased
Mullally et al. (2010)	129Sv/C 57Bl/6	Mouse	Jak2-	E2a-	PV-like	Unchanged
Li et al. (2010)	129Sv/C 57Bl/6	Human	Jak2-	Mx-	PV-like	Decreased

1.4.4 Hematopoietic Stem Cell Compartment in JAK2V617F mice models.

The hematopoietic compartment contains a hierarchy of cell types responsible for the function and maintenance of the BM and blood system. All peripheral blood cells differentiate from a common pool of hematopoietic stem cells and progenitor cells (HSPC) located within the BM(PMID: 21982230). The HSPC can be divided into three subpopulations: long-term hematopoietic stem cells (LT-HSC), short-term hematopoietic stem cells (ST-HSC), and multipotent progenitor cells (MPP). Common myeloid progenitor cells (CMP) and common lymphoid progenitor cells (CLP) populations are present in the MPP. These progenitor cell populations differentiate into peripheral cell populations within each lineage, such as erythrocytes, platelets and neutrophils within the myeloid lineage, B and T cells within the lymphoid lineage(PMID: 16550195,PMID: 15979407).

During steady-state hematopoiesis, the majority of adult HSCs are quiescent and only rarely divide in order to maintain the appropriate amount of differentiated blood cells and renew the HSC pool (Figure 6). Under certain circumstances, some HSCs will undergo one of several fates: apoptosis, generation of more hematopoietic progenitor cells (HPCs), or migration. These fates are largely controlled by specific local microenvironments (ie, “niches”), in which HSCs and HPCs reside. Although the HSC niche was first conceptualized in the 1970s, the precise location and nature of the HSC niche has been

increasingly proposed in recent years with the development of mouse genetic models and in vivo microscopy. Self-renewal is regulated by the interaction of intrinsic factors such as transcription factors, cell cycle states and metabolic pathways, as well as by external local and systemic environment. The localized environment in the bone marrow is known as the stem cell niche[85,86]. Signals from the niche are believed to be vital for the regulation of HSC self-renewal as well as for differentiation decisions[85,87–89].

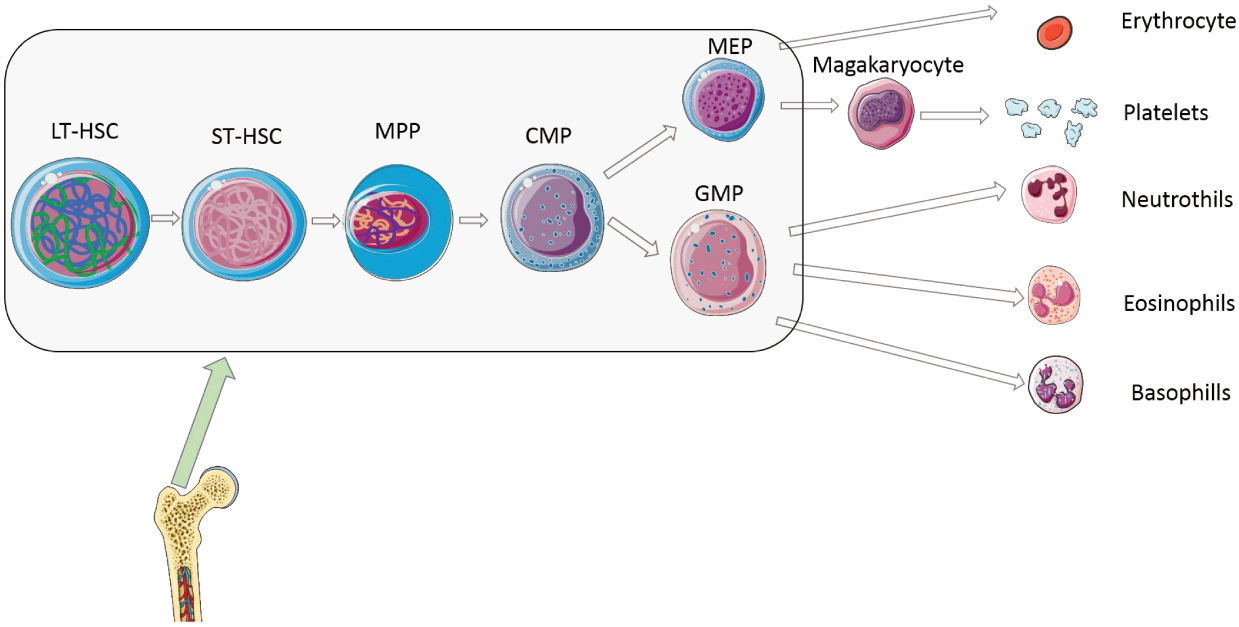

Figure 6: Development of different blood cells.

LT-HSC: long-term hematopoietic stem cells; ST-HSC: short-term hematopoietic stem cells; MPP: myeloid progenitor populations; CMP: common myeloid progenitor; GMP: granulocyte-macrophage progenitors; MEP: megakaryocyte-erythroid progenitors.

In recent years, there have been many studies devoted to the cellular components of the mouse bone marrow niche and hematopoietic progenitor cells that interact directly or indirectly with HSCs and may contribute to the

regulation of HSC self-renewal and differentiation[86,90–96]. Human studies demonstrated that the JAK2V617F appeared not only in mature cells but also in stem cells and progenitor compartments[8,65,97–100]. But the JAK2V617F mutation effects on HSC is still a matter of debate. The conditional knock-in mouse models identified a JAK2V617F effect on HSC cells but this effect was lacking in either transgenic mouse or retroviral transduction mouse models. Studies in primary human jak2V617F cells in vitro showed also different results, JAK2V617F increased the HSC populations in some studies[83,101] but others[67,84] did not found any expansion of HSC compartments in their studies. The xenograft study with transplantation of MPN patient's $CD34^+$ cells into mouse did not demonstrate any advantage of JAK2V617F cells over normal cells[66,102].

As described before, the JAK2V617F KI mouse under the control of V*av* promoter restricts the mutation expression in hematopoietic and endothelial cells and showed PV phenotype with secondary myelofibrosis. In these mice, LSK population was increased 6-fold compared to normal mice in BM and 9-fold increase in spleen. Competitive graft using 30% JAK2V617F mixed with 70% WT found the JAK2V617F increased to more than 80% in 17 weeks and 100% in 35 weeks, demonstrating here a huge JAK2V617F-induced advantage in the HSC compartment[101]. Similar results were also observed in the Salma's study. Using *Vav-Cre* inducible knock-in system (the mouse model we use in our experiments). These mice showed PV-like phenotype while the number of Lin^-, LSK and SLAM in the BM and spleen increased progressively with age

suggesting a JAK2V617F-modest proliferative advantage in the HSC compartment. In addition, these authors also used the 30% JAK2V617F and 70% WT for competitive transplantation and showed that Lin^-, LSK and SLAM in the BM and spleen cells of the mice increased to about 100%. However, some results were different from the previous studies in these competitive transplantation since JAK2V617F KI mice developed a MPN similar to human PV with a short disease latency and lower survival. In contrast to the above studies, these investigators found that CMP and GMP compartments were unchanged in JAK2V617F mice when LSK and MEP compartments slightly increased. In addition, hypersensitivity to EPO was identified in unfractionated BM cells and MEP population with MEP expressing higher phospho-Stat5 signaling under stimulation with EPO and IL-3. Lastly, these authors sorted the LSK, MEP and GMP compartments and grafted cellular compartments in irradiated animals. Only mice grafted with LSK cells developed MPN similar to mice receiving the total BM cells. In order to better understand the JAK2V617F effects in LSK compartments they also tested the number of LT-, ST-HSC and MPP, but they did not find any difference between mutated and WT mice. At last, phospho-STAT5 levels were not different in LSK populations of JAK2V617F BM cells even activated with EPO and IL-3 when compared to normal cells. These results suggest that the JAK2V617F mutation has a quite modest effect on the LSK compartment. To further demonstrate a JAK2V617F-induced advantage in LSK population, the authors performed competitive transplantations with

different ratios of mutant and WT cells. All recipients showed the same degree of splenomegaly and erythroid cells in spleen. BM chimerism ratio slightly increased in blood myeloid population but did not show variations in the different ratio groups. All these results suggest that the LT-HSC has a critical role in MPN but HSC have only a subtle competitive advantage during stress hematopoiesis.

However, other studies demonstrated contradictory results (for instance Li et al) with limited self-renewal ability and number of mutant HSC although JAK2V617F increases the division and expansion of early downstream progenitor cells, explaining why the total LSK numbers were relatively lower than the others populations. In this study, JAK2V617F mutation increased DNA damage and senescence induction and decreased apoptosis and cell cycle. With time, the number of stem cell and progenitor populations (except MEP and CMP) decreased and the competitive graft showed a decreased chimerism of JAK2V617F cells. This study suggested that JAK2V617F reduces the function and number of HSC and simultaneously induce their subsequent more mature populations toward differentiation and proliferation. This leads to the hypothesis that additional genetic lesions are required to truly increase the clonal expansion.

Overall, the function of JAK2V617F in MPN development and progression is still a matter of debate. Animal models demonstrating different results.

1.5 Stress Erythropoiesis

Infection and inflammation due to tissue damage are common, but the decreased ability to produce erythrocytes from steady-state is compensated for in healthy individuals, so that potentially fatal anemia is not observed. One study showed increased erythropoiesis in the spleen of mice in a mouse model of infection and aseptic inflammation[103–106]. Once the mice infected with *Salmonella* they develop anemia, but the anemia can be compensated with spleen erythropoiesis which increased EPO production by the liver and kidney also[107–109]. The same as the infection models, sterile inflammation also increased splenic erythropoiesis. The mice injected with *Brucella abortus* develop anemia in 2-week period which was associated with the bone marrow erythropoiesis decreased. But at day 7 the mice spleen erythropoiesis increased and the mice recover by 4 weeks[104,105,110]. All of these conditions are harmful for the steady state erythropoiesis but stress erythropoiesis can compensate for the infected and inflammation to maintain homeostasis.

Erythropoiesis is classically driven by EPO, which binds to EPOR to trigger the binding of phosphorylated JAK2 to STAT5, then the JAK2-STAT5 complex translocates into the nucleus and induces target gene expression[111]

Erythropoiesis is a multilevel process that begins with the differentiation of self-renewing bone marrow stem cells into multipotent progenitors[112], followed by the differentiation of myeloid progenitors into MEPs and then into a series

of early and late erythroid cells that eventually become mature erythroid cells (In Figure 7). In the steady state, erythropoiesis occurs at a constant rate, with senescent cells being replaced by newly generated erythrocytes. Normally, the red bone marrow is the major source of erythropoiesis, but under conditions of acute blood loss or demands for increased oxygenation (like infections, inflammatory reactions), the existing cellular hypoxia controls EPO expression through hypoxia inducible factor alpha 2 (HIF2α). Upregulated EPO expression elicits an increased erythropoietic response, referred to as stress erythropoiesis [113]. It is faster than the steady-state erythropoiesis and aims to ensure a homeostatic state in the body until the steady-state erythrocytes are normalized[113–116].

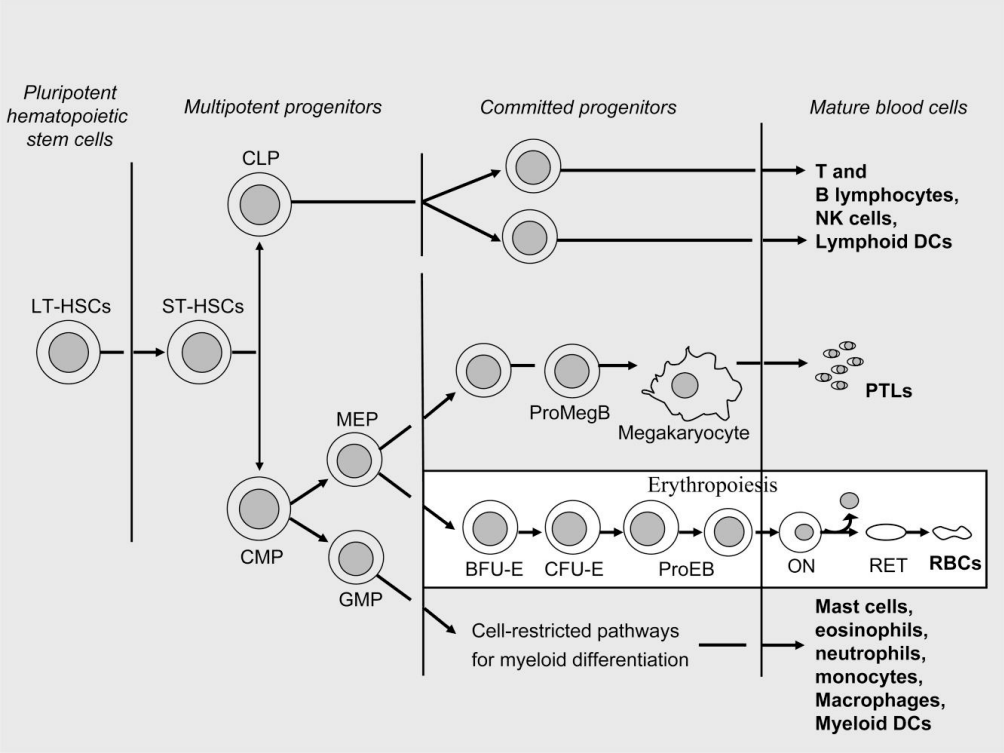

Figure 7: Normal blood cell production schema and red blood cell development

pathway[112]

The presence of signals and progenitor cells that would not be present in steady-state erythropoiesis in the bone marrow is characteristic of stress erythropoiesis. Some of these signals are not associated with erythropoiesis but are more common in stem cell-mediated tissues (like the bone marrow and fetal liver)[117], and these include mainly bone morphogenetic protein 4 (BMP4), growth/differentiation factor 15 (GDF15), and hedgehog (HH) whose functions are associated with SCF and EPO[115,116,118,119]. These signals along with SCF rapidly promote massive proliferation of early stress erythroid progenitors, but the signals also require elevated serum EPO levels to stimulate the production of stress BFU-E and thus differentiation[114,118,119] Steady-state erythroid progenitors developed from a defined hierarchy of myeloid differentiation which results in the development of MEP[120,121]. Spleen is also an important organ in mice for erythropoiesis especially under the stress condition[122]. Stress erythroid progenitors in the spleen are derive from ST-HSC, which migrate to spleen. Once in the spleen these cells become committed to the stress erythroid fate and undergo an initial expansion stage where cells maintain their stem cell characteristics but are unable to differentiate[123].

Erythrocyte stress is divided into the four main stages (Figure 8)[124]: the first stage is the specification of the fate of stress erythrocytes[114,119]. ST-HSC in BM migrate to spleen where the HH ligands act with BMP4 to specify the stress

erythroid fate. The next stage is the expansion of a transient amplifying population of immature stress progenitors. In this period the stress erythroid progenitors (SEP) amplification with a fast rate[124]. Some signals promote the amplification of SEP, like GDF15 which is one of the TGFβ family members, potentiates the hypoxia response by repressing the E3 ubiquitin ligase VHL, which promotes the degradation of the hypoxia inducible transcription factor Hif1α[125]. The overall process of terminal differentiation of SEP is similar to that of the steady state, but with certain differences. During the differentiation stage of steady-state progenitors, Kit expression is downregulated and CD71 and Ter119 expression is increased, whereas SEP maintain Kit expression even at late stages of differentiation[126].

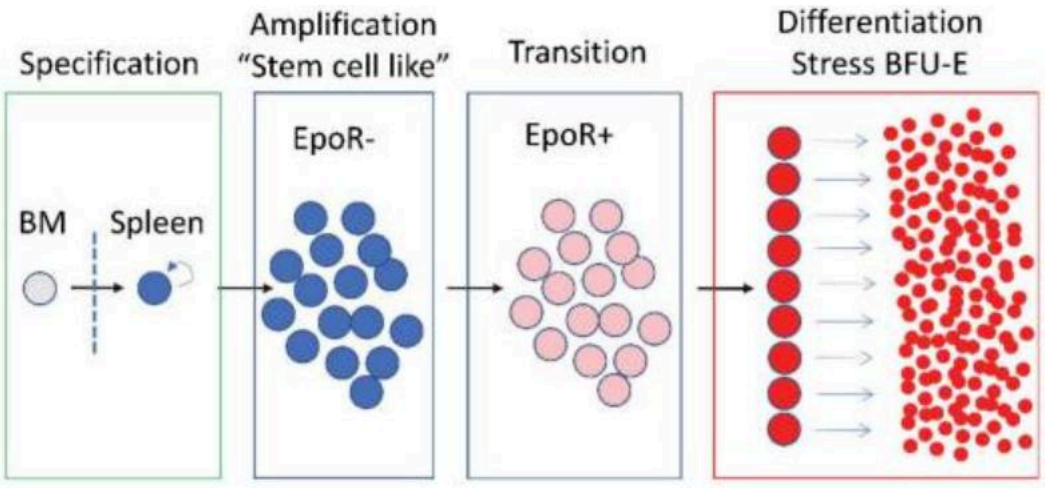

Figure 8: Schematic diagram of stress erythropoiesis[124]

Periods of infection and inflammation often cause a stress-induced hematopoietic response marked by an increase in myeloid lineage of bone marrow HSC and HSPC and mobilization of bone marrow neutrophils and HSPC

to peripheral tissues. In the same way, hematopoiesis switches to erythropoiesis in stressful conditions such as anemia and hemorrhage. The hematopoietic system is able to cope with a variety of stressful situations and its remarkable adaptability is essential for survival. Myeloid cells are mostly acquired and need to be generated from bone marrow HSPC when they are depleted during the fight against infection. In response to infection, committed bone marrow progenitor cells are induced to proliferate and mature as a rapid and immediate response[127].

1.5.1 Hematopoietic stem cells/progenitors respond for the stress.

Immune cells are the first one to respond for the bacterial infection; but in the same time HSPC also respond.

Unlike steady-state erythroid progenitors, stress erythroid progenitors are predominantly converted from ST-HSC, whereas hematopoietic stem cells become erythroid-like after restricted migration to the spleen[114].

In recent years studies have found that uncommitted HSPCs are also actively involved in stress-induced hematopoiesis. HSPC may contribute to the reaction to infection through several mechanisms: (1) Responding to inflammatory factors produced during infection. There is evidence that HPSC and even LT-HSC can respond directly to inflammatory factors, including TPO, SCF, Flt3 ligand, interferons, IL-3, IL-6, TNFα, TGFβ, G-CSF and M-CSF (2). Although it is not clear

how HPSC senses changes in peripheral neutrophils, a "neutrostat" system has been found to sense changes in neutrophils during infection, which triggers differentiation of HPSC in the bone marrow to compensate for the loss of cells; (3) Responding to exogenous signals in the stem cell niche. Stem cell niche cells such as osteoblasts, mesenchymal stem cells, perivascular stromal cells and endothelial cells are affected in many ways during the infection process, thus affecting the proliferation and differentiation of HPSC; (4) Responding to pathogen-associated molecular patterns (PAMPs) and danger-associated molecular patterns (DAMPs) via to Toll-like receptors (TLRs); (5) In theory, HSPC can be affected by pathogens and thus influence of their activity. But until now there is no study support this hypothetical.

Early studies have found that acute anemia leads to tissue hypoxia, which leads to the induction of EPO expression. Increased levels of EPO in serum mobilize cells in the bone marrow, which migrate to the spleen, where expansion and differentiation occur[128,129]. This is also a good explanation for EMH. Stress erythropoiesis takes place mainly during the development in fetal liver and in the adult liver and spleen[130,131]. The unique microenvironment of the spleen supports an extensive erythropoiesis[132]. Steady-state erythroid progenitors develop from a defined hierarchy of myeloid differentiation which leads to the development of erythroid-committed progenitors. But the progenitors of stress erythropoiesis differ from the steady-state progenitors[120,121]. There is an important distinction between the steady-state erythropoiesis and stress

erythropoiesis since BFU-E respond to BMP4 in the stress erythropoiesis but does not express BMP4 receptor in the steady-state hematopoiesis. And the stress erythropoiesis is not continuous like steady-state erythropoiesis. It appears in expanded, transitional and differentiated coupled waves[114,119]. After this, these new cells are required to transfer to the spleen and restart the cycle. Such properties characterize a stress response pathway in which stress elicits a short-term biochemical or cellular response designed to mitigate that stress until homeostatic mechanisms are able to restore and maintain homeostasis.

1.5.2 Phenylhydrazine and stress

1.5.2.1 Phenylhydrazine structure and function

Phenylhydrazine is a chemical compound and first reported by Hermann Emil Fischer in 1875. The chemical structure of PHZ is C6H8N2 and molecular weight is 108 (In Figure 9). PHZ was initially used to treat fever, but was discontinued because of its toxicity to red blood cells until 1933 when Falconer reported that PHZ could be used to treat patients with PV. PHZ was used orally for the treatment of various blood disorders at the beginning of the last century, and the therapeutic effect was evident in some patients[133,134].

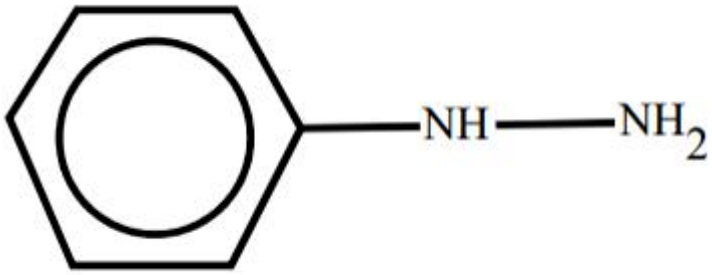

Figure 9: Chemical structure of PHZ

1.5.2.2 Toxicity of Phenylhydrazine

The lethal dose (LD50) of PHZ is 80-188 mg/kg body weight, aspiration and skin contact are the main routes of infection[135]. PHZ can cause red cells rupture induce acute anemia and consequently effect to other organs like spleen and liver[136,137]. Exposed to PHZ in vitro can cause gene mutation and also has the genotoxic in vivo. There is a study showed that the PHZ was carcinogenic and induce cancer in hematopoietic system in the mice[138,139].

1.5.2.3 Phenylhydrazine for the stress Erythropoiesis

Anemic stress in mice compensated for low bone marrow erythroid output by increasing splenic erythropoiesis[115,128,140–142]. Splenomegaly, elevated hemoglobin concentration, and increased erythroblasts frequency in the bone marrow are characteristic of anemia mice. The early study on the reflection of anemia was that PHZ injection caused hemolytic anemia. PHZ was first tested on rats with the dose 20 mg/kg body weight at 1942, inducing the blood cells lowered to 50% than normal and hemoglobin was also decreased around 60%

in day 4. This study also showed that the PHZ led to BFU-E and multilineage CFU-mix decreased in the bone marrow while the BFU-E, CFU-E and CFU-mix increased in the spleen[128,140,143,144].The progenitors were also tested in the peripheral blood. This suggesting that the erythropoietic stimulation post hemolytic anemia mobilized progenitors to migrate from bone marrow to spleen.

A mouse model in which flexed-tail (f) mutant showed endogenous splenic stress erythroid progenitors was also used to study stress erythropoiesis[113]. The f/f mice developed fetal neonatal anemia that disappeared within about 2 weeks after birth. Afterwards, the mice had stable erythropoiesis and normal amount of BFU-E and CFU-E in the bone marrow[145–148].The f/f mice showed a delayed response with more pronounced anemia treated with PHZ[149,150]. This suggests that the f locus modulates the erythrocyte response to anemia, but do not modulates the homestatic erythropoiesis. The phenotype of f/f mice revealed defective expansion of endogenous erythroid progenitor cells in the spleen as a cause of the inability to respond to anemic stress[147]. These data suggest that stress erythropoiesis generates endogenous splenic stress erythroid progenitors that differ from steady-state erythroid progenitors[113].

With the development of biotechnology more and more other species were used to test the PHZ function for the hematopoietic system. Recently, the dose of 90 mg/kg was widely used for the in *vivo* test. It showed that the 90 mg/kg

PHZ induced normal erythrocyte and packed cell volume were decreased 45-53% while hemoglobin increased 60% on day 3; reticulosis was declined 75% and erythrocytes with Howell-Jolly bodies exhibited on day 7[151].

Hemolytic anemia is caused by the ingestion of erythrocytes by macrophages in the spleen, and the translocation of phosphatidylserine from the inner to the outer plasma membrane is a signal of macrophage phagocytosis. Reactive oxygen species (ROS) was identified but surprisingly, lipid peroxidation or phosphatidylserine externalization were not found in the humans and rats red cells exposed to PHZ. ROS was produced by oxidative and denatured hemoglobin and cytoskeleton membrane. Thus, the hemolytic damage induced by PHZ is more a consequence of oxidative changes of erythrocytes than changes in the membrane lipids content.

PHZ induced hemolytic anemia (by the oxidative stress on erythrocytes) but also other effects on other cell lineages that have never fully studied.

1.6 Tumor Protein p53

The P53 protein encoded by *TP53*, was first identified as an oncogene in 1979, but was recognized as a tumor suppressor gene in 1989[152]. The tumor suppressor P53 protein, considered as the "guardian of the genome", maintains genomic stability under cellular stress and is engaged in a variety of processes in development, differentiation, aging and disease[153].

1.6.1 *TP53* gene structure

The human *TP53* gene is localized to 17p13 while the murine *Tp53* is localized to chromosome 11. A non-functional pseudogene was also found on chromosome 14 in mice. *TP53* has an unusually similar gene structure, about 20 Kb long, both consisting of 11 exons and 10 introns, the first exon is non-coding and exons 2, 4, 5, 7, 8, respectively, encode five evolutionarily highly conserved structural domains, the five highly conserved regions of the *TP53* gene, namely the 13th-19th, 117-142, 171-19 2, 236-258, 270-286 coding regions. The *TP53* gene is transcribed into a 2.5 Kb mRNA encoding a 393 amino acid protein with a molecular weight of 43.7 KD. The P53 transcription factor is composed of four structural domains: transactivation domain, DNA binding domain, tetramerization domain and regulatory domain. The majority of *TP53* mutations identified localize to the DNA binding domain covering exons 5-8. The expression of the P53 is controlled at least at both transcriptional and post-transcriptional levels.

In continuously growing cells, mRNA levels did not change significantly with the cell cycle, but decreased after induction of differentiation, partly due to post-transcriptional regulation. The transcription of *TP53* gene is controlled by two promoters, P1 and P2. The P1 is located upstream of the first exon and P2 is located in the first intron, which contains an NF1 protein binding site and a transcription factor AP1-related protein binding site. For normal *TP53* gene

transcription, not only the balance of the two promoters is required, but also the intron of the *TP53* gene plays a role, such as positive regulation in the intron, and its regulation is tissue-specific[154].

1.6.2 The functions of TP53

The functions of *TP53* are mainly related to cell cycle arrest, apoptosis, DNA repair, senescence and, autophagy. (Figure 10).

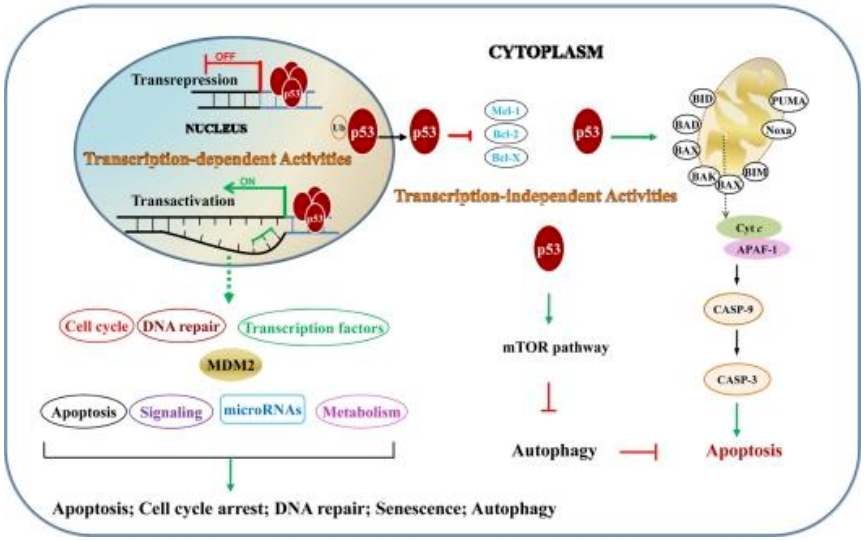

Figure 10: The function of TP53[154]

The normal cells always undergo cell proliferation and apoptosis at a steady rate and process to maintain a stable state. P53 plays a critical role in this process, while defective P53 may prevent cells from controlling proliferation, leading to abnormal cell growth and cancer development. In physiological conditions, P53 protein expression is minimal while DNA damage or any stress signal can increase the P53 expression. The increased expression of P53 allows the cell to repair DNA damages. First, the growth arrest triggered by P53 can

stop the cell cycle progression to terminate the impaired DNA replication. When the cell cycle is arrested, the transcription of protein involved in DNA repair are activated by P53 to repair the impaired DNA. If the DNA is severely damaged, P53 can activate the apoptosis pathway to eliminate DNA-damaged cells.

TP53 mutations are relatively common in many malignancies due to the multiple activities of P53. In fact, more than 50% of all malignancies harbor mutations in the *P53* gene, and other tumors without mutations also express diminished P53 activity[155,156]. Therefore, *P53* mutated or null mice are prone to the onset of tumor development[157–160], especially lymphomas[157–160].

1.6.3 TP53 and MDM2

The level of P53 expression needs to be tightly regulated. High level of P53 leads cells to enter senescence and rapidly activates the apoptosis pathway. Murine double minute 2 homolog (MDM2) is the primary negative regulator of P53 expression, as it can induce the P53 degradation by ubiquitin system.

The expression of MDM2 is activated by P53, and P53 degradation is also triggered by the MDM2. However, once P53 is phosphorylated at Ser15, Ser20 or Thr18 the MDM2/TP53 complex may be disrupted eventually leading to elevated P53 level (Figure 11).

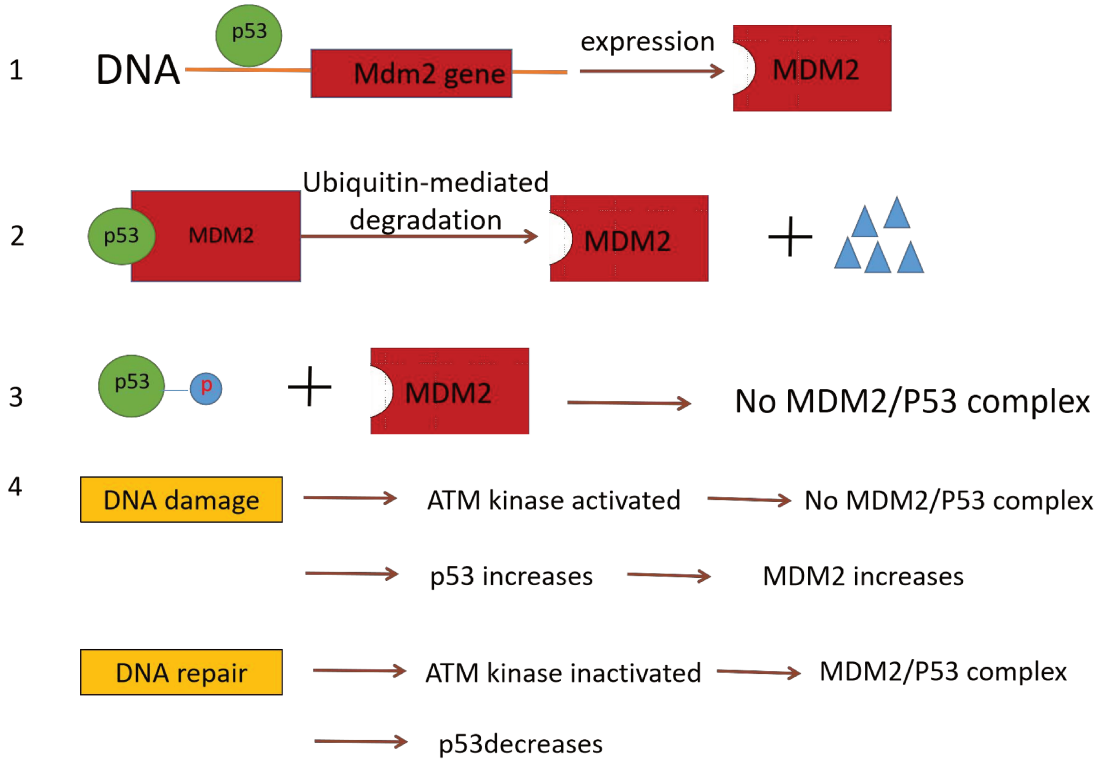

Figure 11: The TP53 and MDM2 interaction under different conditions.

TP53 is expressed in all tissues, the half-life of protein is roughly 20 min due to MDM2 induced ubiquitination and proteasomal degradation in normal conditions[161] (Figure 11). MDM2 overexpression in transformed hematopoietic cells is associated with drug resistance and poor prognosis. MDM2 accumulates in BCR/ABL-expressing cells[162] and its down modulation by an antisense oligonucleotide promotes growth factor deprivation-induced apoptosis[163].

Cell lines and primary cells from MPN patients revealed that JAK2V617F strongly inhibited p53 stabilization after DNA damage induction through

phosphatidylinositol 3-kinase (PI3K)/AKT/mTOR pathway-dependent increase in MDM2 translation(PMID: 21785463).

The inhibitor of MDM2/P53 interaction, nutlin-3a, inhibits cytokine-independent growth of JAK2V617F-mediated cell lines suggesting an important role of the MDM2/P53 axis in JAK2V617F-mediated proliferation.

1.6.4 TP53 in MPN

The treatment of MPN patients has improved considerably with the continuous advances in medical biological research, but a proportion of MPN patients still transform into secondary AML. The conversion rate of secondary leukemia in patients with ET, PV, and PMF is 1%, 4%, and 20%, respectively[74]. Post-MPN patients always have a dismal outcomes with a less 6 months median survival[75]. Gene studies showed that the mutated *NPM1*, *DNMT3A* and *FLT3* are expressed in de novo AML[164] but *TET2*, *SRSF2*, *TP53* and *IDH1/2* are common in post-MPN AML than in novo AML[164–167]. This suggests that the *TP53* is one of the major genes which contribute post-MPN AML transformation. Rampal et al. demonstrates that in JAK2V617F post-MPN AML, the most common co-occurring mutations were *TP53* (44%), *ASXL1* (44%), and *IDH2* (44%). However, there did not such *TP53* mutation in JAK2-wild-type post-MPN AML. The authors also generated a mouse model of loss of *TP53* combination with JAK2V617F retroviral overexpression that eventually developed post-MPN AML. This leukemia was transplantable and enriched with hematopoietic stem and

progenitor cell compartments, particularly MEPs[168]. Another study reported homozygous mutation of *TP53* in HEL and SET-2 cells that harbor JAK2V617F mutation, but R248W (which is the common mutation of p53) was found in SET-2 cells only. Moreover, the high level of p53 protein was also identified in both cells[169] This suggests that the JAK2V617F and *TP*53 mutations coexist in leukemia cells, and JAK2V617F could be the driver gene for the post-MPN AML when the *TP53* mutated.

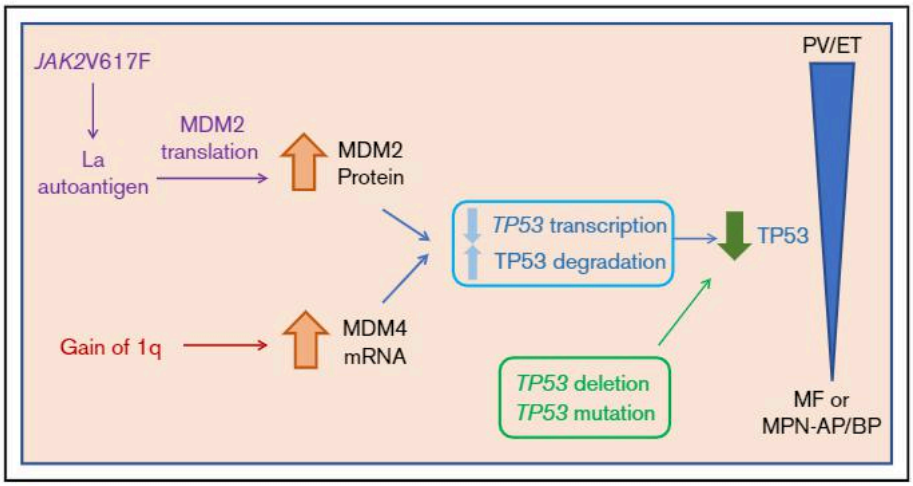

Figure 12: Suggested role of TP53 deficiency in MPN evolution[170] .

P53 inactivating mutations are found in 15% of chronic hematologic disease, including chronic myeloid leukemia[171–173], PV[174] and PMF[175,176] and over half of transformed-MPN[177]. However, chronic-phase MPN patients can also harbor *TP53* mutations persisting at low level for several years without an immediate risk of progression tempering the *TP53* mutated associated risk[178].

In mouse models, *TP53* mutations and inactivation also induce contrasting results. *TP53* knockout mice have a significant rate of cancer, especially lymphatic system tumors. The deletion of *TP53* can accelerate the MDS mouse carrying oncogenic *NRAS* mutations to AML with increased size of immature cell population especially the MEP progenitors[180].

Despite evidence of p53-related pathogenesis in hematologic malignancies, the functional contribution of p53 deficiency to MPN leukemic transformation remains elusive. There is a study in which the JAK2V617F mice express PV-like disease but with the cooperation with *TP53* homozygous deletion the disease would progressed to AML[181]. In this study the authors transducedd the *JAK2V617F* mutant with retroviral transduction into hematopoietic progenitor cells from P53 knockout or wild-type mice to get the *JAK2V617F*/P53$^{+/+}$ (PV-like) and *JAK2V617F*/P53$^{-/-}$(post-PV AML) mice model. The *JAK2V617F*/P53$^{-/-}$ mice have severe anemia, splenomegaly, and expansion of erythroid progenitors. Comparing with *JAK2V617F*/P53$^{+/+}$ mice, the LSK, MEP and CD71^{+} cells from the *JAK2V617F*/P53$^{-/-}$ mice have leukemia-initiating capacity while Mac-1^{+} cells did not recapitulate disease. This suggests that P53 loss is sufficient to induce AML transformation in JAK2V617F MPN

MATERIALS AND METHODS

2.1 Generation of the JAK2V617F KI P53$^{-/-}$ mice

Mice were bred and maintained in pathogen-free conditions in our Institute Animal facilities Unit for Laboratory Animal Medicine at the Université de Paris, Centre Hayem, Saint Louis hospital. All procedures performed were approved by the local Committee on the Use and Care of Animals and by the Institutional Animal Care and Use Committee.

C57BL/6 Ly5.2 and Ly5.1 mice obtained from Janvier, (Le Genest, France). B6, Cg-Commd10$^{Tg(Vav1\text{-}iCre)A2KIO/J}$ mice abbreviated as *Vav-Cre* obtained from Jackson Laboratory (USA)[182–184], TP53 mutation mice were gift from Dr. KAWAKITA(Figure 13)[158].

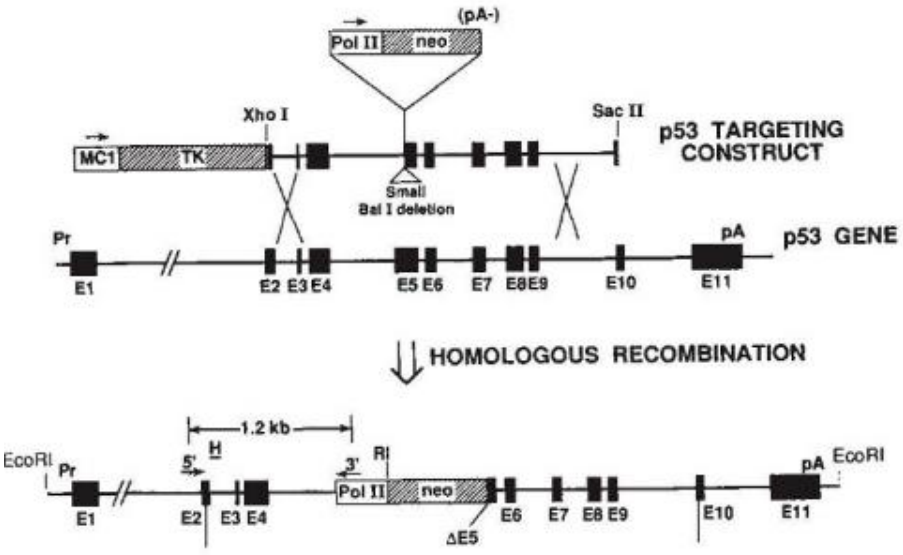

Figure 13: The gene structure of TP53 mutation mice.

Above is the targeting construct disrupting *TP53*. Crossed the endogenous *TP53* with targeting construct to induce the homologous recombination *TP53* mouse[158] .

The conditional flexed JAK2 (JAK2FLEX/1 or L2/1) KI mice were friendly given by Dr. Villeval (Figure 14)[101]. To express the mutation, KI mice were crossed with *Vav-Cre* TG mice. These heterozygous recombined JAK2V617F/WT mice (JAK2VF/1) were termed as JAK2wild-type (WT) and mutated JAK2 allele termed as JAK2V617F KI mice. The JAK2V617F KI mice at the first month old exhibit no hair below the head. The $p53^{-/-}$ mice were crossed with JAK2WT to get the JAK2WT/$p53^{+/-}$ mice crossed them back with $p53^{-/-}$ mice to get JAK2WT/$p53^{-/-}$ mice, at the same time crossed the $p53^{-/-}$ mice with *Vav-Cre* mice to get the Vav-Cre/$p53^{+/-}$ mice. Then crossed the JAK2WT/$p53^{-/-}$ mice with Vav-Cre/$p53^{+/-}$ to get the JAK2V617F/$p53^{-/-}$ mice (Figure 15). The genotyping of JAK2V617F, JAK2WT, *Vav-Cre* and $p53^{-/-}$ were tested by PCR.

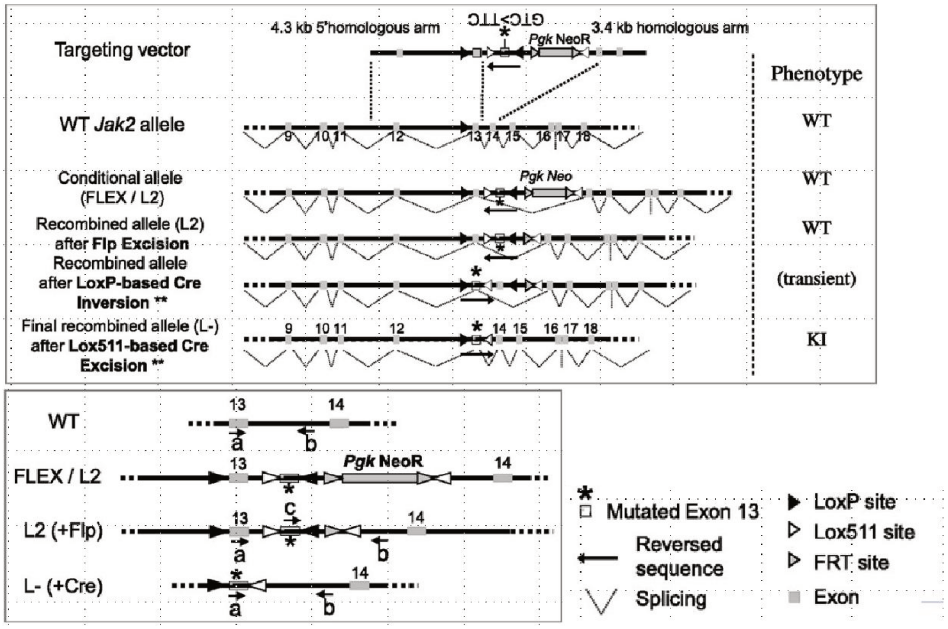

Figure 14: Sketch of targeting vector and modified allele for generating Jak2V617F KI mouse model. [101]

The tails were obtained from the 3-4 week-old mice. The DNA was extracted

with the KAPA Express Extract (KK7100) (Sigma Aldrich Chimie, France) kit from mice tails. REDTaq®ReadyMix™PCR Reaction Mix (ThermoFisher Scientific,) was used to do the PCRs to test the genotype of mice.

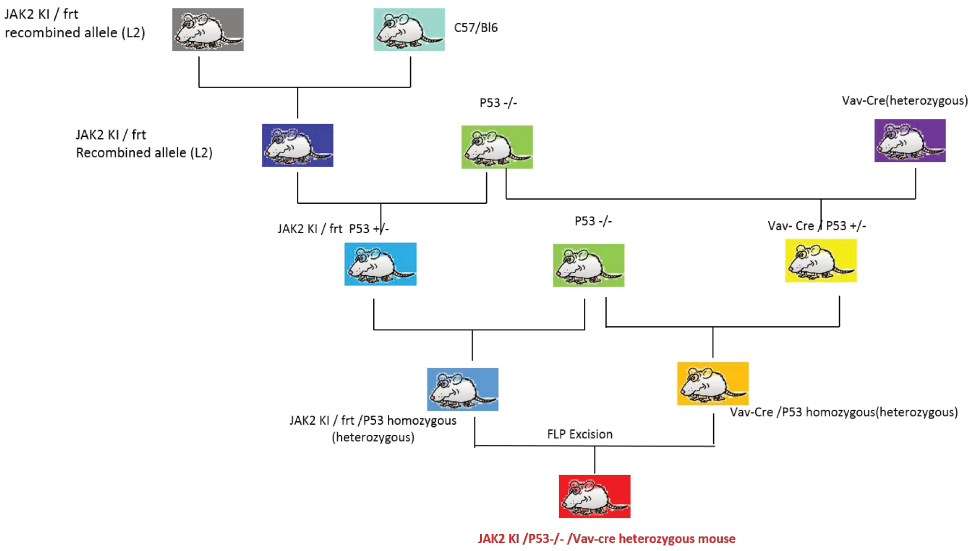

Figure 15: Generation of JAK2V617F/Vav-Cre/P53-/- mouse schematic.

2.2 Genotyping of mice

For the genotype of each mouse the PCR mix solution include 10 µL RedTaq ReadyMix (R2523-100RXN, SIGMA-ALDRICH CHIMIE, Quentin Fallavier Cedex), 0.2 µL primer (10 µM), 1 µL template DNA and dosing with PCR-grade water up to 20 µL. Gels (2% agarose) were run for 30 mins and exposed to UV. The primers for genotype of mice were the followings:

Table 3: primers for the genotype of mice

JAK2 conditional allele Forward 5’-3’:	GTC-TGT-CCA-AAG-AGT-CTG-TAA-GTA-C
JAK2 conditional allele Reverse 5’-3’:	GCT-CCA-GGG-TTA-CAC-GAG-TC
Vav-Cre Forward 5’-3’:	GGT-GTT-GTA-GTT-GTC-CCC-ACT
Vav-Cre Reverse 5’-3’:	CAG-GTT-TTG-GTG-CAC-AGT-CA
Vav-Cre Internal Positive Control Forward 5’-3’:	CTA-GGC-CAC-AGA-ATT-GAA-AGA-TCT
Vav-Cre Internal Positive Control Reverse 5’-3’:	GTA-GGT-GGA-AAT-TCT-AGC-ATC-ATC-C
P53_KS 5’-3’:	GCC-TTC-TAT-CGC-CTT-CTT-GAC-GAG-T
P53_WA 5’-3’:	AGA-CGC-ACA-AAC-CAA-AAC-AAA-ATT-ACA
P53_WS 5’-3’:	CGA-CCT-CCG-TTC-TCT-CTC-CTC-TCT-T

2.3 Treatment and analysis of mice

Peripheral blood of each mouse was collected by facial vein with 20 -gauge needle and EDTA tube (BD Bioscience) after one-month. The complete blood count were analyzed using automated counter (MS9; Schloessing Melet, France). Intraperitoneal injection and retro-orbital injection were performed for the needed treatment. Spleen and BM were fixed according to standard hematologic techniques. For the blood smear, placed a drop of blood on the surface of the first slide near the end then the second labeled slide in contact

with the first so that the blood drop was within an acute angle between the two slides. Work as fast as possible with a single, steady motion to spread the blood across the slide and air dried the smear. For the BM smears, a small portion of bone marrow was extracted with a needle, gently prepped by touch on a slide, then the sample was gently compressed with a second slide on top (no additional pressure) and the slide was carefully pulled straight out in the opposite direction. Slides were stained within Wright-Giemsa under 48 hours.

Both femurs and tibias were collected after the mouse were sacrificed with cervical dislocation. Removal of muscle and residual tissue around the femur and tibia and then cut the bone ends, 23-gauge needle and 1 ml syringe filled with ice-cold DMEM to rinse the bone marrow into a 70 µm cell filter placed in a 50 ml tube (Falcon). Centrifuge cells at 1,200 rpm for 10 min at 4 degree and discard the supernatant. The BM cells were resuspended into PBS again and count to do the other experiments. The spleen was weighted and split into pieces to prepare for histology and others. For the spleen cells suspension, remove the plunger of sterile 5 ml syringe. The flat end of the plunger was used to crush the spleen with a gentle circular motion to release the splenocytes. The suspension was filtered through a 70 µm cell strainer into a sterile 50 ml tube. Centrifuge the suspension with 1,200 rpm for 10 mins at 4 °C. The cells were Resuspended into PBS for the other assays which need splenocytes. To test response to stress, we induced chemical hemolytic anemia using phenyhydrazine PHZ (Sigma-aldrich). We calculate the concentration of PHZ

needed for a dose of 60 mg/kg in 100 µL of sterile PBS. The solution was made freshly prior to use and protected from light. IP injection of PHZ to the mice and then count the blood cells number, each population number and BrdU positive in each population in BM and spleen at different time points: D0, D3, D5, D7, D10, D15 and D30 time points. The experiment schedule as Figure 16

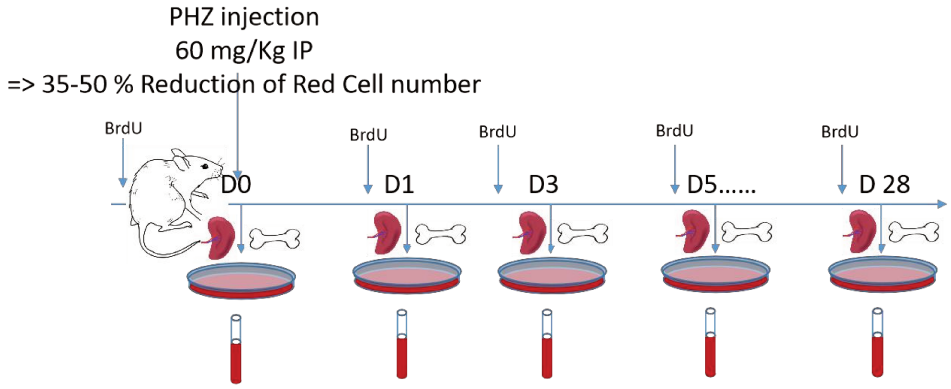

Figure 16: The Schedule of Experiment for the stem cells/progenitors population test after PHZ treated

2.4 Flow cytometry assay

For the chimerism test, 35µL PB and 1µL FITC anti-mouse CD45.1, A20 (Biolegend) and 2µL PE anti-mouse CD45.2, 104 (Biolegend) were incubated 20 min then lysed the RBC with FACS™ Lysing Solution (1×)(BD Biosciences) at room temperature 10 min and washed with 2 ml PBS centrifuge 1,200 rpm 10 mins. Discard the supernatant and wash the cells with PBS again then go to BD FACSCanto™ ‖ to do test. The ratio of CD45.1 as the control and CD45.2 as the JAK2V617F compartment. To test the JAK2V617F/Vav-Cre/p53$^{-/-}$ ratio in triple

competitive graft, we do the CFU with the bone marrow cells from the triple competitive graft mouse. After 10 days of incubation picked out at least 50 colonies from the CFU plate and then genotype the $p53^{-/-}$ in these 50 colonies.

To identify the number of stem and progenitor populations and the actively cycling cell populations in each of these compartments, IP injection of BrdU-containing solution (1mg/mouse, *BD Pharmingen, USA*) into mice 12-15 hours ago of test. The stem cells and progenitors population were labeled with different fluorescent antibodies. We first selected the Lin^- cells population with Biotin anti-mouse Lineage Panel (145-2C11;RB6-8C5;RA3-6B2;Ter-119;M1/70; Biolegend), in Lin^- population we then select the LSK population with $Lin^-Sca^+c\text{-}kit^+$ (BV 510™ anti-mouse Ly-6A/E (Sca-1), D7, Biolegend; BB700 Rat Anti-Mouse CD117 (PerCP), 2B8, BD Biosciences), and LK population with $Lin^-Sca^-c\text{-}kit^+$. We select the stem cells populations form LSK compartment which include ST-HSC ($Lin^-sca^+c\text{-}kit^+CD150^+CD48^-$), LT-HSC ($Lin^-sca^+c\text{-}kit^+CD150^-CD48^-$), and MPP ($Lin^-sca^+c\text{-}kit^+CD150^-CD48^+$) with BV711 anti-mouse CD48, HM48-1; PE/Cy7 anti-mouse CD150 (SLAM), TC15-12F12.2 (Biolegend). Progenitor populations were select from LK ($Lin^+sca^+c\text{-}kit^+$) which contain CMP ($Lin^-sca^+c\text{-}kit^+CD34^+CD16/32^-$), GMP ($Lin^-sca^+c\text{-}kit^+CD34^+CD16/32^+$), MEP ($Lin^-sca^+c\text{-}kit^+CD34^-CD16/32^-$) with Alexa Fluor® 647 Rat anti-Mouse CD34, RAM34 (RUO) and BV786 Rat Anti-Mouse CD16/CD32, 2.4G2(RUO) (BD Biosciences).The BrdU positive cells were tested with Alexa Fluor 488 anti-BrdU Antibody, 3D4 (Biolegend) according to the BD Pharmingen™

BrdU flow kits instruction manual protocol. 3×10^7 BM cells and 2×10^7 spleen cells of each mouse were prepared for the incubation of antibodies. Zombie (Zombie UV™ Fixable Viability Kit, Biolegend) was diluted with PBS to one time and incubated 100 µL of zombie 20 min at room temperature in dark. Then Lin Panel antibodies (Ter-119, M1/70, RB6-8C5, 145-2C11, RA3-6B2) 10 µL/10^7 cells were incubated 20 min at ice, wash the cells with PBS+FBS solution (20% FBS) and centrifuge 1,200 rpm 10 min. After that surface antibodies Sca-1, c-kit, CD16/32 (3 µL/10^7 cells), CD150 (5 µL/10^7 cells), CD48, CD34 and CD135 (5µL/10^7 cells) and 1× Streptavidin APC-Cy7 (Biolegend) were incubated with the cells 20 min at ice. Washed the cells with PBS and centrifuged 10 min. After that fix and permeabilize the cells with Cytofix/ Cytoperm buffer 200 µL/tube for 20 min at cold, washed with Perm/Wash buffer (1×) and centrifuged 10 min. Then resuspend the cells in 100 µL of Cytoperm Permeabilization buffer Plus/tube and incubated 10 min at cold. Washed the cells and then refixed cells with 100 µL of Cytofix/Cytoperm buffer for 5 min. After washing incubate the cells with 100 µL of diluted DNase (diluted to 300 µg/mL in DPBS)/tube for 1 hour at 37°C. One hour later washed the cells with Perm/Wash buffer and then incubated the BrdU antibody (10 µL/tube) for 30 min at room temperature. Washed the cells and suspended the cells into 1 mL Perm/Wash buffer to go to test the samples with flow cytometer. Data acquisition and/or data analysis were performed on the Cochin Cytometry and Immunobiology Facility

Cytometry analyses on a Fortessa cytometer LSRII (BD Biosciences) (Becton Dickinson), and analyses were done on Kaluza software.

To assess cell viability, surface labelled cells were resuspended in Annexin V binding buffer, and Annexin V (FITC) was added 15 min before analysis (FITC-conjugated Annexin V labeling detection kit, BD Biosciences).

2.5 Competitive Bone Marrow Transplantation

Recipient mice (CD45.1+45.2) were irradiated (9Gy) before 24 hours of bone marrow transplantation (BMT). The donor cells from the unisolated bone marrow of JAK2V617F/Vav-Cre and /or JAK2VF/Vav-Cre/$p53^{-/-}$ mice were mixed with the bone marrow cells from WT mice (CD45.1) to do the BMT by retro-orbital injection. There were three group of recipients mice which were engrafted with 5×10^6 WT cells (50%) plus with 5×10^6 JAK2V617F /Vav-Cre cells(50%) in each mouse as the first group; 5×10^6 WT cells (50%) plus with 5×10^6 JAK2V617F/Vav-Cre/$p53^{-/-}$ cells (50%) as the second group; 5×10^6 WT cells (50%) plus with $2{,}5\times10^6$ JAK2V617F/Vav-Cre cells(25%) and plus $2{,}5\times10^6$ JAK2V617F/Vav-Cre/$p53^{-/-}$ cells (25%) as the third group. Each group also has two mice which were uninjected as the negative control. WBC, RBC, hemoglobin, HCT, and PLT counts were tested from first month of graft. chimerism was also performed each time of blood collection. And begin to treat the mice with a pegylated form of murine IFN-α (peg-IFN- α) (600ng) by IP

one time a week until 2 months. Following the mice to get the survival plot. Meanwhile the same number of mice as the uninjected mice in each group

2.6 RNA Sequencing Sample Preparation

BM cells of C57, JAK2V617F/*Vav-Cre* and JAK2V617F/*Vav-Cre* /p53$^{-/-}$ were suspended with PBS and incubated the Lin$^-$ panel antibodies (Ter-119 20μL/10^8 cells, B220 20 μL/10^8 cells, GR1 20μL/10^8 cells, CD3ε 5μL/10^8 cells, CD116 10μL/10^8 cells) in rotation for 20 min at clod room. Then washed the cells with PBS and centrifuged 10 min at 1,200 rpm. Resuspend the cells into Mouse Depletion Dynabeads^{TM} For untouched kits (Invitrogen, Thermo Fisher Scientific) and rotated 15 min at room temperature. After that the tubes were put into magnetic field 2-3 min, and recovered the Lin$^-$ cells in supernatant. Incubated the surface antibodies for Lin$^-$ cells suspension. The volume of each surface antibody as following: Sca-1 1μL/10^7 cells, c-kit, CD150, CD48, CD16/32 and CD34 2μL/10^7 cells. 30 min incubation at room temperature and then washed the cells into 4 mL PBS. Resuspend the cells in MEMα medium at 10% FCS at a rate of 0.5 ml for 1.5 ×10 ^{7} cells. BD FACSAria^{TM} III cell sorter (BD Bioscience) was used to sort the LT-HSC, ST-HSC, MPP, CMP, GMP and MEP populations of each mice. Each population of cells was collected into 100 μL of buffer RL from the single cell RNA purification kit (Norgen Biotek Corp). RNAs were quantified using Nanodrop (100 ng/uL) and qualified in a Bioanalyzer (Agilent). The RNA-Seq analysis was performed at the Cochin Institute genomic platform

(Paris).

After the paired end (2 ×75 bp) sequencing, a primary analysis based on AOZAN software (ENS, Paris) was applied to demultiplex and control the quality of the raw data (based of FastQC modules / version 0.11.5). Obtained fastq files were then aligned using STAR algorithm (version 2.7.1a) on the GRCm38 reference from Ensembl, release 101, and quality control of the alignment realized with Picard tools (version 2.8.1). STAR parameters were the following: --sjdbOverhang 74 --twopassMode Basic –outFilterType BySJout --quantMode TranscriptomeSAM. Reads were then count using RSEM (v1.3.1) with the Aligned to Transcriptome bam files and the statistical analyses on the read counts were performed with theDESeq2 package version 1.24.0 to determine the proportion of differentially expressed genes between two conditions. During the statistical analysis, we filter out annotations where there are less than 3 samples with normalized counts greater than or equal to 10.

Analyzes were pursued with Database for Annotation, Visualization and Integrated Discovery (DAVID) and Gene Set Enrichment Analysis (GSEA) using the following parameters for signification: $p<0.05$ for DAVID, a False discovery rate (FDR) <0.25 and a Normalized Enrichment Score (NES) >1.

2.7 Method to identify enriched pathways

For each experimental comparison, differentially expressed genes with adjusted p values≤ 0.05, from DESeq2 algorithm, were selected. Log fold

change values were used to pre-rank differentially expressed genes. Fast Gene Set Enrichment Analysis (FGSEA)25 implemented in the R Bioconductor package was applied to the ranked gene lists. Enriched pathways identified by FGSEA with significant adjusted p values were considered.

2.8 Colony-forming unit (CFU) assays

To set up the CFU assay, the MethoCult™ medium was dispensed 3 mL per tube for 1.1 mL duplicate cultures. 5 $\times 10^{6}$ BM cells were diluted with IMDM + 2% FBS (0.3 mL) and added to a pre-aliquoted 3 mL MethoCult™ tube and vortexed the tube to mix the contents thoroughly. Fill the Petri dish (35×10 mm) with the mixture and incubate at 37°C under 5% CO2 in the incubator (NAPCO, Series 5400) for 7 days. After that colonies were picked to perform the PCR to test the ratio of $p53^{-/-}$ and JAK2V617F/Vav-Cre.

2.9 Statistic Analysis

All of the data were presented as mean ± standard deviation (SD) and analyzes by one-way analysis of variance (ANVOVA) using Graph Pad 8.0 software. In all figures *p<0.05, **p<0.01,***p<0.001.

RESULTS

Results will be presented as papers that are currently under revision for Part1, (Dynamic regulation from Stem to Red Cells in unperturbed and stress hematopoiesis) and still under writing Part 2 (Part2: Mechanisms of Clonal selection in myeloproliferative neoplasms (JAK2V617F) Subclonal selection and transformation after *TP53* inactivation).

Hematopoiesis provides lifelong supply of mature blood cells derived from bone marrow stem cells characterized by self-renewal and differentiation. Emerging data having highlighted fundamental differences between stress and unperturbed hematopoiesis, mathematical modelling integrating both behaviors should be a powerful approach to address key questions in hematopoiesis. Here, we developed a 6-cell amplification compartment model focused on early steps of erythropoiesis, able to accurately reproduce unperturbed erythropoiesis. Such model was then applied to stress hematopoiesis such as red blood cell destruction after phenylhydrazine treatment. Based on our biological data, we modeled plasticity of erythropoiesis recapitulating steady-state and stress behavior, by introducing time-dependent regulations, depending indirectly on compartment sizes through the dynamics of two regulators (ur and ud) modulating self-renewal and differentiation.

JAK2V617F is a common mutation in MPN phenotype, and *TP53* mutations are important secondary events in MPN progression. In a previously described mouse model it has been demonstrated that JAK2V617F overexpression in a

TP53 inactivated context can lead to erythleukemia in mice when JAK2V617F alone did not. Patient studies also showed the *TP53* is one of the major mutated genes in post-MPN leukemias. Here we used Vav-Cre expression to get the JAK2V617F/Vav-Cre conditional knock in mice in hemtopoietic cells and *TP53* knock out mice to get the JAK2V617F/Vav-Cre/TP53 mouse model and check the consequences of inactivation of *TP53* for the MPN progression. We did not find that inactivation of *TP53* modify the phenotype of MPN or induce MPN transformation. However, in a competitive graft with JAK2V617F cells, we found that the JAK2V617F/Vav-Cre/TP53 cells have a proliferative advantage over JAK2V617F/Vav-Cre cells after stress (reconstitution after Bone marrow transplantation). Furthermore, we also found that the JAK2V617F/Vav-Cre transplanted mice have a different response to the treatment with IFN-α when compared with JAK2V617F/Vav-Cre/TP53 mice. This relatively lower sensitivity could explain the higher risk of acute transformation in the long term.

3.1 Part1. Dynamic regulation from Stem to Red Cells in unperturbed and stress hematopoiesis

Combined biological and modelling Approach of Hematopoiesis: From Native to stressed Erythropoiesis.

Céline Bonnet*[3], Panhong Gou*[1], Simon Girel[3], Vincent Bansaye[3], Catherine Lacout[1], Karine Bailly[2], Marie-Hélène Schlagetter[1], Evelyne Lauret☼[2] Sylvie Méléard☼[3,4], and Stéphane Giraudier☼[1].

*These two authors contribute equally to this work.

☼ These three authors are co-last authors.

[1]Université de Paris, Hôpital Saint Louis, INSERM U1131, F-750 Paris, France

[2] Université de Paris, Institut Cochin, INSERM U1016, CNRS UMR8104, F-75014 PARIS, France

[3] CMAP, CNRS, Ecole polytechnique, Institut Polytechnique de Paris, 91128, Palaiseau.

[4] Institut universitaire de France

Short title: Modelling hematopoiesis from stem to red cells (50 characters)

Corresponding author: Stéphane Giraudier

Address: INSERM U1131, Centre Hayem, Hôpital Saint Louis, 1 avenue Claude Vellefaux, 75010 Paris, France Phone: +33 (0)1 Fax: +33 (0)1 e-mail: stephane.giraudier@aphp.fr

Supported by grants from the INSERM and INCa 2018 and fellowships from The Research ministry of China.

Abstract

We developed here a new mathematical modelling approach which reconciliates native and stress hematopoiesis, focused on hematopoietic stem and progenitor compartments. We first proposed an erythropoiesis model leaning on a minimum of 6 cell-amplification compartments, able to reproduce native erythropoiesis. A phenylhydrazine-induced hemolytic stress was next applied, and *in vivo* data were used to estimate model parameters through an optimized algorithm and integrated regulatory processes. A reduction of all stem cell compartments was observed, due to a drastic differentiation without proliferation during 7 days, followed by a huge proliferation in all compartments including long-term hematopoietic stem cells, before returning to normal values. The 6-compartment model applied to stress erythropoiesis was complexified by integrating regulatory processes. Thus, regulation of hematopoiesis appears dispensable during native hematopoiesis but mandatory for stress hematopoiesis. In conclusion this multi-step and time-dependent model of immature hematopoiesis opens new opportunities to understand development of normal or pathological hematopoiesis.

INTRODUCTION

Hematopoiesis provides the lifelong supply of mature blood cells derived from a rare population of bone marrow (BM) multipotent hematopoietic stem cells (HSCs) (Orkin and Zon, 2008; Till and McCulloch, 2012). The lineage relationship between HSCs and mature cells was first proposed as a multistep

process in which generations of diverse blood cells are coupled with movement through consecutive Hematopoietic Stem and Progenitor Cell (HSPC) amplification motors, from HSC to mature blood cells. HSPC division and differentiation are controlled by extracellular signals, and by intracellular networks. In the classical model, successive HSPC compartments, Long-Term HSC (LT-HSC), Short-Term HSC (ST-HSC), MultiPotent Progenitor (MPP), etc. along hematopoietic differentiation process are defined on their immunophenotypic level, typically by the expression of cell surface marker combinations (Eich et al., 2019; Notta et al., 2016). In this context, since the 1960s, HSCs are typically functionally defined by their ability to sustain multi-lineage engraftment for an extended period of time upon serial transplantation into irradiated recipient mice (Till and McCulloch, 2012). Recently, new generation of experimental tools allowing in situ analysis of HSC output has challenged the classical model by pointing out fundamental differences between physiological unperturbed hematopoiesis and stress hematopoiesis (Busch et al., 2015; Carrelha et al., 2018; Chapple et al., 2018; Pei et al., 2017, 2020; Rodriguez-Fraticelli et al., 2018; Säwen et al., 2018; Sun et al., 2014). In particular, in native hematopoiesis, progenitors directly downstream of LT-HSCs (ST-HSC, MPP…) serve as a major, nearly self-renewing source of day-to-day hematopoiesis, rendering blood and immune system less dependent on LT-HSC, in agreement with the quiescence of adult LT-HSCs (Busch and Rodewald, 2016; Busch et al., 2015; Foudi et al., 2009; Schoedel et

al., 2016). In addition, recent single cell profiling analysis has unveiled the tremendous heterogeneity of each previously defined compartment leading to a continuum in hematopoiesis process (Giladi et al., 2018; Laurenti and Göttgens, 2018; Paul et al., 2015; Velten et al., 2017). However, punctuated transitions across this continuous gene expression landscape may still exist and represent functionally distinct groups of cells (Liggett and Sankaran, 2020).

Mathematical modelling integrating both unperturbed and stress hematopoiesis should be a powerful approach to address key questions in hematopoiesis, able to provide qualitative and quantitative insights into stem cell dynamics and fate commitment. To date, most of hematopoiesis modelling is based on the existence of few cell compartments (stem cells, progenitors and mature cells) (Crauste et al., 2008, 2010). Rodewald's group has introduced a major breakthrough by modelling hematopoiesis based upon stem compartments from LT-HSC to MPP in unperturbed hematopoiesis (Busch et al., 2015). Nevertheless, they notice that their steady state model cannot recapitulate stress hematopoiesis such as 5-fluorouracile (5-FU) treatment, suggesting that unperturbed and stress hematopoiesis do not follow the same biological rules.

Here we want to recapitulate in a single mathematical model stress and steady-state hematopoiesis, based on in vivo experiments. We focused our attention on erythroid response since erythroid cells represent ~95% of blood cells. We chose a "peripheral stress" through hemolytic anemia

(phenylhydrazine administration known to destroy mature red blood cells, RBC) to avoid direct alterations of the stem cell compartments (Hara and Ogawa, 1976; Klinken et al., 1987). So far, most of studies focused their attention on committed progenitors, the effects on more immature compartments being poorly addressed.

Here, we demonstrate that stress and unperturbed hematopoiesis can be combined in a single system based on a 6-compartment modeling. We conducted in silico modelling and in vivo experiments to integrate homeostasis and stress hematopoiesis. We observed that transient hematopoietic stress impacts all primitive HSPC compartments, with a large rebound effect inducing a delay in the hematopoietic system. A steady state model (i.e. with constant parameter values) cannot explain the fast return of RBC to equilibrium and a model whose regulation depends directly on the different compartment sizes cannot explain the observed rebound effect. Then, these effects were taken into account in our in silico model: We integrated time-dependent regulations depending indirectly on compartment sizes. Self-renewal and differentiation dynamics were modulated through the dynamics of two regulators (ur and ud). The model was finely calibrated using a novel stochastic optimization algorithm (CMA-ES) (Hansen and Ostermeier, 2001) based on the experimental observations .

RESULTS

We first developed a mathematical model able to recapitulate steady-state hematopoiesis from quiescent LT-HSC to RBC. Modelling quiescence/kinetics of proliferation/differentiation processes requires a theoretical number of compartments between LT-HSC and RBC. However, deciphering an exact compartment number remains elusive since nature and number of compartments are not standardized from one study to another. Using a mathematical modelling, we deduced that the theoretical number of compartments should rely upon at least 3 criteria for each compartment: 1-size, 2- duration of proliferative steps and 3-self-renewal versus differentiation capacities.

We assumed that an accurate model should integrate stochasticity and amplification in each compartment as well as plasticity in the number of intermediate compartments. Then, a stochastic multi-type branching process was designed to recapitulate native (unperturbed) hematopoiesis, leading to derivation of a macroscopic deterministic system. In vivo steady-state parameters applied to this model helped us to determine the minimal number of amplification motors (k cell compartments) necessary to obtain a lifelong stable RBC production.

Modelling of unperturbed early erythropoiesis

Our model describes a hierarchy of k cell compartments evolving over time. Each cell of a given compartment divides with a constant rate independently

from the others and is characterized by its division rate, its self-renewal and differentiation capacity, and for the last compartment (corresponding to RBC), its death rate. The entire dynamics of hematopoiesis presented in Figure 1A and 1B is summarized as follows:

1- For any i=1 , k−2, a cell belonging to the i compartment divides at rate $\tau i>0$ in two cells of the same compartment with a probability 0<pir<1 (self-renewal) or in two cells of compartment i+1 with a probability µi pid (=µi (1−pir)) (erythroid differentiation). The pid probability corresponds to differentiation, and µi to commitment towards erythroid rather than non-erythroid lineages. The i=1 compartment corresponds to LT-HSC and i=k to mature RBC.

2- A (k-1)-type cell “divides” at rate $\tau\ k\ -1\ >0$. Upon division, the cell renews with probability 0<prk-1<1, and gives rise to 2n k-type cells with probability pdk-1=1–prk−1. This dynamic summarizes the n mitosis with negligible self-renewal observed at the end of erythroid differentiation. This amplification was simplified as 2n RBC issued from 1 cell of the previous compartment since terminal erythroid differentiation has been largely modeled before and is not our main concern.

3 - A k-type cell corresponding to mature RBC dies at rate $\tau k >0$. The estimation HSPC death rate is estimated to 2-4% per day and then was neglected in our modeling (Domen et al., 2000).

We were aware that stem cell division could be asymmetric (a cell of type i giving birth to two daughter cells, one of type i and the other of type i+1).

However, from our data, it was not possible to distinguish symmetrical from asymmetrical divisions. We therefore neglected the latter for parameter identifiability purpose.

Furthermore, presuming that LT-HSC compartment is at equilibrium, the number of self-renewing LT-HSC is equal to the number of differentiating LT-HSC, i.e p1d=p1r. Moreover, for any i $\in$ {2, k-1}, pid−pir >0 to ensure the stability of the system. For any type i=2, k−1, the i-compartment differentiation factor is defined as Di=pid−pir. Since pid+pir =1, Di =1-2 pir =2 pid -1.

According to the literature (Ethier and Kurtz, 1986), LT-HSC number was large enough to approximate the stochastic model by a differential equation system (Figure 1C); therefore compartment sizes at equilibrium can be expressed (Figure 1D). In particular, the i compartment size relies upon the one of compartment i-1 multiplied by 1/Di, meaning that the smaller the Di, the bigger the i compartment size.

As a first step, we assumed that the Di are equal to a positive D value and the μi probabilities equal to 1. Then a direct relationship can be computed between the LT-HSC number, their division rate, the D parameter, the n number of final mitoses, the RBC number, and their death rate (Figure 1E). The minimal number of amplification motors / compartments was computed based on this formula. Such method was drafted in Dingly et al. 2007 (Dingli et al., 2007) with a simple model which does not include temporal dynamics.

Determination of the minimal compartment number

The determination of the theoretical minimum number of compartments was based on Figure 1E. The RBC number and their death rate are known (ie≈10^{10} cells/mouse, and 40-day life expectancy). LT-HSC number was evaluated from the proportion of LT-HSC (Lin^- $Sca\text{-}1^+$ $c\text{-}kit^+$, LSK $CD150^+CD48^-$) estimated as described in Figure S1. Knowing that a C57Bl6 mouse displays ≈250x10^6 BM cells (Boggs, 1984; Chervenick et al., 1968; Mahajan et al., 2015), the LT-HSC number was around 15248 ± 2200/mouse. The LT-HSC division rate was computed from the proportion of LT-HSC retaining their phenotype after 20 hours of BrdU incorporation at steady state (1.82 in [0-4.7] % of cycling LT-HSC) (Figure 1F and Figure S1). Hence LT-HSC division rate was approximated by 1/100 per day. Assuming that Di must increase as a function of i and since Dk=1 (no self-renewal), Di belongs to [D2;1]. As in Busch's report (Busch et al., 2015), the second compartment corresponds to the ST-HSC compartment. Then minimal value for D2 (D2≥0.16) was computed (Figure 1D) with bounds for division rate (Figure 1F and Table 1).

The n number of mitosis between the two last compartments was assessed as follows: we assume that the k-1 compartment is upstream of BFU-E (Burst-Forming-Unit Erythroid)-enriched cells known to perform 11 cell divisions to in vitro generate mature RBC (Li et al., 2019). Therefore "n" should be over 12.

Taking into consideration all these parameters (Figure 1E), we computed that if

k=5, then D=0.12; if k=6, then D=0.23; if k=7, then D=0.35. Therefore, the minimum compartment number to obtain D ∈ [0.16; 1] was 6. As previously assessed, the last steps (MEP to RBC) was simplified as 2n RBC from 1 MEP. We focused our attention on HSPC compartments and roughly summarized behavior of committed erythroid progenitors. To match these 6 compartments to cytometric analysis of hematopoiesis, we then in vivo evaluated the cell number and division rates of LT-HSC, ST-HSC, MPP, CMP, MEP, and MEP to RBC compartments (Table 2).

Parameter calibration of the mathematical model for steady-state erythropoiesis.

We first gave bounds to the division rate per day. By considering variations due to BrdU experimental procedure, we used bounds rather than median values to delineate division rates (Figure 1F). Bounds offered the opportunity to include standard deviation from one experiment to another and variability of the time interval between BrdU injection and analysis (20h ± 4h).

We then computed appropriate values of all parameters (Table 2). We took into consideration 1- population size (Table 1), 2- μi probabilities of differentiation toward the erythroid lineage (based on Busch's data), 3- decreased probability of self-renewal along the differentiation process, and 4- bounds of the division rate of each cell type. The μi erythro-myeloid commitment probabilities were obtained considering Busch et al. data (Busch et al., 2015) and dividing the differentiation rate toward erythro-myeloid lineages by the sum of

differentiation rates toward all lineages. Based on decreasing probability of self-renewal in the different compartments along the differentiation process, Di were computed allowing calibration of the model (Figure 1D). Our results (Table 2) showed that this steady state erythropoiesis model was able to reproduce unperturbed native hematopoiesis for at least two years, the normal mouse lifetime.

Steady-state model applied to acute erythroid stress.

In order to validate the 6-amplification compartment model in stress hematopoiesis, we induce an acute hemolytic anemia using phenylhydrazine (PHZ) administration (Figure S2A). After a 40%-hemolysis stress observed at day 3, a rapid recovery of RBC was evidenced after 10-16 days (Figure 2A). Our 6-step model was applied to recapitulate RBC recovery but the recovery time exceeded one month, in total discrepancy with observed biological data (Figure 2A). This indicated that, although able to fulfill steady state hematopoiesis, this model was unable to recapitulate the hematopoietic stress response just like previously observed by Busch et al. using their own model (Busch et al., 2015). We then considered that our model requires additional regulations during stress hematopoiesis.

Analysis of compartment kinetics during acute hematopoietic stress.

In order to decrypt biological mechanisms responsible for this fast RBC recovery, we analyzed all compartment modifications after PHZ injection in blood, BM, and spleen. Briefly, during the first 3 days after injection, we observed a drastic

RBC fall, and an increase in platelets and leukocytes counts (Figure 2A-C). While total number of BM cells was slightly reduced at day 3 (-25%) and enhanced at day 10 (+33%) (Figure 2G), spleen weight strongly increased 24h after PHZ injection (Figure 2D-F), becoming 3 times larger than normal at day 3, as previously observed after erythroid (Hara and Ogawa, 1976; Sanchez et al., 2006) and social stress in mice (McKim et al., 2018). The three hematopoietic tissues were analyzed to assess proportion and absolute cell numbers in the different compartments (LT-HSC, ST-HSC, MPP, CMP, and MEP) as well as their percentages into cell cycle (BrdU incorporation), and apoptosis (AnnexinV labelling) during the hemolytic phase. In BM, a decrease in the size of all compartments (from LT-HSC to CMP) was evidenced. BM MEP population remained relatively stable during this phase, while a huge increase in the number of splenic MEP was observed 3 and 5 days after PHZ injection (Figure 2G). No difference in BrdU incorporation was noticed at day 3 in the different BM compartments except for MEP, which displayed a 2-fold increased cell proliferation, as compared to D0 (Figure S2F). To further get insight into mechanisms involved in the drastic decrease of compartment size, we analyzed apoptosis. No increase in the proportion of AnnexinV-labelled cells was observed whatever the progenitor compartment examined, allowing us to exclude any excess of cell death in the BM progenitor compartments (Figure S3B). Blood cell analysis performed at day 1 and 3 after PHZ injection showed a 15-fold increase in the number of mononuclear cells (Figure 2B) yet with a

negligible proportion of Lin- cells, precluding an egress of LSK from BM to blood (Figure S3A). In spleen, a stress erythropoietic organ in mouse, the number of mature cells increased (3-fold) (Figure 2E) whereas LSK and CMP compartments displayed no significant variations in cell number, ruling out any role of splenic immature progenitors at day 3 (Figure 2G). Lastly, to confirm stemness properties of LT-HSC assessed by cytometry, competitive BM transplantation with 50% of CD45.1 BM cells from untreated animals and 50% of total BM cells from day 3-PHZ-treated mice were performed in CD45.2 9.5 Gy-irradiated recipients. Blood chimerism analysis 3 months post-transplantation showed a decreased proportion, confirming the decrease number of LT-HSC in BM of day3-PHZ-treated mice (Figure S3C).

The decrease of BM progenitor compartment sizes, without increased proliferation or apoptosis or egress to the spleen or the blood, together with a stable number of MEP displaying a two-fold increased proliferation in BM and spleen, was the result of a rapid differentiation process, like a flush, to quickly compensate loss of RBC through a versatile mechanism.

Recovery of progenitor compartment after PHZ stress.

To assess dynamics of progenitor compartments during recovery after PHZ treatment, we analyzed at days 3, 5, 7, 10, 16 and 28 the different compartment sizes and proliferation rates. Recovery was almost effective in all compartments at day 7-10 (Figure 4A). Surprisingly, at day 10, all compartments displayed a 2-3-fold increased cell numbers before returning to

normal values at day 28. In parallel, BrdU analysis showed that all BM compartments exhibited a drastic increased cell proliferation at day-10 (the time point of the hematocrit normalization). Thereafter, BrdU incorporation returned to normal values at days 16 and 28 (Figure S2C-G).

Modelling steady-state and stress hematopoiesis by adding compartment regulations

The steady state model previously introduced could not recapitulate the fast return of RBC to equilibrium. Therefore, to model all at once unperturbed and stress hematopoiesis, we introduced regulations by assuming that previously defined parameters depend indirectly upon compartment size through dynamics of two regulators (ur and ud) modulating self-renewal and differentiation, bringing positive and negative effects on compartment sizes, respectively (Figure 3A).

Dynamics of the two regulators followed a double system of production and clearance. The production is given by Michaelis-Menten type functions depending on BM cell numbers. The clearance of the regulator after its production is given by a linear degradation term (Figure 3B). This modelling induced a delay between dynamics of the regulators and changes in compartment sizes, explaining the huge oscillations in cell numbers after PHZ injection.

Assuming that the proliferation rate during late erythropoiesis is regulated in a specific manner (Erythropoietin, Stem Cell Factor, etc…), RBC production

dynamics from MEP is controlled with a third type of regulation. MEP differentiation gives birth to 2n (t) RBC summarizing the n(t) last mitosis with a Hill function (Michaelis-Menten's type) of the RBC number (Figure 3C). In addition, we hypothesized that differentiation towards a non-erythroid lineage was not affected by all these regulators. Parameters of the regulated-model were calibrated using a stochastic optimization algorithm based on a CMA-ES method (Covariance Matrix Adaptation in Evolution Strategy), which minimizes discrepancy between in silico simulated and experimental data (see Suppl. data). Optimal parameters obtained by this method are presented in Table 3 and the corresponding cell dynamics in Figure 4B. The later matched with the experimental data in all compartments in stress condition (the oscillation effect) as well as in steady state (second part of the trajectory). Moreover, division rate values were deduced as function of time for each cell type (Table 4).

DISCUSSION

Our present work provides a mathematical model able to reconcile steady state and stress hematopoiesis. Furthermore, it highlights a mechanism by which transient stress exposure leads to a protracted influence on all progenitor compartments including LT-HSC, leading to a fast repopulation of mature compartment.

To decipher mechanisms involved in the normalization of RBC number at steady state and after an acute stress, we first developed a compartmental model of hematopoiesis. The theoretical number of compartments sufficient to

fulfill stable erythropoiesis was relied upon the number of LT-HSC and mature RBC. Our modelling proposes that 6-amplification compartments are sufficient to ensure steady state erythropoiesis. We hypothesized that the last compartment was resumed from MEP to RBC as a simple amplification factor according to the n number of mitosis required from 1 MEP to RBC. Based on the division number between BFU-E and erythrocytes, this n number could vary from 11 to 14 (Li et al., 2019). We neglected megakaryocytic differentiation that theoretically only corresponds to 20% of the MEP differentiation (Mori et al., 2015) and other myelo-lymphoid cells representing quantitative minorities. Then, this 6-compartment model parallels the generally assessed compartment hierarchy with LT-HSC, ST-HSC, MPP, CMP, MEP and RBC.

Our “stress model” was initially the destruction of RBCs by chemical hemolysis. Nevertheless, this process also induced a huge inflammatory response leading to changes in all blood cell types and a huge cytokine storm in the next few days after hemolysis (data not shown), confirming that stress hematopoiesis relied on regulatory mechanisms different from those of unperturbed hematopoiesis, as previously illustrated by the megakaryocytic and the granulocytic differentiation processes (Haas et al., 2015; Kang et al., 2020). Based on our data and modelling, we demonstrate here that (ur and ud) regulations of compartment proliferation and differentiation are required to reproduce stress response while dispensable for steady-state erythropoiesis,

these regulators remaining constant in the latter.

Previous mathematical models based on in vivo experiments mostly described hematopoiesis dynamics at steady state. These studies rely upon parameters such as cell division rates or probabilities of self-renewing (Abkowitz et al., 2000; Busch et al., 2015; Foudi et al., 2009; Klose et al., 2019; MacKey, 2001; Manesso et al., 2013; Sawai et al., 2016). Models integrating steady state as well as in vivo stress hematopoiesis rarely reproduce oscillations observed in the size of the progenitor compartments apart from the modelling (Angulo et al., 2018; Crauste et al., 2008, 2010; Klose et al., 2019; Loeffler et al., 1989; Manesso et al., 2013; Marciniak-Czochra et al., 2009; Roeder et al., 2005). These reports modelized the regulation dynamics by a differential equation with a delay, enabling to predict the oscillating behavior of progenitor compartments characterized by a regulated self-renewal. However they integrated only a theoretical 3-compartment model (stem cells/progenitors/mature erythrocytes) based on RBC recovery data after stress. Other regulation-based models have been developed but did not integrated in vivo data (Kirouac et al., 2010; Mahadik et al., 2019).

In contrast, our present 6-compartment model was designed to reproduce the in vivo dynamics observed throughout unperturbed and stress erythropoiesis, using 8 differential equations, including two for regulator dynamics and naturally created a delay in the oscillation phenomenon due to the duration needed for regulator production and clearance and then better match with

hematopoiesis process.

Little is known regarding in vivo consequences of a “peripheral” stress on upstream progenitor compartments such as LT-, ST-HSC, MPP, CMP, and MEP. Our experiments demonstrated that after an acute stress destroying RBC, the first compensatory mechanism entails all compartments, from LT-HSC to CMP, and surprisingly, induces as a first step, differentiation without proliferation just like a flush. Thereafter, all depleted compartments enter into proliferation during a recovery phase, the division rate of each progenitor compartment reaching its maximum value around day 11 but still remain lower than 3 divisions per day (in accordance with biological data) (Table 4). This recovery phase not only replenishes the different “flushed” compartments but exceeds steady-state values. Normalization of all compartment sizes occurs in a third phase just like spring oscillation around the standard values.

These oscillations in cell number from each compartment are in accordance with in vivo data previously reported in post-chemotherapy stressed hematopoiesis (Busch et al., 2015). In contrast, the MEP compartment was not subjected to such a high regulation process in the bone marrow probably because of the well-known spleen stress erythropoiesis process that follows a different kind of regulation as reported here and in previous reports (Perry et al., 2009).

In conclusion, we modeled the plasticity of hematopoiesis recapitulating steady-state as well as stress hematopoiesis, no compartment being

“protected” from stress consequences. Our mathematical model suggests that regulators of hematopoiesis are dispensable during steady-state hematopoiesis. Thus, our model opens the way to better understand malignant clonal development and invasion: Stem cell disorders just like leukemias and more generally cancers could arise from successive stress if pathological clonal cells react differently from normal cells in response to aggression.

References

Abkowitz, J.L., Golinelli, D., Harrison, D.E., and Guttorp, P. (2000). In vivo kinetics of murine hemopoietic stem cells. Blood *96*, 3399–3405.

Angulo, O., Gandrillon, O., and Crauste, F. (2018). Investigating the role of the experimental protocol in phenylhydrazine-induced anemia on mice recovery. J Theor Biol *437*, 286–298.

Boggs, D.R. (1984). The total marrow mass of the mouse: a simplified method of measurement. Am. J. Hematol. *16*, 277–286.

Busch, K., and Rodewald, H.-R. (2016). Unperturbed vs. post-transplantation hematopoiesis: both in vivo but different. Curr Opin Hematol *23*, 295–303.

Busch, K., Klapproth, K., Barile, M., Flossdorf, M., Holland-Letz, T., Schlenner, S.M., Reth, M., Höfer, T., and Rodewald, H.-R. (2015). Fundamental properties of unperturbed haematopoiesis from stem cells in vivo. Nature *518*, 542–546.

Carrelha, J., Meng, Y., Kettyle, L.M., Luis, T.C., Norfo, R., Alcolea, V., Boukarabila, H., Grasso, F., Gambardella, A., Grover, A., et al. (2018). Hierarchically related lineage-restricted fates of multipotent haematopoietic stem cells. Nature *554*, 106–111.

Chapple, R.H., Tseng, Y.-J., Hu, T., Kitano, A., Takeichi, M., Hoegenauer, K.A., and Nakada, D. (2018). Lineage tracing of murine adult hematopoietic stem cells reveals active contribution to steady-state hematopoiesis. Blood Adv *2*, 1220–1228.

Chervenick, P.A., Boggs, D.R., Marsh, J.C., Cartwright, G.E., and Wintrobe, M.M. (1968). Quantitative studies of blood and bone marrow neutrophils in normal mice. Am. J. Physiol. *215*, 353–360.

Crauste, F., Pujo-Menjouet, L., Génieys, S., Molina, C., and Gandrillon, O. (2008). Adding self-renewal in committed erythroid progenitors improves the biological relevance of a mathematical model of erythropoiesis. J Theor Biol *250*, 322–338.

Crauste, F., Demin, I., Gandrillon, O., and Volpert, V. (2010). Mathematical study of feedback control roles and relevance in stress erythropoiesis. J Theor Biol *263*, 303–316.

Dingli, D., Traulsen, A., and Pacheco, J.M. (2007). Compartmental architecture and dynamics of hematopoiesis. PLoS One *2*, e345.

Domen, J., Cheshier, S.H., and Weissman, I.L. (2000). The role of apoptosis in the regulation of hematopoietic stem cells: Overexpression of Bcl-2 increases both their number and repopulation potential. J Exp Med *191*, 253–264.

Eich, M., Trumpp, A., and Schmitt, S. (2019). OMIP-059: Identification of Mouse Hematopoietic Stem and Progenitor Cells with Simultaneous Detection of CD45.1/2 and

Controllable Green Fluorescent Protein Expression by a Single Staining Panel. Cytometry A *95*, 1049–1052.

Ethier, S., and Kurtz, T. (1986). Markov Processes: Characterization and Convergence. In Markov Processes: Characterization and Convergence, (John Wiley & Sons, Inc.), p.

Foudi, A., Hochedlinger, K., Van Buren, D., Schindler, J.W., Jaenisch, R., Carey, V., and Hock, H. (2009). Defining hematopoietic stem and progenitor cell turnover by analysis of histone 2B-GFP dilution. Nature Biotechnology *27*, 84.

Giladi, A., Paul, F., Herzog, Y., Lubling, Y., Weiner, A., Yofe, I., Jaitin, D., Cabezas-Wallscheid, N., Dress, R., Ginhoux, F., et al. (2018). Single-cell characterization of haematopoietic progenitors and their trajectories in homeostasis and perturbed haematopoiesis. Nat Cell Biol *20*, 836–846.

Haas, S., Hansson, J., Klimmeck, D., Loeffler, D., Velten, L., Uckelmann, H., Wurzer, S., Prendergast, Á.M., Schnell, A., Hexel, K., et al. (2015). Inflammation-Induced Emergency Megakaryopoiesis Driven by Hematopoietic Stem Cell-like Megakaryocyte Progenitors. Cell Stem Cell *17*, 422–434.

Hansen, N., and Ostermeier, A. (2001). Completely derandomized self-adaptation in evolution strategies. Evolutionary Computation *9*, 159–195.

Hara, H., and Ogawa, M. (1976). Erthropoietic precursors in mice with phenylhydrazine-induced anemia. Am J Hematol *1*, 453–458.

Kang, Y.-A., Pietras, E.M., and Passegué, E. (2020). Deregulated Notch and Wnt signaling activates early-stage myeloid regeneration pathways in leukemia. J. Exp. Med. *217*.

Kirouac, D.C., Ito, C., Csaszar, E., Roch, A., Yu, M., Sykes, E.A., Bader, G.D., and Zandstra, P.W. (2010). Dynamic interaction networks in a hierarchically organized tissue. Mol Syst Biol *6*, 417.

Klinken, S.P., Holmes, K.L., Fredrickson, T.N., Erner, S.M., and Morse, H.C. (1987). Phenylhydrazine stimulates lymphopoiesis and accelerates Abelson murine leukemia virus-induced pre-B cell lymphomas. J Immunol *139*, 3091–3098.

Klose, M., Florian, M.C., Gerbaulet, A., Geiger, H., and Glauche, I. (2019). Hematopoietic Stem Cell Dynamics Are Regulated by Progenitor Demand: Lessons from a Quantitative Modeling Approach. Stem Cells *37*, 948–957.

Laurenti, E., and Göttgens, B. (2018). From haematopoietic stem cells to complex differentiation landscapes. Nature *553*, 418–426.

Li, H., Natarajan, A., Ezike, J., Barrasa, M.I., Le, Y., Feder, Z.A., Yang, H., Ma, C., Markoulaki, S., and Lodish, H.F. (2019). Rate of Progression through a Continuum of Transit-Amplifying Progenitor Cell States Regulates Blood Cell Production. Dev Cell *49*, 118-129.e7.

Liggett, L.A., and Sankaran, V.G. (2020). Unraveling Hematopoiesis through the Lens of Genomics. Cell *182*, 1384–1400.

Loeffler, M., Pantel, K., Wulff, H., and Wichmann, H.E. (1989). A mathematical model of erythropoiesis in mice and rats. Part 1: Structure of the model. Cell Tissue Kinet *22*, 13–30.

MacKey, M.C. (2001). Cell kinetic status of haematopoietic stem cells. Cell Prolif *34*, 71–83.

Mahadik, B., Hannon, B., and Harley, B.A.C. (2019). A computational model of feedback-mediated hematopoietic stem cell differentiation in vitro. PLoS One *14*, e0212502.

Mahajan, M.M., Cheng, B., Beyer, A.I., Mulvaney, U.S., Wilkinson, M.B., Fomin, M.E., and Muench, M.O. (2015). A quantitative assessment of the content of hematopoietic stem cells in mouse and human endosteal-bone marrow: a simple and rapid method for the isolation of mouse central bone marrow. BMC Hematol *15*, 9.

Manesso, E., Teles, J., Bryder, D., and Peterson, C. (2013). Dynamical modelling of haematopoiesis: an integrated view over the system in homeostasis and under perturbation. J R Soc Interface *10*, 20120817.

Marciniak-Czochra, A., Stiehl, T., Ho, A.D., Jäger, W., and Wagner, W. (2009). Modeling of asymmetric cell division in hematopoietic stem cells--regulation of self-renewal is essential for efficient repopulation. Stem Cells Dev *18*, 377–385.

McKim, D.B., Yin, W., Wang, Y., Cole, S.W., Godbout, J.P., and Sheridan, J.F. (2018). Social Stress Mobilizes Hematopoietic Stem Cells to Establish Persistent Splenic Myelopoiesis. Cell Rep *25*, 2552-2562.e3.

Mori, Y., Chen, J.Y., Pluvinage, J.V., Seita, J., and Weissman, I.L. (2015). Prospective isolation of human erythroid lineage-committed progenitors. Proc Natl Acad Sci U S A *112*, 9638–9643.

Notta, F., Zandi, S., Takayama, N., Dobson, S., Gan, O.I., Wilson, G., Kaufmann, K.B., McLeod, J., Laurenti, E., Dunant, C.F., et al. (2016). Distinct routes of lineage development reshape the human blood hierarchy across ontogeny. Science *351*, aab2116.

Abkowitz, J.L., Golinelli, D., Harrison, D.E., and Guttorp, P. (2000). In vivo kinetics of murine hemopoietic stem cells. Blood *96*, 3399–3405.

Angulo, O., Gandrillon, O., and Crauste, F. (2018). Investigating the role of the experimental protocol in phenylhydrazine-induced anemia on mice recovery. J Theor Biol *437*, 286–298.

Boggs, D.R. (1984). The total marrow mass of the mouse: a simplified method of measurement. Am. J. Hematol. *16*, 277–286.

Busch, K., and Rodewald, H.-R. (2016). Unperturbed vs. post-transplantation hematopoiesis: both in vivo but different. Curr Opin Hematol *23*, 295–303.

Busch, K., Klapproth, K., Barile, M., Flossdorf, M., Holland-Letz, T., Schlenner, S.M., Reth, M., Höfer, T., and Rodewald, H.-R. (2015). Fundamental properties of unperturbed haematopoiesis from stem cells in vivo. Nature *518*, 542–546.

Carrelha, J., Meng, Y., Kettyle, L.M., Luis, T.C., Norfo, R., Alcolea, V., Boukarabila, H., Grasso, F., Gambardella, A., Grover, A., et al. (2018). Hierarchically related lineage-restricted fates of multipotent haematopoietic stem cells. Nature *554*, 106–111.

Chapple, R.H., Tseng, Y.-J., Hu, T., Kitano, A., Takeichi, M., Hoegenauer, K.A., and Nakada, D. (2018). Lineage tracing of murine adult hematopoietic stem cells reveals active contribution to steady-state hematopoiesis. Blood Adv *2*, 1220–1228.

Chervenick, P.A., Boggs, D.R., Marsh, J.C., Cartwright, G.E., and Wintrobe, M.M. (1968). Quantitative studies of blood and bone marrow neutrophils in normal mice. Am. J. Physiol. *215*, 353–360.

Crauste, F., Pujo-Menjouet, L., Génieys, S., Molina, C., and Gandrillon, O. (2008). Adding self-renewal in committed erythroid progenitors improves the biological relevance of a mathematical model of erythropoiesis. J Theor Biol *250*, 322–338.

Crauste, F., Demin, I., Gandrillon, O., and Volpert, V. (2010). Mathematical study of feedback control roles and relevance in stress erythropoiesis. J Theor Biol *263*, 303–316.

Dingli, D., Traulsen, A., and Pacheco, J.M. (2007). Compartmental architecture and dynamics of hematopoiesis. PLoS One *2*, e345.

Domen, J., Cheshier, S.H., and Weissman, I.L. (2000). The role of apoptosis in the regulation of hematopoietic stem cells: Overexpression of Bcl-2 increases both their number and repopulation potential. J Exp Med *191*, 253–264.

Eich, M., Trumpp, A., and Schmitt, S. (2019). OMIP-059: Identification of Mouse Hematopoietic Stem and Progenitor Cells with Simultaneous Detection of CD45.1/2 and Controllable Green Fluorescent Protein Expression by a Single Staining Panel. Cytometry A *95*, 1049–1052.

Ethier, S., and Kurtz, T. (1986). Markov Processes: Characterization and Convergence. In Markov Processes: Characterization and Convergence, (John Wiley & Sons, Inc.), p.

Foudi, A., Hochedlinger, K., Van Buren, D., Schindler, J.W., Jaenisch, R., Carey, V., and Hock, H. (2009). Defining hematopoietic stem and progenitor cell turnover by analysis of histone 2B-GFP dilution. Nature Biotechnology *27*, 84.

Giladi, A., Paul, F., Herzog, Y., Lubling, Y., Weiner, A., Yofe, I., Jaitin, D., Cabezas-Wallscheid, N., Dress, R., Ginhoux, F., et al. (2018). Single-cell characterization of haematopoietic progenitors and their trajectories in homeostasis and perturbed haematopoiesis. Nat Cell Biol *20*, 836–846.

Haas, S., Hansson, J., Klimmeck, D., Loeffler, D., Velten, L., Uckelmann, H., Wurzer, S., Prendergast, Á.M., Schnell, A., Hexel, K., et al. (2015). Inflammation-Induced Emergency Megakaryopoiesis Driven by Hematopoietic Stem Cell-like Megakaryocyte Progenitors. Cell Stem Cell *17*, 422–434.

Hansen, N., and Ostermeier, A. (2001). Completely derandomized self-adaptation in evolution strategies. Evolutionary Computation *9*, 159–195.

Hara, H., and Ogawa, M. (1976). Erthropoietic precursors in mice with phenylhydrazine-induced anemia. Am J Hematol *1*, 453–458.

Kang, Y.-A., Pietras, E.M., and Passegué, E. (2020). Deregulated Notch and Wnt signaling activates early-stage myeloid regeneration pathways in leukemia. J. Exp. Med. *217*.

Kirouac, D.C., Ito, C., Csaszar, E., Roch, A., Yu, M., Sykes, E.A., Bader, G.D., and Zandstra, P.W. (2010). Dynamic interaction networks in a hierarchically organized tissue. Mol Syst Biol *6*, 417.

Klinken, S.P., Holmes, K.L., Fredrickson, T.N., Erner, S.M., and Morse, H.C. (1987). Phenylhydrazine stimulates lymphopoiesis and accelerates Abelson murine leukemia virus-induced pre-B cell lymphomas. J Immunol *139*, 3091–3098.

Klose, M., Florian, M.C., Gerbaulet, A., Geiger, H., and Glauche, I. (2019). Hematopoietic Stem Cell Dynamics Are Regulated by Progenitor Demand: Lessons from a Quantitative Modeling Approach. Stem Cells *37*, 948–957.

Laurenti, E., and Göttgens, B. (2018). From haematopoietic stem cells to complex differentiation landscapes. Nature *553*, 418–426.

Li, H., Natarajan, A., Ezike, J., Barrasa, M.I., Le, Y., Feder, Z.A., Yang, H., Ma, C., Markoulaki, S., and Lodish, H.F. (2019). Rate of Progression through a Continuum of Transit-Amplifying Progenitor Cell States Regulates Blood Cell Production. Dev Cell *49*, 118-129.e7.

Liggett, L.A., and Sankaran, V.G. (2020). Unraveling Hematopoiesis through the Lens of Genomics. Cell *182*, 1384–1400.

Loeffler, M., Pantel, K., Wulff, H., and Wichmann, H.E. (1989). A mathematical model of erythropoiesis in mice and rats. Part 1: Structure of the model. Cell Tissue Kinet *22*, 13–30.

MacKey, M.C. (2001). Cell kinetic status of haematopoietic stem cells. Cell Prolif *34*, 71–83.

Mahadik, B., Hannon, B., and Harley, B.A.C. (2019). A computational model of feedback-mediated hematopoietic stem cell differentiation in vitro. PLoS One *14*, e0212502.

Mahajan, M.M., Cheng, B., Beyer, A.I., Mulvaney, U.S., Wilkinson, M.B., Fomin, M.E., and Muench, M.O. (2015). A quantitative assessment of the content of hematopoietic stem cells

in mouse and human endosteal-bone marrow: a simple and rapid method for the isolation of mouse central bone marrow. BMC Hematol *15*, 9.

Manesso, E., Teles, J., Bryder, D., and Peterson, C. (2013). Dynamical modelling of haematopoiesis: an integrated view over the system in homeostasis and under perturbation. J R Soc Interface *10*, 20120817.

Marciniak-Czochra, A., Stiehl, T., Ho, A.D., Jäger, W., and Wagner, W. (2009). Modeling of asymmetric cell division in hematopoietic stem cells--regulation of self-renewal is essential for efficient repopulation. Stem Cells Dev *18*, 377–385.

McKim, D.B., Yin, W., Wang, Y., Cole, S.W., Godbout, J.P., and Sheridan, J.F. (2018). Social Stress Mobilizes Hematopoietic Stem Cells to Establish Persistent Splenic Myelopoiesis. Cell Rep *25*, 2552-2562.e3.

Mori, Y., Chen, J.Y., Pluvinage, J.V., Seita, J., and Weissman, I.L. (2015). Prospective isolation of human erythroid lineage-committed progenitors. Proc Natl Acad Sci U S A *112*, 9638–9643.

Notta, F., Zandi, S., Takayama, N., Dobson, S., Gan, O.I., Wilson, G., Kaufmann, K.B., McLeod, J., Laurenti, E., Dunant, C.F., et al. (2016). Distinct routes of lineage development reshape the human blood hierarchy across ontogeny. Science *351*, aab2116.

Orkin, S.H., and Zon, L.I. (2008). Hematopoiesis: an evolving paradigm for stem cell biology. Cell *132*, 631–644.

Paul, F., Arkin, Y., Giladi, A., Jaitin, D.A., Kenigsberg, E., Keren-Shaul, H., Winter, D., Lara-Astiaso, D., Gury, M., Weiner, A., et al. (2015). Transcriptional Heterogeneity and Lineage Commitment in Myeloid Progenitors. Cell *163*, 1663–1677.

Pei, W., Feyerabend, T.B., Rössler, J., Wang, X., Postrach, D., Busch, K., Rode, I., Klapproth, K., Dietlein, N., Quedenau, C., et al. (2017). Polylox barcoding reveals haematopoietic stem cell fates realized in vivo. Nature *548*, 456–460.

Pei, W., Shang, F., Wang, X., Fanti, A.-K., Greco, A., Busch, K., Klapproth, K., Zhang, Q., Quedenau, C., Sauer, S., et al. (2020). Resolving Fates and Single-Cell Transcriptomes of Hematopoietic Stem Cell Clones by PolyloxExpress Barcoding. Cell Stem Cell *27*, 383-395.e8.

Perry, J.M., Harandi, O.F., Porayette, P., Hegde, S., Kannan, A.K., and Paulson, R.F. (2009). Maintenance of the BMP4-dependent stress erythropoiesis pathway in the murine spleen requires hedgehog signaling. Blood *113*, 911–918.

Rodriguez-Fraticelli, A.E., Wolock, S.L., Weinreb, C.S., Panero, R., Patel, S.H., Jankovic, M., Sun, J., Calogero, R.A., Klein, A.M., and Camargo, F.D. (2018). Clonal analysis of lineage fate in native haematopoiesis. Nature *553*, 212–216.

Roeder, I., Kamminga, L.M., Braesel, K., Dontje, B., de Haan, G., and Loeffler, M. (2005). Competitive clonal hematopoiesis in mouse chimeras explained by a stochastic model of stem cell organization. Blood *105*, 609–616.

Sanchez, M., Weissman, I.L., Pallavicini, M., Valeri, M., Guglielmelli, P., Vannucchi, A.M., Migliaccio, G., and Migliaccio, A.R. (2006). Differential amplification of murine bipotent megakaryocytic/erythroid progenitor and precursor cells during recovery from acute and chronic erythroid stress. Stem Cells *24*, 337–348.

Sawai, C.M., Babovic, S., Upadhaya, S., Knapp, D.J.H.F., Lavin, Y., Lau, C.M., Goloborodko, A., Feng, J., Fujisaki, J., Ding, L., et al. (2016). Hematopoietic Stem Cells Are the Major Source of Multilineage Hematopoiesis in Adult Animals. Immunity *45*, 597–609.

Säwen, P., Eldeeb, M., Erlandsson, E., Kristiansen, T.A., Laterza, C., Kokaia, Z., Karlsson, G., Yuan, J., Soneji, S., Mandal, P.K., et al. (2018). Murine HSCs contribute actively to native hematopoiesis but with reduced differentiation capacity upon aging. Elife *7*.

Schoedel, K.B., Morcos, M.N.F., Zerjatke, T., Roeder, I., Grinenko, T., Voehringer, D., Göthert, J.R., Waskow, C., Roers, A., and Gerbaulet, A. (2016). The bulk of the hematopoietic stem cell population is dispensable for murine steady-state and stress hematopoiesis. Blood *128*, 2285–2296.

Sun, J., Ramos, A., Chapman, B., Johnnidis, J.B., Le, L., Ho, Y.-J., Klein, A., Hofmann, O., and Camargo, F.D. (2014). Clonal dynamics of native haematopoiesis. Nature *514*, 322–327.

Till, J.E., and McCulloch, E.A. (2012). A direct measurement of the radiation sensitivity of normal mouse bone marrow cells. 1961. Radiat Res *178*, AV3-7.

Velten, L., Haas, S.F., Raffel, S., Blaszkiewicz, S., Islam, S., Hennig, B.P., Hirche, C., Lutz, C., Buss, E.C., Nowak, D., et al. (2017). Human haematopoietic stem cell lineage commitment is a continuous process. Nat Cell Biol *19*, 271–281.

MATERIALS AND METHODS

Animals

We used adult 6-12 weeks old C57BL/6 Ly5.2 and Ly5.1 mice obtained from Janvier (Le Genest, France). Mice were bred and maintained in pathogen-free conditions in our Institute Animal facilities Unit for Laboratory Animal Medicine at the Université de Paris. All procedures performed were approved by local Committee on the Use and Care of Animals and by the Institutional Animal Care and Use Committee.

Hematologic evaluations

Orbital plexus blood was collected in EDTA tubes from anesthetized mice. Blood cell counts were determined using automated blood coulter (MS9, Schloessing Melet, Cergy-Pontoise, France). Blood samples were used for cytometry analysis. Serum were collected, stored at -20°C before assessing cytokine levels. **BM and spleen Analysis**

Mice were killed by cervical dislocation. Bones (femurs, tibias, pelvis and humerus) and spleen were harvested, muscle and tendon tissue were removed using a scalpel and kimwipes. BM and spleens were used for cell count, and cytometry.

BM fraction was flushed out using a syringe containing 1xPBS complemented with 2% Fetal Bovine Serum (FBS). The resulting cell suspension were filtered through a 40µM cell strainer (Corning, NY, USA) and pelleted by centrifugation.

For mechanical grinding, spleens were smashed and ground between rough

sides of frosted glass slides, and cells were collected in DMEM containing 2% FBS. After incubation in a 24-well plate for 30min at 37°C in a humidified incubator, cell suspensions were passed through a 40µm cell strainer, and cells were re-suspended in DMEM containing 10%FBS. Suspensions were subjected to cytometry analysis after RBC lysis.

Cytometry analysis

Erythrocytes were lysed using ACK Lysing Buffer (Lonza, Basel, Switzerland) before flow cytometry stainings. Total BM and spleen cells were stained with Zombie Viability kit for 15min at room temperature, and thereafter stained with biotinylated anti-mouse Lineage Cocktail antibodies for 30 min (Biolegend). After washing, cells were stained for 30 min using the following monoclonal antibodies in the BD Horizon Brilliant staining buffer: anti-CD117/c-Kit (2B8)-BB700 and anti-CD34 (RAM34)-AF647 (BD Pharmingen); anti-Ly6a/Sca-1 (D7)-BV510; anti-CD150 (TC15-12F12.2)-PE-Cy7; anti-CD48 (HM48-1)-BV711 ; Streptavidin APC-Cy7 (Biolegend).

For proliferation analysis, surface stainings were performed as described above, and cells were proceeded for cell proliferation according to manufacturer's recommendations (BD Pharmingen BrdU Flow kits) with BrdU-AF488 (BD Biosciences, Franklin Lakes, NJ, USA). Data acquisition and/or data analysis were performed on the Cochin Cytometry and Immunobiology Facility Cytometry analyses on a Fortessa cytometer (Becton Dickinson), and analyses were done on Kaluza software.

To assess cell viability, surface labelled cells were resuspended in AnnexinV binding buffer, and AnnexinV (FITC) was added 15min before analysis (FITC-conjugated AnnexinV labeling detection kit, BD Pharmingen).

Reconstitution assays

Donor cells were isolated from 6-12-week-old B6.SJL-PtprcaPepcb/BoyCrl Congenic mice (Ly5.1) and Ly5.2 mice after Phenylhydrazine (PHZ) (60 mg/Kg, IP) injection or not. From these mice, hind limbs were extracted and cleaned. Total BM were flushed, then passed through a 70µM cell strainer to obtain a single cell suspension. A mix of cells from PHZ-treated mouse and untreated mouse was prepared in a 1:1 ratio. A mix of 5x106 cells were resuspended in a total volume of 0.2 mL and transplanted into 5 irradiated (9Gy) CD45.1 C57/BL6 recipient mice. Chimerism analysis was performed three months post-reconstitution using cytometry.

Statistical analysis

Results are presented as mean ± SD. Data were analyzed through 2-tailed Student t-test.

ACKNOWLEDGMENTS

The authors are grateful to C. Chomienne for helpful discussions and improving the English manuscript. The authors greatly acknowledge the Cochin Cytometry and Immunobiology Facility and the IRSL Animal Facility, Université de Paris.

AUTHORSHIP

CB, SiG, VB, SM conducted modeling of the paper, PG, CL, KB, MHS, EL and StG conducted in vivo experimental procedures, EL and SG performed the analysis of the data. CB, SiG, EL, SM and StG wrote the paper.

DISCLOSURE OF CONFLICT INTEREST. The authors declare no competing financial interests.

TABLES

Cell Type	***n (10^6/mouse)***	***BrdU (%)***
LT-HSC	0.011+/-0.070	2.35+/-2.71
ST-HSC	0.022+/-0.013	0.90+/-0.75
MPP	0.066+/-0.045	6.32+/-3.58
CMP	0.196+/-0.111	12.42+/-2.31
MEP	0.358+/-0.189	31.75+/-1.15
GMP	0.677+/-0.430	19.50+/-7.50

Table 1: Determination of the cell number of each compartment per mouse and the % of BrdU positive cells in steady state hematopoiesis.Each value is the mean of at least 6 mice.

Compartment	**1 LT-HSC**	**2 ST-HSC**	**3 MPP**	**4 CMP**	**5 MEP**	**6 RBC**
Division rate/ day	$\tau_1^*= 0.01$	$\tau_2^*= 0.03$	$\tau_3^*= 0.07$	$\tau_4^*= 0.16$	$\tau_5^*=0.35$	$\tau 6^*= 1/40$
Cell number (10^3/mouse)	$x_1^*= 11$	$x_2^*= 22.5$	$x_3^*= 67$	$x_4^*= 196$	$x_5^*= 359$	$x_6^*= 5.17\ 10^7$
D (Differentiation factor)	$D_1= 0$	$D_2= 0.16$	$D_3= 0.167$	$D_4= 0.174$	$D_5= 0.176$	

Table 2: Determination of the division rate/day, the size, and the differentiation factor for each compartment at steady state.

Proliferation rate	$r_1= 9.2$	$r_2= 6.4$	$r_3= 6.4$	$r_4= 2.8$	$r_5= 0.33$
Erythroid Differentiation rate	$d_1=10$	$d_2=8.4$	$d_3=7.7$	$d_4=7.4$	$d_5=4.3$
Regulator clearance (/day)	$m_1=0.03$	$m_2=0.2$			
Constants of the regulators production functions	$a= 10^{-4}$	$b= 100$			
Last mitosis number	$c_1=1.18$	$c_2= 31.3$			
Steady state value of regulator u_1	$u^*_1=1/(m_1(a+5))$				
Steady state value of regulator u_2	$u^*_2=5/(m_2(b+5))$				

Table 3: Constants of proliferation and erythroid differentiation rate of compartments; regulator parameter values and mitosis number from MEP to mature RBC after stress._

Cell type division rate value (/day)	***LT-HSC***	***ST-HSC***	***MPP***	***CMP***	***MEP***
Day 0	$\tau_1^* = 0.01$	$\tau_2^* = 0.03$	$\tau_3^* = 0.07$	$\tau_4^* = 0.16$	$\tau_5^* = 0.35$
Day 5	0.37	0.24	0.57	0.28	0.21
Day 11	0.97	1.4	2.4	2.7	2
Day 16	0.12	0.14	0.34	0.33	0.48

Table 4: Division rates at different time points in the different compartments after PHZ administration.

FIGURE LEGENDS

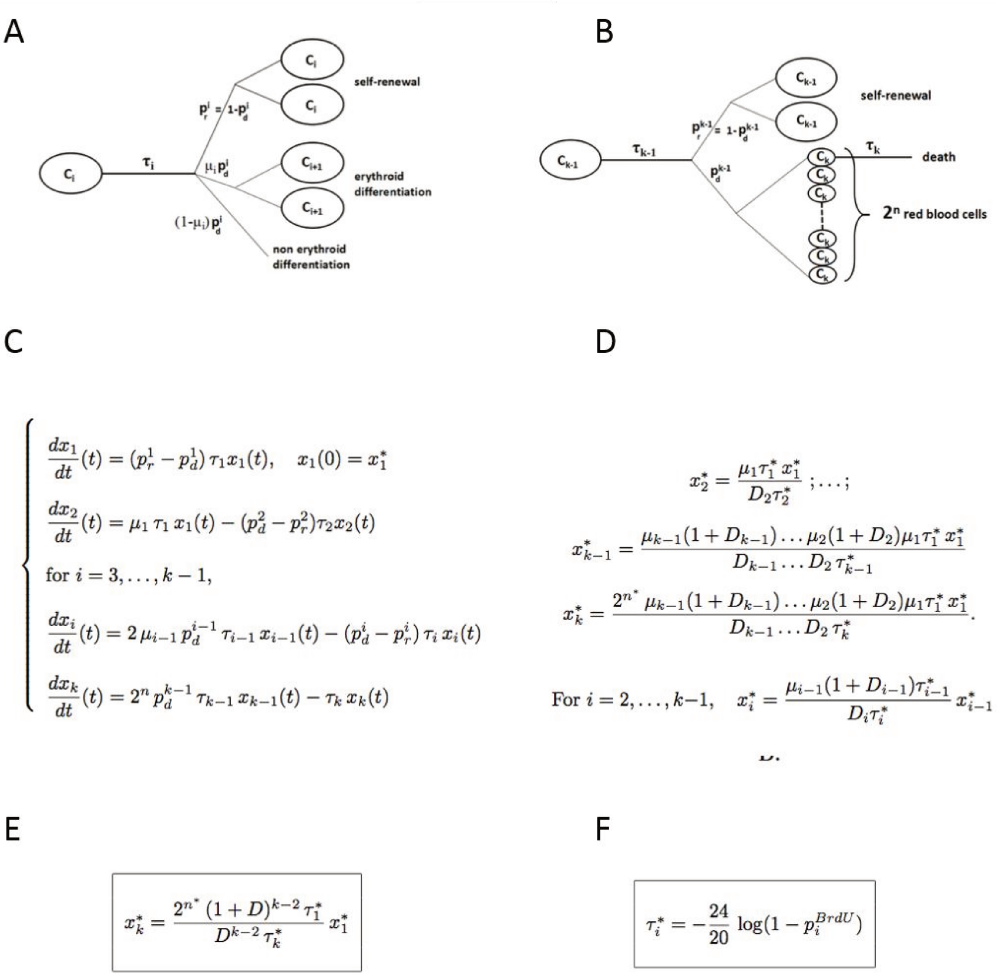

Figure 1: Mathematical parameters required to model steady state Erythropoiesis.

(*A*) Scheme of the cell dynamics of i = 1 to k-2 cell type. *C_i : cell of i-type. τ_i : division rate of i-type cells. (B)* Scheme of the cell dynamics of the two last compartments. *τ_{k-1} : division rate of (k-1)-type cells. τ_k : death rate of RBC (k-type cells). (C)* Differential system modeling steady-state erythropoiesis. *τ_i : division rate of i-type cells. τ_k : death rate of RBC dx_i/dt (t) : derivative of the x_i function at t time. 2^n : number of RBC (type k cells) generated after differentiation of (k-1)-type cell. (D)* Steady state values according to Figure 1C depending on differentiation factors $D_i = p^i_d - p^i_r$. (*E*) Estimation of the RBC number at equilibrium, for the differentiation factors D_i, i=2,⋯,k−1, equal to D and the μ_i probabilities equal to 1. (*F*) Estimation of the division rate at equilibrium for each cell type based on BrdU data. p_i^{BrdU} : proportion at steady-state of $BrdU^+$ i-type cells 20 hours after BrdU incorporation. (see Figure S1 and supplemental information in supplemental appendix).

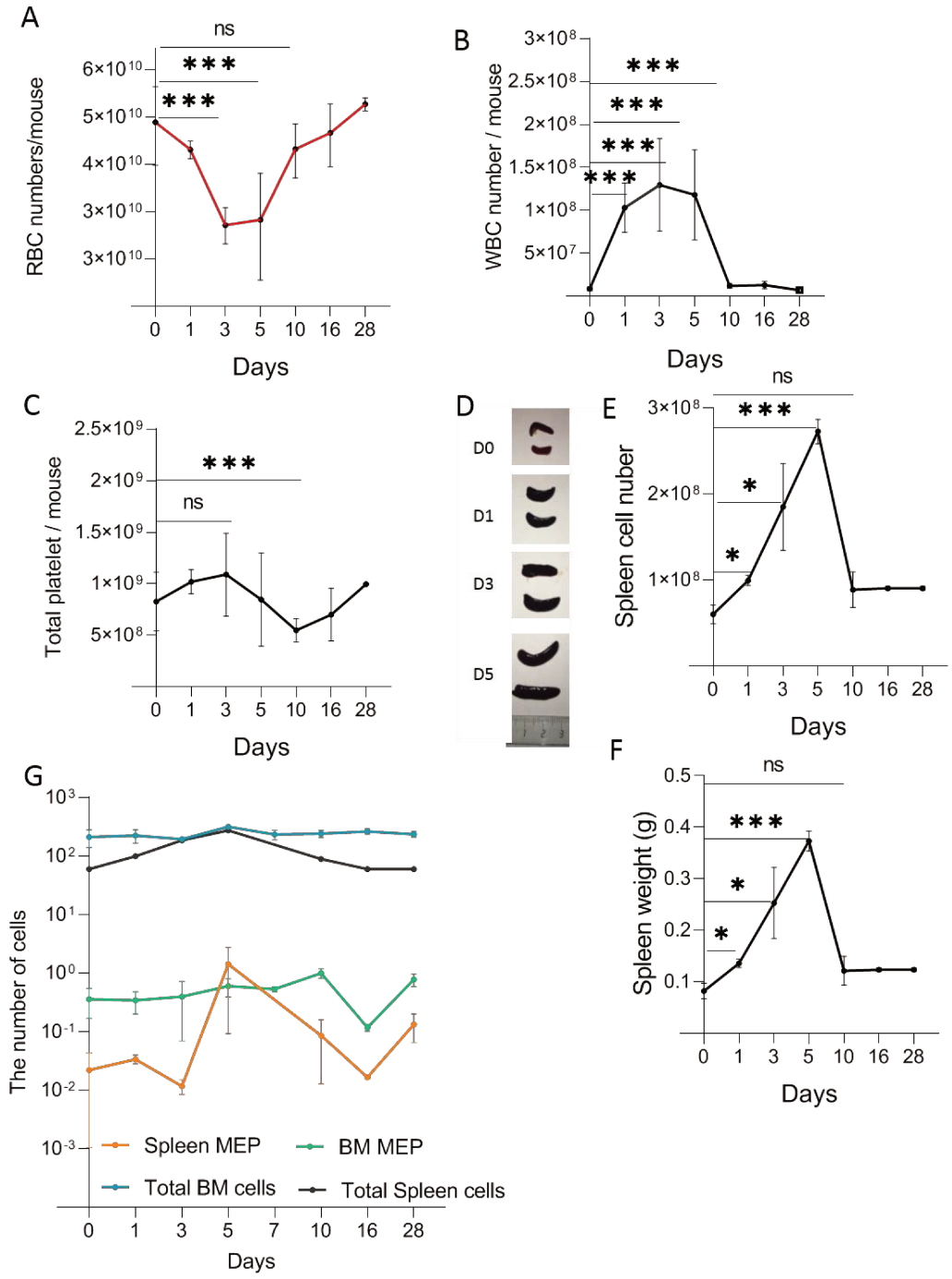

Figure 2: Analysis of Blood, Spleen and BM parameters after PHZ-mediated chemical hemolysis.

Mice were injected with PHZ (60 mg/kg). Blood, BM and spleen were harvested at the indicated times. (*A*) RBC counts (x10^9/mouse) (orange line, biological values, black line, computed values). (*B*) White blood cells (x10^6/mouse) and (*C*) platelets (x10^6/mouse). (*D*) Spleen morphological changes (photographs at day 0, 1, 3 and 5). (*E*) Total spleen cell number per mouse (x10^6/mouse). (*F*) Spleen weight variations. (*G*) Follow-up of total cell and MEP numbers for BM and Spleen (total bone marrow cells, blue line; total spleen cells, black line; Spleen MEP, Green line; BM MEP, orange line). Mean ± SEM of at least 4 mice. * $p<0.05$, *** $p<0.01$.

A

$$\begin{cases} p_r^i(t)\,\tau_i(t) = p_r^i\,\tau_i^*\left(\dfrac{u_r(t)}{u_r^*}\right)^{r_i} \\ \mu_i(t)\,p_d^i(t)\,\tau_i(t) = \mu_i\,p_d^i\,\tau_i^*\left(\dfrac{u_d(t)}{u_d^*}\right)^{d_i} \end{cases}$$

where $(r_i)_i$, $(d_i)_i$, u_r^* and u_d^* are positive parameters.

B

$$\begin{cases} \dfrac{du_r(t)}{dt} = \dfrac{1}{a+y(t)} - m_r\,u_r(t) \\ \dfrac{du_d(t)}{dt} = \dfrac{y(t)}{b+y(t)} - m_d\,u_d(t) \end{cases}$$

with $y(t) = \dfrac{x_1(t)}{x_1^*} + \dfrac{x_2(t)}{x_2^*} + \dfrac{x_3(t)}{x_3^*} + \dfrac{x_4(t)}{x_4^*} + \dfrac{x_5(t)}{x_5^*}$

C

$$n(t) = n^* \frac{c_1}{1+(c_1-1)\left(\frac{x_6(t)}{x_6^*}\right)^{c_2}}.$$

Figure 3 : Mathematical parameters required to Model stress Erythropoiesis.

(*A*) Effects of u_r and u_d regulators on self-renewal and differentiation rates. $p^i_r(t)$: self-renewal probability at t time of i-type cells. $p^i_d(t)$: differentiation probability at t time of i-type cells. $u_r(t)$) : self-renewal regulation effect at t time. $u_d(t)$: Differentiation regulation effect at t time r_i : sensitivity of the i-type cell to u_r regulator. d_i sensitivity of the i-type cell to u_d regulator. (*B*) Dynamics of the u_r and u_d regulators. du_r /dt (t) : derivative of the u_r function at t time (similar notation for u_d). $u_r(t)$ and $u_d(t)$: self-renewal and differentiation regulation effect at t time. a >0 and b>0: Michaelis-Menten's type constant of the u_r and u_d regulator. m_r and m_d : clearance rate of the u_r and u_d regulators. *(C*). Regulation of the terminal erythroid production (from MEP to RBC). $2^{n(t)}$: number of RBC (k-type cells) generated after differentiation of a (k-1)-type cell at time t. c_1>1 and c_2 >0 : Hill constants of the regulated terminal mitosis of erythropoiesis. τ_i^* : steady-state division rate of i-type cells. p^i_r : steady-state self-renewal probability of i-type cells. p^i_d : steady-state differentiation probability of i-type cells. μ_i: steady-state erythro-myeloid commitment probability of i-type cells. $x_i(t)$: number of i-type cells at t time. x_i^* : steady-state number of i-type cells. 2^{n^*} : steady-state number of RBC (type k cells) generated after differentiation of a (k-1)-type cell. k: number of compartments considered.

A

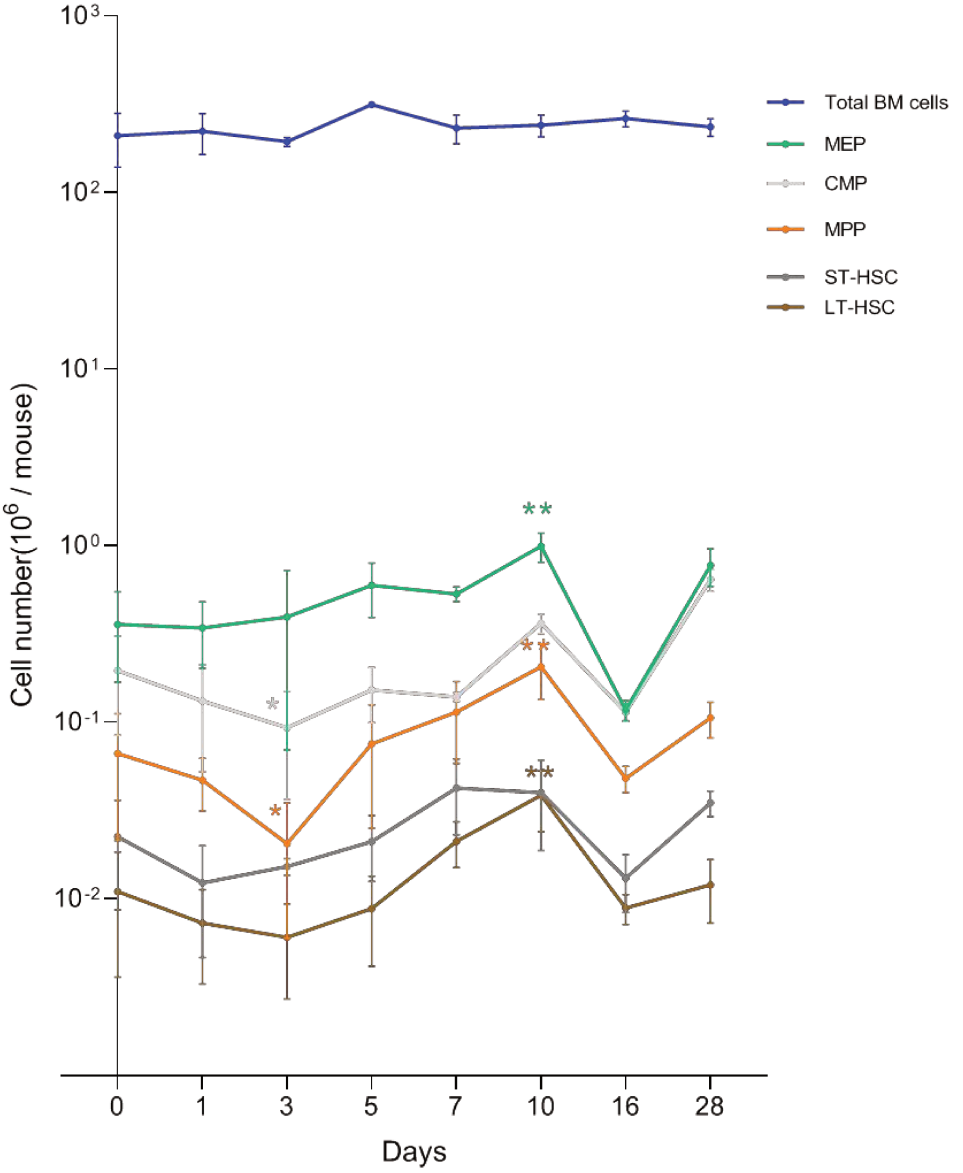
Total BM cells
MEP
CMP
MPP
ST-HSC
LT-HSC
Cell number(10^6 / mouse)
10^3
10^2
10^1
10^0
10^{-1}
10^{-2}
0
1
3
5
7
10
16
28
Days
*
**
**
*
**

B

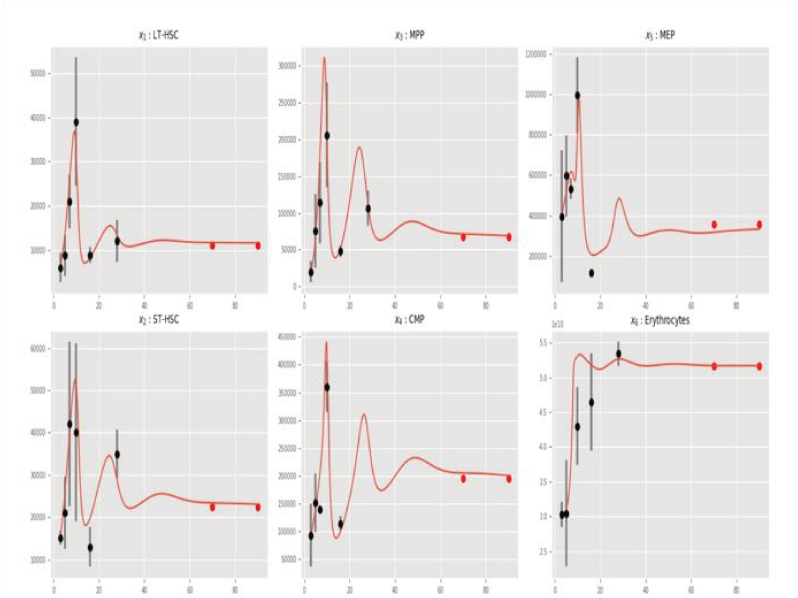
LT-HSC
MPP
MEP
ST-HSC
CMP
Erythrocytes

Figure 4: Evolution of experimental and model parameters after PHZ-mediated chemical hemolysis.

Blood Red Cell and bone marrow cell numbers per mouse (x10^6/mouse) assessed from experiments (red points: Red Blood cells, blue points: Total BM cells, green points: BM MEP, grey points: BM CMP, orange points: BM MPP, dark blue points: BM ST-HSC, brown points: BM LT-HSC). * p<0.05, ** p<0.01. (*B*). Experimental data generate values and standard errors from each time points. Evolution curves are deduced from the modeling and represent the number of cells corresponding to the x_i^* given in Table 2 (See supplemental information).

STAR METHODS

Reagent or Resource	Source	Identifier
Antibodies		
Biotin anti-mouse Lin Panel	Biolegend	133307
Ter-119, M1/70, RB6-8C5, 145-2C11, RA3-6B2,		
A PC/Cy7 Streptavidin	Biolegend	405208
BV 510™ anti-mouse Ly-6A/E (Sca-1-) D7	Biolegend	108129
BV421 anti-mouse CD135 A2F10	Biolegend	135315
BV711 anti-mouse CD48 HM48-1	Biolegend	103439
PE/Cy7 anti-mouse CD150 TC15-12F12.2	Biolegend	115914
BB700 Anti-Mouse CD117 (PerCP) 2B8	BD Pharmingen	566414
BV786 Anti-Mouse CD16/CD32 2.4G2	BD Pharmingen	740851
Alexa Fluor® 647 anti-Mouse CD34 Ram34	BD Pharmingen	560230
Alexa Fluor 488 anti-BrdU Antibody	Biolegend	364105
FITC anti-mouse CD45.1 A20	Biolegend	110705
PE anti mouse CD45.2 104	Biolegend	109808
Chemicals, Peptides, and Recombinant Proteins		
PHZ (Phenylhydrazine)	Sigma-Aldrich	P26252
Critical Commercial Assays		
Zombie UV fixable viability kit	Ozyme	BLE423107
BD Horizon Brilliant staining buffer	BD Pharmingen	563794
Ultracomp ebeads	Life Technologies	01-2222-42

Rainbow Calibration Particles (8 - PEaks), 3.0-3.4 mm SPHERO Particles	BD Pharmingen	559123
BD Pharmingen BrdU Flow Kit	BD Pharmingen	557892
FITC Annexin V Apoptosis Detection Kit	BD Pharmingen	559763
ACK Lysing Buffer, Quality Biological	VWR	10128-802

Experimental Models: Organisms/Strains

C57BL/6J	Janvier (Le Genest, France)
B6.SJL-Ptprc^{a}Pepc^{b}/BoyCrl Congenic (Ly5.1 mice)	Janvier (Le Genest, France)

Software and Algorithms

Diva software	Beckman
Kakuza software	Beckman
Covariance matrix adaptative in Evolution algorithm (CMAES)	Python language

SUPPLEMENTAL FIGURES

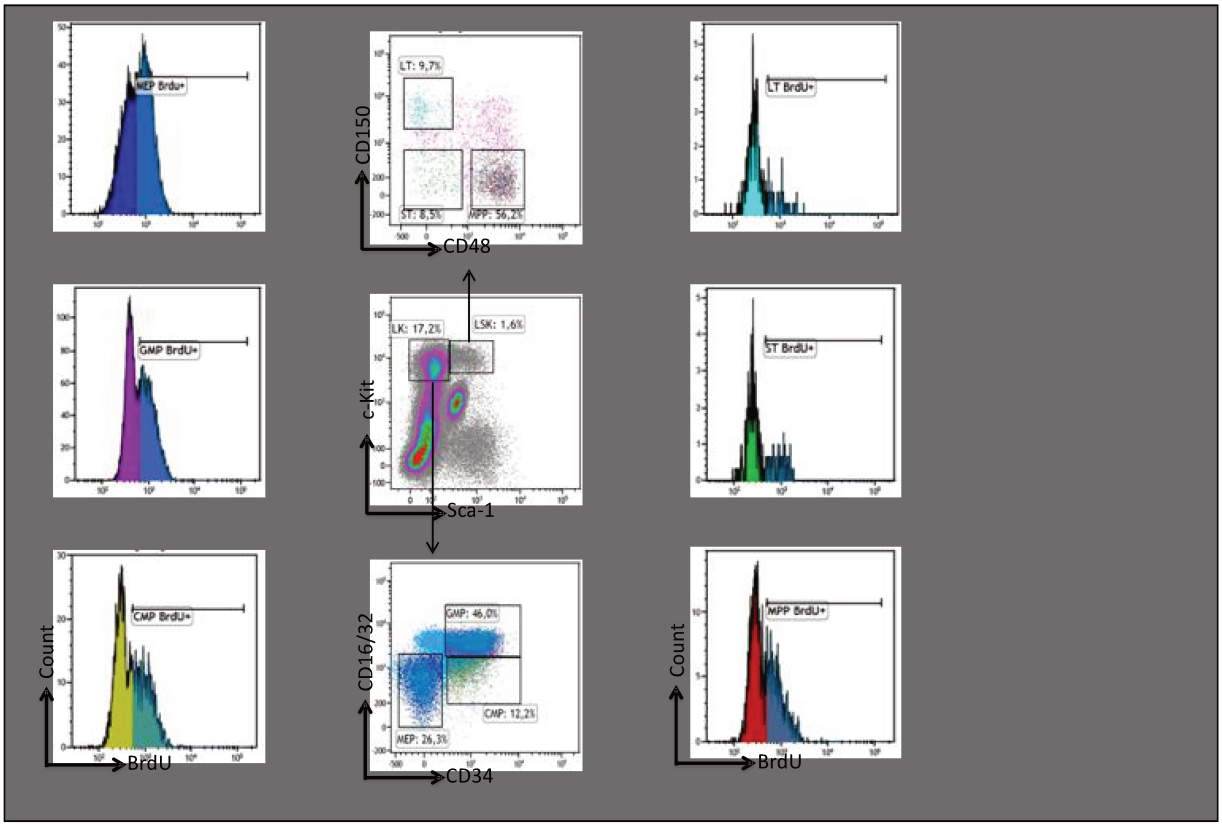

Figure S1: Single staining 9-parameter analysis of mouse bone marrow cells.

After RBC lysis, cellular debris or doublets were discriminated from single cells by analyzing the side scatter area and width signals. Single cells were then stained with the life/dead discriminator (Zombie), and alive cells were then plotted for lineage markers (CD3e, CD11b, B220, Gr1, and Ter119). Lineage negative cells were analyzed for c-Kit and Sca-1 to define the LSK and LS-K cell populations. LS-K cells were discriminated by expression of CD16/32 and CD34 to identify GMP, CMP and MEP populations. LSK cells were discriminated by expression of CD150 and CD48 to identify LT-HSC, ST-HSC and MPP populations. BrdU incorporation was assessed in all these populations.

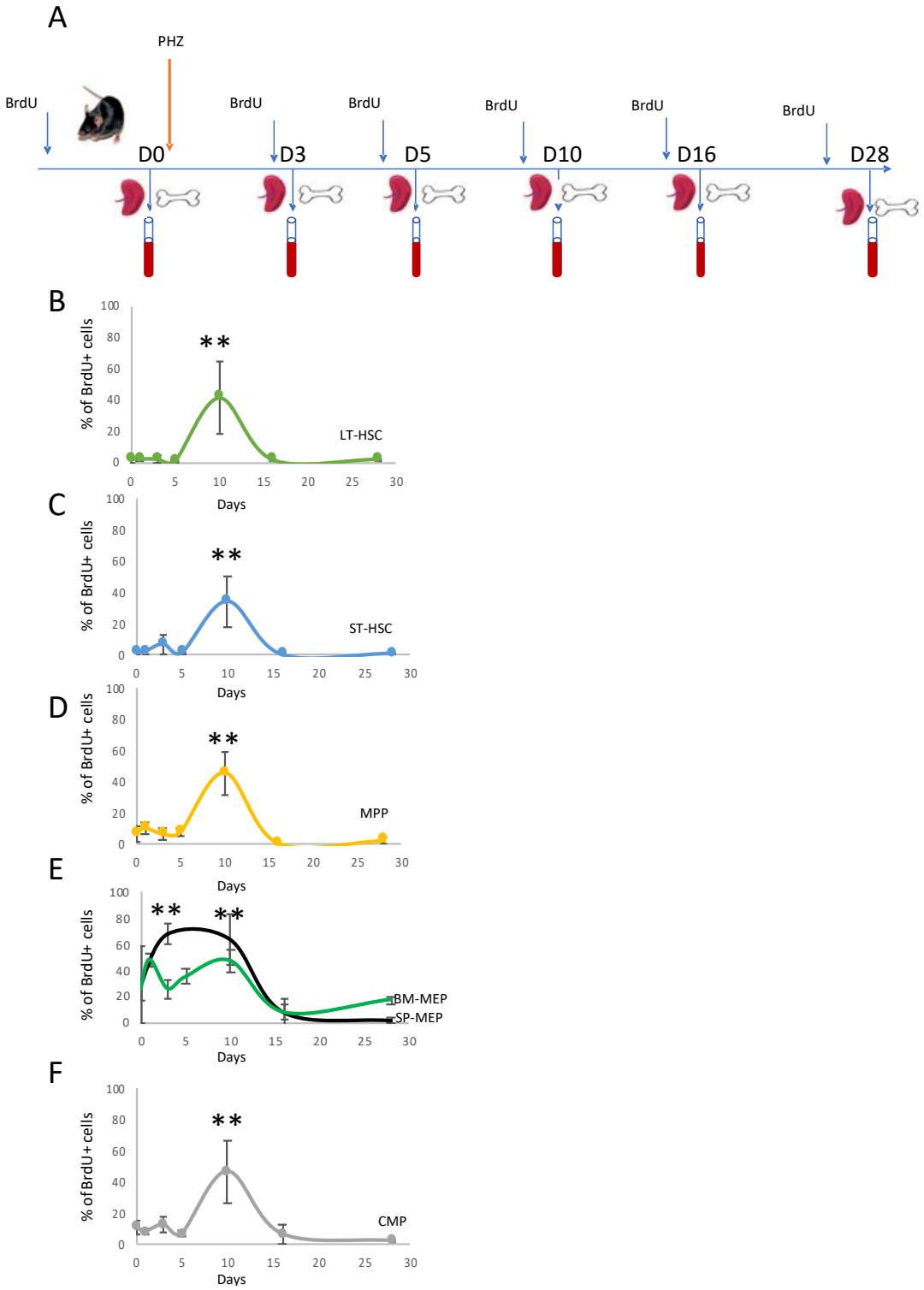

Figure S2: Analysis of BrdU incorporation in HSPCs at different time points after PHZ administration. *(A)* Summary scheme of PHZ treatment. (*B-F*) Percentage of BrdU$^+$ cells 16h after intraperitoneal BrdU injection. (*B*) BM LT-HSC, (*C*) BM ST-HSC, (*D*) BM MPP, (*E*) MEP from BM (green) and spleen (black), (*F*) BM CMP. ** p<0.01 (n=5).

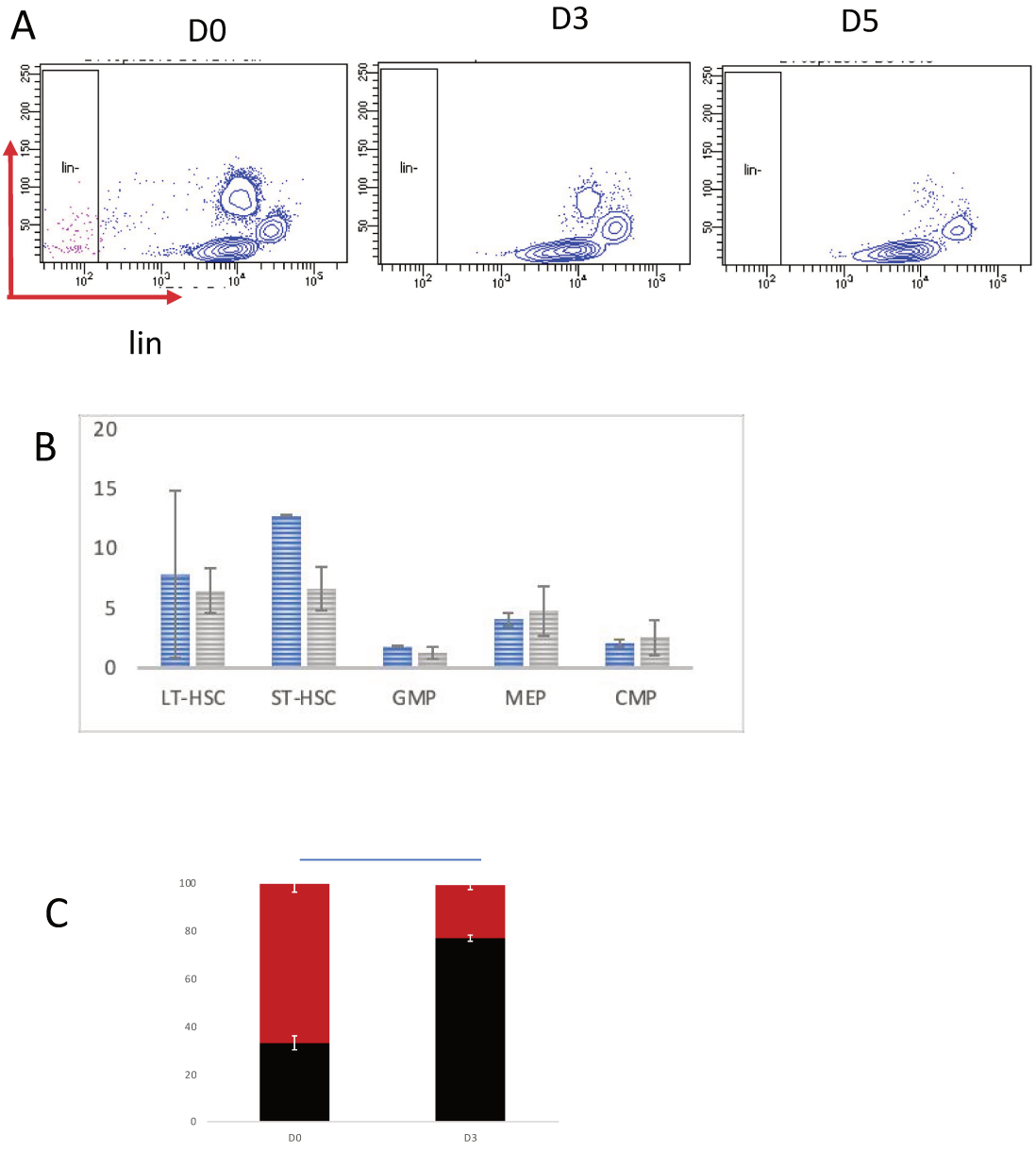

Figure S3: Analysis of peripheral blood, BM and spleen after PHZ administration.

(*A*) Cytometric analysis to detect the presence of Lin^- cells in the peripheral blood. (*B*) Cytometric analysis of apoptosis (AnnexinV positive cells) in the different progenitor compartments at day 3 after PHZ treatment. (*C*) Three days after PHZ administration, lethally irradiated C57BL/6-Ly5.1 mice received 10^6 BM cells from PHZ-treated C57BL/6 (Ly5.2) mice, in competition with the same amount of BM cells from Ly5.1 mice. Presence of CD45.2+ PB cells of engrafted mice was assessed 3 months later by flow cytometry. Data are expressed as mean ± SEM. **P < .01; (Student t test).

SUPPLEMENTAL DATA

1- Complementary informations for Figure 1*F*.

Table 1 presents the % of $BrdU^+$ cells of each compartment at the steady state, which corresponds to the proportion of cells having performed at least one division during 20 hours. Here, we will relate these informations to the steady-state division rates of each cell type: τ_i^*. Before BrdU injection, the system is at equilibrium and all cells are unlabeled by BrdU. The numbers of $BrdU^+$ and unlabeled i-type cells at time t of the experiment are denoted by $N_i^m(t)$ and $N_i(t)$. Then $N_i^m(0)=0$ and $N_i(0)=x_i^*$.

During the experiment, when an unlabeled cell of i type divides, it becomes $BrdU^+$. Thus the dynamics of unlabeled i-type cell number is expressed as an exponential decrease at τi^* rate. Throughout the experiment, the system is considered to be at steady state. Therefore, for any i = 1,...,k-1, and for any $t \in [0,24h]$, $N_i^m(t) + N_i(t) = x_i^*$. The formula in Figure 1F is then deduced

2- Calibration of the regulated-erythropoiesis model

Parameters of the regulated model were calibrated from data of the 6 population sizes dynamics after PHZ induced hemolysis. In order to model the return to the equilibrium (given in Figure 4B), we considered day 3 as the initial time. Hence initial conditions of the model are given by : $x_1(\text{day 3}) = 0.006 \cdot 10^6$ cells/mouse, $x_2(\text{day 3}) = 0.0152 \cdot 10^6$ cells/mouse,

x_3(day 3) = 0.02 . 10^6 cells/mouse, x_4(day 3) = 0.093 . 10^6 cells/mouse,

x_5(day 3) = 0.395 . 10^6 cells/mouse, x_6(day 3) = 0.94 . 10^{10} cells/mouse.

Using a stochastic optimization algorithm based on a CMA-ES method (Covariance Matrix Adaptation Matrix in Evolution Strategy), developed on Python by the INRIA team RandOpt (Hansen and Ostermeier, 2001) and least-squares cost function, we minimized the discrepancy between *in silico* simulated and experimental data. Results were summarized in Table 3. In such algorithms, identifiability is numerically accepted when identical results for a large number of independent runs are obtained.

References

Hansen, N., and Ostermeier, A. (2001). Completely derandomized self-adaptation in evolution strategies. Evolutionary Computation *9*, 159–195.

3.2 Part2. Genomic and Functional impact of TP53 mutations in JAK2V617F myeloproliferative neoplasms.

Short Title: JAK2V617F & TP53mut in MPN

Panhong Gou[2,3], Saravan Ganesan[#2,3], Evelyne Lauret[5], Veronique Montcuquet[2,6], Véronique Meignin[2,7], Nabih Maslah[1,2,3], Jean-Jacques Kiladjian[2,3,4] Bruno Cassinat[1,3##], and Stephane Giraudier[1,2,3]

[1] Service de Biologie Cellulaire, Hôpital Saint-Louis, APHP, Paris, France

[2] Université de Paris, Paris, France

[3]INSERM UMR-S 1131, Hôpital Saint-Louis, Paris, France

[4]Centre Investigations Cliniques, Hôpital Saint-Louis, Paris, France

[5]Université de Paris, Institut Cochin, INSERM U1016, CNRS UMR 8104, F-75014 Paris, France

[6]Animal Facility Unit, IRSL, Université de Paris , Paris, France

[7]Histo-pathological Department, Hôpital Saint-Louis, Paris, France

Keywords: Myeloproliferative neoplasms, *TP53* mutation, JAK2V617F, Interferon a,

Corresponding author: Pr Stephane Giraudier
INSERM UMR-S 1131,
Hopital Saint-Louis
1 Avenue Claude Vellefaux
75010, Paris, France
Phone: +33 1 42 49 94 02
Fax: +33 1 42 38 54 76
Email: stephane.giraudier@aphp.fr

INTRODUCTION

Classical myeloproliferative neoplasms (MPNs) are hematopoietic disorders characterized by clonal proliferation of mature myeloid elements which manifests clinically as an excess of red blood cells, platelets and / or white blood cells[1]. Mutations in kinases such as JAK2 have been identified in the majority of patients with PV, ET, and PMF, underscoring the importance of activated transduction signaling in the pathogenesis of these disorders[2–6]. Despite the use of empiric and targeted therapies, a subset of MPN patients transforms to secondary acute myeloid leukemia (AML). The outcome of such transformation remains desperately poor with a median survival of less than 6 months[7]. Advanced age (>60 y), exposure to chemotherapy and mutations of genes involved in splice remodeling, structure of DNA or cell cycle (just like TP53) increase the risk of leukemic transformation [7–9]

TP53 mutations have been described as associated to post-MPN AML transformation in 25-50% of cases[10,11] suggesting that inactivation of P53 anti-oncogene could be a cooperating event in transformation in combination with over-signaling due to JAK2 gain of function mutation.

Preclinical data implicating mouse models with JAK2V617F retrovirally overexpressed in inactivated *TP53* cells suggest that the combination of this sole abnormality in a JAK2V617F overexpressing cell could be sufficient to cause acute transformation[12]. However, clinical data tempered these results since AML is unusual (∼5% of associated malignancies) among Li-Fraumeni

syndrome associated with germline *TP53* mutations [13,14] and also because long survival patients with chronic phase MPN and harboring *TP53* mutations have been described[15–17].

Recent study suggests that more than the existence of *TP53* mutation, the quantity of *TP53* mutated cells could be responsible for the transformation, then, “small TP53 mutated clones” could have a neutral impact when larger clones could be detrimental[16,18,19] . In order to better define the impact of *TP53* mutations in MPN evolution, we studied mice combining *TP53* inactivation and JAK2V617F mutation expressed at a “normal” level and not overexpressed via a viral ectopic overexpression. Altogether our data suggest that *TP53* inactivation and *JAK2* mutation expressed at a “physiological” level may facilitate clonal progression and resistance to therapies but are not sufficient to induce transformation of chronic phase MPN suggesting that acute transformation of such pathologies may require more than two hits.

RESULTS

1. Constitutive expression of JAK2V617F/Vav-Cre in TP53 inactivated cells results in MPN-like phenotype

We get the JAK2V617F conditional allele mice from Dr. Villeval (**Figure 14**). We crossed the JAK2V617F conditional allele mice with Vav-Cre TG mice to generate the JAK2V617F/Vav-Cre mice. In order to know the function of TP53 inactivation in the background of JAK2V617F, we created JAK2V617F/Vav-Cre/TP53KO mice as shown in methods.

Blood counts demonstrated a similar phenotype in JAK2V617F mice and JAK2V617F/Vav-cre/TP53$^{-/-}$ mice. WBC of JAK2VF/Vav-cre (43.12 ± 12.10 G/L) and JAK2V617F/Vav-Cre/TP53$^{-/-}$(48.30 ± 12.83 G/L) was significantly higher (4 folds) than the control mice (9.94 ± 1.18 G/L) one month after birth and continues to rise at the second (54.78 ± 15.91 G/L) and third month (66.73 ± 27.07 G/L respectively for JAK2V617F/Vav-Cre/TP53$^{-/-}$). Hematocrit in JAK2V617F/Vav-Cre/TP53$^{-/-}$ mice was increased (61.89% ± 9.70%) at one month as compared to 67.87% ± 8.19% in JAK2VF/Vav-Cre mice. The Platelet count was higher than normal level at on month in both JAK2V617F/Vav-Cre and JAK2V617F/Vav-Cre/TP53$^{-/-}$ mice. Patelet count of JAK2V617F/Vav-Cre continues to rise from 1571 G ± 491 G/L to 3497 ± 948 G/L with age, JAK2V617F/Vav-Cre/TP53$^{-/-}$ mice having the same trend of increase from one month-old to three months-old animals (Figure 17A, 17B, 17C). Blood smears analysis was not able to detect blast cells at one or three months of age both in JAK2V617F/Vav-cre mice and JAK2V617F/Vav-cre/TP53$^{-/-}$ mice.

Spleen weights were enlarged in the same order of magnitude (5-fold at three months) in both JAK2V617F/Vav-cre and JAK2V617F/Vav-cre/TP53$^{-/-}$ mice and increased gradually during time in both backgrounds. (Figure 17E).

Bone marrow histological analysis were performed at one and three months. As previously reported, the megakaryocytic density of JAK2VF/Vav-Cre mice was higher than observed in normal mice, just as observed in myeloproliferative neoplasms in humans. No difference was observed in

JAK2V617F/Vav-Cre/TP53$^{-/-}$ mice compared to JAK2V617F/Vav-cre mice. Older-age mice do not reveal differences between these two backgrounds. Because mice were relatively young, reticulin fiber deposits were not prominent in JAK2V617F/Vav-Cre at one or three months but neither in JAK2V617F/Vav-Cre/TP53$^{-/-}$ mice(Figure 17D).

Lastly, survival analysis showed that the JAK2V617F/Vav-Cre mice median survival was around two months when no treatment (or venesections) were performed but TP53 inactivation did not shortened JAK2V617F/Vav-Cre mice lifespan (Figure 17F).

Collectively, these data show that heterozygous endogenous JAK2V617F expression in hematopoietic cells leads to hyperplasia of mature and maturing erythroid, granulocytic, and megakaryocytic cells in blood and hematopoietic tissues whatever the p53 status, suggesting that the JAK2V617F induced phenotype is TP53 independent.

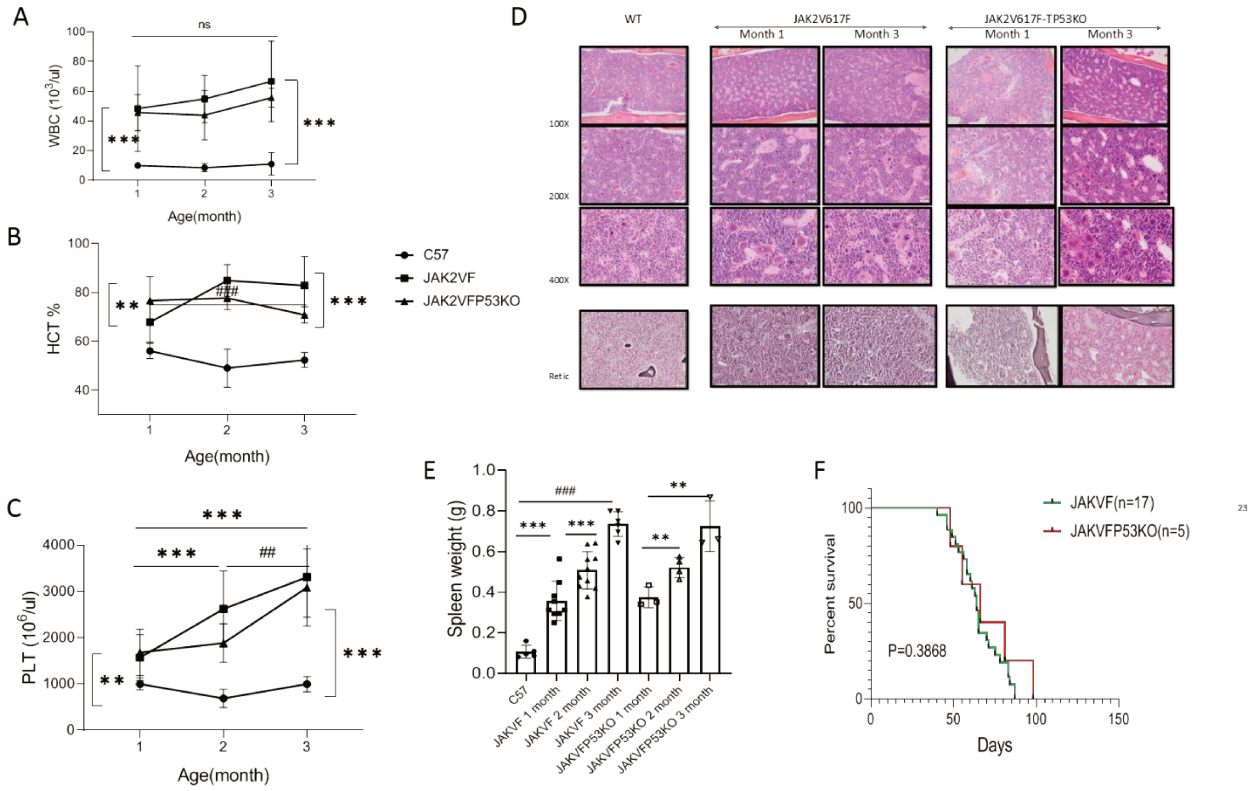

Figure 17: The inactivation of TP53 does not transform the JAK2V617F-induced MPN phenotype into AML.

(A-C) Data of cell count of PB from JAK2V617F/Vav-Cre, JAK2V617F/*Vav-Cre*/TP53$^{-/-}$ and C57Bl/6 mice (A: white blood cell, B: hematocrit, C: platelete.The black round dot is the C57 mice; black square is JAK2V617F/*Vav-Cre* mice; black triangle is JAK2V617F/*Vav-Cre*/TP53$^{-/-}$ mice). (D) Histopathologic characterization of the BM. The first column was the BM of C57Bl/6, second column was one month-old JAK2V617F/*Vav-Cre* BM, third column was three month-old JAK2V617F/*Vav-Cre* BM, fourth column was one month-old JAK2V617F/*Vav-Cre* /TP53$^{-/-}$ BM, and fifth column was three month-old JAK2V617F/*Vav-Cre* /TP53$^{-/-}$BM. The first row to third row are respectively the 100 ×, 200 ×, and 400 × objective. The fourth row was sliver staining and the others are hematoxylin and eosin (HE) staining (E) The spleen weight from C57Bl/6 mice, JAK2V617F/*Vav-Cre*, and JAK2V617F/*Vav-Cre*/TP53$^{-/-}$ at one to three month-old.(F) Percent survival of JAK2V617F/*Vav-Cre*, and JAK2V617F/*Vav-Cre*/TP53$^{-/-}$ mice.

2 TP53 inactivation confers a proliferative advantage to JAK2V617F cells

As previously described, endogenous JAK2V617F expression increases early stages of differentiation (cell numbers) and proliferation. We then analyzed immature cell populations frequencies and absolute numbers in JAK2V617F/Vav-cre and JAK2V617F/Vav-cre/TP53$^{-/-}$ mice and their proliferative

capacities in vivo. We firstly analyzed by flow cytometry LT-HSC, ST-HSC, MPP, CMP, MEP and GMP cells at 2 to 3 months of age. At these ages, bone marrow cellularity was not affected by either molecular change. Mice demonstrated in marrow no change in the numbers of Lin^- cells, GMP or MEP but an increase in most immature LSK, LT-HSC, and MPP cells when compare to normal mice (Figure 18D). These increases in cell numbers were noticed in JAK2V617F/Vav-cre mice as well as in JAK2V617F/Vav-cre/$TP53^{-/-}$ mice and were in the same order of magnitude. (Figure 18D). In the spleen, the percentages of LK, LSK, CMP, GMP and MEP and the more immature LT-HSC and ST-HSC and MPP were drastically increased as previously observed, but these features were also found in JAK2V617F/Vav-cre/$TP53^{-/-}$ mouse spleens (Figure 18E). These results show that endogenous JAK2V617F amplifies all stages of differentiation but TP53 inactivation do not increase these frequencies suggesting that JAK2V617F immature cells proliferation is TP53 independent.

In order to confirm the lack of proliferative advantage compared to JAK2V617F/Vav-cre cells in the most immature compartments induced by TP53 inactivation, BrdU analysis was conducted.

BrdU positive S-phase fraction of DNA-synthesizing cells was statistically increased in BM LT-HSC from JAK2V617F/Vav-cre mice whatever the TP53 status and not different in the two backgrounds of mice and this finding was limited to LT-HSC immature compartments in BM (Figure 18F).

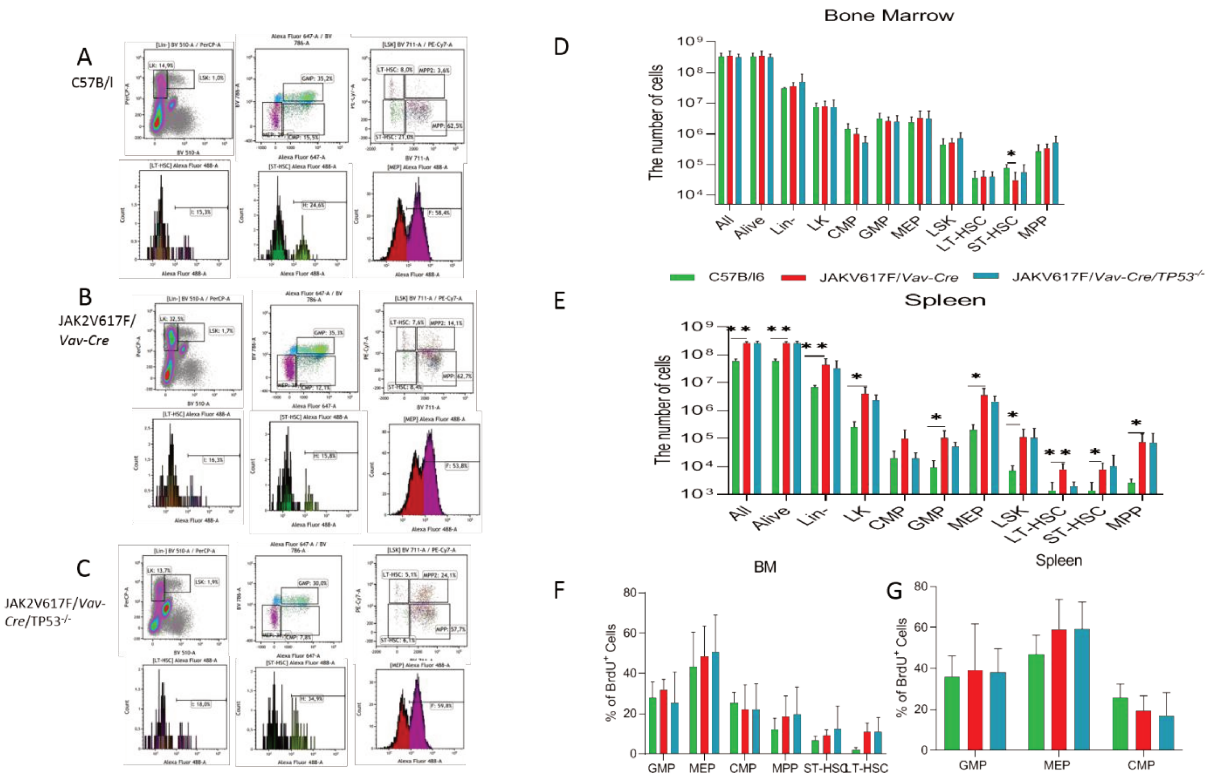

Figure 18: Inactivation of TP53 does not lead to expansion of immature progenitors in JAK2V617F/Vav-Cre mice.

(A-C) Representative flow cytometric plots of BM cells from C57B/l, JAK2V617F/*Vav-Cre*, and JAK2V617F/*Vav-Cre*/p53$^{-/-}$ mice. (D)The total number of all cells, alive cells, Lin^{-} cells, LK cells, CMP cells, GMP MEP LSK LT-HSC ST-HSC MPP from C57B/l6, JAK2V617F/*Vav-Cre*, and JAK2V617F/*Vav-Cre*/p53$^{-/-}$ mice bone marrow. (E) The total number of all cells, alive cells, Lin^{-} cells, LK cells, CMP cells, GMP MEP LSK LT-HSC ST-HSC MPP from C57B/l6, JAK2V617F/*Vav-Cre*, and JAK2V617F/*Vav-Cre*/p53$^{-/-}$ mice spleen.(F) The percentage of BrdU^{+} cells in progenitor and stem cell populations in C57B/l6, JAK2V617F/*Vav-Cre*, and JAK2V617F/*Vav-Cre*/p53$^{-/-}$ mice bone marrow. (G) The percentage of BrdU^{+} cells in progenitor and stem cell populations in C57B/l6, JAK2V617F/*Vav-Cre*, and JAK2V617F/*Vav-Cre*/p53$^{-/-}$ mice spleen. Data are mean ± s.d. *P<0.05, **P<0.01

However, because BrdU analysis can have a relatively low sensibility to modest changes in cell proliferation and particularly in rare populations such as LT-HSC, repopulation competitions were performed using CD45.2 JAK2V617F/Vav-Cre

mice and CD45.2 TP53 inactivated JAK2V617F/Vav-Cre mice as donors in competition with CD45.1 normal mice.

We firstly performed CD45.1 normal BM cells and CD45.2 JAK2V617F/Vav-Cre BM cells or CD45.1 normal BM cells and CD45.2 JAK2V617F/Vav-Cre/TP53$^{-/-}$ BM cells competitions. Whatever the TP53 status, the JAK2V617F cells have a huge advantage on normal cells, chimerism analysis performed 3 months after graft showing a >90% of JAK2V617F/Vav-Cre CD45.2 cells(Figure 19B-C). In all cases, mice developed a MPN phenotype during the first two months and half life expectancy of grafted mice was reduced to 100 to 120 days. (Figure 19A).

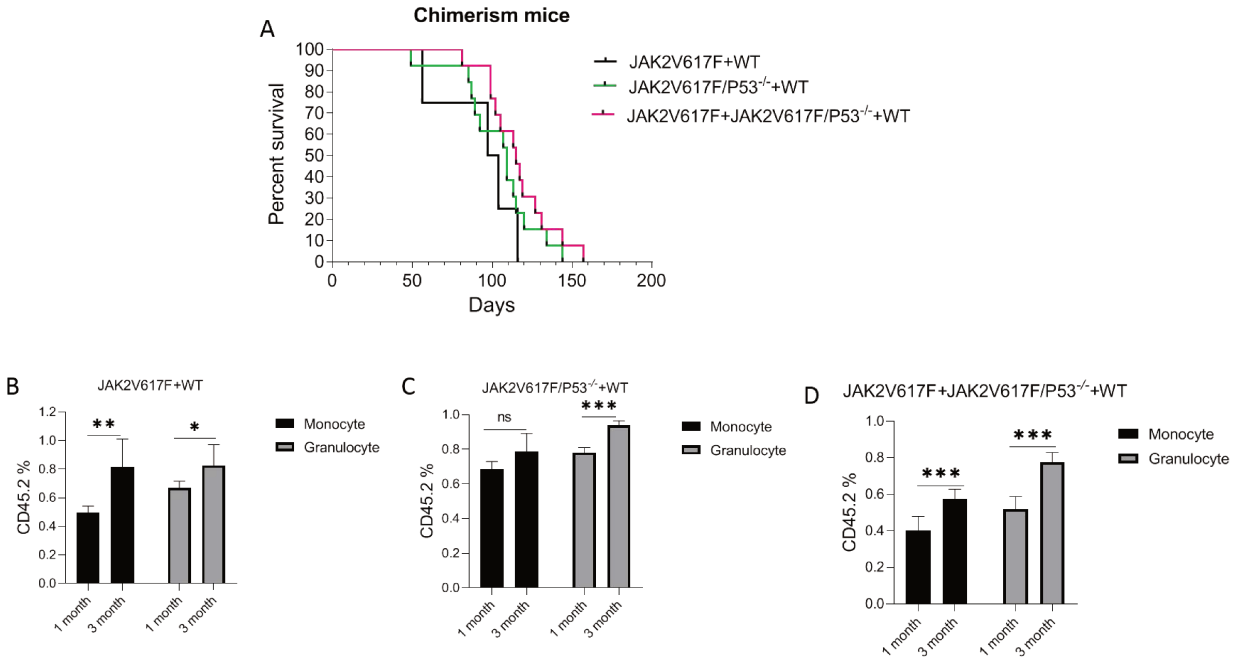

Figure 19: Competitive graft of JAK2V617F/Vav-Cre and JAK2V617F/Vav-Cre/TP53$^{-/-}$ murine cells

(A)The survival of JAK2V617F/Vav-Cre (50%) + WT (50%); JAK2V617F/Vav-Cre/TP53$^{-/-}$ (50%) + WT (50%); and JAK2V617F/Vav-Cre (25%) + JAK2V617F/Vav-Cre/TP53$^{-/-}$ (25%) + WT (50%). (B) The percentage of CD45.2 (JAK2V617F/Vav-Cre cells) in blood Monocyte and Granulocyte cells of JAK2V617F/Vav-Cre (50%) + WT (50%) recipients(C) The percentage of CD45.2 (JAK2V617F/Vav-Cre/TP53$^{-/-}$ cells) in blood Monocyte and Granulocyte cells of

JAK2V617F/Vav-Cre/TP53$^{-/-}$ (50%) + WT (50%) recipients. (D) The percentage of CD45.2 (JAK2V617F/Vav-Cre and JAK2V617F/Vav-Cre/TP53$^{-/-}$ cells) in blood Monocyte and Granulocyte cells of JAK2V617F/Vav-Cre (25%) + JAK2V617F/Vav-Cre/TP53$^{-/-}$ (25%) + WT (50%) recipients. Data are mean ± s.d. *P<0.05, **P<0.01, ***P<0.001

We then analyzed by flow cytometry chimerism three months after transplantation of normal BM cells (50%) associated to different mix of JAK2V617F/Vav-Cre/TP53$^{-/-}$ and JAK2V617F/Vav-Cre cells. We (and others) previously demonstrated that a graft with 50% of WT BM cells and 50% of JAK2V617F induce a MPN disorder in mouse in 3 months and a chimerism of 100% of JAK2V617F/Vav-Cre cells, illustrating the JAK2V617F-induced proliferative advantage/invasion property of these pathological cells. In all cases, chimerism at three months demonstrates an advantage to the JAK2V617F/Vav-Cre cells, whatever the ratio between the two JAK2V617F/Vav-cre and JAK2V617F/Vav-cre/TP53$^{-/-}$ mutated grafts. We took advantage of this property and grafted irradiated mice with mix of 50% WT cells + 25% of JAK2V617F/Vav-Cre cells + 25% of JAK2V617F/Vav-Cre/TP53$^{-/-}$ cells (ratio 2:1:1); 50% of WT cells + 35% of JAK2V617F/Vav-Cre cells + 15% of JAK2V617F/Vav-Cre/TP53$^{-/-}$ (ratio 3:2:1); 50% of WT cells + 45% of JAK2V617F/Vav-Cre cells + 5% of JAK2V617F/Vav-Cre/TP53$^{-/-}$ (ratio 10:9:1); or 50% of WT cells + 49% of JAK2V617F/Vav-Cre cells + 1% of JAK2V617F/Vav-Cre/TP53$^{-/-}$ (ratio 50:49:1). Then, BM cells from 3-months transplanted animals were platted, cultured for 10-12 days, myeloid colonies were picked and genotyped for JAK2 and TP53 status. All BM colonies harbored the JAK2V617F/Vav-Cre recombination and respectively 100%, 94%, 47% and

0% were inactivated for TP53 illustrating the huge invasion property of JAK2V617F/Vav-Cre/TP53$^{-/-}$ cells during stress hematopoiesis (Figure 20).

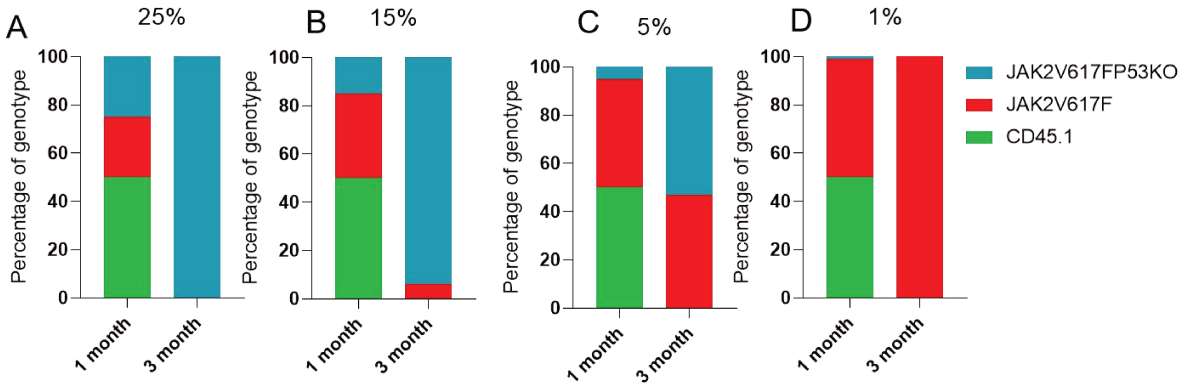

Figure 20: The percentage of genotyping in different competitive graft groups.

(A) The group of 25% competitive graft. 50% WT cells + 25% of JAK2V617F/Vav-Cre cells + 25% of JAK2V617F/Vav-Cre/TP53-/- cells (B) The group of 15% competitive graft.50% of WT cells + 35% of JAK2V617F/Vav-Cre cells + 15% of JAK2V617F/Vav-Cre/TP53-/- (C) The group of 5% competitive graft. 50% of WT cells + 45% of JAK2V617F/Vav-Cre cells + 5% of JAK2V617F/Vav-Cre/TP53-/- (D) The group of 1% competitive graft 50% of WT cells + 49% of JAK2V617F/Vav-Cre cells + 1% of JAK2V617F/Vav-Cre/TP53-/-.

These results confirm that JAK2V617F/Vav-Cre provides a competitive advantage to hematopoietic cells at early stages of differentiation but also that TP53 inactivation associated to JAK2V617F/Vav-Cre mutation provides a higher advantage than JAK2V617F/Vav-Cre mutation alone to these compartments during reconstitution.

3 Genomic analysis reveals TP53 dependent and independent JAK2V617F deregulations in vivo.

To better understand changes in immature cells related to TP53 inactivation in a JAK2V617F context, RNA-Seq analysis was performed on cell sorted immature populations (LT-HSC, ST-HSC, MPP, CMP, MEP, GMP) from normal, JAK2V617F/Vav-Cre and JAK2V617F/Vav-Cre/TP53$^{-/-}$ mice.

Unsupervised analysis classifies the type of cell compartment (but ST and LT-HSC that were not drastically differentiated the ones from the others) but the distinction according to the genotypes was less drastic, JAK2V617F/Vav-Cre/TP53$^{-/-}$ cells being clustered with normal cells in all compartments. (Figure 21A).

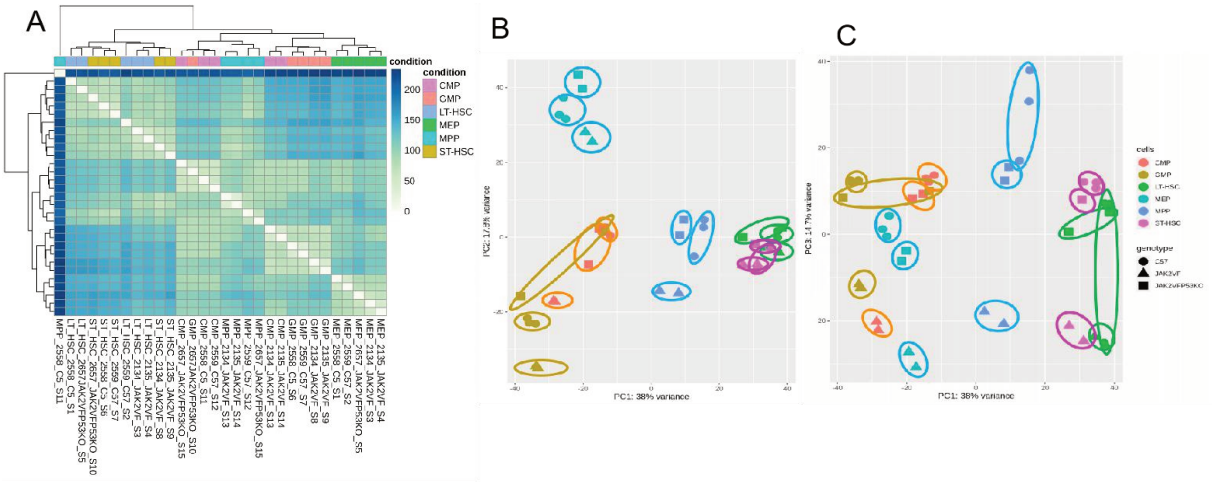

Figure 21: TP53 dependent and independent JAK2V617F deregulations in vivo

(A)Unsupervised analysis with different populations from C57B/l6, JAK2V617F/Vav-cre and JAK2V617F/Vav-cre/TP53$^{-/-}$ mice. (B)Principal component analysis with PC1 and PC2. (C)Principal component analysis with PC1 and PC3

Principal component analysis confirmed the unsupervised findings, demonstrating that RNA-Seq was able to distinguish each type of immature compartment with a gradient in PC1 (38% variance). PC2 and PC3 (respectively 17.8% and 14.7% variance) demonstrate that RNA-Seq was also powerfull to distinguish JAK2V617F/Vav-Cre from WT cells but the JAK2V617F/Vav-Cre/TP53$^{-/-}$ cells were closer to normal cells than JAK2V617F/Vav-Cre cells (Figure 21B-C).

Based on these findings, we firstly isolated JAK2V617F/Vav-Cre statistically significant deregulated genes and found that the proportion of “JAK2V617F”

specific genes vary from 6.65% (GMP compartment) to 22.2% (MPP compartment) with a median of 11.1% of deregulated genes (Figure 22A). Analyzing these JAK2V617F deregulated genes in the JAK2V617F/Vav-cre and in JAK2V617F/TP53$^{-/-}$ cell compartments, we found that approximatively 61% (37% to 77%) of these deregulations were TP53 dependent, confirming previous studies about the main role of TP53 in JAK2 signaling.

Because the phenotype (MPN) was strikingly equivalent during the first three months of life in the JAK2V617F/Vav-Cre and the JAK2V617F/Vav-Cre/TP53$^{-/-}$ mice, we hypothesized that the MPN-phenotype per se was TP53 independent and focus our analysis on these genes deregulated in the same way in JAK2V617F/Vav-Cre and JAK2V617F/Vav-Cre/TP53$^{-/-}$ mice.

We also analyzed JAK2V617F deregulated pathways that are TP53 independent (ie deregulated genes in the JAK2V617F cell compartments and not in the JAK2V617F/Vav-Cre/TP5$^{-/-}$ cell compartments). We particularly focus on IFN pathway since IFNα has been clinically demonstrated as a drug able to preferentially target JAK2V617F cells and because it has been demonstrated that the IFN signaling was uniquely enriched in HSCs from individual diagnosed with ET. We confirmed this enrichment in all JAK2V617F/Vav-Cre immature compartments in mouse but this was not the case in the JAK2V617F/Vav-Cre/TP53$^{-/-}$ cell compartments (Figure 22B-D), suggesting a potential difference in the response to IFN-based therapies.

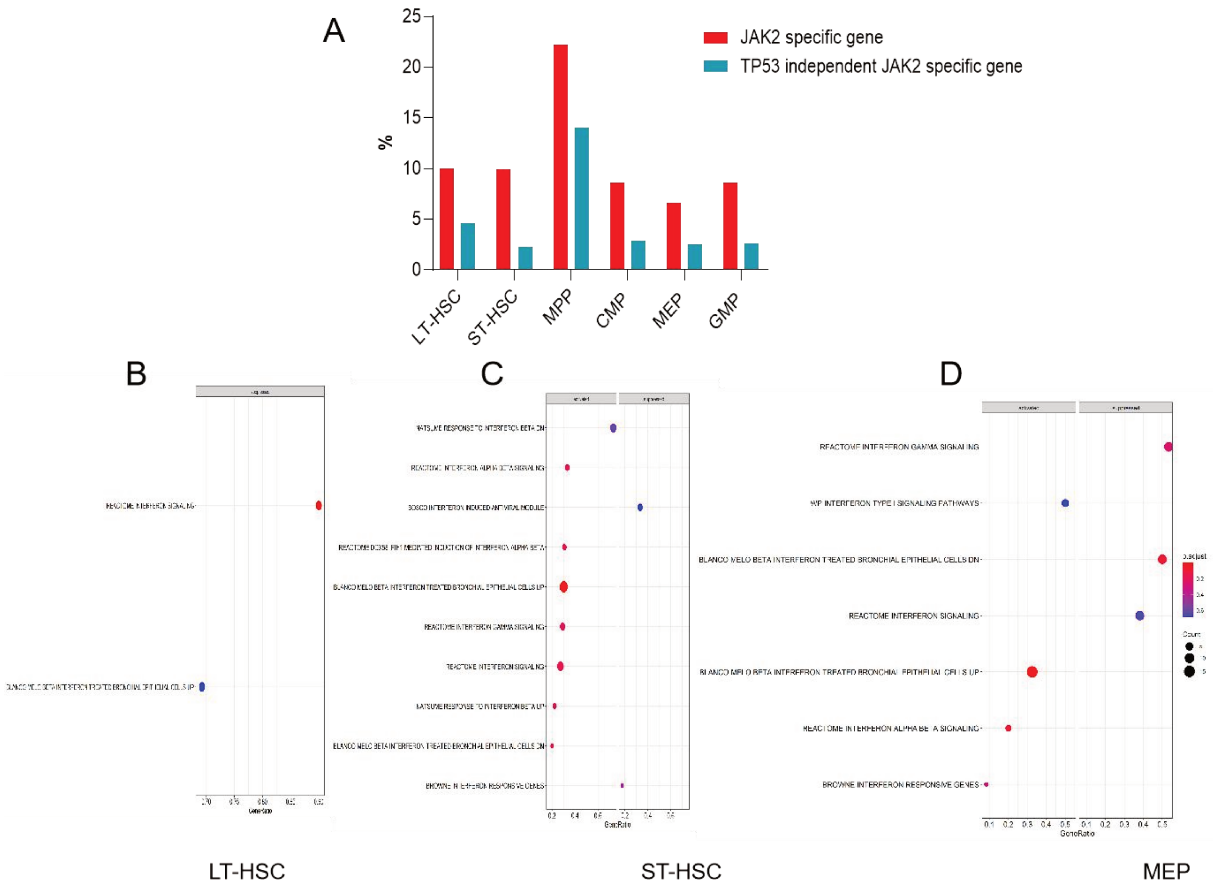

Figure 22: Specific gene between JAK2V617F/Vav-cre and JAK2V617F/Vav-cre/TP53$^{-/-}$ mice

(A)Specific JAK2V617F/Vav-cre gene and TP53 independent gene in different populations between JAK2V617F/Vav-cre and JAK2V617F/Vav-cre/TP53$^{-/-}$ mouse (B)IFN pathway response genes relative expression in LT-HSC of JAK2V617F/Vav-cre mice (C))IFN pathway response genes relative expression in ST-HSC of JAK2V617F/Vav-cre and JAK2V617F/Vav-cre/TP53$^{-/-}$mice. (D) IFN pathway response genes relative expression in MEP of JAK2V617F/Vav-cre and JAK2V617F/Vav-cre/TP53$^{-/-}$mice.

4 IFNα is not effective to treat JAK2V617F/TP53KO MPN in vivo.

IFNα treatment was initiated in 2 groups of CD45.1 WT recipient mice 4-6 weeks after the transplantation of 50% of CD45.1 BM WT cells with 50% JAK2V617F/Vav-Cre or 50% JAK2V617F/Vav-Cre/TP53$^{-/-}$ CD45.2 BM cells collected from 1- to 3-month-old donor mice as previously shown. Treatment was repeated for 8 weeks and stopped. For JAK2V617F/Vav-Cre transplanted

mice, IFNα treatment induced a suppression of leukocytosis, normalization of platelet count and hematocrit after 4 to 8 weeks (despite relapse after IFN withdrawal) (Figure 23A-C) when the treatment of the JAK2V617F/Vav-Cre/TP53$^{-/-}$ transplanted mice do not induce hematological response (Figure 24A-C). Chimerism analysis confirmed a drastic reduction in the JAK2V617F/Vav-Cre proportion of myeloid cells in the blood of the JAK2V617F/Vav-Cre recipients, persisting one month post IFN withdrawal (Figure 23D-G) while no change in chimerism analysis was noticed despite IFN-therapy in the JAK2V617F/Vav-Cre/TP53$^{-/-}$ recipient mice (Figure 24D-F). These hematological and chimerism findings were confirmed by the survival analysis with a significant increase of survival for JAK2V617F/Vav-Cre IFNα treated mice (Figure 23H) and not for the JAK2V617F/Vav-Cre/TP53$^{-/-}$ recipient treated mice (Figure 24G).

These results confirm that IFNα hampers JAK2V617F cell proliferation with normalization of most blood hematological values and reduction of the proliferative advantage of JAK2V617F/Vav-Cre over WT cells but is not as efficient in JAK2V617F/Vav-Cre/TP53$^{-/-}$ mouse cells.

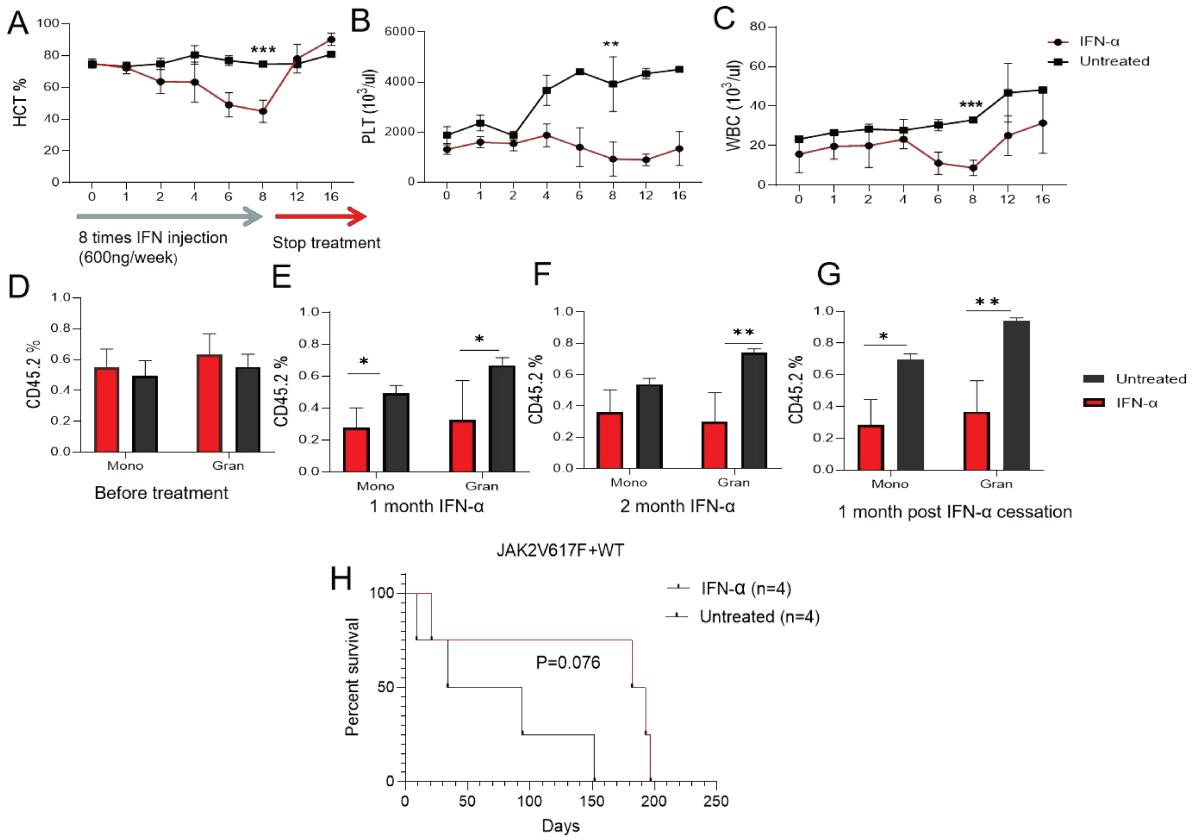

Figure 23: JAK2V617F/Vav-Cre mice respond for the IFNα treatment.

(A-C)The number of PB between IFNα treatment and untreated mice in the recipients of JAK2V617F/*Vav-Cre* mice and Ly5.1 mice. (A)The percentage of HCT. (B)The number of PLT. (C)The number of WBC. (D-G) The percentage of CD45.2 (JAK2V617F/*Vav-Cre* cell) in blood chimerism of treatment and untreatment mice. (H)The survival of treatment and untreatment mice. Data are mean ± s.d. *P<0.05, **P<0.01

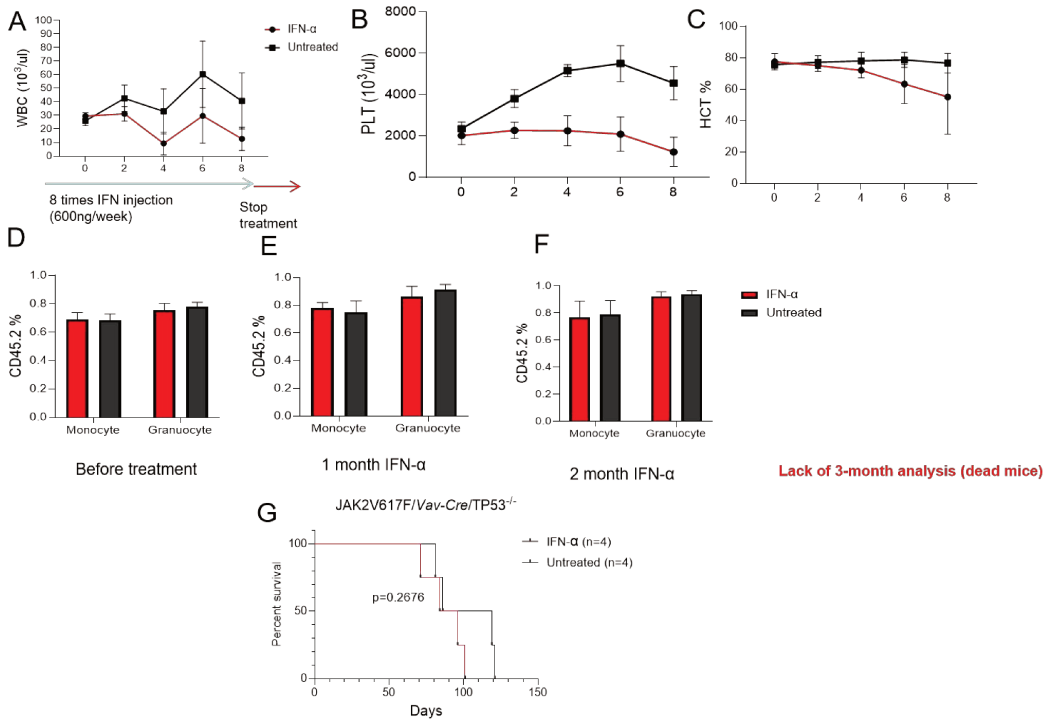

Figure 24: JAK2V617F/Vav-Cre/TP53$^{-/-}$ mice respond for the IFNα treatment.

(A-C)The number of PB between IFNα treatment and untreated mice in the recipients of JAK2V617F/*Vav-Cre* mice and Ly5.1 mice. (A) The number of WBC. (B) The number of PLT. (C) The percentage of HCT. (D-F) The percentage of CD45.2 (JAK2V617F/*Vav-Cre*/TP53$^{-/-}$ cell) in blood chimerism of treatment and untreatment mice. (G) The survival of treatment and untreatment mice. Data are mean ± s.d. *P<0.05, **P<0.01

DISCUSSION

TP53 mutations are the most frequent molecular abnormalities detected in cancer and focus on this molecule and its role on cancer development have been studied for a long time. Because p53 play a main role in cell cycle arrest and apoptosis induction, its inactivation can be directly linked to cancer. However, it does not directly induce transformation of the cell and external damaging stresses are needed when p53 is loss to stabilize proliferative cells acquiring DNA defects. P53 exerts also a peculiar function on the hematopoietic stem cells, regulating the quiescence of the cells. P53 loss induces proliferation of HSC pool in mice[26–30] that engraft more efficiently than normal cells[27–30].

TP53 mutations are relatively rare events in chronic phase MPN[18] but are more frequently detected during evolution and particularly during leukemic transformation[31]. This leads to the hypothesis of a link between P53 inactivation and transformation of signal transduction activation pathologies. This hypothesis has been reinforced by the demonstration that viral-induced overexpression of JAK2V617F in a P53 inactivated context induce leukemias in mice.

However, recent data on p53 mutations in MPN demonstrated that P53 mutations *per se* are not associated to higher risk of transformation (at least when the P53 mutation VAF is low) and can exist for extended period of time. Moreover, the acquisition of TP53 mutations seems to be late events during

the course of the disease questioning the causality of such mutation in the transformation of MPN.

At the biochemical level, cross-talks between JAK2V617F mutation and P53 have been largely described. JAK2V617F (and other MPN-associated mutations able to activate the JAK/STAT pathway) activates STAT3 and STAT5 that are able to inhibit p53 effects via a MDM2 activation (STAT5) or via a nucleophosmin 1 (NPM1) down-expression regulation (NPM1 reduces p53 level) or directly binding the p53 promoter, inhibiting its expression (STAT3)[32,33]. Direct interactions (and inhibition) of STAT5 proteins by p53 have also been described[34] . JAK2V617F has also been shown to induce La accumulation, a protein that can interact and stabilize MDM2 mRNA, increasing its translation and then inhibiting p53[35]. This JAK2/MDM2 pathway has been clinically reinforced since MDM2 inhibitor (Nutlin-3) significantly reduces MPN-$CD34^+$ cell proliferation when associated to IFN[36]. Lastly, other JAK2-dependant transduction pathways just like RAS/MAPK or AKT/mTOR also regulates p53 functions since ERK phosphorylation upregulate MDM2 expression[37]. Taken together, these results suggest that JAK2V617F mutation and inactivation of p53 could be redundant events in MPN suggesting that p53 inactivation do not induce large modifications in chronic MPN phenotypes.

The contradictory data on JAK2V617F and p53 mutations prompt us to develop a more physiological model of JAK2V617F expression in a context of p53 inactivation in the BM immature cells. Our results demonstrate that p53

inactivation do not modify the MPN phenotype at least during the first months, and then is not able to directly induce transformation of MPN. Surprisingly, modifications in the phenotype between WT and p53 inactivated mice in a JAK2V617F context were very mild, reinforcing the hypothesis of a redundancy between JAK2V617F activation and the p53 inactivation.

However, some genetic and phenotypic traits seem to remain p53 dependent in a JAK2V617F context. Firstly, bone marrow competition between JAK2V617F/TP53WT and JAK2V617F/TP53$^{-/-}$ BM cells demonstrate a huge advantage to p53 inactivated cells. It has been suggested previously that 30 LT-HSC are warranted to develop in 100% of mice a JAK2V617F-induced MPN phenotype. Here, we tested this hypothesis. In our hands, WT mice harbored 11027±742 LT-HSC while JAK2V617F or JAK2V617F/TP53$^{-/-}$ mice harbored 33250±25000 LT-HSC, meaning that JAK2V617F mice have a 3-fold increase in LT-HSC number. Triple competitive BM transplantations with different ratio of WT, JAK2V617F and JAK2V617F/TP53$^{-/-}$ cells, led us to inject 262, 157, 52 or 10 JAK2V617F/TP53$^{-/-}$ cells in recipients. In all cases but when mice received only 10 LT-HSC, cells are sufficient to generate MPN with complete penetrance (and p53 inactivation in more than 90% of the colonies) confirming previous data on the necessity to transplant at least 30 LT-HSC to fully develop a MPN in mouse. Moreover, these triple competitive BM transplantations demonstrate in vivo that 52 JAK2V617F/TP53$^{-/-}$ cells can overgrowth 472 JAK2V617F LT-HSC suggesting an over 9-fold capacity to invade the hematopoietic system over

JAK2V617F only cells when JAK2V617F LT-HSC have approximatively the same advantage over normal cells as reported previously[38]. Thus, JAK2V617F/TP53$^{-/-}$ cells could have a 20-fold proliferative advantage over WT cells during stress hematopoiesis. Second, molecular analysis performed during steady-state tends to demonstrate that a large set of JAK2V617F-induced deregulated genes are p53 dependent since immature populations of JAK2V617F/TP53$^{-/-}$ cells are closer to normal than JAK2V617F/TP53 WT cells. Such set of genes include the IFN pathway associated genes that are clearly upregulated in the JAK2V617F context (probably explaining the high sensitivity of these cells to IFN therapy) and comparatively downregulated when p53 is inactivated, suggesting a lower sensitivity of these cells to IFN therapy. We confirmed this differential sensitivity to IFNα therapy in JAK2V617F cells compared to WT or JAK2V617F/p53KO cells *in vivo*. This suggests that patients harboring p53 mutations in chronic MPN could be less sensitive to IFN-based regimen; This need to be confirmed in IFNα treated patients in order to decipher whether screening on p53 mutations need to be performed before IFNα therapy in humans, just like hypothesized by our group for the use of MDM2 modulators[39]. IFNα has been previously suggested as able to induce p53 dependent apoptosis via Fas[40,41], a death receptor expressed on cycling HSC[42]. Thus, modulating Fas expression could be a way to prevent IFN resistance for these patients.

In conclusion, our results show that endogenous P53 inactivation in a JAK2V617F context is not sufficient to directly induce transformation of MPN

but induce a proliferative advantage over p53 WT cells. Our data also suggest that p53 inactivation could induce a resistance to IFN therapy. This finding needing to be confirmed with clinical studies.

REFERENCES

1. Peter J Campbell ARG. The myeloproliferative disorders. *N Engl J Med*. 2006;355(23):2452–66.
2. Ugo V, James C, Vainchenker W. A unique clonal JAK2 mutation leading to constitutive signalling causes polycythaemia vera. *Nature*. 2005;434(7037):1144–8.
3. Kralovics R, Passamonti F, Buser AS, et al. A Gain-of-Function Mutation of JAK2 in Myeloproliferative Disorders. *N. Engl. J. Med.* 2005;352(17):1779–1790.
4. E Joanna Baxter, Linda M Scott, Peter J Campbell, Clare East, Nasios Fourouclas, Soheila Swanton, George S Vassiliou, Anthony J Bench, Elaine M Boyd, Natasha Curtin, Mike A Scott, Wendy N Erber, Anthony R Green CGP. Acquired mutation of the tyrosine kinase JAK2 in human myeloproliferative disorders. *Lancet*. 2005;365(9464):1054–61.
5. Zhao R, Xing S, Li Z, et al. Identification of an Acquired JAK2 Mutation in Polycythemia Vera. *J. Biol. Chem.* 2005;280(24):22788–22792.
6. Ross L Levine, Martha Wadleigh, Jan Cools, Benjamin L Ebert, Gerlinde Wernig, Brian J P Huntly, Titus J Boggon, Iwona Wlodarska, Jennifer J Clark, Sandra Moore, Jennifer Adelsperger, Sumin Koo, Jeffrey C Lee, Stacey Gabriel, Thomas Mercher, Alan D'Andrea, DGG. Activating mutation in the tyrosine kinase JAK2 in polycythemia vera, essential thrombocythemia, and myeloid metaplasia with myelofibrosis. *Cancer Cell*.

2005;7(4):387–97.

7. Mesa RA, Li CY, Ketterling RP, et al. Leukemic transformation in myelofibrosis with myeloid metaplasia: A single-institution experience with 91 cases. *Blood*. 2005;105(3):973–977.

8. Ayalew Tefferi AP. Essential thrombocythemia. *Consult. Obstet. Anesthesiol.* 2019;381(22):2135–2144.

9. Kennedy JA, Atenafu EG, Messner HA, et al. Treatment outcomes following leukemic transformation in Philadelphia-negative myeloproliferative neoplasms. *Blood*. 2013;121(14):2725–2733.

10. Harutyunyan AS, Kralovics R. Role of Germline Genetic Factors in MPN Pathogenesis. *Hematol. Oncol. Clin. North Am.* 2012;26(5):1037–1051.

11. F Cervantes, D Tassies, C Salgado, M Rovira, A Pereira CR. Acute transformation in nonleukemic chronic myeloproliferative disorders: actuarial probability and main characteristics in a series of 218 patients. *Acta Haematol*. 1991;85(3):124–7.

12. T Tsuruta-Kishino , J Koya, K Kataoka, K Narukawa, Y Sumitomo , H Kobayashi , T Sato MK. Loss of p53 induces leukemic transformation in a murine model of Jak2 V617F-driven polycythemia vera. *Oncogene*. 2017;36(23):3300–3311.

13. S Srivastava , Z Q Zou, K Pirollo, W Blattner EHC. Germ-line transmission of a mutated p53 gene in a cancer-prone family with Li-Fraumeni syndrome. *Nature*. 1990;348(6303):747–9.

14. Molica M, Mazzone C, Niscola P, de Fabritiis P. TP53 Mutations in Acute Myeloid Leukemia: Still a Daunting Challenge? *Front. Oncol.* 2021;10:.

15. Lundberg P, Karow A, Nienhold R, et al. Clonal evolution and clinical correlates of somatic mutations in myeloproliferative neoplasms. *Blood*. 2014;123(14):2220–2228.

16. Harutyunyan A, Klampfl T, Cazzola M, Kralovics R. p53 Lesions in Leukemic Transformation. *N. Engl. J. Med.* 2011;364(5):488–490.

17. Beer PA, Delhommeau F, LeCouédic JP, et al. Two routes to leukemic transformation after a JAK2 mutation-positive myeloproliferative neoplasm. *Blood*. 2010;115(14):2891–2900.

18. Kubesova B, Pavlova S, Malcikova J, et al. Low-burden TP53 mutations in chronic phase of myeloproliferative neoplasms: Association with age, hydroxyurea administration, disease type and JAK2 mutational status. *Leukemia*. 2018;32(2):450–461.

19. Sallman DA, Padron E. Integrating mutation variant allele frequency into clinical practice in myeloid malignancies. *Hematol. Oncol. Stem Cell Ther.* 2016;9(3):89–95.

20. Hasan S, Lacout C, Marty C, et al. JAK2V617F expression in mice amplifies early hematopoietic cells and gives them a competitive advantage that is hampered by IFNa. *Blood*. 2013;122(8):1464–1477.

21. Ogilvy S, Elefanty AG, Visvader J, et al. Transcriptional regulation of vav, a gene expressed throughout the hematopoietic compartment. *Blood*. 1998;91(2):419–430.

22. Ogilvy S, Metcalf D, Gibson L, et al. Promoter elements of vav drive transgene expression in vivo throughout the hematopoietic compartment. *Blood*. 1999;94(6):1855–1863.

23. D R Shimshek, J Kim, M R Hübner, D J Spergel, F Buchholz, E Casanova, A F Stewart, P H Seeburg RS. Codon-improved Cre recombinase (iCre) expression in the mouse. *Genesis*.

2002;32(1):19–26.

24. Learning M, Cookbook R. Mice deficient for p53 are developmentally normal but susceptible to spontaneous tumours. *Nature*. 1992;356(6366):215–21.

25. Gennady Korotkevich, Vladimir Sukhov, Nikolay Budin, Boris Shpak, Maxim N. Artyomov AS. Fast gene set enrichment analysis. *bioRxiv*. 2021;

26. Pant V, Quintás-Cardama A, Lozano G. The p53 pathway in hematopoiesis: Lessons from mouse models, implications for humans. *Blood*. 2012;120(26):5118–27.

27. Liu Y, Elf SE, Miyata Y, et al. p53 Regulates Hematopoietic Stem Cell Quiescence. *Cell Stem Cell*. 2009;4(1):37–48.

28. Chen J, Ellison FM, Keyvanfar K, et al. Enrichment of hematopoietic stem cells with SLAM and LSK markers for the detection of hematopoietic stem cell function in normal and Trp53 null mice. *Exp. Hematol.* 2008;36(10):1236–43.

29. TeKippe M, Harrison DE, Chen J. Expansion of hematopoietic stem cell phenotype and activity in Trp53-null mice. *Exp. Hematol.* 2003;31(6):521–7.

30. Akala OO, Park IK, Qian D, et al. Long-term haematopoietic reconstitution by Trp53-/-p16 Ink4a-/-p19Arf-/- multipotent progenitors. *Nature*. 2008;453(7192):228–32.

31. Paz DL, Jouanneau-Courville R, Riou J, et al. Leukemic evolution of polycythemia vera and essential thrombocythemia: Genomic profiles predict time to transformation. *Blood Adv.* 2020;4(19):4887–4897.

32. Ren Z, Aerts JL, Vandenplas H, et al. Phosphorylated STAT5 regulates p53 expression via BRCA1/BARD1-NPM1 and MDM2. *Cell Death Dis.* 2016;7(12):e2560.

33. Raivola J, Haikarainen T, Abraham BG, Silvennoinen O. Janus kinases in leukemia. *Cancers (Basel).* 2021;13(4):800.

34. Goyal H, Chachoua I, Pecquet C, Vainchenker W, Constantinescu SN. A p53-JAK-STAT connection involved in myeloproliferative neoplasm pathogenesis and progression to secondary acute myeloid leukemia. *Blood Rev.* 2020;42:100712.

35. Nakatake M, Monte-Mor B, Debili N, et al. JAK2 V617F negatively regulates p53 stabilization by enhancing MDM2 via la expression in myeloproliferative neoplasms. *Oncogene*. 2012;31(10):1323–33.

36. Lu M, Xia L, Li Y, Wang X, Hoffman R. The orally bioavailable MDM2 antagonist RG7112 and pegylated interferon α 2a target JAK2V617F-positive progenitor and stem cells. *Blood*. 2014;124(5):771–9.

37. Steelman LS, Chappell WH, Abrams SL, et al. Roles of the Raf/MEK/ERK and PI3K/PTEN/Akt/mtor pathways in controlling growth and sensitivity to therapy-implications for cancer and aging. *Aging (Albany. NY).* 2011;3(3):192–222.

38. Dagher T, Maslah N, Edmond V, et al. JAK2V617F myeloproliferative neoplasm eradication by a novel interferon/arsenic therapy involves PML. *J. Exp. Med.* 2020;218(2):e20201268.

39. Rafael Daltro De Oliveira, Juliette Soret-Dulphy, Lin-Pierre Zhao, Clemence Marcault, Nicolas Gauthier, Emmanuelle Verger, Nabih Maslah, Nathalie Parquet, Emmanuel Raffoux, William Vainchenker, Christine Chomienne J-JK. Interferon-Alpha (IFN) Therapy Discontinuation Is Feasible in Myeloproliferative Neoplasm (MPN) Patients with Complete Hematological Remission.

40. Kim SG, Ravi G, Hoffmann C, et al. p53-Independent induction of Fas and apoptosis in leukemic cells by an adenosine derivative, Cl-IB-MECA. *Biochem. Pharmacol.* 2002;63(5):871–80.

41. Barber GN. Host defense, viruses and apoptosis. *Cell Death Differ.* 2001;8(2):113–26.

42. Bryder D, Ramsfjell V, Dybedal I, et al. Self-renewal of multipotent long-term repopulating hematopoietic stem cells is negatively regulated by Fas and tumor necrosis factor receptor activation. *J. Exp. Med.* 2001;194(7):941–952.

DISCUSSION

Until 2005, MPN were considered as clonal disorders based on X chromosome inactivation studies, rare karyotype abnormalities and by analogy to Chronic Myeloid Leukemia and its characteristic clonal BCR-ABL translocation. The discovery of the JAK2V617F mutation in 2005 confirmed the clonal nature of MPN and gave clues for the understanding of disease development. In the following decade, other molecular abnormalities have been found in MPN such as *JAK2* exon 12 mutations, *CALR* mutations or *MPL* mutations. All these abnormalities retain a unique characteristic: Activation of the JAK2 transduction pathway.

Because this pathway plays a major role on myeloid (but also lymphoid) physiology, mouse models were decisive to demonstrate that unregulated activation of this pathway is causal in MPN development.

However, the mild proliferative advantage due to the mutations opens new questions about the emergence of these diseases. If the mutation is causal and acquired in a stem cell, then, the development of the disease needs this quiescent (by definition) stem cell to proliferate.

In mouse (and it can be hypothesized that it is the same in human) the more immature stem cells are quiescent for very long term and in fact are dispensable in “steady state”, ST-HSC and MPP being able to assure the long-term repopulation of mice. This illustrates the quiescence process characterizing the LT-HSC. In mouse, it is now clearly demonstrated that these cells enter in mitosis one time every 100 days approximatively[209]. This means

that a LT-HSC, during the life a mouse (2 years) makes 6 mitoses only. It has been demonstrated that JAK2V617F-mutated LT-HSC are able to enter cell cycle more efficiently than normal stem cells[59]. However, in CML as well as in JAK2V617F models, the proliferative advantage of mutant HSCs is not so clear. In our study, in steady state, 1% of normal LT-HSC enter cell cycle each day compared to 2% for JAK2V617-mutated LT-HSCs. We then could hypothesize that the cycling capacity of JAK2V617F-mutated LT-HSC is doubled when compared to normal cells, leading to 12 mitoses only during the life of the mouse. Then, from one LT-HSC acquiring a JAK2V617F mutation, the probability to develop a MPN disease after 1 year should be very low. The second point to take into consideration is the mutation acquisition time. MPN are considered as acquired pathologies and then it is currently admitted that the first mutated stem cell should emerge during the adulthood. Furthermore, it is hard to understand how a quiescent stem cell could acquire a mutation. For almost a hundred years, geneticists have believed that the more a cell divides the more mutations it acquires, rendering the LT-HSC “resistant” to mutation acquisition. However, it has been shown that quiescent cells, which do not divide, also acquire particular type of mutation such as deletions. However, the acquisition of JAK2V617F mutation does not correspond to this type of mutation (but it could be the case for CALR mutations).

Then, if we postulate that the *JAK2* mutation is acquired during the adulthood in a single cycling stem cell, then the probability of developing MPN disorders

appears very low, or impossible. Another alternative could be the emergence of *JAK2* mutations during the fetal life, when stem cells proliferate quickly to create the stem cell pool, in the fetal liver.

Our initial aim was to demonstrate using mathematical approach the impossibility (or extremely low probability) to develop a JAK2V617F disorder if the mutation emerged in a single LT-HSC during the adulthood and to back-track mathematically the time of emergence during fetal period.

To this end, we first needed to analyze the normal behavior of stem cells in mice. Few mathematical models focused on the immature compartment behaviors. Moreover, the main mathematical models focused on the equilibrium (steady-state) hematopoiesis whereas we hypothesized that stress represents an important factor explaining the capacity of JAK2V617F-mutated cells to expand and compete wild-type cells. Thus, we first decided to model normal immature hematopoiesis combining steady-state and stress hematopoiesis. To this end, modeling need to precisely define a minimum number of immature compartments, a number of cells by compartments, the state of the cells in each compartment (cycling or not) to precisely define the new model. Because regulations concerning the immature compartments (cytokines, chemokines, stress-sensors, neuronal interactions, cell-cell interactions, localization in the niche, etc…) are not well known, we decided to resume these regulators using two equations only, the first one as a positive regulator and the second one as a negative regulator. These regulators were

calibrated using the results obtained in vivo after stress.

Our model presents limitations since we resume all hematopoiesis production to red cells production. We made this hypothesis because red cells represent more than 90% of circulating cells in the blood and hematopoietic tissues. Thus, our model cannot precisely describe what happens in “non-erythroid” differentiation processes.

Despite this limitation, it was possible to validate the model using different “in silico” stresses just like 5-FU treatment, phlebotomy, or LT-HSC suppression. After these extreme stresses, the model demonstrates regulations and return to normal hematopoietic values according to biological data obtained from the literature. Thus, the model being validated, our aim is now to determine the outcome of a mutant LT-HSC (and its own proliferative properties) to determine when and with which probability a MPN phenotype could develop after a single mutant LT-HSC will appears. To this end, we reproduced in JAK2V617F transgenic mice the stress previously analyzed in normal mice. Applying the data from mutant mice to the mathematical model, we hope it will be possible to determine 1- which factors have to be modified in the model, illustrating mathematically the consequences of JAK2V617F mutation on hematopoiesis. 2- Using the mutant mice parameters, we will be able to determine the minimal number of mutant LT-HSC that will be allowed to induce a MPN phenotype with a probability equal to the one of MPN emergence in the general population. This LT-HSC number will correspond to the date of emergence of

the first mutant LT-HSC that will be necessary to induce a MPN. We hope to have the ability to clearly demonstrate that MPN are in fact pathologies emerging during the fetal life. 3- we would like to also demonstrate that stresses are mandatory to induce the emergence of MPN phenotype using comparisons between stress and steady state normal and pathological hematopoiesis. The in vivo data have been collected and the mathematical modeling will be developed during the next few years.

After this first part trying to better understand how and when MPN emerge, the second part of our work concerned the MPN evolution.

During the last decade, it became more and more clear that additional mutations were present in a subset of patients in association to the “driver” mutations such as JAK2V617F. These mutations target several genes involved in various pathways such as epigenetics, mRNA splicing, intracellular signaling or gene expression. These events are acquired in a subset of cells leading to sub-clonal evolution. The development of NGS analysis and more recently the use of single cell sequencing, led to the demonstration that a large subset of patients present driver mutations associated to sub-clonal mutations[210].

Clinical studies demonstrated that some of these additional mutations are associated to poor prognosis in MPN patients. One of the most interesting gene involved in the transformation of MPN is *TP53*[39,170]. Indeed, the p53 protein encoded by *TP53* gene is usually defined as the guardian of the genome. It is mutated in the vast majority of cancers. Surprisingly *TP53* is rarely mutated in

spontaneous acute leukemia but more frequently in secondary acquired leukemias[211]. It has been suggested that *TP53* loss of function mutations could be responsible of acute leukemic transformation in combination with MPN driver mutation[178]. Reinforcing this hypothesis, overexpression of JAK2V617F in *TP53* inactivated cells using retroviral expression induces leukemias in mice. However, other data are confusing: It has been clearly demonstrated that some MPN patients harboring *TP53* mutations do not develop leukemias for long times, particularly when the *TP53* mutation allele burden is low[178]. This suggests that the clonal advantage of the *TP53* mutated cells in a JAK2V617F context is not so high. Moreover, mouse models developed previously used overexpression of JAK2V617F at very high levels that are not compatible with what is observed in humans (despite some patients present more than 2 copies of *JAK2* mutated gene).

We then developed a triple transgenic model using the JAK2V617F model of mouse previously developed by Villeval et al. In the novel model we created JAK2V617F was expressed at a physiological level using a vav-cre recombination in a *TP53* knock-out syngeneic mouse strain. Using these mice, we demonstrated that at steady-state, when hematopoiesis is not stressed, the mice present the same MPN characteristic than JAK2V617F only mice. We analyzed blood parameters, histology of bone marrow and spleen, survival, cell cycle of all immature populations and failed to find any difference between the two strains suggesting that TP53 is not a key player in the MPN phenotype. We

also compared the RNA-Seq from JAK2V617F and JAK2V617F/TP53$^{-/-}$ mice in all immature compartments. Using this approach, we were capable to define which gene expressions (modified by JAK2V617F) were *TP53* dependent or independent. The *TP53*-independent genes are involved in the MPN phenotype since the phenotype was observed in triple transgenic mice. Using pathway analysis comparison, we found that one main differentially regulated pathway was the IFN-α signaling pathway. Indeed, the JAK2V617F strain have a significant overexpression of genes involved in IFN pathway whereas this pathway was down modulated in JAK2V617F/TP53$^{-/-}$ strains, whatever the compartment (LT-HSC to MEP). This suggests that JAK2V617F cells could be hypersensitive to IFN (this correlates with clinical results where a clear decrease in the JAK2V617F clonal size is observed in MPN patients treated for a long time with IFN-α) while JAK2V617F cells harboring an inactivation of *TP53* could be less sensitive to this treatment. To demonstrate this, we used competitive repopulation of irradiated mice and treated these mice with IFN-α. Using this approach, we clearly observed that JAK2V617F/*TP53* mutated cells have a lower sensitivity to IFN-α. This resistance to therapy could be an explanation to the higher probability for leukemia emergence with large delay when TP53 subclones are small. In accordance with this hypothesis, it has been recently reported that *TP53*-mutated clones may emerge in MPN patients receiving MDM2 inhibitor therapy. Interestingly, such *TP53* subclones may decline after the therapy is stopped, suggesting that these clones have a low

potential to outcompete the JAK2V617F / *TP53* wild type ones.

In conclusion, our work focused on MPN emergence and transformation. We currently do not apply our modeling to MPN, and then this part of the work has to be continued. The second part of our work demonstrates that *TP53* inactivation in combination to JAK2V617F is not sufficient to induce transformation of MPN, suggesting that in MPN, like in other cancers, the cellular defense mechanisms are important and then that more than two gene alterations are necessary to induce cancer.

BIBLIOGRAPHY

BIBLIOGRAPHY

1. Fernández KS, de Alarcón PA. Development of the hematopoietic system and disorders of hematopoiesis that present during infancy and early childhood. *Pediatr. Clin. North Am.* 2013;60(6):1273–1289.
2. Hindorf C, Glatting G, Chiesa C, Lindén O, Flux G. EANM dosimetry committee guidelines for bone marrow and whole-body dosimetry. *Eur. J. Nucl. Med. Mol. Imaging*. 2010;37(6):1238–1250.
3. Schermer KL. Aneurysm of the hepatic artery: report of a case. *J Indiana State Med Assoc*. 1967;60(12):1652–4.
4. L E Gerlowski RKJ. Microvascular permeability of normal and neoplastic tissues. *Microvasc Res*. 1986;31(3):288–305.
5. Peter J Campbell ARG. The myeloproliferative disorders. *N Engl J Med*. 2006;355(23):2452–66.
6. Kralovics R, Passamonti F, Buser AS, et al. A Gain-of-Function Mutation of JAK2 in Myeloproliferative Disorders. *N. Engl. J. Med.* 2005;352(17):1779–1790.
7. Ross L Levine, Martha Wadleigh, Jan Cools, Benjamin L Ebert, Gerlinde Wernig, Brian J P Huntly, Titus J Boggon, Iwona Wlodarska, Jennifer J Clark, Sandra Moore, Jennifer Adelsperger, Sumin Koo, Jeffrey C Lee, Stacey Gabriel, Thomas Mercher, Alan D'Andrea, DGG. Activating mutation in the tyrosine kinase JAK2 in polycythemia vera, essential thrombocythemia, and myeloid metaplasia with myelofibrosis. *Cancer Cell*. 2005;7(4):387–97.
8. E Joanna Baxter, Linda M Scott, Peter J Campbell, Clare East, Nasios Fourouclas, Soheila Swanton, George S Vassiliou, Anthony J Bench, Elaine M Boyd, Natasha Curtin, Mike A Scott, Wendy N Erber, Anthony R Green CGP. Acquired mutation of the tyrosine kinase JAK2 in human myeloproliferative disorders. *Lancet*. 2005;365(9464):1054–61.
9. Crisà E, Venturino E, Passera R, et al. A retrospective study on 226 polycythemia vera patients: Impact of median hematocrit value on clinical outcomes and survival improvement with anti-thrombotic prophylaxis and non-alkylating drugs. *Ann. Hematol.* 2010;89(7):691–699.
10. Lengfelder E, Berger U, Hehlmann R. Interferon α in the treatment of polycythemia vera. *Ann. Hematol.* 2000;79(3):103–109.
11. Gioia Colafigli , Emilia Scalzulli , Sara Pepe , Alessio Di Prima , Fabio Efficace , Maurizio Martelli , Robin Foà MB. The advantages and risks of ruxolitinib for the treatment of

polycythemia vera. *Expert Rev Hematol*. 2020;13(10):1067–1072.

12. S Cortelazzo, P Viero, G Finazzi, A D'Emilio, F Rodeghiero TB. Incidence and risk factors for thrombotic complications in a historical cohort of 100 patients with essential thrombocythemia. *J Clin Oncol*. 1990;8(3):556–62.
13. P Fenaux, M Simon, M T Caulier, J L Lai, J Goudemand FB. Clinical course of essential thrombocythemia in 147 cases. *Cancer*. 1990;66(3):549–56.
14. Reynaud D, Pietras E, Barry-Holson K, et al. IL-6 Controls Leukemic Multipotent Progenitor Cell Fate and Contributes to Chronic Myelogenous Leukemia Development. *Cancer Cell*. 2011;20(5):661–673.
15. Carobbio A, Thiele J, Passamonti F, et al. Risk factors for arterial and venous thrombosis in WHO-defined essential thrombocythemia: An international study of 891 patients. *Blood*. 2011;117(22):5857–5859.
16. Tefferi A, Barbui T. Polycythemia vera and essential thrombocythemia: 2017 update on diagnosis, risk-stratification, and management. *Am. J. Hematol.* 2017;92(1):94–108.
17. Briére JB. Essential thrombocythemia. *Orphanet J. Rare Dis.* 2007;2(1):.
18. Harrison CN, Campbell PJ, Buck G, et al. Hydroxyurea Compared with Anagrelide in High-Risk Essential Thrombocythemia. *N. Engl. J. Med.* 2005;353(1):33–45.
19. Gisslinger H, Gotic M, Holowiecki J, et al. Anagrelide compared with hydroxyurea in WHO-classified essential thrombocythemia: The ANAHYDRET Study, a randomized controlled trial. *Blood*. 2013;121(10):1720–1728.
20. Bianca Rocca, Alberto Tosetto, Silvia Betti, Denise Soldati, Giovanna Petrucci , Elena Rossi , Andrea Timillero , Viviana Cavalca , Benedetta Porro , Alessandra Iurlo , Daniele Cattaneo , Cristina Bucelli , Alfredo Dragani , Mauro Di Ianni , Paola Ranalli VDS. A randomized double-blind trial of 3 aspirin regimens to optimize antiplatelet therapy in essential thrombocythemia. *Blood*. 2020;136(2):171–182.
21. F Cervantes, F Passamonti GB. Life expectancy and prognostic factors in the classic BCR/ABL-negative myeloproliferative disorders. *Leukemia*. 2008;22(5):905–14.
22. Cervantes F, Dupriez B, Pereira A, et al. New prognostic scoring system for primary myelofibrosis based on a study of the International working group for myelofibrosis research and treatment. *Blood*. 2009;113(13):2895–2901.
23. Barosi G, Mesa RA, Thiele J, et al. Proposed criteria for the diagnosis of post-polycythemia vera and post-essential thrombocythemia myelofibrosis: A consensus statement from the international working group for myelofibrosis research and treatment [6]. *Leukemia*. 2008;22(2):437–438.
24. Tefferi A. Primary myelofibrosis: 2017 update on diagnosis, risk-stratification, and

management. *Am. J. Hematol.* 2016;91(12):1262–1271.

25. Ayalew Tefferi WV. Myeloproliferative neoplasms: molecular pathophysiology, essential clinical understanding, and treatment strategies. *J Clin Oncol*. 2011;29(5):573–82.
26. Barbui T, Barosi G, Birgegard G, et al. Philadelphia-negative classical myeloproliferative neoplasms: critical concepts and management recommendations from European leukemiaNet. *J. Clin. Oncol.* 2011;29(6):761–770.
27. Mclornan DP, Mead AJ, Jackson G, Harrison CN. Allogeneic Stem Cell Transplantation for Myelofibrosis in 2012. *Br. J. Haematol.* 2012;157(4):413–425.
28. Dameshek W, Dameshek. EDITORIAL Some Speculations on the Myeloproliferative Syndromes. *Blood*. 2016;6(4):372–5.
29. J F Prchal AAA. Letter: Bone-marrow responses in polycythemia vera. *N Engl J Med*. 1974;290(24):1382.
30. Ugo V, James C, Vainchenker W. A unique clonal JAK2 mutation leading to constitutive signalling causes polycythaemia vera. *Medecine/Sciences*. 2005;21(6–7):669–670.
31. O'shea JJ, Holland SM, Staudt LM. JAKs and STATs in Immunity, Immunodeficiency, and Cancer HHS Public Access. *N Engl J Med*. 2013;368(2):161–170.
32. Rawlings JS, Rosler KM, Harrison DA. The JAK/STAT signaling pathway. *J. Cell Sci.* 2004;117(8):1281–1283.
33. Murray PJ. The JAK-STAT Signaling Pathway: Input and Output Integration. *J. Immunol.* 2007;178(5):2623–2629.
34. Ludwig RJ, Gadina M, Yamaoka K, et al. Targeting the Janus Kinase Family in Autoimmune Skin Diseases. *Front. Immunol. | www.frontiersin.org*. 2019;10:2342.
35. Neal K Williams, Rebecca S Bamert, Onisha Patel, Christina Wang, Patricia M Walden, Andrew F Wilks, Emmanuelle Fantino, Jamie Rossjohn ISL. Dissecting specificity in the Janus kinases: the structures of JAK-specific inhibitors complexed to the JAK1 and JAK2 protein tyrosine kinase domains. *J Mol Biol*. 2009;387(1):219–32.
36. Howell MD, Kuo FI, Smith PA. Targeting the Janus Kinase Family in Autoimmune Skin Diseases. *Front. Immunol.* 2019;10:2342.
37. Quintás-Cardama A, Kantarjian H, Cortes J, Verstovsek S. Janus kinase inhibitors for the treatment of myeloproliferative neoplasias and beyond. *Nat. Rev. Drug Discov.* 2011;10(2):127–140.
38. Mead AJ, Mullally A. Myeloproliferative neoplasm stem cells. *Blood*. 2017;129(12):1607–1616.
39. Grabek J, Straube J, Bywater M, Lane SW. MPN: The Molecular Drivers of Disease

Initiation, Progression and Transformation and their Effect on Treatment. *Cells*. 2020;9(8):.

40. Klampfl T, Gisslinger H, Harutyunyan AS, et al. Somatic Mutations of Calreticulin in Myeloproliferative Neoplasms. *N. Engl. J. Med.* 2013;369(25):2379–2390.
41. Scott LM, Tong W, Levine RL, et al. JAK2 Exon 12 Mutations in Polycythemia Vera and Idiopathic Erythrocytosis. *N. Engl. J. Med.* 2007;356(5):459–468.
42. Ugo V, James C, Vainchenker W. A unique clonal JAK2 mutation leading to constitutive signalling causes polycythaemia vera. *Nature*. 2005;434(7037):1144–8.
43. Zhao R, Xing S, Li Z, et al. Identification of an Acquired JAK2 Mutation in Polycythemia Vera. *J. Biol. Chem.* 2005;280(24):22788–22792.
44. Bandaranayake RM, Ungureanu D, Shan Y, et al. Crystal structures of the JAK2 pseudokinase domain and the pathogenic mutant V617F. *Nat. Struct. Mol. Biol.* 2012;19(8):754–759.
45. Toms A V, Deshpande A, McNally R, et al. Structure of a pseudokinase-domain switch that controls oncogenic activation of Jak kinases. *Nat. Struct. Mol. Biol.* 2013;20(10):1221–1224.
46. Shan Y, Gnanasambandan K, Ungureanu D, et al. Molecular basis for pseudokinase-dependent autoinhibition of JAK2 tyrosine kinase. *Nat Struct Mol Biol*. 2014;21(7):579–84.
47. Ungureanu D, Wu J, Pekkala T, et al. The pseudokinase domain of JAK2 is a dual-specificity protein kinase that negatively regulates cytokine signaling. *Nat. Struct. Mol. Biol.* 2011;18(9):971–976.
48. Brooks AJ, Dai W, O'mara ML, et al. Mechanism of Activation of Protein Kinase JAK2 by the Growth Hormone Receptor. *Science (80-.).* 2014;344(6185):1249783.
49. Lu X, Levine R, Tong W, et al. Expression of a homodimeric type I cytokine receptor is required for JAK2V617F-mediated transformation. *Proc. Natl. Acad. Sci. U. S. A.* 2005;102(52):18962–18967.
50. Lu X, Huang LJS, Lodish HF. Dimerization by a cytokine receptor is necessary for constitutive activation of JAK2V617F. *J. Biol. Chem.* 2008;283(9):5258–5266.
51. Pradhan A, Lambert QT, Reuther GW. Transformation of hematopoietic cells and activation of JAK2-V617F by IL-27R, a component of a heterodimeric type I cytokine receptor. *Proc. Natl. Acad. Sci. U. S. A.* 2007;104(47):18502–18507.
52. Pradhan A, Lambert QT, Griner LN, Reuther GW. Activation of JAK2-V617F by components of heterodimeric cytokine receptors. *J. Biol. Chem.* 2010;285(22):16651–16663.

53. Chen E, Mullally A. How does JAK2V617F contribute to the pathogenesis of myeloproliferative neoplasms? *Hematol. (United States)*. 2014;2014(1):268–276.
54. Grinfeld J, Nangalia J, Green AR. Molecular determinants of pathogenesis and clinical phenotype in myeloproliferative neoplasms. *Haematologica*. 2017;102(1):7–17.
55. Julia R Pon MAM. Driver and passenger mutations in cancer. *Annu Rev Pathol*. 2015;10:25–50.
56. Stratton MR. Exploring the genomes of cancer cells: Progress and promise. *Science (80-.).* 2011;331(6024):1553–1558.
57. Stratton MR, Campbell PJ, Futreal PA. The cancer genome. *Nature*. 2009;458(7239):719–724.
58. Vogelstein B, Papadopoulos N, Velculescu VE, et al. Cancer Genome Landscapes. *Science (80-.).* 2013;339(6127):1546–58.
59. Lundberg P, Takizawa H, Kubovcakova L, et al. Myeloproliferative neoplasms can be initiated from a single hematopoietic stem cell expressing JAK2-V617F. *J. Exp. Med.* 2014;211(11):2213–2230.
60. Jamieson CHM, Gotlib J, Durocher JA, et al. The JAK2 V617F mutation occurs in hematopoietic stem cells in polycythemia vera and predisposes toward erythroid differentiation. *Proc. Natl. Acad. Sci. U. S. A.* 2006;103(16):6224–6229.
61. Sabrina Dupont, Aline Massé, Chloé James, Irène Teyssandier, Yann Lécluse, Frédéric Larbret, Valérie Ugo, Patrick Saulnier, Serge Koscielny, Jean Pierre Le Couédic, Nicole Casadevall, William Vainchenker FD. The JAK2 617V>F mutation triggers erythropoietin hypersensitivity and terminal erythroid amplification in primary cells from patients with polycythemia vera. *Comp. Study*. 2007;110(3):1013–21.
62. François Delhommeau, Sabrina Dupont, Carole Tonetti, Aline Massé, Isabelle Godin, Jean-Pierre Le Couedic, Najet Debili, Patrick Saulnier, Nicole Casadevall, William Vainchenker SG. Evidence that the JAK2 G1849T (V617F) mutation occurs in a lymphomyeloid progenitor in polycythemia vera and idiopathic myelofibrosis. *Blood*. 2007;109(1):71–7.
63. Takefumi Ishii , Edward Bruno, Ronald Hoffman MX. Involvement of various hematopoietic-cell lineages by the JAK2V617F mutation in polycythemia vera. *Blood*. 2006;108(9):3128–34.
64. Larsen TS, Christensen JH, Hasselbalch HC, Pallisgaard N. The JAK2 V617F mutation involves B- and T-lymphocyte lineages in a subgroup of patients with Philadelphia-chromosome negative chronic myeloproliferative disorders. *Br. J. Haematol.* 2007;136(5):745–751.

65. Anand S, Stedham F, Beer P, et al. Effects of the JAK2 mutation on the hematopoietic stem and progenitor compartment in human myeloproliferative neoplasms. *Blood*. 2011;118(1):177–181.
66. James C, Mazurier F, Dupont S, et al. The hematopoietic stem cell compartment of JAK2V617F-positive myeloproliferative disorders is a reflection of disease heterogeneity. *Blood*. 2008;112(6):2429–2438.
67. Mullally A, Lane SW, Ball B, et al. Physiological Jak2V617F Expression Causes a Lethal Myeloproliferative Neoplasm with Differential Effects on Hematopoietic Stem and Progenitor Cells. *Cancer Cell*. 2010;17(6):584–596.
68. Li J, Kent DG, Godfrey AL, et al. JAK2V617F homozygosity drives a phenotypic switch in myeloproliferative neoplasms, but is insufficient to sustain disease. *Blood*. 2014;123(20):3139–3151.
69. Kent DG, Li J, Tanna H, et al. Self-Renewal of Single Mouse Hematopoietic Stem Cells Is Reduced by JAK2V617F Without Compromising Progenitor Cell Expansion. *PLoS Biol.* 2013;11(6):.
70. Rumi E, Cazzola M. Diagnosis, risk stratification, and response evaluation in classical myeloproliferative neoplasms. *Blood*. 2017;129(6):680–692.
71. Vainchenker W, Kralovics R. Genetic basis and molecular pathophysiology of classical myeloproliferative neoplasms. *Blood*. 2017;129(6):667–679.
72. Tiedt R, Hao-Shen H, Sobas MA, et al. Ratio of mutant JAK2-V617F to wild-type Jak2 determines the MPD phenotypes in transgenic mice. *Blood*. 2008;111(8):3931–3940.
73. Ortmann CA, Kent DG, Nangalia J, et al. Effect of Mutation Order on Myeloproliferative Neoplasms. *N. Engl. J. Med.* 2015;372(7):601–612.
74. F Cervantes, D Tassies, C Salgado, M Rovira, A Pereira CR. Acute transformation in nonleukemic chronic myeloproliferative disorders: actuarial probability and main characteristics in a series of 218 patients. *Acta Haematol*. 1991;85(3):124–7.
75. Mesa RA, Li CY, Ketterling RP, et al. Leukemic transformation in myelofibrosis with myeloid metaplasia: A single-institution experience with 91 cases. *Blood*. 2005;105(3):973–977.
76. Dunbar A, Nazir A, Levine R. Overview of transgenic mouse models of myeloproliferative neoplasms (MPNs). *Curr. Protoc. Pharmacol.* 2017;77:14.40.1-14.40.19.
77. Lacout C, Pisani DF, Tulliez M, et al. JAK2V617F expression in murine hematopoietic cells leads to MPD mimicking human PV with secondary myelofibrosis. *Blood*. 2006;108(5):1652–1660.

78. Wernig G, Mercher T, Okabe R, et al. Expression of Jak2V617F causes a polycythemia vera-like disease with associated myelofibrosis in a murine bone marrow transplant model. *Blood*. 2006;107(11):4274–4281.

79. Zaleskas VM, Krause DS, Lazarides K, et al. Molecular pathogenesis and therapy of polycythemia induced in mice by JAK2 V617F. *PLoS One*. 2006;1(1):.

80. Bumm TGP, Elsea C, Corbin AS, et al. Characterization of Murine JAK2 V617F-Positive Myeloproliferative Disease. *Cancer Res*. 2006;66(23):11156–65.

81. Shide K, Shimoda HK, Kumano T, et al. Development of ET, primary myelofibrosis and PV in mice expressing JAK2 V617F. *Leukemia*. 2008;22(1):87–95.

82. Xing S, Ho WT, Zhao W, et al. Transgenic expression of JAK2 V617F causes myeloproliferative disorders in mice. *Blood*. 2008;111(10):5109–5117.

83. Akada H, Yan D, Zou H, et al. Conditional expression of heterozygous or homozygous Jak2V617F from its endogenous promoter induces a polycythemia vera-like disease. *Blood*. 2010;115(17):3589–3597.

84. Juan Li, Dominik Spensberger, Jong Sook Ahn, Shubha Anand, Philip A Beer, Cedric Ghevaert, Edwin Chen, Ariel Forrai, Linda M Scott, Rita Ferreira, Peter J Campbell, Steve P Watson, Pentao Liu, Wendy N Erber, Brian J P Huntly, Katrin Ottersbach ARG. JAK2 V617F impairs hematopoietic stem cell function in a conditional knock-in mouse model of JAK2 V617F-positive essential thrombocythemia. *Blood*. 2010;116(9):1528–38.

85. Morrison SJ, Scadden DT. The bone marrow niche for haematopoietic stem cells. *Nature*. 2014;505(7483):327–334.

86. Jiwang Zhang, Chao Niu, Ling Ye, Haiyang Huang, Xi He, Wei-Gang Tong, Jason Ross, Jeff Haug, Teri Johnson, Jian Q Feng, Stephen Harris, Leanne M Wiedemann, Yuji Mishina LL. Identification of the haematopoietic stem cell niche and control of the niche size. *Nature*. 2003;425(6960):836–41.

87. Seita J, Weissman IL. Hematopoietic stem cell: Self-renewal versus differentiation. *Wiley Interdiscip. Rev. Syst. Biol. Med.* 2010;2(6):640–653.

88. Mendelson A, Frenette PS. Hematopoietic stem cell niche maintenance during homeostasis and regeneration. *Nat. Med.* 2014;20(8):833–846.

89. Ito K, Suda T. Metabolic requirements for the maintenance of self-renewing stem cells. *Nat. Rev. | Mol. CELL Biol.* 2014;15(4):243–56.

90. Bruns I, Lucas D, Pinho S, et al. Megakaryocytes regulate hematopoietic stem cell quiescence through CXCL4 secretion. *Nat Med*. 2014;20(11):1315–20.

91. Hashimoto D, Chow A, Noizat C, et al. Tissue-resident macrophages self-maintain

locally throughout adult life with minimal contribution from circulating monocytes. *Immunity*. 2013;38(4):792–804.

92. Chow A, Huggins M, Ahmed J, et al. CD169^{+} macrophages provide a niche promoting erythropoiesis under homeostasis and stress. *Nat Med*. 2013;19(4):429–436.
93. Winkler IG, Barbier V, Nowlan B, et al. Vascular niche E-selectin regulates hematopoietic stem cell dormancy, self renewal and chemoresistance. *Nat. Med.* 2012;18(11):1651–1657.
94. Yamazaki S, Ema H, Karlsson G, et al. Nonmyelinating schwann cells maintain hematopoietic stem cell hibernation in the bone marrow niche. *Cell*. 2011;147(5):1146–1158.
95. Ingrid G Winkler, Natalie A Sims, Allison R Pettit, Valérie Barbier, Bianca Nowlan, Falak Helwani, Ingrid J Poulton, Nico van Rooijen, Kylie A Alexander, Liza J Raggatt J-PL. Bone marrow macrophages maintain hematopoietic stem cell (HSC) niches and their depletion mobilizes HSCs. *Blood*. 2010;116(23):4815–28.
96. Méndez-Ferrer S, Michurina T V, Ferraro F, et al. Mesenchymal and haematopoietic stem cells form a unique bone marrow niche. *Nature*. 2010;466(7308):829–834.
97. Akada H, Akada S, Hutchison RE, et al. Critical role of Jak2 in the maintenance and function of adult hematopoietic stem cells. *Stem Cells*. 2014;32(7):1878–1889.
98. Carolyn M Butcher, Jonathon F Hutton, Uwe Hahn, L Bik To, Peter Bardy, Ian Lewis RJD. Cellular origin and lineage specificity of the JAK2(V617F) allele in polycythemia vera. *Blood*. 2007;109(1):386–7.
99. Delhommeau F, Dupont S, Tonetti C, et al. Evidence that the JAK2 G1849T (V617F) mutation occurs in a lymphomyeloid progenitor in polycythemia vera and idiopathic myelofibrosis. *Blood*. 2007;109(1):71–77.
100. Dupont S, Massé A, James C, et al. The JAK2 617V>F mutation triggers erythropoietin hypersensitivity and terminal erythroid amplification in primary cells from patients with polycythemia vera. *Blood*. 2007;110(3):1013–1021.
101. Hasan S, Lacout C, Marty C, et al. JAK2V617F expression in mice amplifies early hematopoietic cells and gives them a competitive advantage that is hampered by IFNa. *Blood*. 2013;122(8):1464–1477.
102. Takefumi Ishii, Yan Zhao, Selcuk Sozer, Jun Shi, Wei Zhang, Ronald Hoffman MX. Behavior of CD34+ cells isolated from patients with polycythemia vera in NOD/SCID mice. *Exp Hematol*. 2007;35(11):1633–40.
103. Bennett LF, Liao C, Quickel MD, et al. Inflammation induces stress erythropoiesis through heme-dependent activation of SPI-C. *Sci. Signal.* 2019;12(598):7336.

104. Sara Gardenghi , Tom M Renaud, Alessandra Meloni, Carla Casu, Bart J Crielaard, Laura M Bystrom, Noa Greenberg-Kushnir, Barbra J Sasu, Keegan S Cooke SR. Distinct roles for hepcidin and interleukin-6 in the recovery from anemia in mice injected with heat-killed Brucella abortus. *Blood*. 2014;123(8):.

105. Airie Kim, Eileen Fung, Sona G Parikh, Erika V Valore, Victoria Gabayan, Elizabeta Nemeth TG. A mouse model of anemia of inflammation: complex pathogenesis with partial dependence on hepcidin. *Blood*. 2014;123(8):1129–36.

106. Sarah Millot, Valérie Andrieu, Philippe Letteron, Saïd Lyoumi, Margarita Hurtado-Nedelec, Zoubida Karim, Olivier Thibaudeau, Samira Bennada, Jean-Luc Charrier, Sigismond Lasocki CB. Erythropoietin stimulates spleen BMP4-dependent stress erythropoiesis and partially corrects anemia in a mouse model of generalized inflammation. *Blood*. 2010;116(26):.

107. Brown DE, Nick HJ, McCoy MW, et al. Increased ferroportin-1 expression and rapid splenic iron loss occur with anemia caused by Salmonella enterica serovar typhimurium infection in mice. *Infect. Immun.* 2015;83(6):2290–2299.

108. Jackson A, Nanton MR, O'Donnell H, Akue AD, McSorley SJ. Innate Immune Activation during Salmonella Infection Initiates Extramedullary Erythropoiesis and Splenomegaly. *J. Immunol.* 2010;185(10):6198–6204.

109. Li LX, Benoun JM, Weiskopf K, Garcia KC, McSorley SJ. Salmonella infection enhances erythropoietin production by the kidney and liver, which correlates with elevated bacterial burdens. *Infect. Immun.* 2016;84(10):2833–2841.

110. Barbra J Sasu, Keegan S Cooke, Tara L Arvedson, Cherylene Plewa, Aaron R Ellison, Jackie Sheng, Aaron Winters, Todd Juan, Hongyan Li, C Glenn Begley GM. Antihepcidin antibody treatment modulates iron metabolism and is effective in a mouse model of inflammation-induced anemia. *Blood*. 2010;115(17):3616–24.

111. Camaschella C, Nai A. Ineffective erythropoiesis and regulation of iron status in iron loading anaemias. *Br. J. Haematol.* 2016;172(4):512–523.

112. Asterios S Tsiftsoglou, Ioannis S Vizirianakis JS. Erythropoiesis: model systems, molecular regulators, and developmental programs. *IUBMB Life*. 2009;61(8):800–30.

113. Paulson RF, Shi L, Wu DC. Stress erythropoiesis: New signals and new stress progenitor cells. *Curr. Opin. Hematol.* 2011;18(3):139–145.

114. Harandi OF, Hedge S, Wu DC, Mckeone D, Paulson RF. Murine erythroid short-term radioprotection requires a BMP4-dependent, self-renewing population of stress erythroid progenitors. *J. Clin. Invest.* 2010;120(12):4507–4519.

115. Lenox LE, Perry JM, Paulson RF. BMP4 and Madh5 regulate the erythroid response to

acute anemia. *Blood*. 2005;105(7):2741–2748.

116. Perry JM, Harandi OF, Porayette P, et al. Maintenance of the BMP4-dependent stress erythropoiesis pathway in the murine spleen requires hedgehog signaling. *Blood*. 2009;113(4):911–918.
117. Ishizuya-Oka A, Hasebe T. Sonic hedgehog and bone morphogenetic protein-4 signaling pathway involved in epithelial cell renewal along the radial axis of the intestine. *Digestion*. 2008;77(SUPPL. 1):42–47.
118. John M Perry , Omid F Harandi RFP. BMP4, SCF, and hypoxia cooperatively regulate the expansion of murine stress erythroid progenitors. *Blood*. 2007;109(10):4494–502.
119. Xiang J, Wu DC, Chen Y, Paulson RF. In vitro culture of stress erythroid progenitors identifies distinct progenitor populations and analogous human progenitors. *Blood*. 2015;125(11):1803–1812.
120. Cornelis J H Pronk DB. Flow cytometry-based identification of immature myeloerythroid development. *Methods Mol Biol*. 2011;699:275–93.
121. Pronk CJH, Rossi DJ, Månsson R, et al. Elucidation of the Phenotypic, Functional, and Molecular Topography of a Myeloerythroid Progenitor Cell Hierarchy. *Cell Stem Cell*. 2007;1(4):428–442.
122. Oda A, Tezuka T, Ueno Y, et al. Niche-induced extramedullary hematopoiesis in the spleen is regulated by the transcription factor Tlx1. *Sci. Rep.* 2018;8(1):8308.
123. Bennett LF, Liao C, Paulson RF. Stress erythropoiesis model systems. *Methods Mol. Biol.* 2018;1698:91–102.
124. Robert F Paulson , Baiye Ruan , Siyang Hao YC. Stress Erythropoiesis is a Key Inflammatory Response. *Cells*. 2020;9(3):634.
125. Hao S, Xiang J, Wu DC, et al. Gdf15 regulates murine stress erythroid progenitor proliferation and the development of the stress erythropoiesis niche. *Blood Adv.* 2019;3(14):2205–2217.
126. John M Perry, Omid F Harandi RFP. BMP4, SCF, and hypoxia cooperatively regulate the expansion of murine stress erythroid progenitors. *Blood*. 2007;109(10):4494–502.
127. Manz MG, Boettcher S. Emergency granulopoiesis. *Nat. Rev. Immunol.* 2014;14(5):302–314.
128. H Hara MO. Erthropoietic precursors in mice with phenylhydrazine-induced anemia. *Am J Hematol*. 1976;1(4):453–8.
129. Broudy VC, Lin NL, Priestley G V, Nocka K, Wolf NS. Interaction of stem cell factor and its receptor c-kit mediates lodgment and acute expansion of hematopoietic cells in the murine spleen. *Blood*. 1996;88(1):75–81.

130. Porayette P, Paulson RF. BMP4/Smad5 dependent stress erythropoiesis is required for the expansion of erythroid progenitors during fetal development. *Dev. Biol.* 2008;317(1):24–35.
131. Lenox LE, Shi L, Hegde S, Paulson RF. Extramedullary erythropoiesis in the adult liver requires BMP-4/Smad5-dependent signaling. *Exp. Hematol.* 2009;37(5):549–558.
132. Obinata M, Yanai N. Cellular and molecular regulation of an erythropoietic inductive microenvironment (EIM). *Cell Struct. Funct.* 1999;24(4):171–179.
133. HERBERT Z. GIFFIN EVA. Experiments With Phenylhydrazine. *Ann. Intern. Med.* 1928;1(9):655–676.
134. HERBERT Z. GIFFIN HMC. The untoward effects of treatment by Phenylhydrazine hydrochloride. *JAMA*. 1929;92(18):1505–1507.
135. Cary R BS and BI. Concise International Chemical Assessment Document 19 PHENYLHYDRAZINE. Published under the joint sponsorship of the United Nations Environment Programme the International Labour Organisation and the World Health Organization and produced within the framew. 2000.
136. Stern A. Drug-induced oxidative denaturation in red blood cells. *Semin Hematol.* 1989;26(4):301–6.
137. Stern A. Drug-induced oxidative denaturation in red blood cells. *Semin Hematol*. 1989;26(4):301–6.
138. H Shimizu, K Hayashi NT. Relationships between the mutagenic and carcinogenic effects of hydrazine derivatives. *Nihon Eiseigaku Zasshi*. 1978;33(3):474–85.
139. Muller W, Engelhart G, Herbold B, Jackh R, Jung R. Evaluation of mutagenicity testing with Salmonella typhimurium TA102 in three different laboratories. *Environ. Health Perspect.* 1993;101(SUPPL. 3):33–36.
140. H Hara MO. Erythropoietic precursors in mice under erythropoietic stimulation and suppression. *Exp Hematol*. 1977;5(2):141–8.
141. Liao C, Sandeep Prabhu K, Paulson RF. Monocyte-derived macrophages expand the murine stress erythropoietic niche during the recovery from anemia. *Blood*. 2018;132(24):2580–2593.
142. Paulson RF, Shi L, Wu D-C. Stress erythropoiesis: new signals and new stress progenitor cells Correspondence to NIH Public Access. *Curr Opin Hematol*. 2011;18(3):139–145.
143. Hara H. Kinetics of pluripotent hemopoietic precursors in vitro after erythropoietic stimulation or suppression. *Exp Hematol*. 1980;8(3):345–50.
144. H Hara MO. Erythropoietic precursors in murine blood. *Exp Hematol*. 1977;5(3):161–5.

145. R J Cole TR. Haemopoietic progenitor cells in prenatal congenitally anaemic “flexed-tailed” (f/f) mice. *Br J Haematol*. 1976;33(3):387–94.
146. R J Cole, T Regan RGT. Haemoglobin synthesis in reticulocytes of prenatal f-f anaemic mice. *Br J Haematol*. 1972;23(4):443–52.
147. C J Gregory, E A McCulloch JET. The cellular basis for the defect in haemopoiesis in flexed-tailed mice. III. Restriction of the defect to erythropoietic progenitors capable of transient colony formation in vivo. *Br J Haematol*. 1975;30(4):401–10.
148. R Mixter HRH. Anemia in the Flexed Tailed Mouse, Mus Musculus. *Genetics*. 1933;18(4):367–87.
149. Laurie E Lenox , John M Perry RFP. BMP4 and Madh5 regulate the erythroid response to acute anemia. *Blood*. 2005;105(7):2741–8.
150. D L Coleman, E S Russell EYL. Enzymatic studies of the hemopoietic defect in flexed mice. *Genetics*. 1969;61(3):631–42.
151. Criswell KA, Sulkanen AP, Hochbaum AF, Bleavins MR. Effects of phenylhydrazine or phlebotomy on peripheral blood, bone marrow and erythropoietin in Wistar rats. *J. Appl. Toxicol.* 2000;20(1):25–34.
152. Bessette H, Brassard F, Salvail G, Smolin L. p53, guardian of the genome. 1992.
153. Levine AJ. The paths to death and differentiation. *Cell Death Differ.* 2011;18(9):1391–1392.
154. Xu-Monette ZY, Jeffrey Medeiros L, Li Y, et al. Dysfunction of the TP53 tumor suppressor gene in lymphoid malignancies. *Blood*. 2012;119(16):3668–3683.
155. B Vogelstein, D Lane AJL. Surfing the p53 network. *Nature*. 2000;408(6810):307–10.
156. P Hainaut, T Hernandez, A Robinson, P Rodriguez-Tome, T Flores, M Hollstein, C C Harris RM. IARC Database of p53 gene mutations in human tumors and cell lines: updated compilation, revised formats and new visualisation tools. *Nucleic Acids Res*. 1998;26(1):.
157. Olive KP, Tuveson DA, Ruhe ZC, et al. Mutant p53 gain of function in two mouse models of Li-Fraumeni syndrome. *Cell*. 2004;119(6):847–860.
158. Learning M, Cookbook R. Mice deficient for p53 are developmentally normal but susceptible to spontaneous tumours. *Nature*. 1992;356(6366):215–21.
159. Gene A Lang, Tomoo Iwakuma, Young-Ah Suh, Geng Liu, V Ashutosh Rao, John M Parant, Yasmine A Valentin-Vega, Tamara Terzian, Lisa C Caldwell, Louise C Strong, Adel K El-Naggar GL. Gain of function of a p53 hot spot mutation in a mouse model of Li-Fraumeni syndrome. *Cell*. 2004;119(6):861–72.
160. Jacks T, Remington L, Williams BO, et al. Tumor spectrum analysis in p53-mutant mice.

Curr. Biol. 1994;4(1):1–7.

161. Chao Dai WG. p53 post-translational modification: deregulated in tumorigenesis. *Trends Mol Med*. 2010;16(11):528–36.
162. Trotta R, Vignudelli T, Candini O, et al. BCR/ABL activates mdm2 mRNA translation via the La antigen. *Cancer Cell*. 2003;3(2):145–160.
163. Goetz AW, Van der Kuip H, Aulitzky WE, Maya R, Oren M. Requirement for Mdm2 in the survival effects of Bcr-Abl and interleukin 3 in hematopoietic cells. *Cancer Res.* 2001;61(20):7635–7641.
164. Zhang SJ, Rampal R, Manshouri T, et al. Genetic analysis of patients with leukemic transformation of myeloproliferative neoplasms shows recurrent SRSF2 mutations that are associated with adverse outcome. *Blood*. 2012;119(19):4480–4485.
165. Anthony Green PB. Somatic mutations of IDH1 and IDH2 in the leukemic transformation of myeloproliferative neoplasms. *N Engl J Med*. 2010;362(4):369–70.
166. Abdel-Wahab O, Manshouri T, Patel J, et al. Genetic analysis of transforming events that convert chronic myeloproliferative neoplasms to leukemias. *Cancer Res.* 2010;70(2):447–452.
167. Harutyunyan A, Klampfl T, Cazzola M, Kralovics R. p53 Lesions in Leukemic Transformation. *N. Engl. J. Med.* 2011;364(5):488–490.
168. Rampal R, Ahn J, Abdel-Wahaba O, et al. Genomic and functional analysis of leukemic transformation of myeloproliferative neoplasms. *Proc. Natl. Acad. Sci. U. S. A.* 2014;111(50):E5401–E5410.
169. Zhao W, Du Y, Ho WT, Fu X, Zhao ZJ. JAK2V617F and p53 mutations coexist in erythroleukemia and megakaryoblastic leukemic cell lines. *Exp. Hematol. Oncol.* 2012;1(1):.
170. Marcellino BK, Hoffman R, Tripodi J, et al. Advanced forms of MPNs are accompanied by chromosomal abnormalities that lead to dysregulation of TP53. *Blood Adv.* 2018;2(24):3581–3589.
171. H M Kantarjian, M Talpaz JG. Biologic therapy of chronic myelogenous leukemia. *Oncol. (willist. Park.* 1987;1(7):35–40.
172. T Hernandez-Boussard, P Rodriguez-Tome, R Montesano PH. IARC p53 mutation database: a relational database to compile and analyze p53 mutations in human tumors and cell lines. International Agency for Research on Cancer. *Hum Mutat*. 1999;14(1):1–8.
173. Feinstein E, Cimino G, Galet RP, et al. p53 in chronic myelogenous leukemia in acute phase. *Proc. Natl. Acad. Sci. USA*. 1991;88(14):6293–6297.

174. G Gaidano, C Pastore, V Santini, J Nomdedeu, B Gamberi, D Capello, F Vischia, L Resegotti, U Mazza, P R Ferrini, F Lo Coco GS. Genetic lesions associated with blastic transformation of polycythemia vera and essential thrombocythemia. *Genes Chromosom. Cancer*. 1997;19(4):250–5.

175. Tsurumi S, Nakamura Y, Maki K, et al. N-ras and p53 gene mutations in Japanese patients with myeloproliferative disorders. *Am. J. Hematol.* 2002;71(2):131–133.

176. Reilly JT. Pathogenesis of acute myeloid leukaemia and inv(16)(p13;q22): A paradigm for understanding leukaemogenesis? *Br. J. Haematol.* 2005;128:18–34.

177. G Gaidano, C Pastore, A Gloghini, G Volpe, D Capello, P Polito, E Vaccher, U Tirelli, G Saglio AC. Human herpesvirus type-8 (HHV-8) in haematopoietic neoplasia. *Leuk Lymphoma*. 1997;24(3–4):257–66.

178. Kubesova B, Pavlova S, Malcikova J, et al. Low-burden TP53 mutations in chronic phase of myeloproliferative neoplasms: Association with age, hydroxyurea administration, disease type and JAK2 mutational status. *Leukemia*. 2018;32(2):450–461.

179. Zhang J, Kong G, Rajagopalan A, et al. p53-/- synergizes with enhanced NrasG12D signaling to transform megakaryocyte-erythroid progenitors in acute myeloid leukemia. *Blood*. 2017;129(3):358–370.

180. T Tsuruta-Kishino , J Koya, K Kataoka, K Narukawa, Y Sumitomo , H Kobayashi , T Sato MK. Loss of p53 induces leukemic transformation in a murine model of Jak2 V617F-driven polycythemia vera. *Oncogene*. 2017;36(23):3300–3311.

181. Ogilvy S, Elefanty AG, Visvader J, et al. Transcriptional regulation of vav, a gene expressed throughout the hematopoietic compartment. *Blood*. 1998;91(2):419–430.

182. Ogilvy S, Metcalf D, Gibson L, et al. Promoter elements of vav drive transgene expression in vivo throughout the hematopoietic compartment. *Blood*. 1999;94(6):1855–1863.

183. D R Shimshek, J Kim, M R Hübner, D J Spergel, F Buchholz, E Casanova, A F Stewart, P H Seeburg RS. Codon-improved Cre recombinase (iCre) expression in the mouse. *Genesis*. 2002;32(1):19–26.

184. Domen J, Cheshier SH, Weissman IL. The Role of Apoptosis in the Regulation of Hematopoietic Stem Cells: Overexpression of BCL-2 Increases Both Their Number and Repopulation Potential. 2000.

185. Dingli D, Traulsen A, Pacheco JM. Compartmental architecture and dynamics of hematopoiesis. *PLoS One*. 2007;2(4):.

186. Boggs DR. The total marrow mass of the mouse: A simplified method of measurement.

Am. J. Hematol. 1984;16(3):277–286.

187. P A Chervenick, D R Boggs, J C Marsh, G E Cartwright MMW. Quantitative studies of blood and bone marrow neutrophils in normal mice. *Am J Physiol*. 1968;215(2):353–60.
188. Mahajan MM, Cheng B, Beyer AI, et al. A quantitative assessment of the content of hematopoietic stem cells in mouse and human endosteal-bone marrow: a simple and rapid method for the isolation of mouse central bone marrow. *BMC Hematol.* 2015;
189. Busch K, Klapproth K, Barile M, et al. Fundamental properties of unperturbed haematopoiesis from stem cells in vivo. *Nature*. 2015;518(7540):542–546.
190. Sanchez M, Weissman IL, Pallavicini M, et al. Differential Amplification of Murine Bipotent Megakaryocytic/Erythroid Progenitor and Precursor Cells During Recovery from Acute and Chronic Erythroid Stress. *Stem Cells*. 2006;24(2):337–348.
191. McKim DB, Yin W, Wang Y, et al. Social Stress Mobilizes Hematopoietic Stem Cells to Establish Persistent Splenic Myelopoiesis. *Cell Rep.* 2018;25(9):2552-2562.e3.
192. Li H, Natarajan A, Ezike J, et al. Rate of Progression through a Continuum of Transit-Amplifying Progenitor Cell States Regulates Blood Cell Production. *Dev. Cell*. 2019;49(1):118-129.e7.
193. Mori Y, Chen JY, Pluvinage J V., Seita J, Weissman IL. Prospective isolation of human erythroid lineage-committed progenitors. *Proc. Natl. Acad. Sci. U. S. A.* 2015;112(31):9638–9643.
194. Kang YA, Pietras EM, Passegué E. Deregulated notch and wnt signaling activates early-stage myeloid regeneration pathways in leukemia. *J. Exp. Med.* 2020;217(3):.
195. Haas S, Hansson J, Klimmeck D, et al. Inflammation-Induced Emergency Megakaryopoiesis Driven by Hematopoietic Stem Cell-like Megakaryocyte Progenitors. *Cell Stem Cell*. 2015;17(4):422–434.
196. J L Abkowitz, D Golinelli, D E Harrison PG. In vivo kinetics of murine hemopoietic stem cells. *Comp. Study*. 2000;96(10):3399–405.
197. Markus Klose, Maria Carolina Florian , Alexander Gerbaulet, Hartmut Geiger IG. Hematopoietic Stem Cell Dynamics Are Regulated by Progenitor Demand: Lessons from a Quantitative Modeling Approach. *Stem Cells*. 2019;37(7):948–957.
198. Mackey MC. Cell kinetic status of haematopoietic stem cells. *Cell Prolif.* 2001;34(2):71–83.
199. Manesso E, Teles J, Bryder D, Peterson C. Dynamical modelling of haematopoiesis: An integrated view over the system in homeostasis and under perturbation. *J. R. Soc. Interface*. 2013;10(80):.

200. Crauste F, Demin I, Gandrillon O, Volpert V. Mathematical study of feedback control roles and relevance in stress erythropoiesis. *J. Theor. Biol.* 2010;263(3):303–316.
201. Crauste F, Pujo-Menjouet L, Génieys S, Molina C, Gandrillon O. Adding self-renewal in committed erythroid progenitors improves the biological relevance of a mathematical model of erythropoiesis. *J. Theor. Biol.* 2008;250(2):322–338.
202. Angulo O, Gandrillon O, Crauste F. Investigating the role of the experimental protocol in phenylhydrazine-induced anemia on mice recovery. *J. Theor. Biol.* 2018;437:286–298.
203. Loeffler M, Pantel K, Wulfff H, Wichmannt HE, Loeffler M. A mathematical model of erythropoiesis in mice and rats Part 1: Structure of the model. 1989.
204. Anna Marciniak-Czochra, Thomas Stiehl, Anthony D Ho, Willi Jäger WW. Modeling of asymmetric cell division in hematopoietic stem cells--regulation of self-renewal is essential for efficient repopulation. *Stem Cells Dev*. 2009;18(3):377–85.
205. Roeder I, Kamminga LM, Braesel K, et al. Competitive clonal hematopoiesis in mouse chimeras explained by a stochastic model of stem cell organization. *Blood*. 2005;105(2):609–616.
206. Kirouac DC, Ito C, Csaszar E, et al. Dynamic interaction networks in a hierarchically organized tissue. *Mol. Syst. Biol.* 2010;6(417):1–16.
207. Mahadik B, Hannon B, Harley BAC. A computational model of feedback-mediated hematopoietic stem cell differentiation in vitro. *PLoS One*. 2019;14(3):.
208. John M Perry , Omid F Harandi, Prashanth Porayette, Shailaja Hegde, Arun K Kannan RFP. Maintenance of the BMP4-dependent stress erythropoiesis pathway in the murine spleen requires hedgehog signaling. *Blood*. 2009;113(4):911–8.
209. Mayle A, Luo M, Jeong M, Goodell MA. Mouse Hematopoietic Stem Cell Identification And Analysis. *Cytometry. A*. 2013;75(1):14–24.
210. Loeb LA, Kohrn BF, Loubet-Senear KJ, et al. Extensive subclonal mutational diversity in human colorectal cancer and its significance. *Proc. Natl. Acad. Sci. U. S. A.* 2019;116(52):26863–26872.
211. Cumbo C, Tota G, Anelli L, et al. TP53 in myelodysplastic syndromes: Recent biological and clinical findings. *Int. J. Mol. Sci.* 2020;21(10):3432.
212. Koeffler HP. Myelodysplastic syndromes (preleukemia). *Semin. Hematol.* 1986;23(4):284–299.
213. Natelson EA, Pyatt D. Acquired myelodysplasia or myelodysplastic syndrome: Clearing the fog. *Adv. Hematol.* 2013;2013:1–11.
214. Rothe A. Contact dermatitis from N- (a- chlorobenzylidene) phenylhydrazine. *Contact*

Dermatitis. 1988;18(1):16–19.

215. Sérgio Paulo Bydlowski F de LJ. Hematopoietic Stem Cell in Acute Myeloid Leukemia Development. *Adv. Hematol. Stem Cell Res.* 2012;261–276.
216. Germing U, Kndgen A, Haas R, Gattermann N. Myelodysplastische Syndrome (MDS). *Dtsch. Medizinische Wochenschrift*. 2012;183–185.
217. Bejar R, Stevenson K, Abdel-Wahab O, et al. Clinical Effect of Point Mutations in Myelodysplastic Syndromes. *N. Engl. J. Med.* 2011;364(26):2496–2506.
218. Fernández-Medarde A, Santos E. Ras in cancer and developmental diseases. *Genes and Cancer*. 2011;2(3):344–358.
219. Suter R, Marcum JA. The molecular genetics of breast cancer and targeted therapy. *Biol. Targets Ther.* 2007;(3):241–258.
220. Takashima A, Faller D V. Targeting the RAS oncogene. *Expert Opin. Ther. Targets*. 2013;17(5):507–531.
221. Adjei AA. Blocking oncogenic Ras signaling for cancer therapy. *J. Natl. Cancer Inst.* 2001;93(14):1062–1074.
222. Wang J, Liu Y, Li Z, et al. Endogenous oncogenic NRAS mutation promotes aberrant GM-CSF signaling in granulocytic/monocytic precursors in a murine model of chronic myelomonocytic leukemia. *Blood*. 2010;116(26):5991–6002.
223. Ricci C, Fermo E, Corti S, et al. RAS mutations contribute to evolution of chronic myelomonocytic leukemia to the proliferative variant. *Clin. Cancer Res.* 2010;16(8):2246–2256.
224. Padua RA, Guinn BA, Al-Sabah AI, et al. RAS, FMS and p53 mutations and poor clinical outcome in myelodysplasias: A 10-year follow-up. *Leukemia*. 1998;12(6):887–892.
225. Omidvar N, Kogan S, Beurlet S, et al. BCL-2 and mutant NRAS interact physically and functionally in a mouse model of progressive myelodysplasia. *Cancer Res.* 2007;67(24):11657–11667.
226. Parikh C, Subrahmanyam R, Ren R. Oncogenic NRAS rapidly and efficiently induces CMML- And AML-like diseases in mice. *Blood*. 2006;108(7):2349–2357.
227. Meek DW. Tumour suppression by p53: A role for the DNA damage response? *Nat. Rev. Cancer*. 2009;714–723.
228. Chen J. The cell-cycle arrest and apoptotic functions of p53 in tumor initiation and progression. *Cold Spring Harb. Perspect. Med.* 2016;6(3):a026104.
229. Aubrey BJ, Kelly GL, Janic A, Herold MJ, Strasser A. How does p53 induce apoptosis and how does this relate to p53-mediated tumour suppression? *Cell Death Differ.* 2018;104–113.

230. Rivlin N, Brosh R, Oren M, Rotter V. Mutations in the p53 tumor suppressor gene: Important milestones at the various steps of tumorigenesis. *Genes and Cancer*. 2011;466–474.

231. Olivier M, Hollstein M, Hainaut P. TP53 mutations in human cancers: origins, consequences, and clinical use. *Cold Spring Harb. Perspect. Biol.* 2010;2;a001008.

232. Perri F, Pisconti S, Vittoria Scarpati G Della. P53 mutations and cancer: A tight linkage. *Ann. Transl. Med.* 2016;4(24):1–4.

233. Salari A, Thomay K, Lentes J, et al. Effect of TP53 contact and conformational mutations on cell survival and erythropoiesis of human hematopoietic stem cells in a long term culture model. *Oncotarget*. 2018;9(52):29869–29876.

234. Kogan SC, Lagasse E, Atwater S, et al. The PEBP2βMYH11 fusion created by Inv(16)(p13;q22) in myeloid leukemia impairs neutrophil maturation and contributes to granulocytic dysplasia. *Proc. Natl. Acad. Sci. U. S. A.* 1998;95(20):11863–11868.

235. Scott C Kogan, Jerrold M Ward, Miriam R Anver, Jules J Berman, Cory Brayton, Robert D Cardiff, John S Carter, Sherri de Coronado, James R Downing, Torgny N Fredrickson, Diana C Haines, Alan W Harris, Nancy Lee Harris, Hiroshi Hiai, Elaine S Jaffe, Ian C M H subcommittee of the MM of HCC. Bethesda proposals for classification of nonlymphoid hematopoietic neoplasms in mice. *Blood*. 2002;100(1):238–45.

236. Le Pogam C, Krief P, Beurlet S, et al. Localization of the NRAS: BCL-2 complex determines anti-apoptotic features associated with progressive disease in myelodysplastic syndromes. *Leuk. Res.* 2013;37(3):312–319.

237. Beurlet S, Omidvar N, Gorombei P, et al. BCL-2 inhibition with ABT-737 prolongs survival in an NRAS/BCL-2 mouse model of AML by targeting primitive LSK and progenitor cells. *Blood*. 2013;122(16):2864–2876.

238. Darley RL, Hoy TG, Baines P, Padua RA, Burnett AK. Mutant N-RAS induces erythroid lineage dysplasia in human CD34+ cells. *J. Exp. Med.* 1997;185(7):1337–1347.

239. Leukemia M, Itzykson R, Kosmider O, et al. Prognostic score including gene mutations in chronic Myelomonocytic Leukemia. *J. Clin. Oncol.* 2013;31(19):2428–2436.

240. Vogiatzi F, Brandt DT, Schneikert J, et al. Mutant p53 promotes tumor progression and metastasis by the endoplasmic reticulum UDPase ENTPD5. *Proc. Natl. Acad. Sci. U. S. A.* 2016;113(52):E8433–E8442.

241. Falchook GS, Lewis KD, Infante JR, et al. Activity of the oral MEK inhibitor trametinib in patients with advanced melanoma: A phase 1 dose-escalation trial. *Lancet Oncol.* 2012;13(8):782–789.

242. Rutkowski P. What is new in melanoma after European Cancer Congress 2017?

Melanoma Manag. 2017;4(2):83–87.

243. Pollyea DA, Amaya M, Strati P, Konopleva MY. Venetoclax for AML: Changing the treatment paradigm. *Blood Adv.* 2019;3(24):4326–4335.

244. Knight T, Edwards H, Taub JW, Ge Y. Evaluating venetoclax and its potential in treatment-naïve acute myeloid leukemia. *Cancer Manag. Res.* 2019;11:3197–3213.

SUPPLEMENTARY

P53 Deficiency in collaboration with NRASD12 accelerates disease in a mouse model of MDS/AML progression

Panhong Gou[1], Saravanan Ganesan[1], Nader Omidvar[2], Caren Brumpt[3], Pierre Lemaire[4], Fortune Hontonnou[1,5], Benoit Hosten[5,6,7]Evelyne Lauret[8], Wenchao Zhang[9], Christophe Leboeuf[10], Anne Janin[10], Marika Pla[1], Niclas Setterblad[11], Nicolas Vignal[7,12,] Christine Chomienne[1], Laure Sarda-Mantel[6,12], Stéphane Giraudier[1,4], Rose Ann Padua[1*], Pierre Fenaux[4,13]

[1]Inserm UMR-S1131, Université de Paris, IRSL, Hôpital Saint-Louis, Paris, France

[2]Cardiff University Medical School, Hematology Department, UKH

[3]Hematology Laboratory, Lariboisière Hospital, Assistance Publique-Hôpitaux de Paris (APHP), Paris, France

[4]Hopital Saint-Louis, APHP, Paris, France

[5]Unité Claude Kellershohn, Université de Paris, IRSL, France

[6]Radiopharmacie, Hôpital St-Louis, APHP, Paris, France

[7]Inserm UMR-S1144, Faculté de Pharmacie, Université de Paris, IRSL, Paris, France

[8]Université de Paris, Institut Cochin, INSERM U1016, CNRS UMR 8104, F-75014 Paris, France

[9]Université de Paris, BFA, UMR 8251, CNRS, F-75013, Paris, France

[10]Inserm UMR-S 942, Université de Paris, France

[11]Imagerie Département, Université de Paris, IRSL, Paris France

[12]Service de Médecine Nucléaire, Hôpital Lariboisière, APHP, Paris, France

[13]Inserm UMR-S944**,** Université de Paris, IRSL, France

*Corresponding author: Rose Ann Padua, Inserm UMR-S1131, Université de Paris, IRSL, Hôpital Saint-Louis, Paris, France,rose-ann.padua@inserm.fr

Running title: NRASD12 and p53 deficiency in MDS/AML progression

Key Points

1. Together with NRASD12 loss of function of one allele of p53 gives rise to a HR-MDS-like disease with increased apoptosis
2. Loss of both p53 alleles gives rise to AML-like disease with decreased apoptosis in mice.

Abstract

NRAS and *p53* mutations are frequently found in myelodysplastic syndromes (MDS) and acute myelogenous leukemia (AML). To define the role of these genes in MDS/AML progression transgenic mice with human *NRASD12* were bred with *p53*-deficient mice. Mice with *NRASD12* alone had lower risk MDS-like disease with increased apoptosis; together with loss of one allele of *p53* bone marrow (BM) blast counts consistent with higher risk MDS (24.8 %) and increased apoptosis was observed; with homozygous loss of *p53*, mice had increased BM blast counts consistent with AML-like disease (37.5%) with decreased apoptosis and thrombocytopenia. The diseases were serially transplantable, illustrating self-renewal properties. The percentage of granulocyte monocyte/macrophage progenitors (GMPs) was increased in the *NRASD12/p53*$^{-/-}$ compared with *NRASD12/p53*$^{+/-}$ mice. The megakaryocyte erythroid progenitors (MEPs) were decreased in *NRASD12* alone and *NRASD12/p53*-deficient mice. The lineage $^{-}$/Sca1^{+}/c-Kit^{+}(LSK) population was increased in BM and spleens of *NRASD12* and *NRASD12/p53*$^{+/-}$ mice, but the long term(LT)- and short term(ST)-hematopoietic stem cells(HSC) were decreased. The use of the BCL-2(ABT-199) and MEK (GDC-0975) inhibitors showed a decrease in progenitors from transplanted mice *ex vivo*; the BCL-2 inhibitor alone was not efficient, but resistance was overcome by the addition of the MEK inhibitor. *In vivo* the BCL-2 inhibitor alone prolonged the lifespan of some mice (responders as visualized by Positron Emission Tomography (PET)

scanning). Post treatment RAS/Bcl-2 co-localization studies showed a mitochondrial localization in the transplanted AML as expected of drug sensitivity, a reduction in activated RASGTP and increase in apoptosis. Thus, p53 deficiency contributes to MDS/AML progression.

Introduction

Myelodysplastic syndromes (MDS) represent a preleukemia state of ineffective hematopoiesis hallmarked by bone marrow dysplasia with peripheral blood cytopenias, which is associated with increased apoptosis[1,2]. Acute myeloid leukemia (AML) results from the accumulation of mutations that deregulate self-renewal, proliferation, and differentiation in hematopoietic stem and progenitor cells (HSPCs)[3–5]. One third of MDS patients progress to AML, but most of the patients do not survive the cytopenia of MDS[6,7].

The *NRAS* gene is a member of the RAS family, which play important roles in cell division, cell differentiation, and the self-destruction of cells[8,9]. The *NRAS* gene is frequently mutated in cancer leading to a constitutively activated MAPK pathway, which is important for oncogenesis, tumor proliferation and survival[8,10,11]. *NRAS* and other *RAS* genes are often mutated in chronic myelomonocytic leukemia (CMML) [12–14] and jeuvenile mylelomonocytic leukemia (JMML)[15,16]. The tumor suppressor protein 53 (TP53) is a transcription factor, mediating a variety of biological processes like DNA repair, metabolism, apoptosis, cell cycle progression and cell differentiation[17–19]. Loss of function of

TP53 can be obtained through *p53* mutation or loss of one or both alleles causing abnormal cancer cell development, survival and uncontrolled proliferation[20]. *P53* mutations have been identified in several solid tumors[21,22] and also prevalent in AML or post- MDS/MPN patients who have complex karyotypes[14,22]. Furthermore, the *p53* mutation is an important negative predictor of survival and relapse after allogeneic transplant in MDS patients[14]. The function of p53 loss in leukemia progression has been elucidated in MDS murine models[23]. In MDS mice, p53 loss has a positive role in restoring the hematopoietic stem/progenitor cell defect. Previous studies showed that *NRAS* and *p53* mutations are concurrent in MDS patients[14]. A study identified 8 of 1238 of myeloid neoplasms patients expressing both *p53* and *RAS* pathway gene mutations; most of them were secondary AML with a dismal prognosis[15]. To better understand if the *NRAS* mutation and *p53* loss to causes progression from MDS transformation into AML, we crossed an NRASD12 transgenic mice [24] with a *p53* deficient mouse[25]

Materials and methods

Mice

All mouse lines were maintained in the friend leukemia virus B (FVB/N) strain from the National Institutes of Health in the barrier facilities of the Institut de la Recherche Saint-Louis, Paris, Hospital Saint-Louis, under the appropriate animal project licenses. All procedures complied with national regulations on

the use of animals for experimentation. Mice were sacrificed based on veterinary advice or when they were moribund. Mice were classified according to the Bethesda method[26].

Mice bearing a constitutive hemizygous *MRP8NRASD12* previously shown to develop MDS[15,24], were crossed to *p53* deficient mice (FVB. 129S2 (B6)-Trp53tm1Tyj)[25] to generate the *MRP8NRASD12/p53*$^{+/-}$ mice. *MRP8NRASD12/p53+/-* mice were crossed to p53$^{+/-}$ or p53$^{-/-}$ mice to generate *MRP8NRASD12/p53*$^{-/-}$ mice. The genotyping of *MRP8NRASD12* and *p53*$^{-/-}$ were tested by polymerase chain reaction (PCR) as previously described[15].

The primers of *NRASD12* and *p53*[25] are: *p53* WT forward primer-5'AGG CTT AGA GGT CGCA AGC TG 3'; *p53* deleted forward primer-5'CAG CCT CTG TTC CAC ATA CAC T 3'; *p53* reverse primer-5' TGG ATG GTG GTA TAC TCA GAG C 3'; *NRASD12* forward primer- 5'GCTGTCTTTCAGAAGACCTG 3'; *NRASD12* reverse primer-5'ACTGGTGGTGGTTGGAGCAG 3'.

Treatment and analysis of mice

For bone marrow transplantation (BMT), BM was isolated from both tibias and femurs were harvested from 6- to 10-week-old *MRP8NRASD12/p53*$^{-/-}$ mice as described above, pooled and divided (10^7 nucleated cell aliquots per recipient) for intravenous (iv) injections into recipient FVB/N mice, which were treated with busulfan (120-150 microlitres of a 6mg/ml solution) 24 hours before transplantation. A mouse was left uninjected as a control for the busulfan conditioning. Successful transfers of the transgene-positive mice were

confirmed by PCR 3 weeks after transplant. Mice were followed for survival. A cohort of primary transplanted mice were treated with ABT-199 (Venetoclax, aBCL -2 inhibitor) (75mg/kg every other day 15 times for 33 days) and transferred into secondary or tertiary recipients. Disease was confirmed by peripheral blood (PB) counts and blast cell counts. White blood cell (WBC), red blood cell (RBC), hemoglobin, hematocrit (HCT), and platelet counts (PLT) were measured with an automated counter (MS9; Schloessing Melet, France) on PB collected from the retro-orbital plexus in EDTA tubes (BD Bioscience, Le Pont de Claix Cedex). Spleens were weighed and single cell suspensions were prepared with PBS. PB and BM smears were prepared according to standard hematologic techniques. Blood and BM smears were stained with Wright Giemsa. Smears were examined by cytologists from the Hospital Saint-Louis and Hospital Lariboisière.

Immunophenotyping by flow cytometry

Mice were anesthetized with isoflurane and PB samples were obtained by orbital bleeds using EDTA as anticoagulant. PB cells were immunophenotyped with antibodies conjugated with either phycoerythrin (PE) or fluorescein isothiocyanate (FITC) to test the Mac-1^{hi}/Gr-1^{lo} (immature myeloid cells) as previously described[15].

Hematopoietic stem cells (HSC) and progenitor population in BM and spleen cells were analyzed using the lineage negative panel (Lin^-), Ly-6A (Sca-1), CD48, CD135, CD150 (Biolegend, Le Pont de Claix Cedex), c-Kit, CD34, and CD16/32

(BD Bioscience) antibodies (Figure S1). 3×10^7 BM and 1×10^8 spleen suspension cells were incubated with surface antibodies to measure the LSK cells ($Lin^-Sca^+c\text{-}Kit^+$) and its subpopulations include short-term-HSCs (ST-HSC) ($Lin^-Sca^+c\text{-}Kit^+CD150^-CD48^-$), long-term-HSCs (LT-HSC) ($Lin^-Sca^+c\text{-}Kit^+CD150^+CD48^-$), multipotent myeloid progenitors (MPPs) ($Lin^-Sca^+c\text{-}Kit^+CD150^-CD48^+$), and LSK cells ($Lin^-Sca^+c\text{-}Kit^+$) and its subpopulations like common myeloid progenitors (CMPs) ($Lin^-Sca^+c\text{-}Kit^+CD34^+CD16/32^-$), granulocyte monocyte/macrophage progenitors (GMPs) ($Lin^+Sca^+c\text{-}Kit^+CD34^+CD16/32^+$) and megakaryocyte erythroid progenitors (MEPs) ($Lin^+Sca^+c\text{-}Kit^+CD34^-CD16/32^-$). To identify the actively cycling cell population a BrdU-containing solution (1mg/mouse, Biolegend, Le Pont de Claix Cedex) was injected intraperitoneally (IP) into mice 12-15 hours before harvesting cells for assay. DNA synthesis in each population was assessed by measuring the incorporation of BrdU. Cells were permeabilized with BD Cytofix/Cytoperm™ buffer and BD Cytoperm™ Permeabilization buffer Plus and labeled with fluorochrome-conjugated anti-BrdU (Biolegend, Le Pont de Claix Cedex) antibody. Cells were analyzed on an LSRII (BD Biosciences) cytometer and analysis was undertaken using the Kaluza Analysis Software.

Immunofluorescence microscopy

Immunofluorescence was performed as described previously[15]. Briefly, BM slides from transplanted *NRASD12/p53*$^{+/-}$ and *NRASD12/p53*$^{-/-}$ mice which were treated with ABT-199 and placebo were prepared by cytospin and stored in

-20°C. Fluorochrome-conjugated NRAS, BCL2 and TOM20 antibodies were incubated overnight at 4°C. The following day cells were washed with PBS, secondary antibodies and WGA-AF488 were incubated for an hour and then washed with PBS. A drop of DAPI was added on each slides and covered with a coverslip. Slides were kept in -20°C until analyzed under a confocal microscope (LSM800, Zeiss) under a X63 objective oil immersion.

Apoptosis assays

The Annexin V-FITC assay Kit (Biolegend, Le Pont de Claix Cedex) was used to test the different groups of mice. BM cells were incubated with Annexin V and propidium iodide (PI) according to the manufacturer's instructions and acquisitions were made with a BD flow cytometer.

BM cells were collected to detect apoptosis using the IncuCyte® Annexin V Red Reagent (Essen Bioscience, UK) for apoptosis. 10,000 BM suspension cells were diluted with PBS and were cultured in triplicate either untreated, or treated with ABT-199 (1 M), or GDC-0975 (1 M), or with ABT-199 and GDC-0975 (1 M of each); 1 l of Annexin V was added to each. The cells were gently vortexed and incubated in the IncuCyte® S3 System for 24 h while taking images every hour. The results were analyzed with the Incucyte software.

Caspase 3/7 Glo assay was employed for apoptosis assessment as described in the manufacturer's instructions (Promega). Briefly, BM hematopoietic cells were incubated overnight in the presence of WEHI-conditioned/serum-rich medium, harvested, and 100µl of cells containing 10,000 cells were seeded in a

96 well plate with 100µl Caspase Glo reagent before luminescence was recorded.

Progenitor Assays

A total of $5x10^4$ BM cells in 1.5 ml media were added to 1.5 mL methylcellulose "MethoCult™ GF M3434" (StemCell Technologies) and plated in three 35 mm plates. BM cells were separated into four groups including untreated, GDC-0975 (1 M MEK inhibitor), ABT-199 (1 M BCL2 inhibitor) and GDC-0975 plus ABT-199 (1 M of each). Cultures in duplicate or quadruplicate were scored after 2 weeks for colony forming colony forming unit granulocyte-macrophage (CFU-GM) assays. The total progenitor cell number was calculated assuming that one femur represents 6% of the total marrow.

[18F]-Fluoro-Thymidine Positron Emission Tomography (PET) scanning

A PET device dedicated to mice (Inveon Siemens Medical Systems) was used to measure blast proliferation in bone marrow after IV injection of [^{18}F]-Fluoro-Thymidine ([^{18}F]-FLT) in *NRASD12/p53*$^{+/-}$ or *NRASD12/p53*$^{-/-}$ transplanted mice before and/or after ABT-199 treatment, as compared to wild type FBVN mice or diseased mice treated with vehicle. [^{18}F]-FLT is a thymidine analog whose uptake is increased in proliferative cells, as thymidine. After [^{18}F]-FLT injection in the tail vein of the mice, PET images were performed 1.5 hours later, visually analyzed for the presence or absence of abnormal signal in the BM, then quantified using the percentage of FLT injected dose per gram of femoral bone marrow in femoral diaphysis and of blood in cardiac

cavities (Inveon Siemens processing software). The contrast of bone marrow signal was quantified using %ID/g in bone marrow/%ID/g in the blood ratio, called FBR (Femur-to-Blood activity Ratio).

RAS activation

Activation sensitive RAS-pulldown assays were carried out using purified protein from prokaryotic cells expressing pGEX-2T-RAF1-RAS Binding Domain as previously described[15].

Statistical analysis

Statistical analysis was performed using Graphpad version 5.0 software. Kruskal Wallis and Wilcoxon signed-rank test was used to compare PB cell counts and Mac-1^{hi}/Gr-1^{lo} expressions in blood, % of BM blasts, TBR in the femurs between groups of mice. A significance value of $p<0.05$ was considered as significant.

Results

Loss of p53 induces MDS to AML progression

To investigate the effect of p53 deficiency in the NRASD12 mice in leukemia, we generated the *NRASD12/p53$^{+/+}$*, *p53$^{-/-}$*, *NRASD12/p53$^{+/-}$* and *NRASD12/p53$^{-/-}$* mice as described in the material and methods. The PB of each mouse was counted (Figure 1); results showed that the number of WBC showed no significant differences in the different groups of mice (Figure 1a), whereas the number of platelets (Figure 1b) in $p53^{+/-}$ (mean=1022 x 10^3/µl)) and $p53^{-/-}$

(mean=1089 x 10^3/µl) mice were not significantly different from the normal FVB/N control mice (mean=1237 x 10^3/µl)), but the *NRASD12/p53*$^{+/+}$ mice (mean=788 x 10^3/ µl) had a lower platelet count than the controls (mean=1237 x 10^3/ µl) ; the *NRASD12/p53*$^{+/-}$ mice also had reduced platelets (mean=708 x 10^3/ µl) than controls; the *p53*$^{-/-}$ platelet count (mean=1089 x 10^3/ µl) was significant decreased compared to controls and the platelet count of the *NRASD12/p53*$^{-/-}$ (mean=574 x 10^3/ µl) had the significantly lowest among all of these mouse groups (Figure 1b); *NRASD12* decreased the number of RBC when compared with controls, but in *NRASD12/p53*$^{+/-}$ and *NRASD12/p53*$^{-/-}$ mice the RBC were not significantly different from each other, similar to *NRASD12/p53*$^{+/+}$ mice (Figure 1c). Percentage of HCT in *NRASD12* mice was lower than controls and *NRASD12/p53*$^{+/-}$ mice had decreased HCT compared with *p53*$^{+/-}$ (Figure 1d). Splenomegaly was obtained in all of the NRASD12 groups (Figure 1e) The BM smears results showed that in the *NRASD12/p53*$^{-/-}$ mice the blast cells number (mean=37.5% SD=12.54) was higher than *NRASD12/p53*$^{+/-}$ (mean=24.8% SD=5.63) and *NRASD12/p53*$^{+/+}$ (mean=9% SD=2.64) mice (Figure 1g).

Hematoxylin and eosin staining of the spleen clearly showed a marked enlargement of the red pulp, with more infiltration of myeloid cells and dysplastic megakaryocytes, characterized by low density in *NRASD12/p53*$^{+/-}$ and *NRASD12/p53*$^{-/-}$ mice. The FVBN, *p53*$^{-/-}$ and *NRASD12/p53*$^{+/+}$ showed no

evidence of infiltration in the liver; there was increase infiltration of myeloid cells in *NRASD12/p53*$^{-/-}$ mice compared with *NRASD12/p53*$^{+/-}$ *(*Figure 1h).

Loss of p53 decreased the BM apoptosis of MDS mice

In order to determine the disease stage in *NRASD12/p53*$^{+/-}$ mice, levels of apoptosis in mouse BM cells were measured. Etoposide was used to induce cell death in different BM cells and apoptosis was measured with Annexin V. The data showed that the percentage of apoptosis in FVB/N was 13.43 % ± 4.776 but with the *NRASD12/p53*$^{+/-}$ mice most of the mice had increased apoptosis (mean= 34.84 % SD=5.643) relative to normal FVB/N cells (Figure 1h). The apoptosis percentage (mean=21.91 % SD=7.889) was decreased in *NRASD12/p53*$^{-/-}$ mice compared to the *NRASD12/p53*$^{+/-}$, which was consistent with AML features (Figure 1h).

Loss of p53 cooperate with NRASD12 modifies the HSCs and progenitors

The number of HSCs and progenitors were examined upon disease progression. The percentage of LSK compartments in *NRASD12/p53*$^{+/+}$ mice were moderately but not significantly expanded (Figure 2a) whereas significantly decreased in *NRASD12/p53*$^{-/-}$ mice compared with in *NRASD12/p53*$^{+/-}$. Interestingly the LT- and ST-HSC almost disappeared in *NRASD12/p53*$^{+/+}$ and *NRASD12/p53*$^{+/-}$ mice except the ST-HSC in *NRASD12/p53*$^{-/-}$ was higher than *NRASD12/p53*$^{+/-}$ (Figure 2a). For the progenitor populations in the BM, we found that the MPPs were increased, but CMPs and MEPs were lower in *NRASD12/p53*$^{+/+}$, *NRASD12/p53*$^{+/-}$ and *NRASD12/p53*$^{-/-}$ compared with controls.

The percentage of GMPs in *NRASD12p53$^{+/+}$*, *NRASD12/p53$^{+/-}$* and *NRASD12/p53$^{-/-}$* mice was expanded but *NRASD12/p53$^{-/-}$* was lower than *NRASD12/p53$^{+/-}$* (Figure 2b). In spleen cells, results showed that the percentage of Lin^{-} cells was expanded in *NRASD12/p53$^{+/+}$* mice compared with controls but significantly decreased in *NRASD12/p53$^{+/-}$* and *NRASD12/p53$^{-/-}$* mice. There were no LSK cells in the spleen of WT mice but increased in *NRASD12/p53$^{+/-}$* mice. The LSK percentage in spleen cells of *NRASD12/p53$^{-/-}$* was lower than *NRASD12/p53$^{+/-}$ (*Figure 2c). The MPPs in spleen cells of *NRASD12/p53$^{+/-}$* expanded but decreased in *NRASD12/p53$^{-/-}$* when compared with the control mice. The *NRASD12/p53$^{+/+}$* gene increased the percentage of CMPs in spleen cells; the percentage of GMPs in *NRASD12/p53$^{+/+}$* mouse spleen was significantly increased compared with control mice but the *p53$^{-/-}$* in the *NRASD12* background had a decreased GMPs population. The MEP population in each group of mouse spleens showed no difference (Figure 2d). To measure the actively cycling cells BrdU was used in each population. The results showed the percentage of BrdU positive in *NRASD12/p53$^{-/-}$* GMPs population was less than *NRASD12/P53$^{+/-}$*. In the other groups almost no differences either in BM or spleen cells in BrdU positive cells was observed (Figure S2).

In order to determine if p53 deficiency can reduce the lifespan of NRASD12 mice, 2x10^{6} BM cells were isolated from each of *NRASD12/p53$^{+/+}$,* *NRASD12/p53$^{+/-}$* and *NRASD12/p53$^{-/-}$* mice and transplanted into individual recipient mice. The recipient mice transplanted with *NRASD12/p53$^{+/+}$* cells

engrafted with a median survival of more than 200 days, whereas the recipients with *NRASD12/p53*$^{+/-}$ cells developed MDS with a median survival of 200 days (Figure 3a). In contrast, the recipients that received *NRASD12/p53*$^{-/-}$ cells with a median survival of 60 days, was significantly shorter than the other groups (Figure 3a).

Acceleration of disease upon serial transplantation

To determine the effect of serial transplantation in second and tertiary recipients, BM from primary recipients of *NRASD12/p53*$^{+/+}$, *NRASD12/p53*$^{+/-}$ or *NRASD12/p53*$^{-/-}$ were transplanted into busulfan conditioned second and tertiary recipients. The median survival in all of the mice were significantly shorter than the preceding transplants (Figures 3b-d). The AML disease of the *NRASD12/p53*$^{-/-}$ mice transplanted to secondary recipients accelerated rapidly with 90% of the recipients developing a lethal AML-like disease within 40 days (Figure 3d).

Altogether these results showed that the p53$^{-/-}$ co-operates with NRASD12 to promote transformation from MDS into AML. The *NRASD12/p53*$^{+/-}$ mice seemed to develop either HR-MDS (24.8% BM blasts) or AML post-MDS (37.5% BM blasts).

Inhibition of MEK and BCL-2 increased the apoptosis of NRASD12/p53-deficient mice bone marrow cells ex vivo

The NRAS/BCL2 complex was previously reported in the MDS patients some of which had *NRAS* mutations. We have also shown that NRASD12 can recruit

endogenous Bcl-2 to remain active[15]. To confirm the NRAS/Bcl-2 complex in the *NRASD12/p53-deficient* mouse models, we used the BCL2 inhibitor ABT-199 and MEK1 inhibitor GDC-0975 on BM cells from normal FVB/N, *p53*$^{-/-}$, *NRASD12/p53*$^{+/+}$, *NRASD12/p53*$^{+/-}$, *NRASD12/p53*$^{-/-}$ ex vivo. Firstly we used the Incucyte Annexin V assay to measure the real time apoptosis under different treatments. The results showed that ABT-199 was ineffective but GDC-0975 increased the apoptosis in each of the different BM cells (Figure 4a-f). The different BM cells were treated with both inhibitors and each inhibitor respectively to check the CFU progenitor numbers showed concordance with the Incucyte; the MEK inhibitor GDC-0975 had reduced number of colonies compared with ABT-199 (Figure 4g).

Effect of BCL2 inhibitor (ABT-199) *in vivo*

The effect of ABT-199 was also determined in vivo. *NRASD12/p53*$^{+/-}$ and *NRASD12/p53*$^{-/-}$ transplanted mice were treated with ABT-199 and PB counts were measured and the number of immature PB myeloid cells (Mac1^{hi+}Grl^{lo}) of each mouse before and after treatment was measured by flow cytometry. The platelet numbers increased from 429 x 10^3/µl to $10^3$1 x 10^3/µl after ABT-199 treatment in *NRASD12/p53*$^{+/-}$ recipients, while the placebo treatment mice platelet number increased from 609 x 10^3/µl to 1025 x 10^3/µl (Figure 5a); the percentage of immature myeloid cells also decreased from 47% to 34% in the ABT-199 treated *NRASD12/p53*$^{+/-}$ recipients (Figure 5b) whereas the untreated *NRASD12/p53*$^{+/-}$ recipients retained higher numbers of immature myeloid cells

(from 62% to 54%). In the *NRASD12/p53*$^{+/-}$ recipients there was no significant difference in survival between the ABT-199 or placebo treated mice (Figure 5c). For the *NRASD12/p53*$^{-/-}$ recipients, the ABT-199 treatment increased the number of platelets (from 465 x 10^3/µl to 744 x 10^3/µl), the number of immature myeloid cells was unchanged, but survival of the ABT-199 treated mice had prolonged survival compared to placebo (Figure 5d-f). [18F]FLT-PET scanning was used to monitor the response to treatment in these mice. Representative PET scans are shown (Figure 5g); the abnormal increased radiotracer uptakes expected in the BM, mostly seen in the femurs, were quantitated. For the treated *NRASD12/p53*$^{+/-}$ mice the PET scans showed no responders (Figure S4). In some *NRASD12/p53*$^{-/-}$ mice presumed to be responders a decrease in the extent and intensity of PET abnormalities after ABT-199 was (Figure 5g) and in mice presumed to be non-responders an increase in the number and intensity of PET abnormalities was observed (Figure 5 h).

RAS/BCL-2 co-localization and RAS-GTP activation in the NRASD12/p53$^{-/-}$ mice treated with BCL2 inhibitor

We have previously shown that the NRAS/BCL2 complex co-localized at the plasma membrane correlated with MDS disease while its presence at mitochondria correlated with AML post-MDS in mice[15] and in patients[27]. In order to determine if ABT-199 was efficacious in the NRASD12/p53-deficient mice, we determined the localization of NRAS and Bcl-2 in the BM cells of

NRASD12/p53$^{+/-}$, NRASD12/p53$^{-/-}$ and control mice. The results showed that in the NRASD12/p53$^{-/-}$ mice the NRAS/Bcl-2 complex localized in the mitochondria and not plasma membrane similar to that observed with the AML mouse model of RAS/BCL-2[28] in placebo and ABT-199 treated mice (Figure 6). BM cells of the NRASD12/p53$^{+/-}$ mice showed localization of the complex in the plasma membrane (Figure S3).

Having previously demonstrated the substantial activation of RAS-GTP in our RAS/BCL-2 models of AML and MDS, using the RAS-GTP assay, we next interrogated RAS activity in the NRASD12/p53$^{-/-}$ model and asked whether it is sustained in the ABT-199 treated animals. RAS-GTP:Bcl-2 complex is significantly upregulated as compared to control in the NRASD12/p53$^{-/-}$ model. Also, although basal levels of RAS-GTP found in wild-type animals is not reached, there is a marked and significant reduction in RAS-GTP:Bcl-2 levels in the ABT-199 treated animals as compared to placebo controls (Fig. 6b; $p<0.01$). Furthermore, ex vivo analysis shows ABT-199 treated animal cells demonstrated a relative induction of high levels of apoptosis as measured by the cleaved Caspase 3/7 (Fig 6c; $p<0.01$), confirming its potency as an inhibitor of the BCL-2 family.

Discussion

In this study we confirmed that the transgenic mice NRASD12 and their recipients cause MDS[15], and together with p53$^{-/-}$ co-operate to accelerate disease from MDS to AML. This is consistent with a previous report showing

that NRASD12/p53$^{-/-}$ cells rapidly develop a highly penetrant AML subtype erythroleukemia. However, in this current report, the mice develop a myeloid disease. The main difference between the previous report of erythroleukemia and this current study is the promoter usage. The conditional p53 deficient mice used in the previous study were driven by the Mxi-Cre, which targets a more primitive progenitor than MRP8, the promoter driving the NRASD12 mice[29]. Introducing a retrovirus with mutant NRAS in primary CD34^{+} cord blood human cells gave rise to erythroid abnormalities[30].

The data shows that the percentage of LSK in BM of *NRASD12* mice is higher than that of controls, but in *NRASD12/p53*$^{+/-}$ mice, due to the difference in MDS progression, there is a diversity in LSK levels. The NRASD12 inhibited the ST/LT-HSC whatever the p53 status. This is consistent with the notion that NRASD12 is the driver for the MDS disease. Although CMPs and MEPs were not found to be expanded in the *NRASD12/p53*$^{-/-}$ mice, the MPPs and GMPs were increased. In these murine models the mutated *NRAS* gene is driven by the MRP8 promoter, which would be expressed in myeloid progenitors, GMPs rather than the MEPs, and may explain why MEPs were not expanded in these mice. CMPs were also decreased in the *NRASD12/p53*$^{+/+}$ and *NRASD12/P53*$^{-/-}$ mice compared to MEPs. However, we found that NRASD12 promotes the number of cycling cells in GMPs, p53$^{-/-}$ seems to have no effect on GMP function. This result is consistent with the high frequency of *NRAS* mutation and rare *p53* mutations in MDS patients[31]. As the disease is transplantable this

underlines the self-renewal capacity of the leukemia initiating cells (LICs), which accelerates upon serial transplantations. Spleen cells from the *NRASD12/p53*$^{-/-}$ mice did not transplant the disease, suggesting that these cells were not invaded with myeloblast, however, the histology shows invasion of myelobalsts. This correlated with the reduced percentage of LT/ST-HSCs in spleen cells of *NRASD12* and *NRAS/p53*$^{-/-}$ mice.

As we know that *p53* mutation may be secondary events for the most of cancer progression[32], in our mouse AML model we believe the NRASD12 is the initiation event and p53 deficiency leads to progression to AML. However, p53 deletion has so far not been reported to be associated with disease progression in MDS patients, but, *p53* mutations leading to TP53 functional deficiency is associated with progressive disease in MDS and AML. Here, we noticed that some of the *NRASD12/p53*$^{+/-}$ had either HR-MDS or AML post-MDS features with the proportion of apoptotic BM cells lower and percentage BM blast cells higher compared with *NRASD12/p53*$^{+/+}$ low-risk MDS mice. Our previous study showed that the mutated *NRAS* gene decreased cell proliferation and differentiation and increased apoptosis, which is consistent with MDS[15,27,28]. When p53$^{+/-}$ co-operates with NRASD12, some of the MDS mice progressed to AML. As p53 deficiency controls apoptosis and the consequent stage of disease and the observation that some *NRASD12/p53*$^{+/-}$ mice tended to be more apoptotic with early HR-MDS than the other mice with AML-like disease, other events may be occurring to result in disease acceleration.

In some MDS patients the NRAS/BCL2 complex is expressed but currently no therapies are approved that directly target mutant NRAS; however, MEK inhibitors have been shown to have some effect in mutant NRAS[33,34]. The BCL-2 inhibitor, Venetoclax (ABT-199) is currently being used to treat AML patients.[35,36] The NRASD12/p53-deficient mouse models we developed were treated with BCL2 and MEK1 inhibitors alone and together. The BCL2 inhibitor caused increased apoptosis of BM cells from the MDS and AML mouse cells, but not as much as the MEK1 inhibitor. As mutant *NRAS* is one of the genes in the diseased mice, this is to be expected as MEK is downstream of RAS. The BCL-2 inhibitor *in vivo* increased the survival of transplanted AML mice and the number of platelets increased, thereby rescuing the platelet abnormality. In *NRASD12/p53*$^{+/-}$ recipients the platelets were increased but some mice did not respond to the inhibitor. In the RAS/BCL-2 models published previously[15] the NRAS/BCL-2 complex is localized to the plasma membrane in the HR-MDS mice; in the AML post-MDS model, the complex is localized in the mitochondria[28]. The NRAS/Bcl-2 complex co-localized in the mitochondria in *NRASD12/p53*$^{-/-}$ mice after ABT-199 or placebo treatment. The ABT-199 prolonged the life of the AML-like mice with a reduction of active RAS-GTP and increased apoptosis. Taken together with the confocal data, these data confirm our previous findings of the localization of the RAS-GTP:Bcl-2 complex correlating with apoptotic activity and demonstrate the potency and efficacy of ABT-199 in improving overall survival.

In conclusion, p53 deficiency accelerates NRASD12 from MDS to AML. Loss of one allele (*p53*$^{+/-}$) accelerates disease progression from early MDS, characteristic of mutant *NRAS* alone, to HR-MDS and given time to AML. NRASD12 with the MRP8 promoter co-operates with p53 deficiency with increased GMPs with transplantable disease. The ABT-199 (Venetoclax) therapy for the NRAS/Bcl-2 complex alleviates disease symptoms but does not necessarily eradicate the disease as a monotherapy and in combination with other targeted reagents such as a MEK inhibitor may overcome resistance.

Acknowledgement

We thank Scott Kogan (UCSF) for the NRASD12 mice and Tyler Jacks (MIT) for the p53 deficient mice, Veronique Parietti and the animal facility and the Imagerie Department. We thank Abbvie and Genentech for providing the BCL-2 and MEK inhibitors. The authors thank the Cytometry and Immunobiology facility of Institut Cochin/ INSERM U1016.

This work was supported by the Groupe Francophone Myelodysplasie, PH is supported by the Chinese Scholarship Council (CSC N°201706180057).

Authorship

Contribution: PH, CC, SGi, RAP, PF designed experiments, analyzed the data and wrote the manuscript, PH, SGa, NO, FH, BH, EL, NS, NV, LSM, MP, WZ, RAP performed experiments and analyzed the data, CB, PL, CL, AJ analyzed the cytology and histology; all of the authors edited the manuscript.

Conflict-of-interest disclosure: RAP is receipt of an Abbvie/Genentech grant (no. 10179).

References

1. Koeffler HP. Myelodysplastic syndromes (preleukemia). *Semin. Hematol.* 1986;23(4):284–299.
2. Natelson EA, Pyatt D. Acquired myelodysplasia or myelodysplastic syndrome: Clearing the fog. *Adv. Hematol.* 2013;2013:1–11.
3. Reilly JT. Pathogenesis of acute myeloid leukaemia and inv(16)(p13;q22): A paradigm for understanding leukaemogenesis? *Br. J. Haematol.* 2005;128:18–34.
4. Rothe A. Contact dermatitis from N- (a- chlorobenzylidene) phenylhydrazine. *Contact Dermatitis*. 1988;18(1):16–19.
5. Sérgio Paulo Bydlowski F de LJ. Hematopoietic Stem Cell in Acute Myeloid Leukemia Development. *Adv. Hematol. Stem Cell Res.* 2012;261–276.
6. Germing U, Kndgen A, Haas R, Gattermann N. Myelodysplastische Syndrome (MDS). *Dtsch. Medizinische Wochenschrift*. 2012;183–185.
7. Bejar R, Stevenson K, Abdel-Wahab O, et al. Clinical Effect of Point Mutations in Myelodysplastic Syndromes. *N. Engl. J. Med.* 2011;364(26):2496–2506.
8. Fernández-Medarde A, Santos E. Ras in cancer and developmental diseases. *Genes and Cancer*. 2011;2(3):344–358.
9. Suter R, Marcum JA. The molecular genetics of breast cancer and targeted therapy. *Biol. Targets Ther.* 2007;(3):241–258.
10. Takashima A, Faller D V. Targeting the RAS oncogene. *Expert Opin. Ther. Targets*. 2013;17(5):507–531.
11. Adjei AA. Blocking oncogenic Ras signaling for cancer therapy. *J. Natl. Cancer Inst.* 2001;93(14):1062–1074.
12. Wang J, Liu Y, Li Z, et al. Endogenous oncogenic NRAS mutation promotes aberrant GM-CSF signaling in granulocytic/monocytic precursors in a murine model of chronic myelomonocytic leukemia. *Blood*. 2010;116(26):5991–6002.
13. Ricci C, Fermo E, Corti S, et al. RAS mutations contribute to evolution of chronic myelomonocytic leukemia to the proliferative variant. *Clin. Cancer Res.* 2010;16(8):2246–2256.
14. Padua RA, Guinn BA, Al-Sabah AI, et al. RAS, FMS and p53 mutations and poor clinical outcome in myelodysplasias: A 10-year follow-up. *Leukemia*. 1998;12(6):887–892.
15. Omidvar N, Kogan S, Beurlet S, et al. BCL-2 and mutant NRAS interact physically and functionally in a mouse model of progressive myelodysplasia. *Cancer Res.* 2007;67(24):11657–11667.
16. Parikh C, Subrahmanyam R, Ren R. Oncogenic NRAS rapidly and efficiently induces CMML- And AML-like diseases in mice. *Blood*. 2006;108(7):2349–2357.
17. Meek DW. Tumour suppression by p53: A role for the DNA damage response? *Nat. Rev. Cancer*. 2009;714–723.
18. Chen J. The cell-cycle arrest and apoptotic functions of p53 in tumor initiation and progression. *Cold Spring Harb. Perspect. Med.* 2016;6(3):a026104.
19. Aubrey BJ, Kelly GL, Janic A, Herold MJ, Strasser A. How does p53 induce apoptosis and how does this relate to p53-mediated tumour suppression? *Cell Death Differ.* 2018;104–113.
20. Rivlin N, Brosh R, Oren M, Rotter V. Mutations in the p53 tumor suppressor gene: Important milestones at the various steps of tumorigenesis. *Genes and Cancer*. 2011;466–474.
21. Olivier M, Hollstein M, Hainaut P. TP53 mutations in human cancers: origins, consequences,

and clinical use. *Cold Spring Harb. Perspect. Biol.* 2010;2;a001008.

22. Perri F, Pisconti S, Vittoria Scarpati G Della. P53 mutations and cancer: A tight linkage. *Ann. Transl. Med.* 2016;4(24):1–4.
23. Salari A, Thomay K, Lentes J, et al. Effect of TP53 contact and conformational mutations on cell survival and erythropoiesis of human hematopoietic stem cells in a long term culture model. *Oncotarget*. 2018;9(52):29869–29876.
24. Kogan SC, Lagasse E, Atwater S, et al. The PEBP2βMYH11 fusion created by Inv(16)(p13;q22) in myeloid leukemia impairs neutrophil maturation and contributes to granulocytic dysplasia. *Proc. Natl. Acad. Sci. U. S. A.* 1998;95(20):11863–11868.
25. Jacks T, Remington L, Williams BO, et al. Tumor spectrum analysis in p53-mutant mice. *Curr. Biol.* 1994;4(1):1–7.
26. Scott C Kogan, Jerrold M Ward, Miriam R Anver, Jules J Berman, Cory Brayton, Robert D Cardiff, John S Carter, Sherri de Coronado, James R Downing, Torgny N Fredrickson, Diana C Haines, Alan W Harris, Nancy Lee Harris, Hiroshi Hiai, Elaine S Jaffe, Ian C M H subcommittee of the MM of HCC. Bethesda proposals for classification of nonlymphoid hematopoietic neoplasms in mice. *Blood*. 2002;100(1):238–45.
27. Le Pogam C, Krief P, Beurlet S, et al. Localization of the NRAS: BCL-2 complex determines anti-apoptotic features associated with progressive disease in myelodysplastic syndromes. *Leuk. Res.* 2013;37(3):312–319.
28. Beurlet S, Omidvar N, Gorombei P, et al. BCL-2 inhibition with ABT-737 prolongs survival in an NRAS/BCL-2 mouse model of AML by targeting primitive LSK and progenitor cells. *Blood*. 2013;122(16):2864–2876.
29. Zhang J, Kong G, Rajagopalan A, et al. p53-/- synergizes with enhanced NrasG12D signaling to transform megakaryocyte-erythroid progenitors in acute myeloid leukemia. *Blood*. 2017;129(3):358–370.
30. Darley RL, Hoy TG, Baines P, Padua RA, Burnett AK. Mutant N-RAS induces erythroid lineage dysplasia in human CD34+ cells. *J. Exp. Med.* 1997;185(7):1337–1347.
31. Leukemia M, Itzykson R, Kosmider O, et al. Prognostic score including gene mutations in chronic Myelomonocytic Leukemia. *J. Clin. Oncol.* 2013;31(19):2428–2436.
32. Vogiatzi F, Brandt DT, Schneikert J, et al. Mutant p53 promotes tumor progression and metastasis by the endoplasmic reticulum UDPase ENTPD5. *Proc. Natl. Acad. Sci. U. S. A.* 2016;113(52):E8433–E8442.
33. Falchook GS, Lewis KD, Infante JR, et al. Activity of the oral MEK inhibitor trametinib in patients with advanced melanoma: A phase 1 dose-escalation trial. *Lancet Oncol.* 2012;13(8):782–789.
34. Rutkowski P. What is new in melanoma after European Cancer Congress 2017? *Melanoma Manag.* 2017;4(2):83–87.
35. Pollyea DA, Amaya M, Strati P, Konopleva MY. Venetoclax for AML: Changing the treatment paradigm. *Blood Adv.* 2019;3(24):4326–4335.
36. Knight T, Edwards H, Taub JW, Ge Y. Evaluating venetoclax and its potential in treatment-naïve acute myeloid leukemia. *Cancer Manag. Res.* 2019;11:3197–3213.

Figure Legends

Figure 1. P53 loss and NRASD12 induce mouse models of HR-MDS and AML. Peripheral blood cell counts and spleen from normal control FVB/N, *p53$^{+/-}$, p53$^{-/-}$, NRASD12*, *NRASD12/p53$^{+/-}$* and *NRASD12/p53$^{-/-}$* mice. (a) white blood cells; (b) Platelet (PLT); (c) red blood cells (RBC) (d) haematocrit (HCT); (e) spleen; (f) bone marrow (BM) and hematoxylin and eosin (H&E) sections of liver and spleen; (g) percentage of BM blasts; (h) percentage BM apoptosis after treatment with etoposide.

Figure 2. P53 loss co-operate with NRASD12 to decrease in stem cells and progenitors. (a) Percentage of BM stem cell populations; (b) percentage of BM progenitor populations; (c) percentage of spleen stem cell populations; (d) percentage of spleen progenitor populations

Figure 3. The serial transplant of second and tertiary recipients of MDS and AML mice developed severe disease (a) Kaplan-Meier comparative survival curves were plotted after transplantation of different mouse models; (b) Kaplan-Meier comparative survival curves after transplantation of *NRASD12* first to third recipients; (c) Kaplan-Meier comparative survival curves after transplantation of *NRASD12/p53$^{+/-}$* first to third recipients; (d) Kaplan-Meier comparative survival curves after transplantation of *NRASD12/p53$^{-/-}$* first to fourth recipients.

Figure 4. The effect of MEK and BCL2 inhibitors in vitro showing increased apoptosis and reduction of progenitors (a-f) Inhibitors on the BM cells of (a)

FVBN; (b) *p53$^{+/-}$*; (c) *p53$^{-/-}$;* (d) *NRASD12*; (e) *NRASD12/53$^{+/-}$;* (f) *NRASD12/p53$^{-/-}$*. Blue is untreated group, red is ABT-199 treated group, green is GDC-0975 treated group, violet is ABT-199+GDC-0975 treated group. (g) BM cells isolated from control, *p53$^{-/-}$, NRASD12*, or *NRASD12/p53$^{-/-}$* mice were plated in semisolid medium without inhibitor or with inhibitor alone or a combination of both. Colonies were counted 14 days after culture.

Figure 5. BCL2 inhibitors in *vivo showing efficacy in AML but not in HR-MDS mice* (a) Platelet number before and after treatment with ABT-199 or placebo in *NRASD12/p53$^{+/-}$* mice; (b) percentage of Mac1hi^{+} Gr1lo^{-} before and after treated with ABT-199 or placebo in NRASD12/P53$^{+/-}$ mice; (c) Kaplan-Meier comparative survival curve of transplanted NRASD12/P53$^{+/-}$ recipients treated with ABT-199 or placebo; (d) platelet number before and after treated with ABT-199 or placebo in NRASD12/P53$^{-/-}$ mice; (e) percentage of Mac1hi^{+}Gr1lo^{-} before and after treated with ABT-199 or placebo in *NRASD12/p53$^{-/-}$* mice[(f) Kaplan-Meier comparative survival curve of *NRASD12/p53$^{-/-}$* recipients treated with ABT-199 or placebo; (g) [18F]FLT-PET Scan of a *NRASD12/p53$^{-/-}$* mouse which responded to the ABT-199 treatment, the arrows show the abnormal hot spots on the PET scan; (h) [18F]FLT-PET Scan of a *NRASD12/p53$^{-/-}$* mouse which did not respond to ABT-199 treatment.

Figure 6. Mitochondrial Co-Localization of NRAS/Bcl-2 complex and RAS activation in NRASD12/p53$^{-/-}$ transplanted mice treated with ABT-199 or placebo. (a) Bone marrow from mice treated in vivo showing mitochondrial

localization by immunofluorescence using TOM20 for the mitochondria or wheat germ agglutinin (WGA) for plasma membraner; (b) decrease in RASGTP upon treatment with ABT-199 ($p<0.01$); (c) caspase 3/7 cleavage showing increased apoptosis ($p<0.01$) upon treatment with ABT-199.

Enliven Archive
Intensifying Thoughts

Research Article www.enlivenarchive.org Enliven: Journal of Stem Cell Research & Regenerative Medicine

ISSN: 2379-5751

Comparison of *In Vivo* [^{18}F]Fluoro-Desoxyglucose and [^{18}F]Fluoro-Thymidine Positron Emission Tomography for Disease Monitoring in a Mouse Model of Higher-Risk Myelodysplastic Syndrome

Laure Sarda-Mantel[1,2], Panhong Gou[3], Fortune Hontonnou[2,3], Benoit Hosten[2,4,5], Nicolas Vignal[1,2], Carine San[2,4], Caren Brumpt[6], Pierre Fenaux[7,8], Christine Chomienne[3], Stephane Giraudier[3,9], and Rose Ann Padua[3]*

[1]*Nuclear Medicine Department, Lariboisière Hospital, Assistance Publique-Hôpitaux de Paris (APHP), 2 rue Ambroise Paré, 75010 Paris, France*
[2]*Claude Kellershohn Unit, Saint-Louis Research Institute, Paris University, 1 avenue Claude Vellefaux, 75010 Paris, France*
[3]*Inserm UMR-S1131, Saint-Louis Research Institute, 1 avenue Claude Vellefaux, 75010 Paris, France*
[4] *Radiopharmacy Department, Saint-Louis Hospital, Assistance Publique-Hôpitaux de Paris (APHP), 1 avenue Claude Vellefaux, 75010 Paris, France*
[5]*Pharmacy Faculty, Paris University, 4 avenue de l'observatoire, 75006 Paris, France*
[6]*Hematology Laboratory, Lariboisière Hospital, Assistance Publique-Hôpitaux de Paris (APHP), 2 rue Ambroise Paré, 75010 Paris, France*
[7]*Inserm UMR-S944, Saint-Louis Research Institute, 1 avenue Claude Vellefaux, 75010 Paris, France*
[8]*Hematology Seniors Department, Saint-Louis Hospital, Assistance Publique-Hôpitaux de Paris (APHP), 1 avenue Claude Vellefaux, 75010 Paris, France*
[9]*Hematology, Saint-Louis Hospital, Assistance Publique-Hôpitaux de Paris (APHP), 1 avenue Claude Vellefaux, 75010 Paris, France*

***Corresponding author**: Pr L. Sarda-Mantel, Nuclear Medicine Department, Lariboisière Hospital, Assistance Publique-Hôpitaux de Paris (APHP), 2 rue Ambroise Paré, 75010 Paris, France, Email: laure.sarda-mantel@aphp.fr

Received Date: 07th March 2021
Accepted Date: 17th May 2021
Published Date: 21st May 2021

Citation: Sarda-Mantel L, Gou P, Hontonnou F, Hosten B, Vignal N, San C, et al. Comparison of In Vivo [18F]Fluoro-Desoxyglucose and [18F]Fluoro-Thymidine Positron Emission Tomography for Disease Monitoring in a Mouse Model of Higher-Risk Myelodysplastic Syndrome. Enliven: J Stem Cells Regen Med. 2021, 5(1):001.

Abstract

Higher-risk myelodysplastic syndrome (HR-MDS) has a poor prognosis in the absence of efficient therapy. The evaluation of new therapies in animal models of HR-MDS is hampered by the absence of accurate in vivo biomarkers of the disease. In this study we compared [18F]Fluoro-desoxyglucose Positron Emission Tomography (FDG-PET/CT) and [^{18}F]Fluoro-thymidine (FLT-PET/CT) imaging for disease follow-up in a triple transgenic *MMTVtTA/TetoBCL-2/MRP8NRASD12* mouse model of HR-MDS. Normal control FVB/N mice (G1, n=9) and HR-MDS mice (G2, n=12) underwent both FDG- and FLT-PET?CT procedures at 2-day intervals, on a dedicated small animal device. Blood cell counting, BCL-2 and Mac-1hi/Gr-1lo expression measurements in blood were performed before each PET/CT procedure. Visually, PET/CT images of G2 mice demonstrated homogeneous FDG uptake in the whole skeleton similar to that observed in G1 mice, and abnormal FLT hot spots in bone marrow not observed in G1 mice. The intensity of FLT hot spots in bone marrow was higher in 3-months old G2 mice than in 2-months old G2 mice, concordant with a higher percentage of cells expressing Mac-1hi/Gr-1lo and lower platelets counts. We conclude that FLT-PET/CT imaging is a more valuable surrogate non-invasive quantitative marker of HR-MDS bone marrow involvement than FDG-PET/CT in our mouse model of HR-MDS.

Keywords: Myelodysplastic syndrome; Positron emission tomography; [^{18}F]fluoro-thymidine; Small animal imaging

Introduction

Myelodysplastic syndromes (MDS) is an orphan disease of myeloid stem cells. It is characterized by ineffective hematopoiesis leading to life threatening blood cytopenias, and a variable risk of progression toacute myeloid leukemia (AML) [1]. In high risk (HR) MDS (defined by an international score, IPSS), the poor median overall survival is only 15 months, except in the small proportion of cases (15%) who benefit from allogeneic stem cell transplantation. A large phase III clinical trial showed that azacitidine (AZA), a hypomethylating agent, significantly increased median survival of HR-MDS to about 24 months. However, 50% of the patients do not respond to AZA, and no drug has demonstrated clear efficacy after AZA failure [2,3]. HR-MDS thus remains an unmet medical need of the elderly. Allogeneic stem-cell transplantation remains, with few exceptions, the only curative treatment of higher-risk myelodysplastic syndromes, with prolonged disease-free survival of 35–50%. However, only about 15% of HR-MDS patients may receive allogeneic SCT, due to the median age of the population (about 70 years) and the absence of an HLA matched donor, justifying the development of other therapeutic approaches.

In MDS, ineffective haemopoiesis results from the increased susceptibility of clonal myeloid progenitors to apoptosis, which leads to cytopenias despite a generally hypercellular marrow. Progression to AML is thought to result from a subsequent shift from apoptosis to proliferation of these clonal progenitors. Expansion of minor subclones can also contribute to transformation to AML.

Positron Emission Tomography (PET/CT) imaging using [^{18}F]fluoro-desoxyglucose (FDG) has proven to be highly efficient for early assessment of therapeutic response in glucose-avid malignant diseases, especially in lymphomas. FDG-PET/CT seems useful for the detection and therapeutic follow-up of extra-medullary lesions in AML. But FDG uptake in bone marrow (BM) is weak [4]. Conversely, few but promising data have been reported on the use of PET/CT imaging with [^{18}F]Fluoro-thymidine (FLT), for the detection and therapeutic monitoring of BM disease in patients with MDS or AML[5-7]. FLT uptake in tissues is correlated with exogenous thymidine uptake and incorporation in DNA during the S mitotic phase [8]. FLT-PET/CT imaging has been used for therapeutic evaluations in several malignant diseases. It demonstrated good correlation with proliferative indexes on histology, and to thymidine kinase 1 (TK1) expression in cells [8].

An animal model of HR-MDS and AML progression was created in Inserm Unit 1131, using mutant NRAS and overexpression of BCL-2 [9], known to be poor prognostic indicators of the human diseases [10]. This model was used to test anti-BCl2 agents ABT737 and ABT199, as well as anti-MEK and anti-p53 agents. However such evaluations are hampered by the absence of accurate *in vivo* biomarkers to follow the therapeutic effects of the treatments. BM biopsy, although feasible, is not easy in mice. Currently, the only valuable end-point in these studies is survival duration.

In this study, our aim was to evaluate the ability of FDG- and FLT-PET/CT to monitor BM involvement in our triple transgenic *MMTVtTA/TetoBCL-2/CT MRP8NRASD12* mouse model of HR-MDS.

Results

We investigated 2 groups of mice (FVB/N strain): normal FVB/N mice (G1, n=9), and triple transgenic mice (G2, HR-MDS, n=12). Mice of G1 aged 2-3 months underwent FDG- and FLT-PET/CT once. HR-MDS mice of G2 underwent FDG- and FLT-PET/CT twice: at the age of 2 months, then 1 month later at 3 months of age. For each imaging set, FDG-PET/CT was performed 48h before or after FLT-PET/CT. For all mice, just before FLT-PET/CT imaging, peripheral blood samples were taken for peripheral blood (PB) cell counts, and for BCL-2 and Mac-1hi/Gr-1lo (blast cells) expression measurements by flow cytometry as described previously [9]. After the last imaging procedure, all mice were sacrificed for BM cytological analysis.

Biological Data

The results of PB parameters in G1 and G2 are reported in Table 1. As expected, BCL-2 and Mac-1hi/Gr-1lo expressions were increased in G2 vs G1. White Blood cells (WBC) counts were higher in G2 than in G1 mice, and higher in 3-months-old G2 mice than in 2-months-old G2 mice. Platelet and Hb counts were lower in G2 than in G1 mice, and decreased between2 months and 3 months in G2 mice. These latter data are consistent with disease progression.

Cytological Data

No blast was observed in PB of all mice. In femoral BM, the percentageof blasts was 4.2±2.2% in FVB/N G1 mice, and 16.3±9.3 in 3-months-old HR-MDS G2 mice ($p<0.04$ vs G1). Dystrophic megakaryocytes were seen in the BM of G2 mice, confirming the diagnosis of MDS. Cell counts in 3-months-old G2 mice were evocative of infection (numerous immature granulocytes and only few erythroblasts).

PET/CT Data

FLT radiosynthesis was achieved in 48 min with a non-corrected yield of 11.5-20.7%. Radiochemical purity was > 99%. Specific activity was 267-1567 GBq/µmol and volumic activity was 1-1.5 GBq/mL. The elution time of FLT was 8.8 min.

Visual analysis of FDG-PET/CT images demonstrated homogeneous FDG uptake in the whole skeleton in all G1 and G2 mice (Figure 1A). Conversely, as compared to FLT-PET/CT images obtained in normal control G1 mice, FLT-PET/CT images of all G2 mice revealed abnormal unilateral or bilateral asymmetric hot spots in femoral diaphysis, in spine and/or in humeral bones (Figure 1B). The abnormalities observed in HR-MDS G2 mice became more intense and/or extensive at the age of 3 months than at the age of 2 months.

The results of FLT- and FDG-PET/CT quantifications obtained in the two groups of mice are reported in Table 1 and Figure 2. On FLT-PET/CT, the femoral BM-to-background bloodpool activity ratio (TBR) was higher in G2 than in G1 mice, and higher in 3-months-old G2 mice than in 2-months-old G2 mice. FDG max %ID/g in femoral bone marrow was higher in G2 than in G1 mice, but decreased between the age of 2 and 3 months in G2 mice.

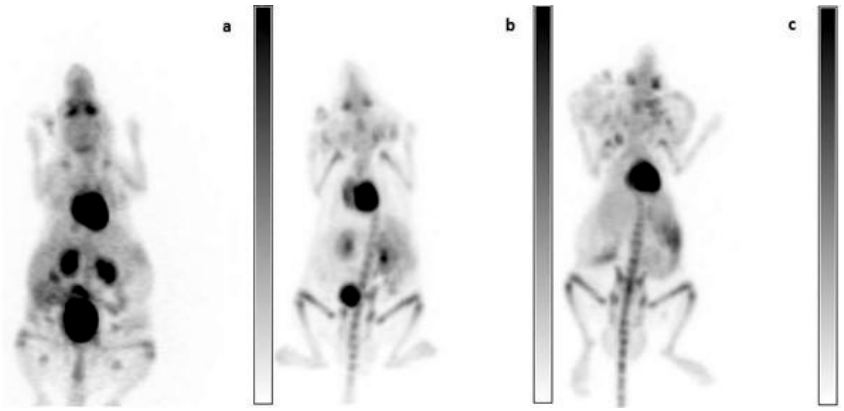

Figure 1A: FDG-PET images (whole-body volumes) of a normal FVB/N (G1) mouse (a) and of a HR-MDS (G2) mouse at 2 months of age (b) then 3 months of age (c).

Visually, all three FDG-PET scans show homogeneous FDG uptake in the whole-skeletal bone marrow.

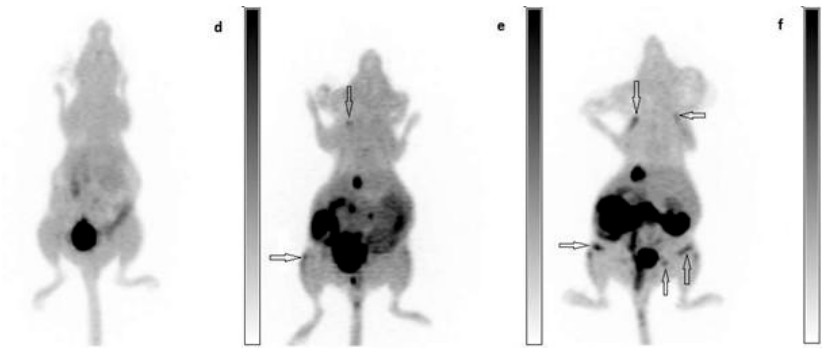

Figure 1B: FLT-PET images (whole-body volumes) of the same normal FVB/N (G1) mouse (d) and HR-MDS (G2) mouse (e,f) than in Figure 1A.
Clear abnormal hot spots are seen in the humerus and the femurs in the HR-MDS mouse (e,f) as compared to the control mouse (d). These abnormalities increase in extent and intensity between the age of 2 (e) and 3 (f) months (arrowed).

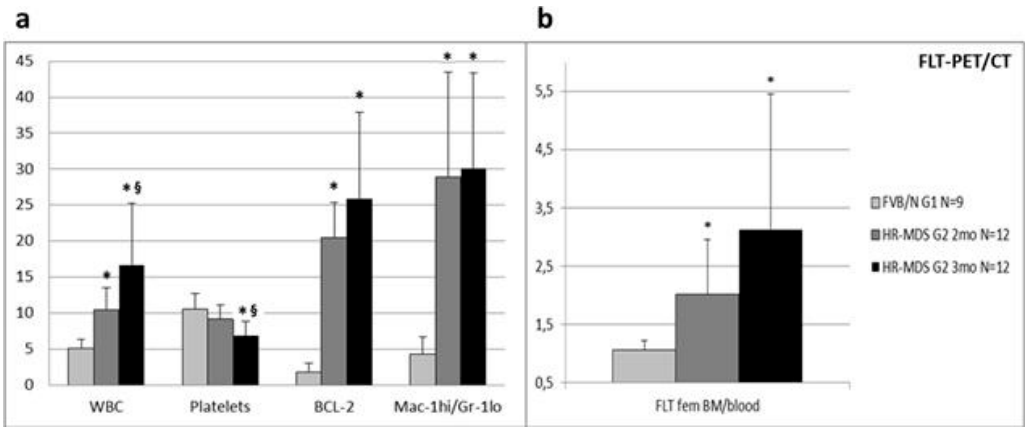

Figure 2: Graphs comparing quantitative PET/CT and PB parameters in G1 and G2.
(a) PB parameters in G1 and G2 (number of WBC $x10^3/\mu l$ of blood, number of platelets $x10^5/\mu l$ of blood, % of blood cells expressing BCL2, % of blood cells expressing Mac-1hi/Gr-1lo).
(b) FLT-PET/CT quantification: femoral BM-to-background (bloodpool) activity ratio on FLT-PET/CT images of G1 and G2.
*: significant difference ($p<0.05$) between G2 and G1. §: significant difference between 3-months-old G2 mice and 2-months-old G2 mice.

Table 1: Peripheral Blood parameters, FLT and FDG quantification on PET/CT images, in normal FVB/N mice (G1) and in 2 months-old then 3 months-old triple transgenic HR-MDS mice (G2).

	G1 normal N=9	G2 2mo HR-MDS N=12	G2 3mo HR-MDS N=12	G2 2mo versus G1 (*p*)	G2 3mo versus G1 (*p*)	G2 3mo versus G2 2mo (*p*)
WBC x 10^3/µl	5.13±1.18	10.39±3.08	16.67±8.56	*<0.03*	*<0.03*	*<0.02*
RBC x 10^3/µl	9.49±0.18	8.65±0.41	7.88±2.58	*<0.02*	*NS*	*NS*
Platelets x 10^3/µl	1055±221	917±198	681±199	*NS*	*<0.04*	*<0.007*
Hb (g/dL)	16.40±0.14	15.27±0.81	13.17±4.48	*NS*	*NS*	*NS*
BCL-2 %	1.8±1.2	20.5±4.9	25.9±12.0	*<0.0002*	*<0.006*	*NS*
Mac-1hi/Gr-1lo %	4.3±2.4	28.9±14.5	30.1±13.62	*NS*	*<0.03*	*NS*
FLT-PET/CT TBR in femoral BM	1.06±0.16	2.02±0.94	3.13±2.32	*<0.002*	*<0.0003*	*= 0.05*
FDG-PET/CT max %ID/g in femoral BM	3.98±1.11	16.50±3.68	12.27±3.58	*<0.007*	*<0.02*	*<0.05*

Peripheral Blood parameters: Number of WBC, Red Blood Cells, and platelets per ml, hemoglobin (Hb) level, percentage of cells expressing BCL-2, percentage of cells expressing Mac-1hi/Gr-1lo in PB.

FLT and FDG quantification on PET/CT images: TBR = the intensity of abnormal hot spots in femoral bone marrow determined on FLT-PET/CT images; max %ID/g in femoral bone marrow = maximal percentage of FDG injected dose per gram in femoral bone marrow on FDG-PET/CT images.

Discussion

In our triple transgenic model of HR-MDS, both FDG-PET/CT and FLT-PET/CT were performed and compared to normal control group of mice. FDG-PET/CT and FLT-PET/CT scans demonstrated different features. FDG-PET/CT showed homogeneous increased FDG uptake in the whole skeleton BM in HR-MDS mice as compared to controls and decreased with age. FLT-PET/CT showed focal abnormalities in one or several bones of HR-MDS mice, the intensity of which increased with age, together with BCL-2 and Mac-1hi/Gr-1lo peripheral blood expression as well as with PB WBC counts and decreased blood platelet counts consistent with disease progression between 2 and 3 months.

To our knowledge, this is the first study reporting a direct comparison between FDG and FLT-PET/CT in HR-MDS disease. FDG and FLT-PET/CT were previously compared in a tumor-bearing mouse model of human chronic myeloid leukemia (K562 cell line [11]). The authors reported increased FLT uptake in the tumors, with a bone marrow-to-background activity ratio of 5.39±0.42 at 30min post-IV, 4.88±0.43 at 1h and 3.81±0.38 at 2h post-IV, whereas FDG-PET/CT scans were negative. Our results show completely different patterns of BM uptake between FLT and FDG in HR-MDS mice.

FDG uptake in BM of our HR-MDS mice was always homogeneous. FDG uptake in MDS was previously described in few clinical case reports: focal abnormalities [12,13] or diffuse increased FDG uptake in the whole skeleton [14] were retrieved. The most important series using FDG-PET/CT in leukemic diseases is that of Li H. et al. in 35 patients suspected of acute leukemia relapse [15]. In this study, only 3 of 16 patients showed focal BM FDG abnormalities, all with positive BM biopsy; 24 showed diffuse increased FDG uptake in BM, among which 14 had positive BM biopsy and 10 negative BM biopsy. Overall, visual analysis achieved a successful diagnosis only in 68.6% (24/35) of patients. In our mice, FDG uptake in BM decreased between the age of 2 and 3 months, whereas all peripheral blood parameters demonstrated more severe disease at 3 months than at 2 months: WBC (including blasts) counts, expression of BCL-2 and of Mac-1hi/Gr-1lo increased, whereas platelet counts decreased. This suggests that FDG uptake in bone marrow may not be an accurate marker of HR-MDS.

FLT-PET/CT allows in vivo quantification of cell proliferation and has been suggested for the diagnosis and follow-up of patients with myelodysplastic disorders [5,6]. Conversely, FLT abnormalities in HR-MDS mice were always focal, and increased in intensity with age. This suggests that: firstly, FLT-PET/CT scans are easier to interpret (normal or abnormal) than FDG-PET/CT scans; secondly, FLT is a valuable quantitative marker of HR-MDS disease. Concordantly to our data in mice, Agool et al reported increased FLT uptake in epiphyses and expansion in diaphysis of peripheral bones in patients with MDS [5,6].

The question of whether blast or normal hematopoietic cells accumulate FLT is still unclear. Authors agree that both types of cells can proliferate in MDS and acute leukemia. Moreover, it seems that not all the blasts proliferate at the same time [16].

Our data suggest that FLT-PET/CT is a better marker of HR-MDS disease than FDG-PET/CT in our mouse model of HR-MDS. If this proves tobe the same in HR-MDS patients, it may allow to avoid or to guide BM biopsy in some cases and to monitor response to therapy. To this regard, Vanderhoeka et al. suggested the potential value of FLT-PET/CT for in vivo chemotherapeutic monitoring in AML patients [7]. FLT uptake in BM was absent in patients with complete remission, whereas significant uptake was still observed in patients with resistant disease, including one with aplastic BM (complete remission) on post-therapy BM biopsy.

Materials and Methods

Animal Models

All mice lines were maintained in Friend leukemia Virus B (FVB/N) strain from the National Institutes of Health.

The triple transgenic *MMTVtTA/TetoBCL-2/MRP8NRASD12* murine model of HR-MDS was previously validated in the lab [9,16,17]. MMTVtTA/TetoBCL-2/MRP8NRASD12 were obtained by crossing MMTVtTA/TBCL-2 mice with mice harboring mutant NRASD12 gene under the regulation of the myeloid promoter MRP8. The mice were genotyped as previously described [9]. The mice develop an MDS-like disease with around 15% BM blasts with a dysplasia, some liver invasion and a relatively indolent disease with a long latency period before they die. Normal FVB/N mice have 0 to 4% of blasts in BM [9,17,18].

All animal experiments were performed in accordance with European guidelines for care of laboratory animals (2010/63/EU) and were approved by the Animal Ethics Committee of Paris Nord.

FLT-PET/CT and FDG-PET/CT

[^{18}F]fluoro-thymidine (FLT) radiosynthesis

FLT was synthetized in the UCK lab on the All-In-One® (Trasis©, Ans, Belgium) radiosynthesis automate by nucleophilic substitution (90°C, 5min) of nosylated precursor (3- N-boc-5-ODMTr-3-O-nosyl-lyxothymidine), after activation of fluorine 18 by TBAHCO3 (100°C, 10min). Further steps area deprotection of the product by acid hydrolysis (1,5mL HCL 2M, 95°C, 5min) then neutralisation (2,4mL NaOH 1M, 40°C). After neutralisation the solution was passed through 2 cartridges (IC-H, Alumina), then the purification was performed using CLHP column Akzo Nobel Kromasil® C18 10µm 250*10mm, in a solution H2O/ethanol (90/10 v/v) at 6 mL/min. The chemical purity, the radiochemical purity (RCP) and specific activity were determined by analytic CLHP (Akzo Nobel Kromasil® column (C18 5µm 250*4,6mm), with an H_2O/acetonitrile gradient starting from 90/10 to 5/95 at 1 mL/min. The identity of the labeled compound [^{18}F]FLT was confirmed by co-injection with a non-radioactive standard of FLT. The FLT concentration in the radioactive sample was obtained using the UV-peak area ratio between the radioactive product and the standard solution.

PET/CT acquisitions

PET/CT imaging was performed as previously described [19] using Inveon PET/CT scanner (Siemens Medical Solutions) designed for small laboratory animals.

Mice were anesthetized (isoflurane/oxygen, 2.5% for induction at 0.8-1.5 L/min and 1.5% at 0.4-0.8 L/min thereafter) during injection of FLT or FDG (7-10 MBq) in a volume of 0.15 mL via the tail vein, and during PET/CT acquisitions. For FLT-PET/CT, mice were kept on standby for 1h after FLT injection, then were re-anesthetized and placed in the PET camera in prone position under isoflurane anesthesia and respiratory monitoring for a 15 min-duration static PET acquisition followed by a 10 min-duration CT acquisition for attenuation correction of PET images and anatomic localization of PET signals. For FDG-PET/CT, mice were kept anesthetized during 60 min after radiotracer injection (to avoid muscular uptake) under a heat lamp to avoid FDG uptake in brown fat tissues, then placed in the PET camera fora static acquisition of 10 min-duration then a CT acquisition of 10 min-duration. The spatial resolution of Inveon PET device was 1.4 mm full-width at half-maximum (FWHM) at the centre of the field of view. Images were reconstructed using a 2-D ordered subset expectation maximization (Fourier rebinning/2-D OSEM) method including corrections for scanner dead time, scatter radiations and randoms.

PET-CT analysis

Qualitative visual analysis of whole-body FLT and FDG uptakes in axial and peripheral skeleton, liver and spleen were performed. Then FLT or FDG uptake was quantified in volumes of interest manually drawn on PET/CT images (IRW 4,2 software, Siemens). The software calculates the percentage of injected dose (Bq) per gram of tissue (%ID/g) in each voxel of the volumes of interest drawn on the images. The max %ID/g values obtained in the volumes of interest were considered for quantitative analysis. For FLT-PET/CT images, max %ID/g obtained in femoral BM was divided by max %ID/ml obtained in the blood (volume of interest drawn on the cardiac area),in order to calculate a bone marrow-to-background (bloodpool) activity ratio. For FDG-PET/CT images, only the max %ID/g obtained in femoral BM was considered. Indeed the bone marrow-to-background (bloodpool) activity ratio could not be calculated on FDG-PET/CT images because of high normal FDG uptake in the myocardium impairing the drawing of blood volumes of interest.

Ex-Vivo Analyses

On the day of FLT-PET/CT imaging, PB samples were taken for red blood cell, leukocyte, and platelet counting, hemoglobin (Hb) dosage and for BCL-2 and Mac-1hi/Gr-1lo (as a marker of primitive cells) expression measurements. After the last set of PET/CT imaging the mice were sacrificed, femoral BM was flushed, and PB and femoral BM were smeared on slides for cytological analysis.

May Grunwald Giemsa stainings were performed on PB and femoral BM smears and examined by a cytologist of Lariboisière Hospital with an Olympus Bx41 microscope. The cell morphology was studied at magnification 100X, 500X and 1000X, according to the WHO 2016 criteria. The percentage of blasts was determined on the BM smears by counting 200 cells at magnification 1000X.

Statistical Analysis

Statistical analysis was performed using Graphpad prism 5 version 5.0 software. Kruskal Wallis and Wilcoxon signed-rank test was used to compare PB cell counts, BCL2 and Mac- 1hi/Gr-1lo expressions in blood, % of blasts on BM smears, FDG-max %ID/g and FLT-bone marrow–to-background activity ratios between groups of mice. A significance value of $p<0.05$ was used.

Conclusion

In our triple transgenic HR-MDS mouse model, FLT-PET/CT imaging demonstrated focal BM abnormalities, with intensity increasing with age concordantly with PB parameters that evidenced more severe disease at the age of 3 months than at the age of 2 months. Whereas FDG-PET/CT imaging demonstrated homogeneous increased FDG uptake in the whole skeleton's BM decreasing with age, thus not correlating with PB parameters. These results suggest that FLT-PET/CT imaging is a more valuable surrogate non-invasive quantitative marker of HR-MDS BM involvement than FDG-PET/CT in our mouse model. It remains to be determined whether this finding may be the same in HR-MDS patients.

Acknowledgements

We thank Scott Kogan (UCSF) for the NRASD12 mice, Lothar Hennighausen (NIH) for the MMTVLTRtTA mice and Veronique Parietti and the animal facility.

Author's Contributions

LSM, PF, CC, SG and RAP participated in research design and in the writing of the manuscript. LSM, PG, FH, BH, NV, CS and RAP participated in the experimental research. BH, NV and CS synthetized the radiotracer. LSM, PG, and CB Participated in data analysis.

Conflict of interest

The authors have no relevant conflict of interest.

Funding

This study was funded by the Saint-Louis Research Institute and Jean Bernard Association. PH is supported by the Chinese Scholarship Council.

References

1. Ades L, Itzykson R, Fenaux P. Myelodysplastic syndromes. Lancet. 2014, 383: 2239-2252.
2. Garcia-Manero G, Fenaux P. Hypomethylating agents and other novel strategies in myelodysplastic syndromes. J Clin Oncol. 2011, 29: 516-523.
3. Fenaux P, Mufti GJ, Hellstrom-Lindberg E, Santini V, Finelli C, Giagounidis A, et al. Efficacy of azacitidine compared with thatof conventional care regimens in the treatment of higher-risk myelodysplastic syndromes: a randomised, open-label, phase III study. Lancet Oncol. 2009, 10: 223-232.
4. Cribe AS, Steenhof M, Marcher CW, Petersen H, Frederiksen H, Friis LS. Extramedullary disease in patients with acute myeloid leukemia assessed by 18F-FDG PET. Eur J Haematol. 2013, 90: 273-278.
5. Agool A, Schot BW, Jager PL, Vellenga E. 18F-FLT PET in hematologic disorders: a novel technique to analyze the bone marrow compartment. J Nucl Med. 2006, 47: 1592-1598.
6. Agool A, Glaudemans AW, Boersma HH, Dierckx RA, Vellenga E, Slart RH. Radionuclide imaging of bone marrow disorders. Eur J Nucl Med Mol Imaging. 2011, 38: 166-178.
7. Vanderhoek M, Juckett MB, Perlman SB, Nickles RJ, Jeraj R. Early assessment of treatment response in patients with AML using [(18)F] FLT PET imaging. Leuk Res. 2011, 35: 310-316.
8. McKinley ET, Ayers GD, Smith RA, Saleh SA, Zhao P, Washington MK, et al. Limits of [18F]-FLT PET as a biomarker of proliferation in oncology. PLoS One. 2013, 8: e58938.
9. Omidvar N, Kogan S, Beurlet S, le Pogam C, Janin A, West R, et al. BCL-2 and mutant NRAS interact physically and functionally in a mouse model of progressive myelodysplasia. Cancer Res. 2007, 67: 11657-11667.
10. Padua RA, Guinn BA, Al-Sabah AI, Smith M, Taylor C, PetterssonT, et al. RAS, FMS and p53 mutations and poor clinical outcome in myelodysplasias: a 10-year follow-up. Leukemia. 1998, 12: 887-892.
11. Lu L, Jiang L, Guan H, Gao Y, Lu H. Imaging proliferation in human leukemia-tumor bearing mice with (18)F-FLT: Comparison with (18) F-FDG PET. Hell J Nucl Med. 2012, 15: 206-209.
12. Valls L, Badve C, Avril S, Herrmann K, Faulhaber P, O'Donnell J, et al. FDG-PET imaging in hematological malignancies. Blood Rev. 2016, 30: 317-331.
13. Liu F, Cao Q. Transformation of myelodysplastic syndrome to acute myeloid leukemia: A case with whole-body 2-[F18] fluoro-2-deoxy-D-glucose positron emission tomography. Indian J Nucl Med. 2011, 26: 104-106.
14. Inoue K, Okada K, Harigae H, Taki Y, Goto R, Kinomura S, et al. Diffuse bone marrow uptake on F-18 FDG PET in patients with myelodysplastic syndromes. Clin Nucl Med. 2006, 31: 721-723.
15. Li H, Xu C, Xin B, Zheng C, Zhao Y, Hao K, et al. (18)F-FDG PET/CT Radiomic analysis with Machine Learning for Identifying Bone Marrow Involvement in the Patients with Suspected Relapsed Acute Leukemia. Theranostics. 2019, 9: 4730-4739.
16. Clarkson B, Ohkita T, Ota K, Fried J. Studies of cellular proliferation in human leukemia. I. Estimation of growth rates of leukemic and normal hematopoietic cells in two adults with acute leukemia given single injections of tritiated thymidine. J Clin Invest. 1967, 46: 506-529.
17. Beurlet S, Omidvar N, Gorombei P, Krief P, Le Pogam C, Setterblad S, et al. BCL-2 inhibition with ABT-737 prolongs survival in an NRAS/BCL-2 mouse model of AML by targeting primitive LSK and progenitor cells. Blood. 2013, 122: 2864-2876.
18. Guerenne L, Beurlet S, Said M, Gorombei P, Le Pogam C, Guidez F, et al. GEP analysis validates high risk MDS and acute myeloid leukemia post MDS mice models and highlights novel dysregulated pathways. J Hematol Oncol. 2016, 9: 5.
19. Rizzo-Padoin N, Chaussard M, Vignal N, Kotula E, Tsoupko-Sitnikov V, Hontonnou F, et al. [18F]MEL050 as a melanin-targeted PET tracer: fully automated radiosynthesis and comparison to 18F-FDG for the detection of pigmented melanoma in mice primary subcutaneous tumors and pulmonary metastases. Nucl Med Biol. 2016, 43: 773-780.

Translational Oncology 14 (2021) 101169

Contents lists available at ScienceDirect

Translational Oncology

journal homepage: www.elsevier.com/locate/tranon

Etoposide, an anticancer drug involved in therapy-related secondary leukemia: Enzymes at play

Wenchao Zhang [a,*], Panhong Gou [b], Jean-Marie Dupret [a], Christine Chomienne [b,c], Fernando Rodrigues-Lima [a,*]

[a] Université de Paris, BFA, UMR 8251, CNRS, Paris F-75013, France
[b] Inserm UMR-S1131, Université de Paris, IRSL, Hôpital Saint-Louis, Paris, France
[c] Service de Biologie Cellulaire, Assistance Publique des Hôpitaux de Paris (AP-HP), Hôpital Saint Louis, Paris, France

ARTICLE INFO

Keywords:
Topoisomerase II poison
Etoposide
Oxidative metabolite
Double-stranded breaks
Therapy-related leukemia

ABSTRACT

Etoposide is a semi-synthetic glycoside derivative of podophyllotoxin, also known as VP-16. It is a widely used anticancer medicine in clinics. Unfortunately, high doses or long-term etoposide treatment can induce therapy-related leukemia. The mechanism by which etoposide induces secondary hematopoietic malignancies is still unclear. In this article, we review the potential mechanisms of etoposide induced therapy-related leukemia. Etoposide related leukemogenesis is known to depend on reactive oxidative metabolites of etoposide, notably etoposide quinone, which interacts with cellular proteins such as topoisomerases II (TOP2), CREB-binding protein (CREBBP), and T-Cell Protein Tyrosine Phosphatase (TCPTP). CYP3A4 and CYP3A5 metabolize etoposide to etoposide catechol, which readily oxidizes to etoposide quinone. As a poison of TOP2 enzymes, etoposide and its metabolites induce DNA double-stranded breaks (DSB), and the accumulation of DSB triggers cell apoptosis. If the cell survives, the DSB gives rise to the likelihood of faulty DNA repair events. The gene translocation could occur in mixed-lineage leukemia (*MLL*) gene, which is well-known in leukemogenesis. Recently, studies have revealed that etoposide metabolites, especially etoposide quinone, can covalently bind to cysteines residues of CREBBP and TCPTP enzymes, . This leads to enzyme inhibition and further affects histone acetylation and phosphorylation of the JAK-STAT pathway, thus putatively altering the proliferation and differentiation of hematopoietic stem cells (HSC). In brief, current studies suggest that etoposide and its metabolites contribute to etoposide therapy-related leukemia through TOP2 mediated DSB and impairs specific enzyme activity, such as CREBBP and TCPTP.

Etoposide is a commonly used anticancer drug

Etoposide is a fundamental and essential part of combination chemotherapies for treating numerous cancers, such as lung cancer, lymphoma, leukemia [1]. Like most anti-neoplastic drugs, etoposide treatment cancer has limited single-agent activity [2,3]. It is mainly associated with cisplatin, carboplatin, and cyclophosphamide in combination chemotherapy [4–6]. Currently, 4 to 6 cycles etoposide and cisplatin combination is the standard therapy commonly used for most small cell lung cancer in the clinic, with a 50%–80% objective response rate [7,8]. In combination with several drugs (lomustine, methotrexate, and prednisone), etoposide is also proposed to be first-line therapy in patients with non-Hodgkin's lymphoma with no major cardiotoxicity [9, 10]. Similarly, in Hodgkin's disease, etoposide is a first-line chemotherapeutic agent in combination with other chemotherapeutic agents (vincristine, chloramphenicol, and prednisolone), was positive (77% response rate) [11]. In addition, it is reported that etoposide was active against gestational trophoblastic disease [12]. Etoposide was used for breast cancer treatment, the single-agent trial in untreated patients showed a response rate of approximately 15% in untreated patients [13]. Oral etoposide has been investigated in many clinical trials for the treatment of ovarian cancer response rates have varied in different studies (20.4% to about 30%), and it seems that the activity of this drug depends to a large extent on the degree of prior treatment [14].

Although etoposide has been widely and successfully used to treat many types of cancer, patients treated with etoposide may develop secondary leukemia. Due to the increases in the overall cure rate of patients, interest has arisen on the adverse effects, and special attention

* Corresponding authors.
E-mail addresses: zhangwch611@gmail.com (W. Zhang), fernando.rodrigues-lima@u-paris.fr (F. Rodrigues-Lima).

https://doi.org/10.1016/j.tranon.2021.101169
Received 28 June 2021; Accepted 29 June 2021
Available online 6 July 2021

has been focused on the potential risk of therapy-related secondary leukemia [15–17] and the FDA (U.S. Food and Drug Administration) and EMA (European Medicines Agency) recommend different doses and treatment periods for different cancers as well [18,19].

Metabolism of etoposide in human body

In cells, the oxidation of etoposide mainly involves cytochrome P450 3A family enzymes and/or peroxidases, such as myeloperoxidase (MPO). CYP3A4 and CYP3A5 are members of the cytochrome P450 superfamily of enzymes (encoded by the *CYP3A4* and *CYP3A5* genes). CYP3A4 and CYP3A5 metabolize etoposide to etoposide catechol, which is readily oxidized to etoposide quinone by cellular peroxidases [20].The induction of CYP3A4 and CYP3A5 can enhance the clearance rate of etoposide [21,22]. Etoposide catechol is oxidized by MPO in liver or bone marrow lysosomes [23,24]. Etoposide can be directly metabolized to etoposide quinone with the assistance of prostaglandin-endoperoxidases 1/2 (PGTS1/2) or by other peroxidases (such as MPO) [25]. Oxidative metabolites of etoposide have a more potent inhibitory activity on DNA TOP2 cleavage near the MLL translocation breakpoint and more remarkable oxidizing ability than etoposide [26]. Etoposide can be cleared by UGT1A1 (UDP-glucuronosyltransferase family 1 member A1) etoposide glucuronides. In addition, etoposide quinone may be transferred to glutathione via GSTT1/GSTP1 (glutathione S-transferase). These two conjugated metabolites seem to inactivate the biological properties of etoposide [27,28]. (Fig. 1)

Mechanism of action of etoposide

Early in the development of etoposide, its mechanism of action was considered similar to its parent compound, podophyllotoxin. These compounds inhibit microtubule assembly by preventing tubulin polymerization and then destroying spindle fibers. When the cells are exposed to podophyllotoxin, sister chromatids cannot be separated during mitosis because of a missing spindle [29]. As a result, cell division is arrested in mitosis with an increased cell number in metaphase. Nevertheless, cells exposed to etoposide show a decreased cell number in metaphase rather than an increase [30]. Simultaneously, studies reported that a low concentration of etoposide blocks the cell cycle in the late S or early G2 phase [31,32]. These are significant indications that etoposide has a different mechanism compared to podophyllotoxin.

Currently, it is well known that etoposide is a TOP2 inhibitor, this inhibition being considered as a major anti-cancer mechanism of etoposide. TOP2 (alpha and beta isoforms) are ubiquitous enzymes that plays a vital role in many basic DNA processes and regulates the under- and over-winding of DNA during DNA replication. TOP2 inhibitors play an integral role in cancer treatment due to the collapse/collision of the resultant bifurcation and unsolved DSB, leading to cancer cell apoptosis. Generally, TOP2 enzymes create a transient TOP2-DNA cleavage complex (TOP2cc) and reseals TOP2cc rapidly. Once the inhibitor interacts with TOP2, the TOP2cc is trapped, leading to an accumulation of DSB. If the DSB cannot be repaired timely, the cell will initiate apoptosis and eventually die [33,34]. In contrast, if the DSB cell survives, it gives riseto the prospect of faulty DNA repair events, and the gene translocation could occur in the *MLL* gene, which is known for leukemogenesis. Chromosomal translocation causes abnormal growth and leads to the development of malignant tumors and neoplasms. More than 10,000 gene fusions have been identified in cancer [35,36]. Etoposide and other chemotherapeutic do not directly cause translocation. However, the DSB caused by these molecules must be repaired, and it is the aberrant repair that can result in a translocation. (Fig. 2)

Topoisomerase II and topoisomerase II poisons

Topoisomerases are classified according to whether they cut one (type I) or two strands (type II) of DNA. Human cells express two TOP2 subtypes, TOP2α and TOP2β. The two subtypes share 70% amino acid sequence identity and encoded by two different genes. TOP2α is encoded by *TOP2A*, which is located at chromosome 17. TOP2β is encoded by

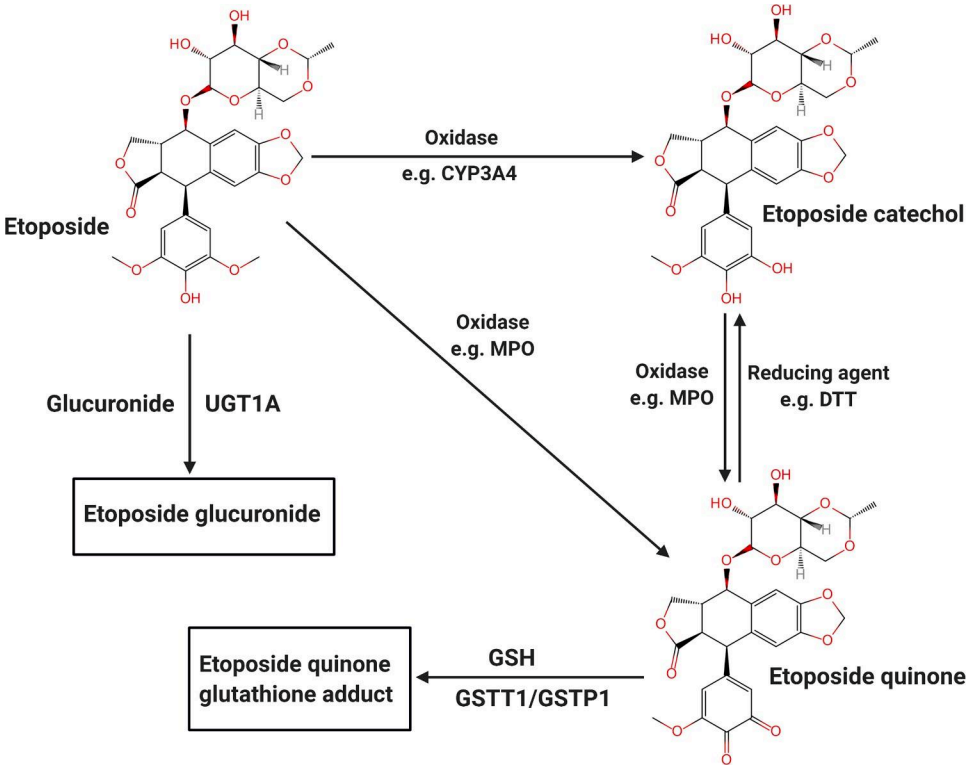

Fig. 1. The main metabolic pathway of etoposide in vivo.

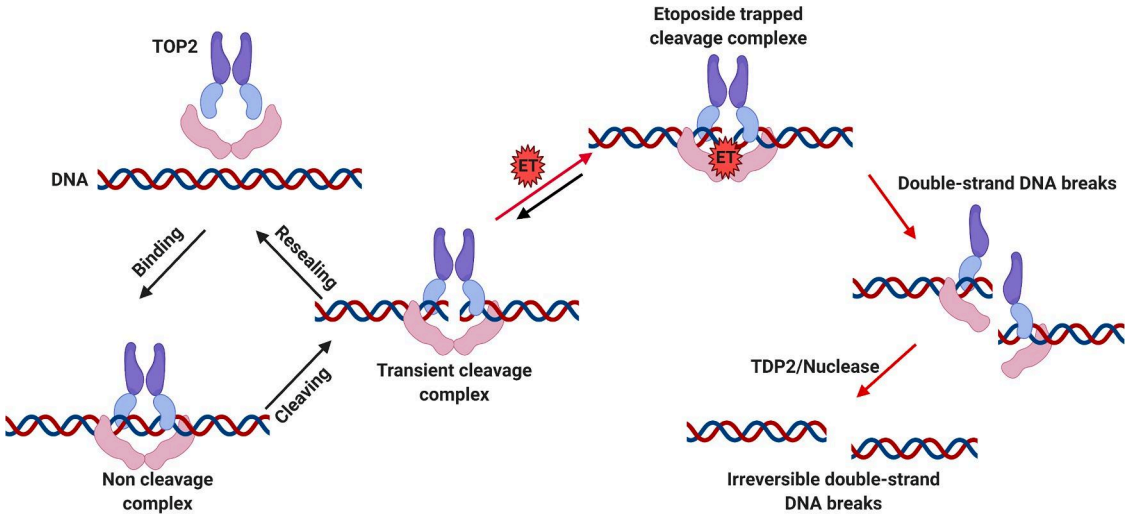

Fig. 2. Etoposide mechanism of action and poisons on TOP2. The normal catalytic activity of TOP2 creates and reseals the DSB, which involves three steps: TOP2 and DNA binding, TOP2 cleavages DNA double strands, and TOP2 reseal the transient cleaved DNA. Etoposide inhibits TOP2 by stabilizing the TOP2cc. If the trapped TOP2cc can not be adequately repaired, the TDP2 or nuclease will remove the TOP2 from the complex, leading to a persistent and irreversible double-strand DNA break.

TOP2B, which is located on chromosome 13 [37–39]. TOP2α is highly expressed in proliferating cells and can be used as a biomarker of cell proliferation. While, TOP2α is poorly expressed in quiescent and differentiated cell populations [37]. In contrast, TOP2β expression was uniformly distributed in all cells [37,40]. Therefore, TOP2α is considered to be an effective target of TOP2 inhibitors, its impairment being considered as a contributor to the anticancer effects of etoposide.

TOP2 enzymes cleave DNA double-strands, which may cause DNA double-strand breaks [41,42]. Chemicals that inhibits TOP2 activity and decreases the levels of TOP2cc are termed TOP2 catalytic inhibitors. Chemicals that increase the levels of TOP2cc can convert the enzymeinto a potential "toxin" that further produces DNA double-strand breaks are called TOP2 poisons [43].

TOP2 poisons can be grouped into two classes based on their mechanism of action. Interfacial poisons, such as etoposide, doxorubicin, or mitoxantrone bind non-covalently to the TOP2cc at the interface of protein-DNA complex and prevent TOP2 from rejoining the DNA ends [44,45]. Covalent poisons such as certain quinones (BQ or etoposide quinone) react with TOP2 at cysteine residues (albeit reaction with other amino acids cannot be ruled out) . Covalent poisons produce irreversible TOP2cc and increase the levels of DSB by altering the conformation of TOP2 [46].

All clinically used TOP2 targeted anticancer drugs impair activities of both TOP2α and TOP2β [37]. However, the extent to which any TOP2 poison targets TOP2α and TOP2β and the relative contribution of either isoform to the drug's therapeutic effect is not well understood [46,47]. It is worth noting that cellular and in vivo studies indicate that TOP2β is the primary enzyme responsible for gene breaks in *MLL* (see below).

Etoposide induced therapy-related leukemia

Leukemia is a carcinoma of the human hematopoietic system, comprising the bone marrow and lymphatic system. The precise causes of leukemia are not understood; cellular disorders and environmental factors are certainly involved [48]. Therapy-related leukemia has been under investigation for decades and is known to be induced by radiation and/or chemotherapy [49]. Drugs that induce secondary leukemia include alkylating agents, TOP2 poisons (for instance, etoposide and teniposide), cyclophosphamide, anthracyclines, and doxorubicin [15]. Etoposide is a well-known TOP2 poison and a commonly used anticancer drug. It is also recognized that etoposide can be leukemogenic, notably through *MLL* gene translocation [26,50].

Etoposide was approved for clinical use by the FDA in 1983, and a first report published in 1987 showed that etoposide treatment has a risk of induction of secondary leukemia in 1987 [51]. Subsequently, studies were published on etoposide and secondary leukemia, particularly acute myeloid leukemia (AML). Le Deley's study showed that a high concentration and continuous etoposide treatment of solid tumors give a higher risk of treatment-related acute myeloid leukemia (t-AML) [52]. The study performed by N. J. Winnick et al. revealed that within 23 to 68 months after etoposide treatment, 10 out of 205 children developed secondary AML, and there was a 5.9% $\pm$ 3.2% risk of developing leukemia in the next four years [53]. Sugita et al. reported a high incidence of etoposide-associated secondary leukemia in children with non--Hodgkin's lymphoma treated by etoposide. In order to reduce the associated secondary AML, the authors recommend giving etoposide treatment twice a week [54]. Kollmannsberger et al. demonstrated that patients receiving etoposide doses in excess of 2 g/m^2 had a 1.3% likelihood of developing s-AML [55]. Meanwhile, Ratain et al. proposed that high-dose etoposide is leukemogenesis in non-small cell lung cancer treatment, and the median dose of etoposide is 6795 mg/m^2 [51]. A study by M.A. Smith et al. found that the cumulative risk of secondary leukemia in six years was observed 3.3% in the low etoposide group, 0.7% in the medium etoposide group, and 2.2% in the high etoposide group, respectively (low: $<$ 1.5 g/m^2; Medium: 1.5 to 2.99 g/m^2; high $\geq$3.0 g/m^2), indicating that factors other than cumulative dose seem to be the main determinants of secondary leukemia risk [56]. Interestingly, it was revealed that receiving etoposide at doses greater than 4000 mg/m^2 tended to increase secondary acute non-lymphoblastic leukemia (s-ANLL). Meanwhile, all leukemias described in the Italian Langerhans cell histiocytosis (LCH) group are acute promyelocytic leukemia, which are not identified in Austria, Germany, Netherlands, and Switzerland (AGDS) groups [57]. It is reported that secondary leukemia does occur after conventional doses of etoposide treatment, but the low incidence does not change the risk-benefit ratio of etoposide-based chemotherapy in germ cell carcinoma [58]. Based on these researches, there is evidence that high-dose and long-term doses are critical factors in secondary leukemia caused by etoposide treatment, while other factors cannot be ruled out.

Topoisomerase II-associated DNA double-strand breakage and repair mechanisms

A critical intermediate in topoisomerase activity is the cleavage complex. Once topoisomerases have cleaved the DNA, each subunit ofthe TOP2 becomes covalently attached to the broken end of the 5′- phosphate group [40]. The cleavage complex is usually transient and naturally results from circumstances that are not clear or induced by the presence of drugs that act as antitumor agents. Topoisomerase inhibitors poison the cleavage intermediates and lead to the formation of an aborted or irreversible TOP2cc [39,47].

In order to repair the TOP2cc captured by the TOP2 poisons, the non-homologous end joining (NHEJ) or homologous recombination (HR) repair pathway is activated. To proceed with NHEJ repair, the trapped TOP2cc is first degraded by the proteasome, and then the remaining tyrosine-linked end can be released by tyrosyl-DNA phosphodiesterase 2 (TDP2) [59,60]. Once the TOP2cc(which is trapped by etoposide), is captured by TDP2, the latter hydrolyzes the phosphodiester bond between TOP2 and DNA through proteasome degradation [61]. The collaboration between TDP2 and proteasome is not well understood. The study by Schellenberg et al. provided some novel findings [62]. First, zinc finger protein 451 (ZNF451) binds and reshapes TOP2cc, thereby opening the complex and allowing TDP2 to access and interact with the cleavage complex. Second, ZNF451 assists small ubiquitin like modifier 2 (SUMO2) protein in SUMOylation of trapped TOP2cc. The interaction of TDP2 with SUMO2 bound to TOP2cc further facilitates the interaction of TDP2 with the cleavage complex. This activity is instru- mental in preventing the formation of the cell-deadly DSB that is typical of TOP2 poisons. To proceed with HR repair, the MRE11-RAD50-NBS1 (MRN) complex cooperates with other repair proteins (e.g., BRCA1 and CtIP) and can directly sever a small segment of DNA ends containing covalently bound TOP2. In case of DNA damage is recognized, the MRN complex recruits and activates ataxia-telangiectasia mutant kinase (ATM) dimers [63]. The activated ATM dimer interacts with the checkpoint kinase, causing the cell cycle to stop at G2/M [64]. Subsequently, the nuclease activity of the MRN complex cleaves the DNA ends, prompting HR repair. Meanwhile, it was demonstrated that MRN, CtIP, and BRCA1 are required to remove TOP2-DNA adducts induced by etoposide treatment, and subsequent excision of TOP2-induced DSB ends. It is revealed that the interaction between CtIP and BRCA1 is necessary for the resistance of cells to etoposide during genomic DNA replication [65]. In addition, the MRN complex is also involved in the repair of NHEJ, and is species-specific in the repair of the hairpin structure, but the exact mechanism is still unclear [66]. The degradation of TOP2 through these two processes will leave free DNA ends, which undergo continuous excision and final repair [67,68].

Once TOP2 is released from the DNA-TOP2 cross-linking adduct, NHEJ or HR repair is initiated. NHEJ repairs DSB directly rejoining DNA terminals, which may produce a perfect repair. If the sequence around the lesion is missing or presenting with other DSB, deletion or translocation may occur [69]. Compared to NHEJ, HR is a more precise mechanism where a homologous sequence is used as a template to guide the repair process. The DSB can be repaired by several homologous mediated pathways, including double-strand break repair (DSBR) and synthesis-dependent strand annealing (SDSA), both of the pathways are initiated by 3′ single-strand DNA [70]. The DSBR pathway produces a crossover or non-crossover product, while the SDSA pathway produces a non-crossover product. Crossover is essential for proper chromosome segregation during meiosis and interprets genetic variation. In fact, it does not rule out that a perfect repair can be produced if the template sequence is the same as the sequence with the break sequence. Rarely, if the template is a non-homologous sequence, it may produce a translocation as well [71]. NHEJ is usually involved in the development of lymphocytes, while HR is thought to be more involved in the catalytic recombination of meiosis [71,72], which suggests that the NHEJ pathway is mainly involved in DSB repair induced by TOP2 poisons. In

this regard, several studies have emphasized that NHEJ pathway plays a vital role in the TOP2 poison induced DSB (etoposide was specifically listed) [73,74] (Fig. 3).

Etoposide and chromosomal translocations

A distinct subset of t-AML is associated closely with TOP2 poisons. t-AML shows unique cytogenetic changes, the most common of which is the destruction of the *MLL* gene on chromosome 11q23 in the 8.3 kb breakpoint cluster region (BCR). The 7 to 13 exon of the *MLL* gene are located in the BCR, where most of the chromosomal translocation breakpoints are located [15,75]. Several lines of evidence suggested that etoposide caused TOP2cc cleavage activities induced site-specific DNA cleavage in the *MLL* BRC [76–78]. Likewise, Martin et al. reported that DNA cleavage within the *MLL* BCR is a specific event in the initial phase of apoptosis that is part of higher-order chromatin fragmentation leading to chromosomal translocations in the *MLL* and *AML1* genes. In addition, in vitro incubation of etoposide with TOP2 enhanced the DNA-TOP2 cleavage complex near the translocation site within the DNA sequence containing *MLL* and partner genes identified in susceptible leukemia [77,79,80]. The partner genes found in *MLL*-related translocations include *AF9, AF4, ENL, AF10, AF6, AF17, EPS15, GAS7, LOC100128568, CREBBP*, and *PTD* [81].

Etoposide metabolites contribute to therapy-related leukemia: TOP2 poison

As described above, etoposide metabolites display activity against TOP2 enzymes, which is similar or greater than etoposide [82–85]. However, studies have shown that etoposide quinone or etoposide catechol has a similar inhibitory activity towards TOP2, when per- formed with a buffer containing a large amount of reducing agents [26, 86,87]. Studies with minimal reducing agents levels have shown that etoposide quinone is several times more effective than the parent com- pound in inducing TOP2-mediated DSB [83,84]. It was simultaneously demonstrated that the inhibition of TOP2 by etoposide quinone is not limited in the same manner as etoposide by blocking ligation as an interfacial poison [37,82–84]. Numerous studies imply that etoposide quinone is a redox-sensitive compound [84,88–90]. More significantly, etoposide quinone was reported to act as a covalent poison, a mecha- nism involving covalent adduction , which may lead to multiple effects: inactivation of the enzyme may occur due to blocking of DNA before binding to the enzyme or stabilizing N-terminal clap after DNA binding to the enzyme [82]. In addition, etoposide quinone is a covalent poison of TOP2α and TOP2β, and its reactivity to TOP2β is reported to be slightly higher than that of TOP2α [85]. Meanwhile, studies have shown that etoposide catechol is 2–3 folds more potent than etoposide and can induce high levels of double-stranded DNA cleavage under oxidative conditions [83]. Compared with etoposide, its metabolites are several times more potent on TOP2, and they induce higher levels of DSB under oxidative reaction conditions.

Benzene is a carcinogen that can induce AML in humans and various tumors in animals. According to several reports, benzene metabolites, including benzoquinone (BQ), are responsible for the genotoxic and leukemogenic effects of benzene . In particular, benzoquinone can directly modify DNA, causing genotoxicity and mutagenesis [91,92]. BQ is a TOP2 poison as well, similar to etoposide quinone, which blocks DNA linkage and produces TOP2-DNA adducts [47,93]. In addition, exposure to benzene metabolites in mouse fetal liver is known to in- crease reactive oxygen species (ROS) [94,95]. ROS has been shown to contribute to the modification of topoisomerases [96,97]. The c-Myb transcription factor has also been shown to be abnormally activated in hematopoietic cells exposed to BQ [98]. In addition, NAD (P)H quinone dehydrogenase 1 (NQO1) is an enzyme that metabolizes BQ into hy- droquinone, which is a less reactive compound. C609T mutation encoding an inactive form of NQO1 has been suggested to increase the

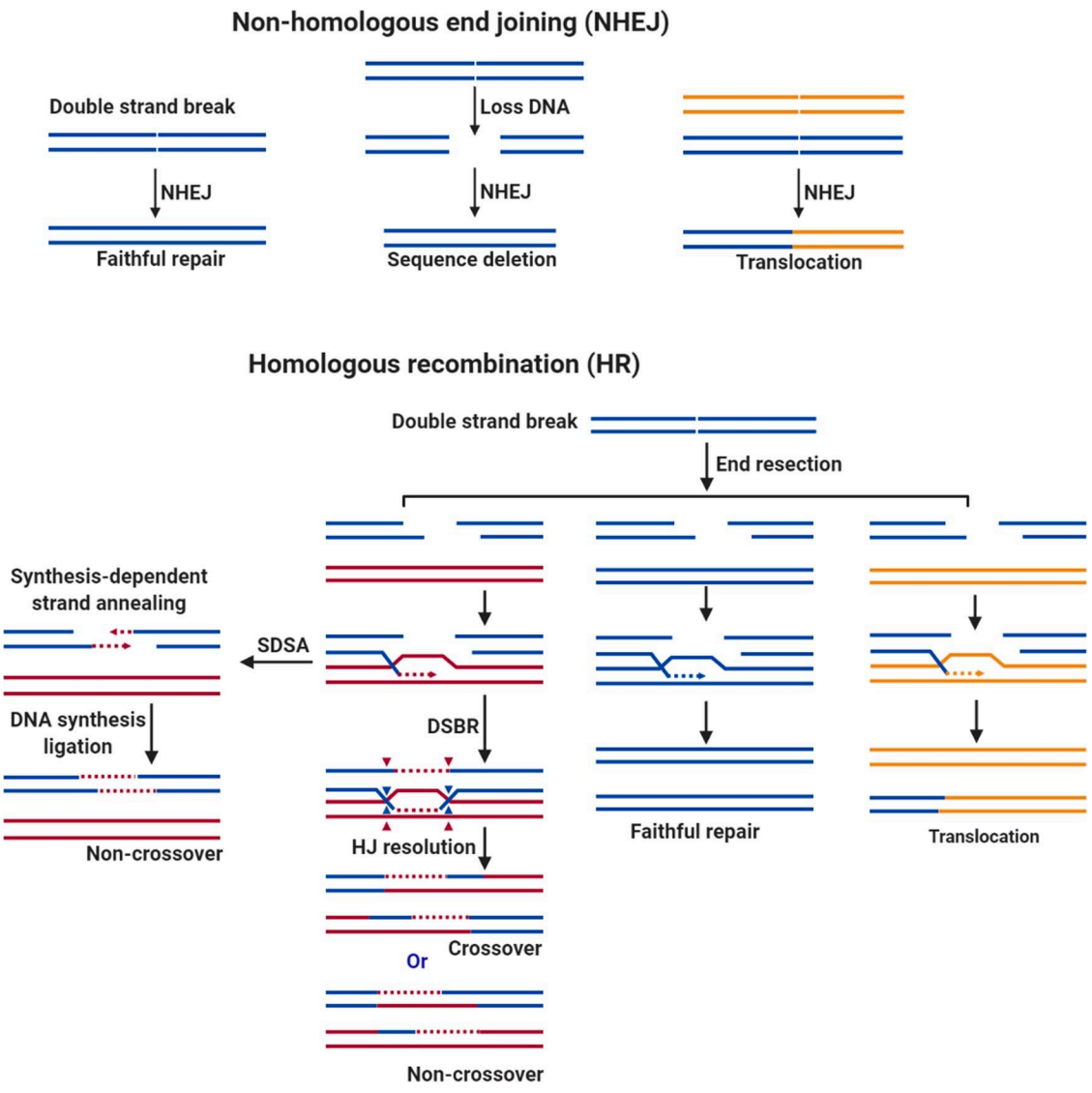

Fig. 3. TOP2 poison induces translocation mediated by the DSB repair pathway. TOP2 poison-mediated DSB is likely to be repaired by two pathways, NHEJ or HR repair. NHEJ can repair precisely when the DSB at a low concentration level. If DSB accumulates to a high concentration level, it may cause sequence deletion and translocation. NHEJ mainly contains three types of repair products, faithful repair, sequence loss, and translocation. HR is mediated by a homologous sequence. According to the model sequence, it may produce a different product. In most cases, HR repair uses homologous sequences as templates. This situation generates mainly a crossover or a non-crossover product through two pathways, including SDSA and DSBR, which play an instrumental role in meiosis. In a few cases, precision repair occurs when HR repair uses the same sequence as a template, and translocations may happen when HR uses a non-homologous sequence as a template. The blue and the red chromosomes are homologous, while the orange indicates a non-homologous chromosome. The blue arrowheads are located at one of the Holliday junctions (HJ), and the red arrowheads are located at the other junctions.

risk of leukemia with chromosome 11q23 translocations [99,100] (particularly prominent in acute non-lymphoblastic leukemia, where the *MLL* gene is fused to the AF-4 gene on chromosome 4) [101]

Etoposide metabolites contribute to therapy-related leukemia: non-TOP2 factors

Exposure to benzene is correlated with the deregulation of the expression of specific genes associated with leukemia and DNA methylation changes [102,103]. Chromatin components, in particular histones may also react with etoposide (or its metabolite) as shown for histone H1 [104]. The benzene metabolite 1,2,4-benzenetriol can influence DNA methylation and histone acetylation in K562 cells [105]. Recently, etoposide quinone has been shown to inhibit certain enzymes, such as the histone acetyltransferase CREBBPwhich is known to be involved in the leukemogenesis [106]. CREBBP(also known as CBP or KAT6A) regulates both normal and malignant hematopoiesis [107], and the majority of $Crebbp^{+/-}$ or $Crebbp^{-/-}$ mice develop malignant hematopoietic pathologies indicating that CREBBP acts as a tumor suppressor and plays a crucial role in hematopoiesis [108–110]. Werecently showed that etoposide quinone can inhibit CREBBP acetyl- transferase activity by reacting with cysteine within zinc fingers do- mains that are key for CREBBP activity[106].

TCPTP (also known as PTPN2) is a member of the protein tyrosine phosphatase (PTP) family, which negatively regulates JAK/STAT (Janus kinase/signaling transducer and activator of transcription) signaling, through dephosphorylation of different tyrosine phosphorylated JAK/STAT proteins, for instance, STAT1 or JAK1. TCPTP plays an essential role in normal and malignant hematopoiesis by regulating the JAK/STAT pathway [111,112]. Deletions or inactivating mutations of TCPTP were identified in non-Hodgkin's lymphoma and T-cell leukemia and associated with elevated STAT signaling and changes in gene expression

[112–114]. The loss of TCPTP phosphatase activity may lead to excessive activation of the JAK/STAT pathway, which further changes the development of HSC. Etoposide and benzene metabolites, including etoposide quinone and benzoquinone, can irreversibly inhibit TCPTP activity, suggesting another new mechanisms for etoposide and benzene to induction of leukemia [115,116]. (Fig. 4)

Conclusion and further challenge

In summary, etoposide and its metabolite etoposide quinone can inhibit TOP2 enzymes, and the accumulation of DSB is the main cause of secondary leukemia. There is still a need to obtain more precise evidence to prove that CREBBP and TCPTP are involved treatment-related leukemia. However, it has been established that etoposide quinone could contribute more importantly to the development of leukemia than etoposide through TOP2 inhibition. It is likely that other mechanisms such as CREBBP and TCPTP inhibition, may also contribute to etoposide treatment-related leukemia.

Similarly, a large amount of evidence has been established that metabolites of benzene are involved in leukemogenesis through other mechanisms than TOP2 inhibition. For instance, chronic occupational exposure to benzene leads to an increase in the expression of genes involved in apoptosis in blood cells [117,118]. Benzene metabolite triggers apoptosis of hematopoietic progenitor cells in a dose-dependent manner in bone marrow [119]. Meanwhile, benzene affects cell apoptosis by inhibiting caspase-3 [120,121], which may promote the survival of cancer cells. It is also well known that inappropriate activation or expression of c-Myb is involved in the process of leukemia. The c-Myb transcription factor has also been shown to be abnormally activated in K562 and mouse models of hematopoietic cells exposed to 1, 4-benzoquinone [122,123]. Moreover, the duration of exposure to benzene is associated with the dysregulation of specific gene expression associated with leukemia and changes in DNA methylation [102,103].

Based on the existence of homologous histone acetyltransferases or protein tyrosine phosphatases , it is likely that etoposide quinone may affect homologs of CREBBP and TCPTP. For example, p300, the homolog of CREBBP, is structurally and functionally similar to CREBBP, notably, on the acetyltransferase catalytic core , including RING andPHD domains. Etoposide quinone covalently binds to CREBBP in the RING and PHD domains [106]. Indeed, p300 has similar RING and PHD domains , It is thus likely that etoposide quinone may also inhibit the acetyltransferase activity of p300. Other histone acetyltransferases , such as TIP60, MOZ, and MOF, contain structural zinc fingers and may also be targets of etoposide quinone. Acetyltransferases, particularly CREBBP/p300, are involved in HR repair by acetylating Recombinant DNA repair protein 52 (RAD52) [124,125]. TIP60 plays a direct role in

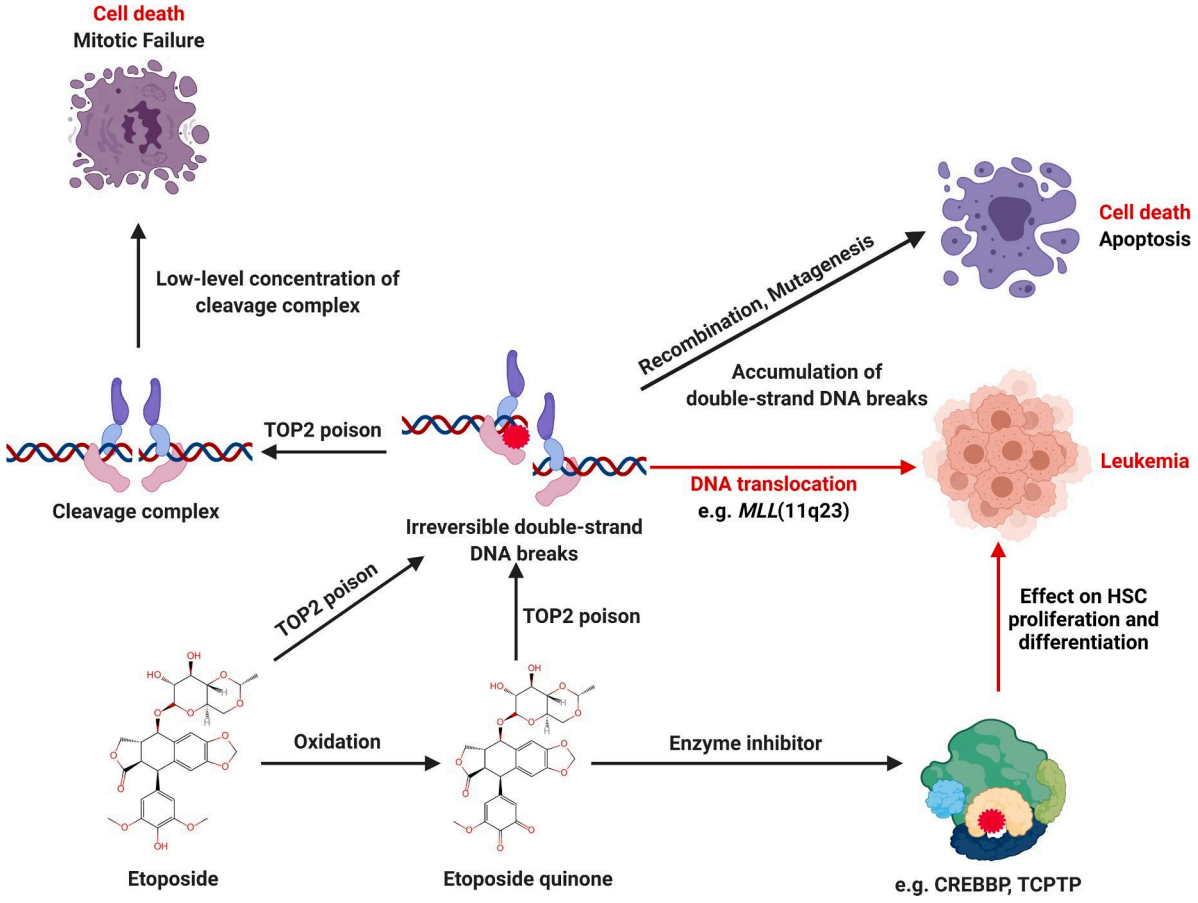

Fig. 4. The underlying mechanism of etoposide induced therapy-related leukemia. TOP2 is an essential as well as a genotoxic enzyme. Typically, the TOP2, DNA, and TOP2-DNA complex are maintained precisely to perform the relevant cellular functions. If the TOP2 enzyme activity is insufficient, the TOP2-DNA complex is lacking, resulting in the inability to release the torsional stress, leading to cell division failure and eventual death due to the failure to unwind the daughter chromosomes. In contrast, TOP2 poisons inactivate the enzymes via interfacial or covalent interaction, resulting in irreversible damage to the TOP2-DNA complex and ultimately creating DSB. Accumulation of DSB inhibits fundamental DNA processes and initiates recombination/repair pathways that produce chromosomal translocations and mutations. If the DSB overwhelms the cells, they will trigger apoptosis, which is the primary anticancer mechanism of etoposide. If the concentration of TOP2 mediated DSB is limited to induce apoptosis, mutations or chromosomal aberrations could occur, and it is possible to develop cancers. Etoposide caused therapy-related leukemia is a chromosomal rearrangement involving the MLL gene on chromosome 11q23. Meantime, etoposide quinone inhibits CREBBP or TCPTP, which has been reported to be associated with leukemogenesis.

activating ATM (an essential DSB repair protein kinase) by acetylating it in response to DNA damage [126,127]. Therefore, the loss of acetyltransferase activity may directly affect DSB repair.

The catalytic cysteine 216 is an essential residue of TCPTP and participates to the enzymatic reaction.Cysteine 216 is a evolutionary conserved residue in the PTP family [128]. Therefore, etoposide quinone may inhibit other PTP family members, possibly leading to a broad loss of PTP activity in cells. This may affect JAK/STAT signal transductionwhich plays a key role inHSC differentiation and proliferation. In parallel, a study reported that deficiency in protein-tyrosine phosphatase 1B (PTP1B) is involved in the development of acute leukemia [129]. In addition, SHP2 (Src homology region 2 domain containing phosphatase 2, also known as PTPN11) is related to hematopoiesis and leukemia [130].

As suggested for benzene-induced leukemia, etoposide-induced secondary leukemia are likely to rely on different mechanisms of actions affecting several and distinct biological processes. More studies are needed to understand the pathogenesis of etoposide therapy-related leukemia. This mayfacilitates the determination of the optimal therapeutic administration methods, including the timing and dosage and thereby advances the prevention and treatment of etoposide therapy-related leukemia.

Declaration of Competing Interest

All authors declare no conflicts of interest.

Acknowledgments

This work was supported by running grants from Université de Paris, CNRS, ANSES (Agence Nationale de Sécurité Sanitaire de l'Alimenta- tion, de l'Environnement et du Travail) and ITMO Cancer (plan Cancer- Environnement). WZ and PG were supported by the China Scholarship Council PhD fellowships. We thank Dr. Rose Ann Padua for English language manuscript reading and comments.

Author contributions

WZ, and PG designed the review. JMD, CC and FRL provided expertise. All authors contributed intellectually and to the writing of the manuscript.

References

[1] P. Meresse, E. Dechaux, C. Monneret, E. Bertounesque, Etoposide: discovery and medicinal chemistry, Curr. Med. Chem. 11 (2012) 2443–2466, https://doi.org/10.2174/0929867043364531.

[2] D.N. Carney, L. Grogan, E.F. Smit, P. Harford, H.H. Berendsen, P.E. Postmus, Single-agent oral etoposide for elderly small cell lung cancer patients, Semin. Oncol. (1990), https://doi.org/10.1016/0169-5002(90)90229-f.

[3] J. Liang, N. Bi, S. Wu, M. Chen, C. Lv, L. Zhao, A. Shi, W. Jiang, Y. Xu, Z. Zhou, W. Wang, D. Chen, Z. Hui, J. Lv, H. Zhang, Q. Feng, Z. Xiao, X. Wang, L. Liu, T. Zhang, L. Du, W. Chen, Y. Shyr, W. Yin, J. Li, J. He, L. Wang, Etoposide and cisplatin versus paclitaxel and carboplatin with concurrent thoracic radiotherapy in unresectable stage III non-small cell lung cancer: a multicenter randomized phase III trial, Ann. Oncol. (2017), https://doi.org/10.1093/annonc/mdx009.

[4] S. Dasari, P.Bernard Tchounwou, Cisplatin in cancer therapy: molecular mechanisms of action, Eur. J. Pharmacol. (2014), https://doi.org/10.1016/j.ejphar.2014.07.025.

[5] Y. Wang, S. Zou, Z. Zhao, P. Liu, C. Ke, S. Xu, New insights into small-cell lung cancer development and therapy, Cell Biol. Int. (2020), https://doi.org/10.1002/cbin.11359.

[6] T. Saito, Y. Hatta, F. Hayakawa, T. Takahashi, M. Hagihara, H. Iida, K. Minauchi, E. Yamazaki, I. Sugiura, T. Murayama, T. Sakura, N. Mori, K. Imai, Y. Yahagi, Y. Atsuta, A.M. Saito, A. Hirakawa, H. Kiyoi, I. Matsumura, Y. Miyazaki, Combination of clofarabine, etoposide, and cyclophosphamide in adult relapsed/refractory acute lymphoblastic leukemia: a phase 1/2 dose-escalation study by the Japan adult leukemia study group, Int. J. Hematol. (2021), https://doi.org/10.1007/s12185-020-03032-3.

[7] Z. Qiu, A. Lin, K. Li, W. Lin, Q. Wang, T. Wei, W. Zhu, P. Luo, J. Zhang, A novel mutation panel for predicting etoposide resistance in small-cell lung cancer, Drug Des. Dev. Ther. (2019), https://doi.org/10.2147/DDDT.S205633.

[8] A. Rossi, M. Di Maio, P. Chiodini, R.M. Rudd, H. Okamoto, D.V. Skarlos, M. Früh, W. Qian, T. Tamura, E. Samantas, T. Shibata, F. Perrone, C. Gallo, C. Gridelli, O. Martelli, S.M. Lee, Carboplatin- or cisplatin-based chemotherapy in first-line treatment of small-cell lung cancer: the COCIS meta-analysis of individual patient data, J. Clin. Oncol. (2012), https://doi.org/10.1200/JCO.2011.40.4905.

[9] H. Nemade, U. Chaudhari, A. Acharya, J. Hescheler, J.G. Hengstler, S. Papadopoulos, A. Sachinidis, Cell death mechanisms of the anti-cancer drug etoposide on human cardiomyocytes isolated from pluripotent stem cells, Arch. Toxicol. (2018), https://doi.org/10.1007/s00204-018-2170-7.

[10] A. Dorigo, R. Mansberg, Y.L. Kwan, Lomustine, etoposide, methotrexate and prednisone (LEMP) therapy for relapsed and refractory non-Hodgkin's lymphoma, Eur. J. Haematol. (1993), https://doi.org/10.1111/j.1600-0609.1993.tb00072.x.

[11] R.B.JM Henwood, Etoposide. A review of its pharmacodynamic and pharmacokinetic properties, and therapeutic potential in combination chemotherapy of cancer, Drugs 39 (3) (1990) 438.

[12] C. Alifrangis, R. Agarwal, D. Short, R.A. Fisher, N.J. Sebire, R. Harvey, P. M. Savage, M.J. Seckl, EMA/CO for high-risk gestational trophoblastic neoplasia: good outcomes with induction low-dose etoposide-cisplatin and genetic analysis, J. Clin. Oncol. 31 (2013) 280–286, https://doi.org/10.1200/JCO.2012.43.1817.

[13] S.G. Jr, Etoposide in the management of metastatic breast cancer, Cancer 1 (1 Sup) (1991), https://doi.org/10.1002/1097-0142(19910101)67, 67https://doi.org/doi::1+ <266::aid-cncr2820671310>3.0.co;2-a.

[14] O. RF, Oral etoposide for the treatment of recurrent ovarian cancer, Drugs 58 (Suppl 3) (1999), https://doi.org/10.2165/00003495-199958003-00007 https://doi.org/doi.

[15] S. Ezoe, Secondary leukemia associated with the anti-cancer agent, etoposide, a topoisomerase II inhibitor, Int. J. Environ. Res. Public Health. 9 (2012) 2444–2453, https://doi.org/10.3390/ijerph9072444.

[16] J. Pedersen-Bjergaard, G. Daugaard, S.W. Hansen, M. R o rth, P. Philip, S. O. Larsen, Increased risk of myelodysplasia and leukaemia after etoposide, cisplatin, and bleomycin for germ-cell tumours, Lancet (1991), https://doi.org/10.1016/0140-6736(91)90490-G.

[17] N. Shimada, N. Ohno, R. Tanosaki, S. Fuji, Y. Suzuki, K. Yuji, K. Uchimaru, A. Tojo, Therapy-related acute myeloid leukemia after the long-term administration of low-dose etoposide for chronic-type adult T-cell leukemia-lymphoma: a case report and literature review, Intern. Med. (2017), https://doi.org/10.2169/internalmedicine.56.7763.

[18] The US Food and drug administration, Acute myeloid leukemia: developing drugs and biological products for treatment, (n.d.) 1–36. 2020. https://www.fda.gov/media/140821/download.

[19] E.M. Agency. https://www.ema.europa.eu/en/documents/referral/etopophos-article-30-referral-chmp-assessment-report_en.pdf.

[20] M.V. Relling, J. Nemec, E.G. Schuetz, J.D. Schuetz, F.J. Gonzalez, K.R. Korzekwa, O-demethylation of epipodophyllotoxins is catalyzed by human cytochrome P450 3A4, Mol. Pharmacol. (1994).

[21] G. Luo, T. Guenthner, L.-S. Gan, W. Humphreys, CYP3A4 induction by xenobiotics: biochemistry, experimental methods and impact on drug discovery and development, Curr. Drug Metab (2005), https://doi.org/10.2174/1389200043335397.

[22] S. Kishi, W. Yang, B. Boureau, S. Morand, S. Das, P. Chen, E.H. Cook, G.L. Rosner, E. Schuetz, C.H. Pui, M.V. Relling, Effects of prednisone and genetic polymorphisms on etoposide disposition in children with acute lymphoblastic leukemia, Blood (2004), https://doi.org/10.1182/blood-2003-06-2105.

[23] Y. Fan, E.M. Schreiber, A. Giorgianni, J.C. Yalowich, B.W. Day, Myeloperoxidase-catalyzed metabolism of etoposide to its quinone and glutathione adduct forms in HL60 cells, Chem. Res. Toxicol. (2006), https://doi.org/10.1021/tx0600595.

[24] J. Yang, A. Bogni, E.G. Schuetz, M. Ratain, M.Eileen Dolan, H. McLeod, L. Gong, C. Thorn, M.V. Relling, T.E. Klein, R.B. Altman, Etoposide pathway, Pharmacogenet. Genom. (2009), https://doi.org/10.1097/FPC.0b013e32832e0e7f.

[25] N. Haim, B.K. Sinha, J. Nemec, J. Roman, Peroxidase-catalyzed metabolism of etoposide (VP-16-213) and covalent binding of reactive intermediates to cellular macromolecules, Cancer Res. (1987).

[26] B.D. Lovett, D. Strumberg, I.A. Blair, S. Pang, D.A. Burden, M.D. Megonigal, E. F. Rappaport, T.R. Rebbeck, N. Osheroff, Y.G. Pommier, C.A. Felix, Etoposide metabolites enhance DNA topoisomerase II cleavage near leukemia-associated MLL translocation breakpoints, Biochemistry (2001), https://doi.org/10.1021/bi002361x.

[27] Z. Wen, M.N. Tallman, S.Y. Ali, P.C. Smith, UDP-glucuronosyltransferase 1A1 is the principal enzyme responsible for etoposide glucuronidation in human liver and intestinal microsomes: structural characterization of phenolic and alcoholic glucuronides of etoposide and estimation of enzyme kinetics, Drug Metab. Dispos. (2007), https://doi.org/10.1124/dmd.106.012732.

[28] Y. Watanabe, M. Nakajima, N. Ohashi, T. Kume, T. Yokoi, Glucuronidation of etoposide in human liver microsomes is specifically catalyzed by UDP-glucuronosyltransferase 1A1, Drug Metab. Dispos. (2003), https://doi.org/10.1124/dmd.31.5.589.

[29] J.D. Hainsworth, F.A. Greco, Etoposide: twenty years later, Ann. Oncol. 6 (1995) 325–341, https://doi.org/10.1093/oxfordjournals.annonc.a059180.

[30] A. Grieder, R. Maurer, H. Stähelin, Effect of an Epipodophyllotoxin derivative (VP 16-213) on macromolecular synthesis and mitosis in mastocytoma cells in vitro, Cancer Res (1974).

[31] T. Colombo, M. Broggini, M. Vaghi, Comparison between VP 16 and VM 26 in Lewis lung carcinoma of the mouse, Eur. J. Cancer Clin. Oncol. (1986).

[32] H. Roed, L.L. Vindelov, I.J. Christensen, M. Spang-Thomsen, H.H. Hansen, The effect of the two epipodophyllotoxin derivatives etoposide (VP-16) and teniposide (VM-26) on cell lines established from patients with small cell carcinoma of the lung, Cancer Chemother. Pharmacol. (1987), https://doi.org/10.1007/BF00296248.

[33] K. Kasahara, Y. Fujiwara, Y. Sugimoto, K. Nishio, T. Tamura, T. Matsuda, N. Saijo, Determinants of response to the DNA topoisomerase II inhibitors doxorubicin and etoposide in human lung cancer cell lines, J. Natl. Cancer Inst. 84 (1992) 113–118, https://doi.org/10.1093/jnci/84.2.113.

[34] C.M. Edwards, B.S. Glisson, C.K. King, S. Smallwood-Kentro, W.E. Ross, Etoposide-induced DNA cleavage in human leukemia cells, Cancer Chemother. Pharmacol. 20 (1987) 162–168, https://doi.org/10.1007/BF00253972.

[35] F. Mitelman, B. Johansson, F. Mertens, The impact of translocations and gene fusions on cancer causation, Nat. Rev. Cancer. (2007), https://doi.org/10.1038/nrc2091.

[36] F. Mertens, B. Johansson, T. Fioretos, F. Mitelman, The emerging complexity of gene fusions in cancer, Nat. Rev. Cancer. (2015), https://doi.org/10.1038/nrc3947.

[37] M.P., Topoisomerase II and leukemia MaryJean, Ann N Y Acad Sci 1310 (2015) 98–110, https://doi.org/10.1111/nyas.12358.Topoisomerase.

[38] F. Gómez-Herreros, DNA Double Strand Breaks and Chromosomal Translocations Induced by DNA Topoisomerase II, Front. Mol. Biosci. 6 (2019) 1–7, https://doi.org/10.3389/fmolb.2019.00141.

[39] J.E. Deweese, N. Osheroff, The DNA cleavage reaction of topoisomerase II: wolf in sheep's clothing, Nucleic Acids Res (2009), https://doi.org/10.1093/nar/gkn937.

[40] S.M. Vos, E.M. Tretter, B.H. Schmidt, J.M. Berger, All tangled up: how cells direct, manage and exploit topoisomerase function, Nat. Rev. Mol. Cell Biol. (2011), https://doi.org/10.1038/nrm3228.

[41] Y. Pommier, Drugging topoisomerases: lessons and Challenges, ACS Chem. Biol. (2013), https://doi.org/10.1021/cb300648v.

[42] A.K. McClendon, N. Osheroff, DNA topoisomerase II, genotoxicity, and cancer, Mutat. Res. - Fundam. Mol. Mech. Mutagen. (2007), https://doi.org/10.1016/j.mrfmmm.2007.06.009.

[43] V.M. Matias-Barrios, M. Radaeva, Y. Song, Z. Alperstein, A.R. Lee, V. Schmitt, J. Lee, F. Ban, N. Xie, J. Qi, N. Lallous, M.E. Gleave, A. Cherkasov, X. Dong, Discovery of new catalytic topoisomerase II inhibitors for anticancer therapeutics, Front. Oncol (2021), https://doi.org/10.3389/fonc.2020.633142.

[44] Y. Pommier, C. Marchand, Interfacial inhibitors: targeting macromolecular complexes, Nat. Rev. Drug Discov. (2012), https://doi.org/10.1038/nrd3404.

[45] C.C. Wu, T.K. Li, L. Farh, L.Y. Lin, T.S. Lin, Y.J. Yu, T.J. Yen, C.W. Chiang, N. L. Chan, Structural basis of type II topoisomerase inhibition by the anticancer drug etoposide, Science (80) (2011), https://doi.org/10.1126/science.1204117.

[46] A.C. Ketron, N. Osheroff, Phytochemicals as anticancer and chemopreventive topoisomerase II poisons, Phytochem. Rev. (2014), https://doi.org/10.1007/s11101-013-9291-7.

[47] J.L. Nitiss, Targeting DNA topoisomerase II in cancer chemotherapy, Nat. Rev. Cancer. (2009), https://doi.org/10.1038/nrc2607.

[48] C.C. Kumar, Genetic abnormalities and challenges in the treatment of acute myeloid Leukemia, Genes Cancer 2 (2011) 95–107, https://doi.org/10.1177/1947601911408076.

[49] M.J. Ratain, J.D. Rowley, Review: therapy-related acute myeloid leukemia secondary to inhibitors of topoisomerase II: from the bedside to the target genes, Ann. Oncol. 3 (1992) 107–111, https://doi.org/10.1093/oxfordjournals.annonc.a058121.

[50] P.H. Domer, D.R. Head, N. Renganathan, S.C. Raimondi, E. Yang, M. Atlas, Molecular analysis of 13 cases of MLL/11q23 secondary acute leukemia and identification of topoisomerase II consensus-binding sequences near the chromosomal breakpoint of a secondary leukemia with the t(4;11), Leukemia (1995).

[51] M.J. Ratain, L.S. Kaminer, J.D. Bitran, R.A. Larson, M.M. Le Beau, C. Skosey, S. Purl, P.C. Hoffman, J. Wade, J.W. Vardiman, K. Daly, J.D. Rowley, H. M. Golomb, Acute nonlymphocytic leukemia following etoposide and cisplatin combination chemotherapy for advanced non-small-cell carcinoma of the lung, Blood (1987), https://doi.org/10.1182/blood.v70.5.1412.1412.

[52] M.C. Le Deley, G. Vassal, A. Taïbi, A. Shamsaldin, T. Leblanc, O. Hartmann, High cumulative rate of secondary leukemia after continuous etoposide treatment for solid tumors in children and young adults, Pediatr. Blood Cancer. (2005), https://doi.org/10.1002/pbc.20380.

[53] N.J. Winick, R.W. McKenna, J.J. Shuster, N.R. Schneider, M.J. Borowitz, W. P. Bowman, D. Jacaruso, B.A. Kamen, G.R. Buchanan, Secondary acute myeloid leukemia in children with acute lymphoblastic leukemia treated with etoposide, J. Clin. Oncol. 11 (1993) 209–217, https://doi.org/10.1200/JCO.1993.11.2.209.

[54] K. Sugita, T. Furukawa, M. Tsuchida, Y. Okawa, S. Nakazawa, J. Akatsuka, M. Ohira, K. Nishimura, High frequency of etoposide (vp-16)-related secondary leukemia in children with non-hodgkin's lymphoma, J. Pediatr. Hematol. Oncol. (1993), https://doi.org/10.1097/00043426-199302000-00013.

[55] C. Kollmannsberger, J. Beyer, J.P. Droz, A. Harstrick, J.T. Hartmann, P. Biron, A. Flechon, P. Schöffski, M. Kuczyk, H.J. Schmoll, L. Kanz, C. Bokemeyer, Secondary leukemia following high cumulative doses of etoposide in patientstreated for advanced germ cell tumors, J. Clin. Oncol. 16 (1998) 3386–3391,https://doi.org/10.1200/JCO.1998.16.10.3386.

[56] M.A. Smith, L. Rubinstein, J.R. Anderson, D. Arthur, P.J. Catalano, B. Freidlin, R. Heyn, A. Khayat, M. Krailo, V.J. Land, J. Miser, J. Shuster, D. Vena, Secondary leukemia or myelodysplastic syndrome after treatment with epipodophyllotoxins, J. Clin. Oncol. (1999), https://doi.org/10.1200/jco.1999.17.2.569.

[57] R. Haupt, T.R. Fears, A. Heise, H. Gadner, G. Loiacono, M. De Terlizzi, M. A. Tucker, Risk of secondary leukemia after treatment with etoposide (VP-16) for Langerhans' cell histiocytosis in Italian and Australian-German populations, Int. J. Cancer. (1997), https://doi.org/10.1002/(SICI)1097-0215(19970328)71,1<9::AID-IJC3>3.0.CO;2-Y.

[58] C.R. Nichols, E.S. Breeden, P.J. Loehrer, S.D. Williams, L.H. Einhorn, Secondary leukemia associated with a conventional dose of etoposide: review of serial germ cell tumor protocols, J. Natl. Cancer Inst. (1993), https://doi.org/10.1093/jnci/85.1.36.

[59] N. Sciascia, W. Wu, D. Zong, Y. Sun, N. Wong, S. John, D. Wangsa, T. Ried, S. F. Bunting, Y. Pommier, A. Nussenzweig, Suppressing proteasome mediated processing of topoisomerase II DNA-protein complexes preserves genome integrity, Elife (2020), https://doi.org/10.7554/eLife.53447.

[60] K. Szlachta, A. Manukyan, H.M. Raimer, S. Singh, A. Salamon, W. Guo, K. S. Lobachev, Y.H. Wang, Topoisomerase II contributes to DNA secondary structure-mediated double-stranded breaks, Nucleic Acids Res (2020), https://doi.org/10.1093/nar/gkaa483.

[61] M. Tsuda, K. Kitamasu, S. Hosokawa, T. Nakano, H. Ide, Repair of trapped topoisomerase II covalent cleavage complexes: novel proteasome-independent mechanisms, Nucleosides, Nucleot. Nucleic Acids (2020), https://doi.org/10.1080/15257770.2019.1674332.

[62] M.J. Schellenberg, J.A. Lieberman, A. Herrero-Ruiz, L.R. Butler, J.G. Williams, A. M. Muñoz-Cabello, G.A. Mueller, R.E. London, F. Cortés-Ledesma, R.S. Williams, ZATT (ZNF451)–mediated resolution of topoisomerase 2 DNA-protein cross-links,Science (80) (2017), https://doi.org/10.1126/science.aam6468.

[63] S.P. Jackson, Sensing and repairing DNA double-strand breaks, Carcinogenesis (2002), https://doi.org/10.1093/carcin/23.5.687.

[64] M.Bala Anuranjani, Concerted action of Nrf2-ARE pathway, MRN complex, HMGB1 and inflammatory cytokines - Implication in modification of radiationdamage, Redox Biol (2014), https://doi.org/10.1016/j.redox.2014.02.008.

[65] T. Aparicio, R. Baer, M. Gottesman, J. Gautier, MRN, CtIP, and BRCA1 mediate repair of topoisomerase II-DNA adducts, J. Cell Biol. (2016), https://doi.org/10.1083/jcb.201504005.

[66] S. Qiu, J. Huang, MRN complex is an essential effector of DNA damage repair, J. Zhejiang Univ. Sci. B. (2021), https://doi.org/10.1631/jzus.B2000289.

[67] R.A. Deshpande, J.H. Lee, S. Arora, T.T. Paull, Nbs1 converts the human Mre11/Rad50 nuclease complex into an endo/exonuclease machine specific for protein-DNA adducts, Mol. Cell. (2016), https://doi.org/10.1016/j.molcel.2016.10.010.

[68] R. Anand, A. Jasrotia, D. Bundschuh, S.M. Howard, L. Ranjha, M. Stucki, P. Cejka, NBS1 promotes the endonuclease activity of the MRE11-RAD50 complex by sensing CtIP phosphorylation, EMBO J. (2019), https://doi.org/10.15252/embj.2018101005.

[69] M.R. Lieber, The biochemistry and biological significance of nonhomologous DNA end joining: an essential repair process in multicellular eukaryotes, Genes to Cells 4 (1999) 77–85, https://doi.org/10.1046/j.1365-2443.1999.00245.x.

[70] A.T. Do, J.T. Brooks, M.K. Le Neveu, J.R. Larocque, Double-strand break repair assays determine pathway choice and structure of gene conversion events in drosophila melanogaster, 4 (2014) 425–432. https://doi.org/10.1534/g3.113.010074.

[71] D.O. Ferguson, F.W. Alt, DNA double strand break repair and chromosomal translocation: lessons from animal models, Oncogene (2001), https://doi.org/10.1038/sj.onc.1204767.

[72] T. Hatkevich, D.E. Miller, J. Sekelsky, C.A. Turcotte, M.C. Miller, A pathway for error-free non-homologous end joining of resected meiotic double-strand breaks, 49 (2021) 879–890. https://doi.org/10.1093/nar/gkaa1205.

[73] M. de Campos-Nebel, I. Larripa, M. González-Cid, Topoisomerase ii-mediated DNA damage is differently repaired during the cell cycle by non-homologous endjoining and homologous recombination, PLoS ONE 5 (2010) 1–13, https://doi. org/10.1371/journal.pone.0012541.

[74] M. Malik, K.C. Nitiss, V. Enriquez-Rios, J.L. Nitiss, Roles of nonhomologous end-joining pathways in surviving topoisomerase II-mediated DNA damage, Mol. Cancer Ther. (2006), https://doi.org/10.1158/1535-7163.MCT-05-0263.

[75] P. Broeker, H. Super, M. Thirman, H. Pomykala, Y. Yonebayashi, S. Tanabe, N. Zeleznik-Le, J. Rowley, Distribution of 11q23 breakpoints within the MLL breakpoint cluster region in de novo acute leukemia and in treatment-related acute myeloid leukemia: correlation with scaffold attachment regions and topoisomerase II consensus binding sites, Blood (1996), https://doi.org/10.1182/blood.v87.5.1912.bloodjournal8751912.

[76] A.C. Winters, K.M. Bernt, MLL-rearranged leukemias- An update on science and clinical approaches, Front. Pediatr (2017), https://doi.org/10.3389/fped.2017.00004.

[77] M. Stanulla, J. Wang, D.S. Chervinsky, S. Thandla, P.D. Aplan, DNA cleavage within the MLL breakpoint cluster region is a specific event which occurs as part of higher-order chromatin fragmentation during the initial stages of apoptosis, Mol. Cell. Biol. 17 (1997) 4070–4079, https://doi.org/10.1128/mcb.17.7.4070.

[78] P.L. Strissel, R. Strick, J.D. Rowley, N.J. Zeleznik-Le, An in vivo topoisomerase II cleavage site and a DNase I hypersensitive site colocalize near exon 9 in the MLL breakpoint cluster region, Blood (1998), https://doi.org/10.1182/blood.v92.10.3793.422a24_3793_3803.

[79] R.J. Whitmarsh, C. Saginario, Y. Zhuo, E. Hilgenfeld, E.F. Rappaport, M. D. Megonigal, M. Carroll, M. Liu, N. Osheroff, N.K.V. Cheung, D.J. Slater, T. Ried, T. Knutsen, I.A. Blair, C.A. Felix, Reciprocal DNA topoisomerase II cleavage events at 5′-TATTA-3′ sequences in MLL and AF-9 create homologous single-stranded overhangs that anneal to form der(11) and der(9) genomic breakpoint

junctions in treatment-related AML without further processing, Oncogene (2003), https://doi.org/10.1038/sj.onc.1207052.
[80] A. Ng, G.M. Taylor, O.B. Eden, Genotoxicity of etoposide: greater susceptibility of MLL than other target genes, Cancer Genet. Cytogenet. 164 (2006) 164–167, https://doi.org/10.1016/j.cancergencyto.2005.08.006.
[81] C. Meyer, T. Burmeister, D. Gröger, G. Tsaur, L. Fechina, A. Renneville, R. Sutton, N.C. Venn, M. Emerenciano, M.S. Pombo-De-Oliveira, C. Barbieri Blunck, B. Almeida Lopes, J. Zuna, J. Trka, P. Ballerini, H. Lapillonne, M. De Braekeleer, G. Cazzaniga, L. Corral Abascal, V.H.J. Van Der Velden, E. Delabesse, T.S. Park, S. H. Oh, M.L.M. Silva, T. Lund-Aho, V. Juvonen, A.S. Moore, O. Heidenreich, J. Vormoor, E. Zerkalenkova, Y. Olshanskaya, C. Bueno, P. Menendez, A. Teigler-Schlegel, U. Zur Stadt, J. Lentes, G. Göhring, A. Kustanovich, O. Aleinikova, B. W. Schäfer, S. Kubetzko, H.O. Madsen, B. Gruhn, X. Duarte, P. Gameiro, E. Lippert, A. Bidet, J.M. Cayuela, E. Clappier, C.N. Alonso, C.M. Zwaan, M. M. Van Den Heuvel-Eibrink, S. Izraeli, L. Trakhtenbrot, P. Archer, J. Hancock, A. Möricke, J. Alten, M. Schrappe, M. Stanulla, S. Strehl, A. Attarbaschi, M. Dworzak, O.A. Haas, R. Panzer-Grümayer, L. Sedék, T. Szczepa, A. Caye, L. Suarez, H. Cavé, R. Marschalek, The MLL recombinome of acute leukemias in 2017, Leukemia (2018), https://doi.org/10.1038/leu.2017.213.
[82] E.G. Gibson, M.M. King, S.L. Mercer, J.E. Deweese, Two-mechanism model for the interaction of etoposide quinone with topoisomerase IIα, Chem. Res. Toxicol. 29 (2016) 1541–1548, https://doi.org/10.1021/acs.chemrestox.6b00209.
[83] D.A. Jacob, E.G. Gibson, S.L. Mercer, J.E. Deweese, Etoposide catechol is an oxidizable topoisomerase II poison, Chem. Res. Toxicol. 26 (2013) 1156–1158, https://doi.org/10.1021/tx400205n.
[84] D.A. Jacob, S.L. Mercer, N. Osheroff, J.E. Deweese, Etoposide quinone is a redox-dependent topoisomerase II poison, Biochemistry (2011), https://doi.org/10.1021/bi200438m.
[85] N.A. Smith, J.A.W. Byl, S.L. Mercer, J.E. Deweese, N. Osheroff, Etoposide quinone is a covalent poison of human topoisomerase IIβ, Biochemistry 53 (2014) 3229–3236, https://doi.org/10.1021/bi500421q.
[86] T.G. Gantchev, D.J. Hunting, Inhibition of the topoisomerase II-DNA cleavable complex by the ortho-quinone derivative of the antitumor drug etoposide (VP-16), Biochem. Biophys. Res. Commun. (1997), https://doi.org/10.1006/bbrc.1997.7063.
[87] T.G. Gantchev, D.J. Hunting, The ortho-quinone metabolite of the anticancer drug etoposide (VP-16) is a potent inhibitor of the topoisomerase II/DNA cleavable complex, Mol. Pharmacol. (1998), https://doi.org/10.1124/mol.53.3.422.
[88] R.H. Lindsey, R.P. Bender, N. Osheroff, Stimulation of topoisomerase II-mediated DNA cleavage by benzene metabolites, Chem. Biol. Interact. 153–154 (2005) 197–205, https://doi.org/10.1016/j.cbi.2005.03.035.
[89] R.P. Bender, H.J. Lehmler, L.W. Robertson, G. Ludewig, N. Osheroff, Polychlorinated biphenyl quinone metabolites poison human topoisomerase IIα: altering enzyme function by blocking the N-terminal protein gate, Biochemistry (2006), https://doi.org/10.1021/bi0524666.
[90] S. Mondrala, D.A. Eastmond, Topoisomerase II inhibition by the bioactivated benzene metabolite hydroquinone involves multiple mechanisms, Chem. Biol. Interact. 184 (2010) 259–268, https://doi.org/10.1016/j.cbi.2009.12.023.
[91] J.L. Bolton, M.A. Trush, T.M. Penning, G. Dryhurst, T.J. Monks, Role of quinones in toxicology, Chem. Res. Toxicol. (2000), https://doi.org/10.1021/tx9902082.
[92] J.L. Bolton, T. Dunlap, Formation and biological targets of quinones: cytotoxic versus cytoprotective effects, Chem. Res. Toxicol. (2017), https://doi.org/10.1021/acs.chemrestox.6b00256.
[93] R.H. Lindsey, K.D. Bromberg, C.A. Felix, N. Osheroff, 1,4-Benzoquinone is a topoisomerase II poison, Biochemistry (2004), https://doi.org/10.1021/bi049756r.
[94] N.A. Philbrook, L.M. Winn, Benzoquinone toxicity is not prevented by sulforaphane in CD-1 mouse fetal liver cells, J. Appl. Toxicol. (2016), https://doi.org/10.1002/jat.3251.
[95] H.J. Badham, S.J. Renaud, J. Wan, L.M. Winn, Benzene-initiated oxidative stress: effects on embryonic signaling pathways, Chem. Biol. Interact. (2010), https://doi.org/10.1016/j.cbi.2009.11.005.
[96] H.R. Lu, H. Zhu, M. Huang, Y. Chen, Y.J. Cai, Z.H. Miao, J.S. Zhang, J. Ding, Reactive oxygen species elicit apoptosis by concurrently disrupting topoisomerase II and DNA-dependent protein kinase, Mol. Pharmacol. (2005), https://doi.org/10.1124/mol.105.011544.
[97] L.H. Meng, J. Ding, Salvicine, a novel topoisomerase II inhibitor, exerts its potent anticancer activity by ROS generation, Acta Pharmacol. Sin. (2007), https://doi.org/10.1111/j.1745-7254.2007.00698.x.
[98] R. Singh, L.M. Winn, The effects of 1,4-benzoquinone on c-Myb and topoisomerase II in K-562 cells, Mutat. Res. - Fundam. Mol. Mech. Mutagen. (2008), https://doi.org/10.1016/j.mrfmmm.2008.08.007.
[99] J.L. Wiemels, A. Pagnamenta, G.M. Taylor, O.B. Eden, F.E. Alexander, M. F. Greaves, A lack of a functional NAD(P)H:quinone oxidoreductase allele is selectively associated with pediatric leukemias that have MLL fusions, Cancer Res (1999).
[100] R.A. Larson, Y. Wang, M. Banerjee, J. Wiemels, C. Hartford, M.M. Le Beau, M. T. Smith, Prevalence of the inactivating 609C → T polymorphism in the NAD(P)H: quinone oxidoreductase (NQO1) gene in patients with primary and therapy-related myeloid leukemia, Blood (1999), https://doi.org/10.1182/blood.v94.2.803.
[101] M.T. Smith, Y. Wang, C.F. Skibola, D.J. Slater, L. Lo Nigro, P.C. Nowell, B. J. Lange, C.A. Felix, Low NAD(P)H: quinone oxidoreductase activity is associated with increased risk of leukemia with MLL translocations in infants and children, Blood (2002), https://doi.org/10.1182/blood-2001-12-0264.

[102] K. Li, Y. Jing, C. Yang, S. Liu, Y. Zhao, X. He, F. Li, J. Han, G. Li, Increased leukemia-associated gene expression in benzene-exposed workers, Sci. Rep. (2014), https://doi.org/10.1038/srep05369.
[103] V. Bollati, A. Baccarelli, L. Hou, M. Bonzini, S. Fustinoni, D. Cavallo, H.M. Byun, J. Jiang, B. Marinelli, A.C. Pesatori, P.A. Bertazzi, A.S. Yang, Changes in DNA methylation patterns in subjects exposed to low-dose benzene, Cancer Res (2007),https://doi.org/10.1158/0008-5472.CAN-06-2995.
[104] E. Chamani, A. Rabbani-Chadegani, Z. Zahraei, Spectroscopic detection of etoposide binding to chromatin components: the role of histone proteins, Spectrochim. Acta - Part A Mol. Biomol. Spectrosc. (2014), https://doi.org/10.1016/j.saa.2014.05.068.
[105] C.H. Yu, Y. Li, X. Zhao, S.Q. Yang, L. Li, N.X. Cui, L. Rong, Z.C. Yi, Benzene metabolite 1,2,4-benzenetriol changes DNA methylation and histone acetylationof erythroid-specific genes in K562 cells, Arch. Toxicol. 93 (2019) 137–147, https://doi.org/10.1007/s00204-018-2333-6.
[106] W. Zhang, J. Berthelet, C. Michail, L.C. Bui, P. Gou, R. Liu, R. Duval, J. Renault, J. M. Dupret, F. Guidez, C. Chomienne, F.R. Lima, Human CREBBP acetyltransferaseis impaired by etoposide quinone, an oxidative and leukemogenic metabolite of the anticancer drug etoposide through modification of redox-sensitive zinc-fingercysteine residues, Free Radic, Biol. Med. (2021), https://doi.org/10.1016/j. freeradbiomed.2020.11.027.
[107] X.J. Sun, N. Man, Y. Tan, S.D. Nimer, L. Wang, The role of histone acetyltransferases in normal and malignant hematopoiesis, Front. Oncol. (2015),https://doi.org/10.3389/fonc.2015.00108.
[108] V.I. Rebel, A.L. Kung, E.A. Tanner, H. Yang, R.T. Bronson, D.M. Livingston, Distinct roles for CREB-binding protein and p300 in hematopoietic stem cell self-renewal, Proc. Natl. Acad. Sci. U. S. A. (2002), https://doi.org/10.1073/pnas.232568499.
[109] S.N. Zimmer, Q. Zhou, T. Zhou, Z. Cheng, S.L. Abboud-Werner, D. Horn, M. Lecocke, R. White, A.V. Krivtsov, S.A. Armstrong, A.L. Kung, D.M. Livingston, V.I. Rebel, Crebbp haploinsufficiency in mice alters the bone marrow microenvironment, leading to loss of stem cells and excessive myelopoiesis, Blood(2011), https://doi.org/10.1182/blood-2010-09-307942.
[110] M. Qian, H. Zhang, S.K.Y. Kham, S. Liu, C. Jiang, X. Zhao, Y. Lu, C. Goodings, T. N. Lin, R. Zhang, T. Moriyama, Z. Yin, Z. Li, T.C. Quah, H. Ariffin, A.M. Tan, S. Shen, D. Bhojwani, S. Hu, S. Chen, H. Zheng, C.H. Pui, A.E.J. Yeoh, J.J. Yang, Whole-transcriptome sequencing identifies a distinct subtype of acute lymphoblastic leukemia with predominant genomic abnormalities of EP300 andCREBBP, Genome Res (2017), https://doi.org/10.1101/gr.209163.116.
[111] K.A. Dorritie, J.A. McCubrey, D.E. Johnson, STAT transcription factors in hematopoiesis and leukemogenesis: opportunities for therapeutic intervention,Leukemia (2014), https://doi.org/10.1038/leu.2013.192.
[112] K.A. Pike, M.L. Tremblay, TC-PTP and PTP1B: regulating JAK-STAT signaling, controlling lymphoid malignancies, Cytokine (2016), https://doi.org/10.1016/j.cyto.2015.12.025.
[113] M. Kleppe, T. Tousseyn, E. Geissinger, Z.K. Atak, S. Aerts, A. Rosenwald, I. Wlodarska, J. Cools, Mutation analysis of the tyrosine phosphatase PTPN2 in Hodgkin's lymphoma and T-cell non-Hodgkin's lymphoma, Haematologica (2011), https://doi.org/10.3324/haematol.2011.041921.
[114] M. Kleppe, I. Lahortiga, T. El Chaar, K. De Keersmaecker, N. Mentens, C. Graux, K. Van Roosbroeck, A.A. Ferrando, A.W. Langerak, J.P.P. Meijerink, F. Sigaux, T. Haferlach, I. Wlodarska, P. Vandenberghe, J. Soulier, J. Cools, Deletion of the protein tyrosine phosphatase gene PTPN2 in T-cell acute lymphoblastic leukemia,Nat. Genet. (2010), https://doi.org/10.1038/ng.587.
[115] Q. Nian, J. Berthelet, W. Zhang, L.C. Bui, R. Liu, X. Xu, R. Duval, S. Ganesan, T. Leger, C. Chomienne, F. Busi, F. Guidez, J.M. Dupret, F.R. Lima, T-cell protein tyrosine phosphatase is irreversibly inhibited by etoposide-quinone, a reactive metabolite of the chemotherapy drug etoposide, Mol. Pharmacol. (2019), https://doi.org/10.1124/mol.119.116319.
[116] R. Duval, L.C. Bui, C. Mathieu, Q. Nian, J. Berthelet, X. Xu, I. Haddad, J. Vinh, J. M. Dupret, F. Busi, F. Guidez, C. Chomienne, F. Rodrigues-Lima, Benzoquinone, a leukemogenic metabolite of benzene, catalytically inhibits the protein tyrosine phosphatase PTPN2 and alters STAT1 signaling, J. Biol. Chem. 294 (2019) 12483–12494, https://doi.org/10.1074/jbc.RA119.008666.
[117] C.M. McHale, L. Zhang, Q. Lan, G. Li, A.E. Hubbard, M.S. Forrest, R. Vermeulen, J. Chen, M. Shen, S.M. Rappaport, S. Yin, M.T. Smith, N. Rothman, Changes in theperipheral blood transcriptome associated with occupational benzene exposure identified by cross-comparison on two microarray platforms, Genomics (2009), https://doi.org/10.1016/j.ygeno.2008.12.006.
[118] C.M. McHale, L. Zhang, Q. Lan, R. Vermeulen, G. Li, A.E. Hubbard, K.E. Porter, R. Thomas, C.J. Portier, M. Shen, S.M. Rappaport, S. Yin, M.T. Smith, N. Rothman, Global gene expression profiling of a population exposed to a rangeof benzene levels, Environ. Health Perspect. (2011), https://doi.org/10.1289/ehp.1002546.
[119] J.L. Moran, D. Siegel, X.M. Sun, D. Ross, Induction of apoptosis by benzene metabolites in HL60 and CD34 human bone marrow progenitor cells, Mol.Pharmacol. (1996).
[120] R. Ruiz-Ramos, M.E. Cebrian, E. Garrido, Benzoquinone activates the ERK/MAPK signaling pathway via ROS production in HL-60 cells, Toxicology (2005), https:// doi.org/10.1016/j.tox.2004.12.035.
[121] M.T. Smith, The mechanism of benzene-induced leukemia: a hypothesis and speculations on the causes of leukemia, Environ. Health Perspect. 104 (1996) 1219–1225, https://doi.org/10.1289/ehp.961041219.
[122] R.G. Ramsay, A.L. Barton, T.J. Gonda, Targeting c-Myb expression in human disease, Expert Opin. Ther. Targets. (2003), https://doi.org/10.1517/14728222.7.2.235.

[123] J. Wan, H.J. Badham, L. Winn, The role of c-MYB in benzene-initiated toxicity, Chem. Biol. Interact. (2005), https://doi.org/10.1016/j.cbi.2005.03.037.
[124] T. Yasuda, W. Kagawa, T. Ogi, T.A. Kato, T. Suzuki, N. Dohmae, K. Takizawa, Y. Nakazawa, M.D. Genet, M. Saotome, M. Hama, T. Konishi, N.I. Nakajima, M. Hazawa, M. Tomita, M. Koike, K. Noshiro, K. Tomiyama, C. Obara, T. Gotoh, A. Ui, A. Fujimori, F. Nakayama, F. Hanaoka, K. Sugasawa, R. Okayasu, P. A. Jeggo, K. Tajima, Novel function of HATs and HDACs in homologous recombination through acetylation of human RAD52 at double-strand break sites, PLoS Genet. (2018), https://doi.org/10.1371/journal.pgen.1007277.
[125] S. Li, B. Shi, X. Liu, H.X. An, Acetylation and deacetylation of DNA repair proteins in cancers, Front. Oncol. (2020), https://doi.org/10.3389/fonc.2020.573502.
[126] T. Ikura, V.V. Ogryzko, M. Grigoriev, R. Groisman, J. Wang, M. Horikoshi, R. Scully, J. Qin, Y. Nakatani, Involvement of the TIP60 histone acetylase complex in DNA repair and apoptosis, Cell (2000), https://doi.org/10.1016/S0092-8674(00)00051-9.
[127] K.K. Lee, Y. Zhang, R. Tirado- Magallanes, D. Rajagopalan, S.S. Bhatia, L. Ng, N. Desi, C.Y. Tham, W.S. Teo, M.M. Hoppe, A. Jeyasekharan, Y. Tay, W.J. Chng, D. Tenen, T. Benoukraf, S. Jha, TIP60 acetylates H2AZ and regulates doxorubicin-induced DNA damage sensitivity through RAD51 transcription, (2020). https://doi.org/10.1101/2020.06.10.145193.
[128] J.N. Andersen, O.H. Mortensen, G.H. Peters, P.G. Drake, L.F. Iversen, O.H. Olsen, P.G. Jansen, H.S. Andersen, N.K. Tonks, N.P.H. Møller, Structural and evolutionary relationships among protein tyrosine phosphatase domains, Mol.Cell. Biol. (2001), https://doi.org/10.1128/mcb.21.21.7117-7136.2001.
[129] S.Le Sommer, N. Morrice, M. Pesaresi, D. Thompson, M.A. Vickers, G.I. Murray, N. Mody, B.G. Neel, K.K. Bence, H.M. Wilson, M. Delibegovic, Deficiency in protein tyrosine phosphatase PTP1B shortens lifespan and leads to development of acute leukemia, Cancer Res (2018), https://doi.org/10.1158/0008-5472.CAN-17-0946.
[130] R. Pandey, M. Saxena, R. Kapur, Role of SHP2 in hematopoiesis and leukemogenesis, Curr. Opin. Hematol. (2017), https://doi.org/10.1097/MOH.0000000000000345.